

Aliphatic Alkynes as versatile Building Blocks for Macromolecular Architectures

Zur Erlangung des akademischen Grades eines

DOKTORS DER NATURWISSENSCHAFTEN

(Dr. rer. nat.)

von der KIT-Fakultät für Chemie und Biowissenschaften
des Karlsruher Instituts für Technologie (KIT)

genehmigte

DISSERTATION

von

M. Sc. Sergej Baraban

aus

Zelinograd, Kasachstan

1. Referent: Prof. Dr. Patrick Théato
2. Referent: Prof. Dr. Michael A. R. Meier
Tag der mündlichen Prüfung: 25.10.2022

"Denn Kunst ist nichts anderes als Gestaltung mit beliebigem Material."

Kurt Schwitters

Declaration

Die vorliegende Arbeit wurde im Zeitraum von Mai 2018 bis August 2022 am Institut für Technische Chemie und Polymerchemie (ITCP) und am Institut für Biologische Grenzflächen III (IBG-3) am Karlsruher Institut für Technologie (KIT) unter der Betreuung von Prof. Dr. Patrick THÉATO angefertigt.

Hiermit versichere ich, dass ich die Arbeit selbstständig angefertigt, nur die angegebenen Quellen und Hilfsmittel benutzt und mich keiner unzulässigen Hilfe Dritter bedient habe. Insbesondere habe ich wörtlich oder sinngemäß aus anderen Werken übernommene Inhalte als solche kenntlich gemacht. Die Satzung des Karlsruher Instituts für Technologie (KIT) zur Sicherung wissenschaftlicher Praxis habe ich beachtet. Des Weiteren erkläre ich, dass ich mich derzeit in keinem laufenden Promotionsverfahren befinde, und auch keine vorausgegangenen Promotionsversuche unternommen habe. Die elektronische Version der Arbeit stimmt mit der schriftlichen Version überein und die Primärdaten sind gemäß Abs. A (6) der Regeln zur Sicherung guter wissenschaftlicher Praxis des KIT beim Institut abgegeben und archiviert.

Ort, Datum

Sergej Baraban

Abstract

Alkynes are a class of hydrocarbons stemming from acetylene, which thus contain a carbon – carbon triple bond, and are widely represented in modern organic chemistry and polymer science. Concerning the broad field of applications however, the use of aliphatic alkynes is limited compared to the corresponding aromatic derivatives. This stands in contrast to the manifold and diverse chemistry that has emerged since FAVORSKII's pioneering work on isometric conversion of unsaturated hydrocarbons at the end of the 19th century.^[1] Furthermore, long-chain hydrocarbons feature desirable traits, such as high melting temperatures and chemical stability, nevertheless, their difficult syntheses has limited their use in polymer science, aside from a few examples.^[2]

On this premise, in the present thesis the synthesis and application of functionalized (long-chain) aliphatic alkynes were investigated. Four distinct projects emerged in this context and are summarized below.

In the first part of this thesis, the synthesis of long-chain α,ω -functionalized hydrocarbons and their respective use in polymer science was investigated. To this end, a modular synthesis strategy based on the alkylation of commercially available short alkynes was devised. Subsequently, the Alkyne Zipper reaction was employed to isomerize the internal alkyne moieties to the chain ends, thus yielding α,ω -functionalized alkynols with up to 25 in-chain methylene units in multi-gram fashion. Importantly, high yields were ensured through an improved reaction protocol, considering the challenging solubility of the long-chain hydrocarbons.

In the second part, a new route towards precise poly(ethylene) *via* SONOGASHIRA polycondensation was investigated. To this end, symmetrical divinyl halide monomers were synthesized and reacted with aliphatic dialkynes to yield polymers with enyne-linkages in the backbone. Initial setbacks, due to the intrinsic instability of these materials, were overcome by *in-situ* hydrogenation, which in turn resulted in a poly(ethylene) derivative with precisely placed ester groups along the main chain.

In the third part of the thesis, the trans-esterification of poly(pentafluorophenyl acrylate) with long-chain α,ω -alkynols was realized, and the thermal properties of the obtained bottlebrush polymers investigated. In a second step the pendant alkyne group of a previously attached alkynol was further modified through a three-component reaction allowing the attachment of a mPEG 400 moiety, thus creating a core-shell bottlebrush copolymer (cs-BBCP) with a cylindrical structure.

Finally, aliphatic dialkynes were reacted with 2,3,4,5,6-pentafluorobenzene-1-thiol (PFTP), yielding a bifunctional pentafluorophenyl vinyl sulfide monomer. The stability of these motifs under *para*-fluoro thiol reaction (PFTR) conditions was shown and the monomer subsequently polymerized with a series of (functional) dithiols successfully. The resulting tetrafluorophenyl vinyl sulfide motifs in the polymers were subsequently examined with regard to its post-polymerization possibilities *via* oxidation, thiol-ene reaction, halogenation and through the derivatization of functional groups of one dithiol.

In summary, the present work shows the importance of alkyne motif for the synthesis of previously unknown polymeric structures, either through direct incorporation or functional derivatives.

Zusammenfassung

Alkine sind eine Klasse von Kohlenwasserstoffen, die von Acetylen abstammen, also eine Kohlenstoff-Kohlenstoff-Dreifachbindung enthalten, und in der modernen organischen Chemie und Polymerwissenschaft weit verbreitet sind. Dabei ist der Anteil der aliphatischen Alkine gegenüber aromatischen Derivaten in der Anwendung relativ gering. Dies steht im Gegensatz zu der vielfältigen Chemie, die sich seit FAVORSKIIs Pionierarbeit über die isometrische Umwandlung ungesättigter Kohlenwasserstoffe Ende des 19. Jahrhunderts herausgebildet hat.^[1] Darüber hinaus weisen langkettige Kohlenwasserstoffe zwar wünschenswerte Eigenschaften, wie hohe Schmelztemperaturen und chemische Stabilität auf, doch ihre komplexe Synthese schränkt ihre Verwendung in der Polymerwissenschaft ein, abgesehen von einigen wenigen Ausnahmen.^[2]

Unter dieser Prämisse wurden in der vorliegenden Arbeit die Synthese und Anwendung von funktionalisierten (langkettigen) aliphatischen Alkinen untersucht. In diesem Zusammenhang wurden vier verschiedene Projekte bearbeitet, die im Folgenden zusammengefasst werden.

Im ersten Teil dieser Arbeit wurde die Synthese von langkettigen α,ω -funktionalisierten Kohlenwasserstoffen für den Einsatz in der Polymerwissenschaft untersucht. Zu diesem Zweck wurde eine modulare Synthesestrategie entwickelt, die auf der Alkylierung kommerziell erhältlicher, kurzer Alkine basiert. Anschließend wurde die Alkin-Zipper-Reaktion eingesetzt, um die interne Alkineinheit zu den Kettenenden zu isomerisieren und so α,ω -funktionalisierte Alkinole mit bis zu 25 Methyleneinheiten in der Kette in Multigrammform zu erhalten. Um hohe Ausbeuten zu gewährleisten, wurde ein optimiertes Reaktionsprotokoll entwickelt, das der schwierigen Löslichkeit der langkettigen Kohlenwasserstoffe Rechnung trägt.

Im zweiten Teil wurde ein neues Herstellungsverfahren von präzise Poly(ethylen) durch SONOGASHIRA-Polykondensation entwickelt. Zu diesem Zweck wurden symmetrische Divinylhalogenidmonomere synthetisiert und mit aliphatischen Dialkinen umgesetzt, um Polymere mit Enin-Verknüpfungen im Rückgrat zu erhalten. Anfängliche Schwierigkeiten, die auf die Instabilität dieser Materialien zurückzuführen waren, wurden durch *in-situ*-Hydrierung überwunden, sodass ein Poly(ethylen) mit präzise angeordneten Estergruppen entlang der Kette erhalten wurde.

Im dritten Teil wurde die Umesterung von Poly(pentafluorphenylacrylat) mit langkettigen α,ω -Alkynolen durchgeführt und die thermischen Eigenschaften der erhaltenen *Bottlebrush*-Polymere untersucht. In einem zweiten Schritt wurde die Alkin-Seitengruppe eines zuvor angefügten Alkynols durch eine Dreikomponentenreaktion (3-CR) weiter modifiziert, was die Anknüpfung einer mPEG 400-Einheit ermöglichte, sodass ein Kern-Schale-*Bottlebrush*-Copolymer (*cs-BBCP*) mit zylindrischer Struktur erhalten werden konnte.

Schließlich wurden aliphatische Dialkine mit 2,3,4,5,6-Pentafluorbenzol-1-thiol (PFTP) umgesetzt, wodurch ein bifunktionelles Pentafluorphenylvinylsulfid-Monomer generiert werden konnte. Die Stabilität der besagten Struktur motive unter den Bedingungen der *para*-Fluor-Thiol-Reaktion (PFTR) wurde nachgewiesen und das Monomer wurde anschließend erfolgreich mit einer Reihe von (funktionellen) Dithiolen polymerisiert. Die resultierenden Tetrafluorphenylvinylsulfid-Motive in den Polymeren wurden anschließend im Hinblick auf ihre Post-Polymerisationsmöglichkeiten durch Oxidation, Thiol-En-Reaktion, Halogenierung und durch die Derivatisierung der funktionellen Gruppen eines der Dithiole untersucht.

Zusammenfassend zeigt die vorliegende Arbeit die Bedeutung des Alkinmotivs für die Synthese bisher unbekannter Polymerstrukturen auf, sei es durch direkten Einbau oder mittels funktionaler Derivate.

Contents

Declaration	I
Abstract	II
Zusammenfassung.....	IV
Contents	VI
1 Introduction	1
2 Theoretical Background	3
2.1 The Alkyne Zipper Reaction.....	3
2.2 The SONOGASHIRA Reaction	6
2.3 Polymer Chemistry & Polymerization Methods.....	9
2.3.2 Post-Polymerization Modification.....	13
2.4 Polymer Architectures.....	15
2.4.1 Bottlebrush Polymers.....	16
2.5 Pentafluoro Motifs in Polymer Chemistry	18
3 Synthesis of α,ω -functionalized Hydrocarbons <i>via</i> Alkyne Zipper Reaction	23
3.1 Motivation	23
3.2 Synthesis of long-chain Hydrocarbons <i>via</i> Alkyne Zipper Reaction	24
3.2.1 General Concept.....	24
3.2.2 Precursor Synthesis and Alkylation	26
3.2.3 α,ω -Alkynol Synthesis <i>via</i> Alkyne Zipper Reaction.....	29
3.3 Conclusion	35
4 Precise Polyethylene <i>via</i> SONOGASHIRA Polycondensation.....	36
4.1 Motivation	36
4.2 General Concept for the Synthesis of unsaturated PE Precursors	38

4.3	Synthesis of modular Monomers and their Polymerization	41
4.3.1	Ester System	41
4.3.1	Diester System.....	47
4.4	Conclusion	51
5	Bottlebrush Architectures <i>via</i> PPM of Poly(Pentafluorophenol acrylate) with long- chain α,ω -Alkynols	52
5.1	Motivation	52
5.2	Polymer Synthesis and Post-Polymerization Reactions with α,ω -Alkynols	54
5.3	Derivatization of precise Bottlebrush Polymers	60
5.4	Conclusion	64
6	Pentafluorophenyl Vinyl Sulfides and their Polymerization	65
6.1	Motivation	65
6.2	PFPT Hydrothiolation & Monomer Synthesis	67
6.3	Polymerization <i>via para</i> -Fluoro Thiol Reaction.....	70
6.4	Post-Polymerization Modification.....	78
6.4.1	Derivatization based on the Dithiol Functional Groups.....	79
6.4.2	Derivatization based on Oxidation.....	81
6.4.3	Derivatization based on the Vinyl Group	85
6.5	Conclusion	92
7	Conclusion and Outlook.....	93
8	Experimental Part	95
8.1	Materials.....	95
8.2	Instrumentation	95
8.2.1	Nuclear Magnetic Resonance (NMR) Spectroscopy	95
8.2.2	Liquid Flash Chromatography Purification.....	95
8.2.3	Size Exclusion Chromatography (SEC).....	96

8.2.4	Thermogravimetric Analysis (TGA).....	97
8.2.5	Differential Scanning Calorimetry (DSC)	97
8.2.6	IR Spectroscopy	97
8.2.7	Centrifuge	97
8.3	Synthesis Procedures	98
8.3.1	Experimental Procedures for Chapter 3.....	98
8.3.1	Experimental Procedures for Chapter 4.....	116
8.3.2	Experimental Procedures for Chapter 5.....	125
8.3.3	Experimental Procedures for Chapter 6.....	132
9	Appendix	146
	List of Schemes, Figures and Tables	149
	Abbreviations	155
	Bibliography.....	156
	Publications	167
	Acknowledgments	168

1 Introduction

Since STAUDINGER's pioneering work on macromolecules at the beginning of the last century, polymers have come to be universally used in the modern world.^[3] Nowadays, almost all aspects of everyday life are in one way or another in contact to polymers, due to their use in nearly every object we encounter, such as the fibers in clothing, detergents, plastic cups, coatings, glues, smartphones and many more. The widespread use of plastics and polymers is due to their special properties, such as formability, hardness, elasticity, breaking strength, temperature and heat resistance, chemical resistance and a high strength-to-weight ratio. Besides their use in everyday life through commercial products, polymers are also found in special applications, such as flame retardants,^[4] high-performance materials in industry^[5] and sports^[6] as well as medical applications (*e.g.*, dental^[7,8] and skin adhesives).^[9] In these areas, functional polymer proved to be of value as their functionalities lead to the abovementioned special inherent properties, that makes them interesting for applications in the areas mentioned above.

The synthesis of such functional polymers can be achieved *via* the polymerization of functional monomers (*e.g.*, pentafluorophenyl acrylate). However, some functionalities (*i.e.*, alkenes and alkynes) are incompatible with the desired polymerization technique, such as free-radical polymerization, for instance. To circumvent this problem, the placement of the desired functionalities on the polymer backbone can be achieved upon the initial polymerization *via* so-called post-polymerization modification (PPM). In doing to, series of functional polymers can be generated from a single parent polymer. In this regard, the combination of desirable properties of commodity polymers, such as high temperature and chemical resistance, and the specialized uses of functional polymers, can be possibly accomplished *via* the incorporation of functional long-chain hydrocarbons in the polymer structure. However, the synthesis of such building blocks is tedious, and thus their application in this context is limited, besides a few examples.^[10,11] In this regard, established Organic Chemistry methods can be transferred to polymer research in order to open up new possibilities for the synthesis of functional synthons.

Among the broad toolbox of reactions, one such example is the Alkyne Zipper reaction, which allows the migration of triple bonds along a carbon chain.^[12] Therefore, aliphatic alkynes and alkynols especially, are a class of molecules with potential for polymer synthesis, either through their direct incorporation in the polymer backbone or *via* PPM approaches. The latter also gained much attention recently, due to another class of molecules that emerged to be of great value for the synthesis of polymer architectures: pentafluorobenzene derivatives. In the form of monomers such as pentafluorotyrene and pentafluorophenyl (meth)acrylates, these substrates allow for the (orthogonal) attachment of (macro)nucleophiles to polymer

backbones. In combination with the very efficient *para*-fluoro thiol reaction (PFTR),^[13] versatile polymer architectures, such as bottlebrush polymers, were achieved.^[14] However, a structural relative of these motifs has been ignored in this context: pentafluorothiophenol (PFTP). This molecule possesses a rich chemistry of addition reactions, and the respective products should be suitable precursors for the *para*-fluoro thiol reaction. Here, especially alkynes could prove to be useful, as their hydrothiolation motif, pentafluorophenyl vinyl sulfides offer great synthetic potential for PPM reactions.

The combination of the possible synthesis of α,ω -functionalized long-chain hydrocarbons *via* the Alkyne Zipper, the incorporation of aliphatic alkynes and alkynols in polymers and the potential use of pentafluorophenyl vinyl sulfides as substrates for the *para*-fluoro thiol reaction offer immense potential for yet unknown polymeric structures and are the topic of the presented work.

Accordingly, the following chapters summarize the distinctive topics that have been investigated in the context of this work. Chapter 3 deals with the synthesis of long-chain α,ω -functionalized hydrocarbons as synthons for direct polymerization or post-polymerization reactions that are based on alkynes, and are covered in the successional chapters. The modular synthesis is based on the connection of short-chain alkynes with haloalkanes and subsequent α,ω -alkynol formation *via* the Alkyne Zipper reaction.

Chapter 4 deals with a new modular approach towards precise poly(ethylene) *via* the SONOGASHIRA coupling reaction. Here, dialkynes are linked with symmetrical divinyl halide monomers to form the carbon backbone, that would then be hydrogenated subsequently to form a poly(ethylene) with precisely placed ester groups along the chain.

In the 5th chapter the post-polymerization modification of poly(pentafluorophenyl acrylate) with the long-chain α,ω -alkynols from Chapter 3 is realized and the thermal properties of the obtained bottlebrush polymers investigated. In a second step the pendant alkyne group of a previously attached alkynol is used for further modification allowing the attachment of a mPEG 400 moiety, thus creating a core-shell bottlebrush copolymer (cs-BBCP) with a cylindrical structure.

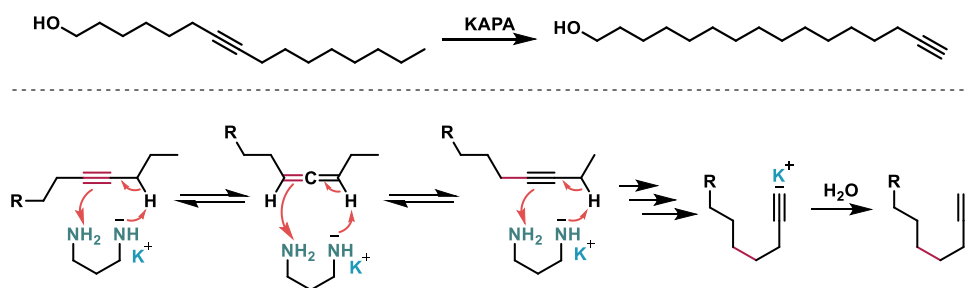
Finally in Chapter 6, the reaction alkynes with 2,3,4,5,6-pentafluorobenzene-1-thiol (**PFTP**) is used for the synthesis of a monomer unit, that is subsequently polymerized with a series of (functional) dithiols *via* *para*-fluoro thiol reaction. The resulting tetrafluorophenyl vinyl sulfide motif in the polymers is subsequently examined regarding its post-polymerization possibilities *via* oxidation, thiol-ene reaction, halogenation and through the derivatization of functional groups of one dithiol derivative.

2 Theoretical Background

The current chapter provides background information for a better understanding of the concepts, methods and reactions mechanisms used within this work. To this end, first some detailed information on two integral reactions in the context of this work, *i.e.*, the Alkyne Zipper and the SONOGASHIRA reaction, is given. Further, fundamental definitions related to polymer science, particularly macromolecular architectures, are elucidated, which in turn was followed up with a detailed information on the chemistry of fluorinated pentafluoro motifs.

2.1 The Alkyne Zipper Reaction

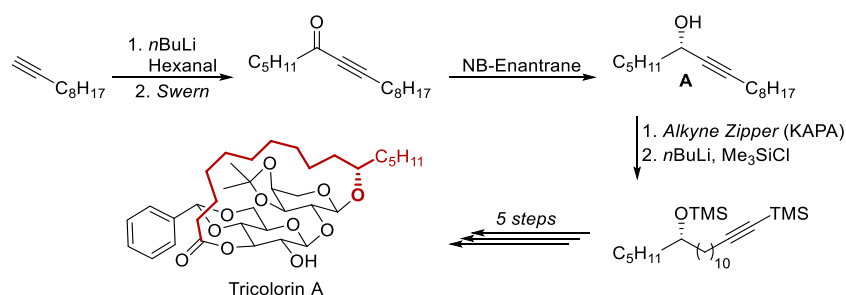
The migration of functional groups is a viable tool in organic chemistry and is found in many famous name reactions such as the Claisen,^[15] Cope^[16] and Carroll^[17] rearrangements, for example. Considering the movement of alkynes, FAVORSKII was the first to observe their movement as early as 1888, albeit from terminal (monosubstituted) to the more stable disubstituted derivatives.^[18] Since then, many reports were published that cover the movement of triple bonds along one position, mostly under very basic conditions (*e.g.* sodium amide in liquid ammonia) in internal alkynes.^[19,20] But it was not until WOTIZ *et al.* reported in 1966 that triple bonds can also isomerize along several carbon atoms, this time with sodium amide in ethylenediamine.^[21,22] However, these reactions resulted in mixtures and were thus unpractical from a synthetic standpoint. Almost a decade later, in 1974, BROWN reported the “Acetylene Zipper”, *i.e.*, the isomerization of internal alkyne bond towards terminal alkynes in the presence of potassium 3-aminopropylamide (KAPA), which is obtained through the reaction of potassium hydride (KH) and 1,3-diaminopropane (DAP), and is coined as a superbase.^[12,23] Shortly after, he applied the reaction to alcohols and successfully isomerized the internal alkyne in hexadec-7-yn-1-ol to the ω -position of the chain (Scheme 2.1 *Top*).^[24] Since, terminal alkynes are less stable (more acidic) compared to internal ones, Brown described the reaction as “contrathermodynamic”.^[12]



Scheme 2.1: *Top:* First example of the isomerization of a longer alcohol (hexadec-7-yn-1-ol) in the presence of potassium 3-aminopropylamide (KAPA). *Bottom:* Mechanism of the Alkyne Zipper reaction.

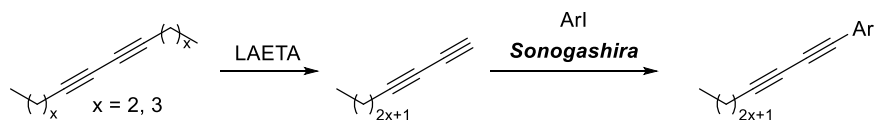
Mechanistically, the Alkyne Zipper reaction is a series of successive reversible alkyne-allene interconversions. The alkyne adjacent position is deprotonated to form an allene, which is rearranged to the alkyne again, thus moving the unsaturated moiety along one carbon (Scheme 2.1 *Bottom*). This process is repeated until the chain terminus is reached, where the acetylide anion is produced and stabilized with the counter ion. The stability of the acetylide is the driving factor in this reaction.^[25] Furthermore, due to the underlying mechanism, isomerizations cannot proceed through branching points, such as alkyl groups or secondary alcohols along the chain. Improvements of the original protocol by BROWN were made through the use of different salts, such as sodium and lithium, as well as the mixed alkali metal procedure reported by ABRAMS.^[26–28]

Due to the extremely basic conditions, the alkyne zipper reaction is mostly employed in the very early stages of total syntheses of complex molecules, as is exemplarily shown in Scheme 2.2 for the synthesis of **Tricolorin A**. The total synthesis involves the preliminary synthesis of chiral alkynol **A**, which is transformed to the terminal alkyne, that in turn is subsequently converted to the final product within total five steps. For a clarification, the pristine carbon skeleton is marked in red.



Scheme 2.2: Synthesis of **Tricolorin A** *via* the Alkyne Zipper reaction employed in the third step of the sequence.

Since the Alkyne Zipper reaction yields terminal alkynes, those isomerized substrates can be employed in SONOGASHIRA reactions. One such example is reported by BALOVA *et al.* and is especially noteworthy (Scheme 2.3).^[29,30]

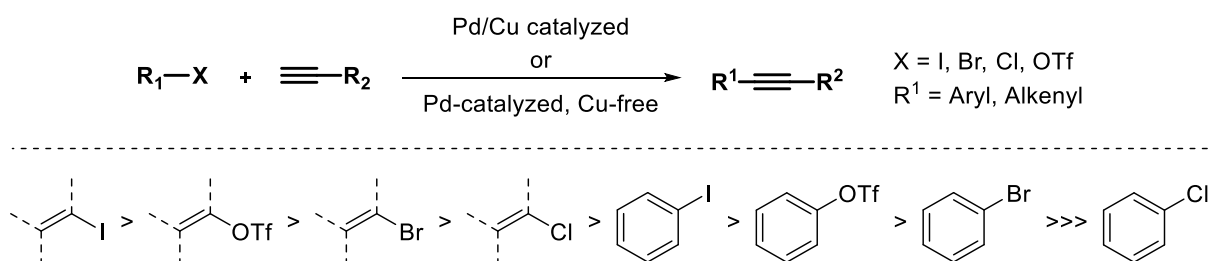


Scheme 2.3: Depiction of the isomerization of 1,3-diynes, which leads towards vicinal alkynes at the same chain end.

Particularly, the isomerization 1,3-diynes was achieved with lithium 2-aminoethylamide (LAETA) as the isomerizing agent and gave products with both alkynes at the same chain terminus. The obtained terminal alkynes were subsequently reacted with aryl iodides *via* SONOGASHIRA coupling, which is covered in more details within the following section.

2.2 The SONOGASHIRA Reaction

The SONOGASHIRA reaction was first described in 1975 and is named after its investigator, Kenkichi SONOGASHIRA.^[31] It is an extension of the CASSAR-HECK reaction protocol^[32,33] and has emerged to be the most important method among C-C linking cross-coupling reactions in organic synthesis for linking terminal alkynes to sp^2 -hybridized carbon atoms, such as aryl or vinyl halides.^[31,34] The generalized reaction scheme is shown in Scheme 2.4 (*top*). This transition-metal-catalyzed cross-coupling reaction is usually performed at atmospheric temperatures with mild bases, such as triethyl amine, which is often also used as the solvent medium. Due to these mild conditions, this reaction has also been employed for the synthesis of myriad complex molecules, such as drug candidates for cancer treatment in kg-scale.^[35] Furthermore, terminal alkynes have been coupled with several aryl and vinyl halides, including iodides, bromides, chlorides and even triflates.^[36] Usually, the reactivity of the substrates is dependent on the employed halide derivative (Scheme 2.4 (*bottom*)). Generally, vinyl halides are more reactive than aryl halides, whereas iodides are more reactive compared to bromides and chlorides.^[36]

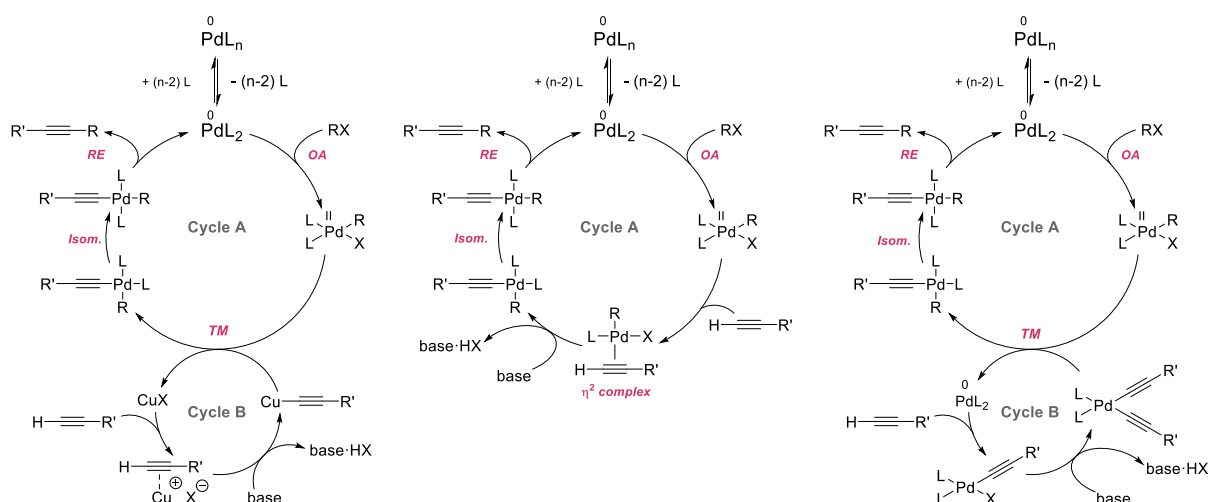


Scheme 2.4: General representation of the SONOGASHIRA reaction (*top*) and relative reactivities of sp^2 -carbon substrates bearing different halides (halides).

The mechanism of the SONOGASHIRA reaction (Scheme 2.5) is divided into the palladium catalytic cycle and the copper catalytic cycle. The activated palladium(0) complex reacts under oxidative addition to the palladium(II) complex, which is subsequently transmetalated with the copper acetylide. This is followed by *cis-trans* isomerization, after which the product is reductively eliminated with the reformation of the palladium(0) complex. The copper catalysis cycle begins with the formation of a π -alkyne complex between the copper(I) ion and the employed alkyne. The subsequent deprotonation by base (usually Et_3N), often also used as the reaction medium, forms the copper acetylide. This is subsequently transmetalated in the palladium cycle, whereby the copper ion is reformed and can undergo further catalytic cycles.

Several modern variants of the SONOGASHIRA reaction allow the bond formation in conditions free of solvents and nitrogen bases, as well as free of a copper cocatalyst.^[37] Since copper favors the formation of undesirable GLASER coupling by-products, the elimination of copper is

of particular interest in order to prevent these side reactions. Thus, many scientific research efforts have been made to exclude the metal from the reaction protocols, especially since the reaction also yields the desired products, albeit under harsher conditions.^[38] For clarity, the copper-free reaction mechanism is depicted in Scheme 2.5.



Scheme 2.5: Depiction of multiple reaction mechanisms of copper- and copper-free variants of the SONOGASHIRA reaction. *Left:* Textbook mechanism for the Pd/Cu catalyzed coupling. *Middle:* Textbook mechanism for the Cu-free variant. *Right:* Recently reported Pd-Pd transmetalation mechanism.^[39] OA – oxidative addition; TM – transmetalation; *Isom.* – *cis-trans* isomerization.

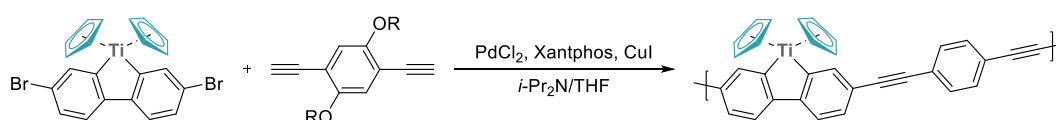
Although the first report on the so-called copper-free SONOGASHIRA reaction was reported more than four decades ago,^[32,33] its mechanism is still not fully understood. In 2003, SOHEILI *et al.* published a proposed mechanism consisting only of oxidative addition and reductive elimination (Scheme 2.5 *middle*).^[40] The mechanism is based on the reversible η^2 -complex formation and subsequent base-mediated deprotonation of the terminal acetylenic proton.

However, this proposed mechanism has not yet been proven. Indeed, recent calculations even suggest that this cycle is unlikely, since the activation barrier for the formation of the complex is much too high.^[41,42] Based on these findings, GAZVODA *et al.* postulated another mechanism (Scheme 2.5 *right*).^[39] According to this study, the copper-free SONOGASHIRA coupling proceeds analogously to the conventional mechanism of the SONOGASHIRA coupling, through a tandem double cycle, where the palladium takes over the role of the copper. Importantly, computational studies and various experiments support this hypothesis.^[39] However, a complete elucidation has not yet been achieved.

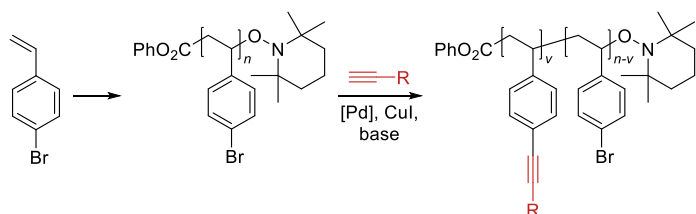
Besides the numerous applications of the SONOGASHIRA reaction in the field of pure Organic Chemistry, it was also extensively employed as a tool for polymer synthesis and modification. As it is not possible to do justice to the countless number of examples, the following three should show the broad possibilities of this method (Scheme 2.6). Thus, TOMITA *et al.* employed

the SONOGASHIRA polycondensation to form linear π -conjugated organometallic polymer by coupling a titanafluorene and arylene ethynylene (*top*). GRUBBS *et al.* used the reaction for the post-polymerization modification of poly(4-bromostyrene) with aliphatic alkynes, which resulted in polymers that cannot be obtained *via* the preceded controlled radical polymerization (*middle*).^[43] Finally, TRUNK *et al.* reacted 1,3,5-triethynylbenzene with various multifunctional iodoarenes in a copper-free SONOGASHIRA-variant with extremely low palladium loadings of 0.65% to form high-surface-area poly(aryleneethynylene) networks.^[44]

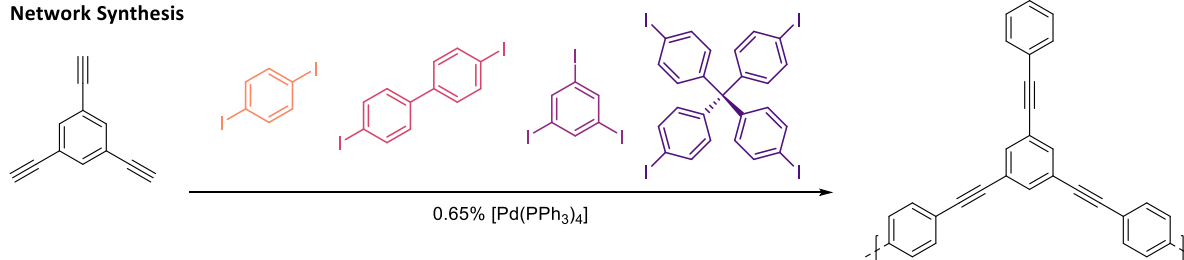
Linear Polymers



Post-Polymerization Modification



Network Synthesis



Scheme 2.6: Depiction of three different examples for the use of the SONOGASHIRA reaction in the field of polymer and material science.

2.3 Polymer Chemistry & Polymerization Methods

Polymers (Greek: *poly-*, "many" and *-mer*, "part") are materials that consist of large molecules (macromolecules), composed of linked repeating subunits (monomer). The idea that polymers constitute of covalently linked repeating units was introduced by Hermann STAUDINGER in his landmark publication "Über Polymerisation" ('On Polymerization') in 1920.^[45] which is recognized as the beginning of modern polymer science. Thus, Staudinger was honored with a Nobel Prize in 1953.

In general, a distinction can be made between natural and synthetic polymers. Natural polymers, also called biopolymers, encompass all polymers that are synthesized in living organisms. These include, for example, carbohydrates, proteins and oligonucleotides in addition to natural rubber. Synthetic polymers, on the other hand, are chemically produced on a laboratory scale, which some of them in turn are also industrially accessible. Some of the best-known examples are poly(ethylene), poly(styrene) and poly(vinyl chloride), since they are utilizable nearly everywhere in everyday life, for example as plastic bags, cups, films, tubing and many more. The process of polymer synthesis is called polymerization. Although many polymerization techniques exist, usually a distinction is made between two mechanisms: Step- and chain-growth.^[46]

In step-growth processes, polymerization takes place in a step-wise manner. Here, another differentiation can be made between polyaddition and polycondensation processes, depending on whether a byproduct, water for instance, is expelled during the formation of the monomer linkage.

A requirement for monomers to undergo step growth is that they need to be bifunctional.^[47,48] Thus, the monomers first form dimers, then trimers or tetramers, which combine again to form oligomers, and their linkage ultimately leads to the desired polymer. As a result, growth is very slow, and large conversions are required to obtain compounds with high molecular weight.^[49] In fact, the correlation between the degree of polymerization and the conversion of the monomers is described by the CAROTHERS equation.^[50]

In contrast, polymers with a very high molecular weight can be obtained at low conversion rates using a chain-growth polymerization technique. Here, initially a radical initiator decomposes and adds to a monomer unit, thus creating a reaction site for further monomer additions until the chain-growth is terminated *via* recombination of two radicals or a chain transfer event. The chain-growth polymerization itself can be further divided into free radical, anionic, cationic and coordinative polymerization.^[46] Since only radical polymerization was employed in the context of this work, it will be described in more detail below.

Within the radical based methods, two types can also be distinguished: Free Radical Polymerization (FRP) and Reversible Deactivation Radical Polymerization (RDRP). FRP is one of

the best known and most widely used polymerization methods. It essentially involves three steps: the initial decomposition of a radical initiator, formation of a reaction center and further additions and termination (recombination of two radicals or chain transfer events). However, especially the latter result in chain breaking, backbiting processes and transfer reactions that prevent homogeneous chain growth and thus lead to polymer chains with different chain lengths.^[46]

Since the polymer properties, such as viscosity, glass transition temperature T_g or rheological parameters, strongly depend on the chain lengths, the determination of the molecular weight plays a vital role. As mentioned, both step-growth and chain-growth polymerizations yield polymer chains of different lengths due to the nature of the polymerization of side reactions. For this reason, polymer samples are obtained as distributions of chain lengths and described through averages.

Most commonly the number-average molecular weight \bar{M}_n (Equation 1) and the weight-average molecular weight \bar{M}_w (Equation 2) are used (respective definitions below).

$$\bar{M}_n = \frac{w}{\sum N_x} = \frac{\sum N_x M_x}{\sum N_x} \quad (1)$$

- Total weight w of all molecules divided by the number of moles present $x = 1 \rightarrow \infty$ over all different polymer sizes. N_x & M_x – number of chains and their respective molecular weight.

$$\bar{M}_w = \frac{\sum c_x M_x}{\sum c_x} = \frac{\sum c_x M_x}{c} = \frac{\sum N_x M_x^2}{\sum N_x} \quad (2)$$

- Sum of the weight concentration, multiplied with the corresponding molecular weight, c_x - weight concentration of M_x molecules. c - total weight concentration of all polymer chains.

The dispersity \mathcal{D} is the quotient of both averages (Equation 3) and describes the molecular weight distribution.

$$\mathcal{D} = \frac{\bar{M}_w}{\bar{M}_n} \quad (3)$$

Since the properties of polymers differ with their chain length usually low distributions are required. In an ideal polymerization, all polymer chains would have the exact same length and thus a dispersity (\mathcal{D}) of 1. However, due to side reactions such as chains-transfer events this is not possible to achieve with FRP. In order to allow for the synthesis of polymers with very narrow distributions, Reversible Deactivation Radical Polymerization (RDRP) techniques, such as Nitroxide-Mediated radical Polymerization (NMP), Atom Transfer Radical Polymerization (ATRP) and Reversible Addition-Fragmentation chain Transfer (RAFT) polymerization, have been developed. The latter is described in the following section.

2.3.1.1 Reversible Addition-Fragmentation Chain Transfer (RAFT) Polymerization

Reversible addition-fragmentation chain transfer (RAFT) polymerization is a reversible-deactivation radical polymerization (RDRP) technique that was first introduced RIZZARDO *et al.* in 1998.^[51] Here, control over the radical polymerization process is gained through the use of mediating molecules, the so-called chain transfer agents (CTA) or simply 'RAFT agents'. Examples include thioesters (A), trithiocarbonates (B), dithiocarbamates (C), and xanthates (D), for instance.^[52] The general structure as well as a representative compound for each class, is presented in Figure 2.1.^[52–54]

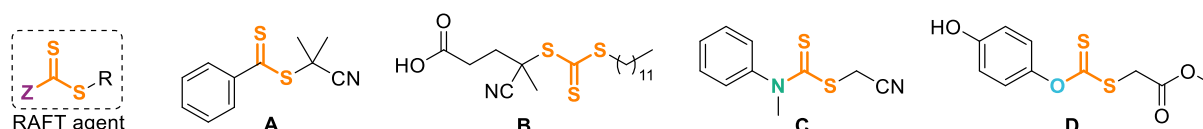
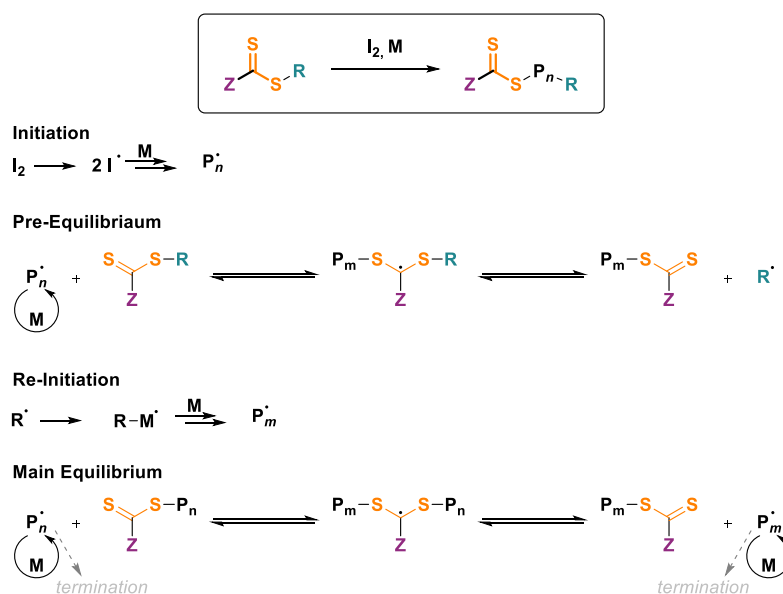


Figure 2.1: Depiction of the general RAFT agent structure as well as selected examples for the class of thioesters (A), trithiocarbonates (B), dithiocarbamates (C) and xanthate esters (D).

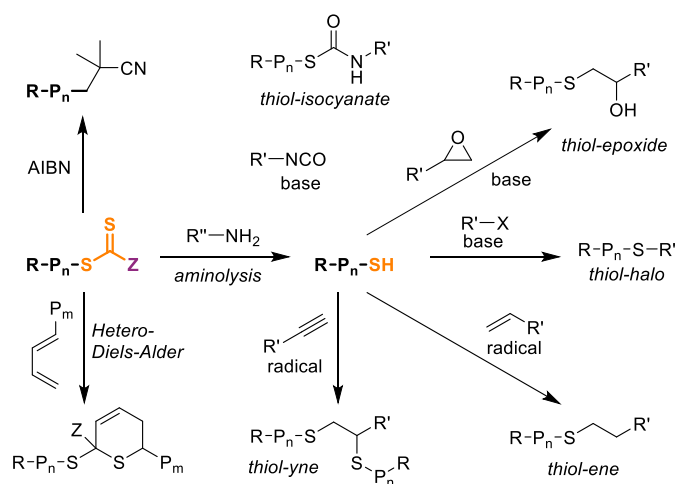
RAFT polymerization is a very versatile method, as it allows the polymerization of electronically different monomers if the RAFT agent is selected accordingly.^[55] Furthermore, in contrast to other RDRP methods, the controlled nature does not stem from all over lowered radical concentrations by reversible trapping of propagating free radicals (NMP, ATRP), but instead is based on a degenerative transfer, *i.e.*, an activation-deactivation process, and thus, the overall radical concentration is not reduced, which in turn allows high polymerization rates.



Scheme 2.7: General reaction scheme (*top*) and mechanism of the RAFT process.

Mechanistically, after initial radical formation and addition to monomer (*Initiation*), the radical species adds to the RAFT agent entering the equilibrium between active and dormant

species (*Pre-Equilibrium*), thereby expelling another radical (R') *via* β -scission. The new radical adds to monomer (*Re-Initiation*) and is again caught by the CTA, thus establishing the main equilibrium. In this manner, the propagating chains are continually reversibly transferred between a propagating and dormant state. Ideally, the rate of the addition-fragmentation steps is higher than the propagating rates, keeping resulting in the addition of less than one monomer *per* scission-propagation-addition sequence, which ensures a similar propagating probability for all chains and thus a narrow dispersity \mathcal{D} . The overall reaction constitutes of the insertion of monomer between the R group and the dithioester moiety. This in turn, results in polymers with the respective functional group at the chain end. Through aminolysis, the terminal CTA group can be transformed into thiols, which can be subsequently used for series of post-polymerization reaction, such as thiol-ene or nucleophilic substitutions, as shown in Scheme 2.8.^[56–60]



Scheme 2.8: Depiction of the varied post-polymerization chemistries that are available to RAFT-polymers.

2.3.2 Post-Polymerization Modification

Despite the numerous polymerization methods available, it is not always possible to achieve the desired functionality or properties of the polymer directly during polymerization. Problems such as different solubilities, stabilities or interactions of the functional groups or their plain incompatibility with the employed polymerization conditions can be overcome by functionalizing polymers after polymerization. For this so-called Post-Polymerization Modification (PPM) approach, functionalized monomers are first polymerized and then modified by orthogonal reactions to obtain their final properties.^[61]

Two early examples for this methodology are the vulcanization of natural rubber with elemental sulfur^[62] (1840) and the production of nitrocellulose^[63] (1847) by nitration of the polysaccharide. Since then, a plethora of organic reactions has been used to modify polymers yielding immensely diverse structures with varying functionalities.^[61] In combination with the mentioned controlled free radical polymerization techniques, the synthesis of well-defined polymers was possible and thus diverse polymer architectures such as micelles, lamellae, brush polymers and many others could be achieved.^[64] In order for an organic reaction to be considered for PMM applications, it should feature several important characteristics, such as high efficiency, chemoselectivity and most importantly, full conversion. In contrast to reactions of small molecules, the separation of incompletely functionalized polymers is extremely difficult, even one could postulate that it is impossible. For this reason, the most employed PPM reactions feature criteria of so-called '*click chemistry*',^[65] including Diels-Alder reactions,^[61] copper(I)-catalyzed alkyne-azide cycloadditions (CuAAC),^[66] thiol-ene^[67,68] as well as thiol-yne reactions (Figure 2.2).^[69,70] Recently, the chemistry of fluorinated moieties, such as pentafluorophenyl esters and pentafluorobenzene-derivates, has gained increasing attention in context of post-polymerization modification reactions.^[61] In the case of the former, the electron-deficient ester can be trans-esterified with alcohols and amines under mild reactions conditions, reaching full conversions, which allows the introduction of varied groups to the polymer backbone.^[71,72] The latter undergoes nucleophilic aromatic substitution (S_NAr) reactions with nucleophiles such as alcohols, amines and thiols. Due to the preferred use of the last, owing to their increased nucleophilicity, the replacement of the *para*-positioned fluorine atom with thiols is referred to as the *para*-fluorine thiol reaction (PFTR).^[73] Beneficially, the conversion of reactions involving both motifs can be easily followed *via* ^{19}F NMR. The combination of both motifs in the polymer backbone further allows the orthogonal functionalization of polymer structures, depending on the employed nucleophile.^[13]

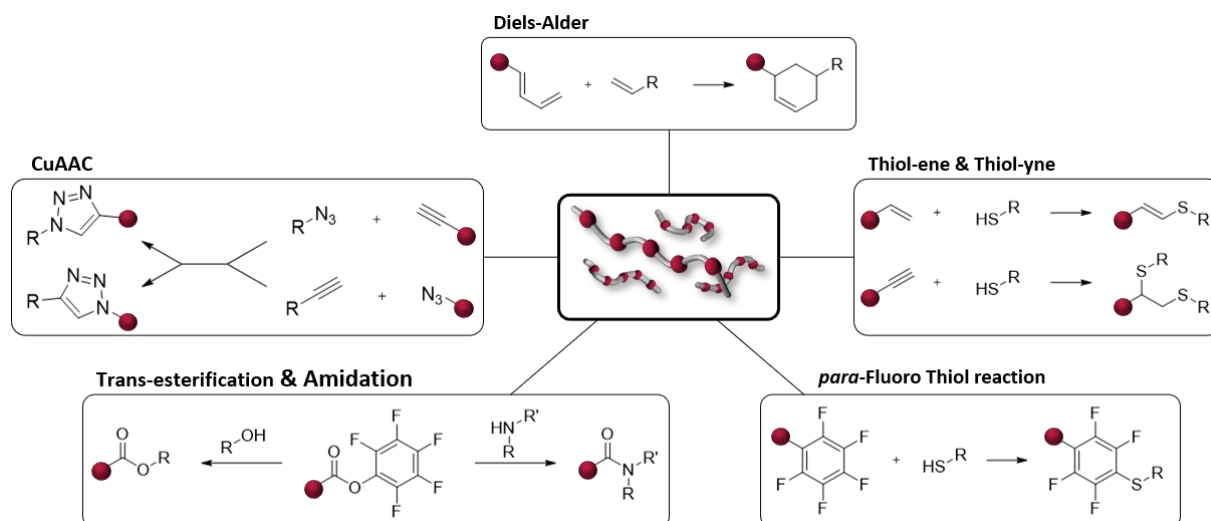


Figure 2.2: Overview over the most common PPM reactions: Diels-Alder, CuAAC, thiol-ene & thiol-yne, trans-esterification and amidation of active-esters in addition to the *para*-Fluoro Thiol reaction (PFTR).

The *para*-Fluoro Thiol reaction is described in detail in Chapter 2.5.1.1. Post-polymerization reactions can also be used for the synthesis of different molecular architectures as shown in following section, as well as in Chapter 5.

2.4 Polymer Architectures

The physical properties of a polymer not only depend on its molar mass, but also on its macromolecular structure, which is determined by the arrangement of the monomers. Thus, polymers can exist as linear chains, branched chains or even as three-dimensional networks. These branching points can either occur randomly during polymerization *via* backbiting, a reaction with another chain, or can be targeted during the synthesis.^[74]

Furthermore, covalent bonds can form between linear chains, generating entire polymer networks, which are thus named crosslinked polymers.^[75] Depending on the degree of crosslinking, several polymer properties such as the glass transition temperature T_g and tensile strength, is influenced. This is especially noticeable in the different types of poly(ethylene) (PE), which accordingly classified as low- or high density PE *inter alia*, and is thus used for very differ applications.^[76]

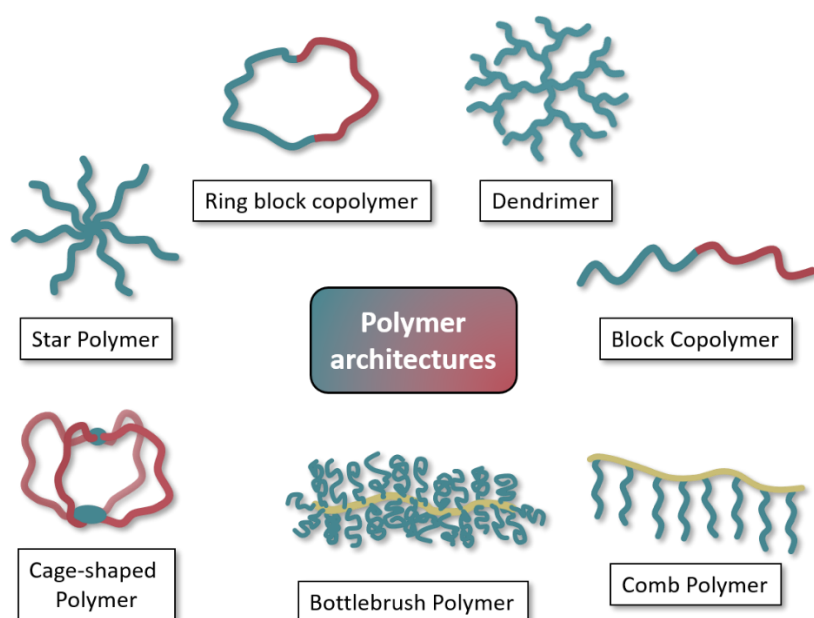
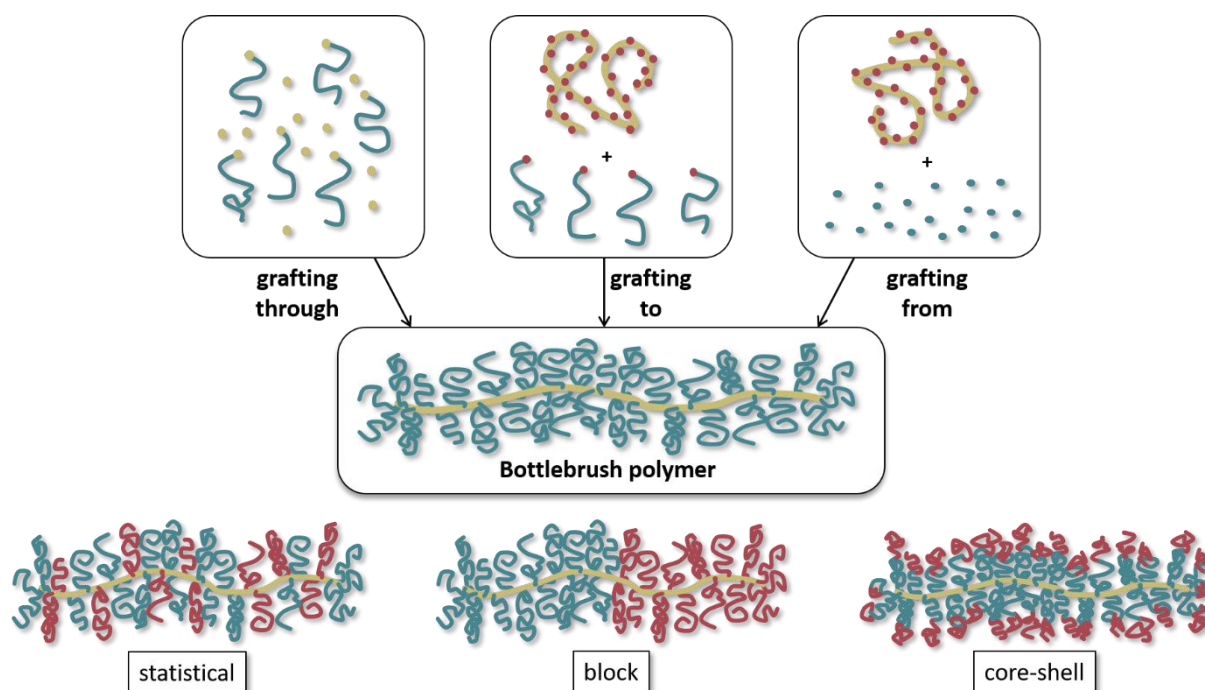


Figure 2.3: Depiction of various polymer architectures that can be generated *via* modern polymerization techniques.

With the aid of modern polymerization techniques, such as reversible addition–fragmentation chain-transfer (RAFT) polymerization for instance, and post-polymerization modification (PPM) reaction, it is possible to generate a large number of structurally different macromolecules in a targeted manner.^[77] Skillful selection of monomers and suitable synthesis methods results in defined macromolecular structures whose properties can be specifically adapted according to their envisioned application. A large number of complex molecular architectures, such as star polymers,^[78] comb polymers,^[79] bottlebrush polymers,^[79–81] dendrimers^[82] and ring (block co-)polymers^[83–85] as well as cage polymers^[86,87] are known (Figure 2.3).

2.4.1 Bottlebrush Polymers

Architecturally, bottlebrush polymers belong to the category of comb polymers, but deviate from such through their very high grafting density.^[79] Structurally, they consist of a linear main chain to which side chains are tethered at more or less regular intervals. The structure and thus also the properties depend on the graft density and the steric repulsion of the side chains. The higher the graft density, the lower the flexibility of the architecture, twisting backbone into an elongated shape and obtaining rod-like properties.^[88,89] Depending on the synthesis method, very different properties can be obtained from the choice of side-chain types (water-soluble PEG vs. poly(styrene) for instance), the length of the side chains as well as the type of monomer for the bottlebrush backbone.^[14,79]



Scheme 2.9: Depiction of different grafting methods for the synthesis of bottlebrush polymers (which can vary as statistical, block and core-shell): grafting through (*left*), grafting to (*middle*) and grafting from (*right*).

The synthesis of bottlebrushes is realized *via* grafting methods, hence the notion as graft polymers. In principle, a distinction can be made between three grafting methods: 'grafting through', 'grafting to' and 'grafting from' (Scheme 2.9).^[14]

The 'grafting through' method is based on the copolymerization of monomer with polymers that carry polymerizable side chains (macromonomers). As the chain grows, the polymerizable side group is integrated into the backbone forming the bottlebrush. One advantage of this approach is the fact that the macromonomer can be tuned in its length *via* controlled radical

polymerization techniques, for instance. More importantly, the macromonomer can be accordingly characterized before its use. Furthermore, the grafting density can be partially controlled through the use of macromonomers consisting of A-branch-B diblock macromonomers, for example.^[90] However, full conversions cannot be reached caused by the increasing steric hindrance during polymerization, and thus the removal of macromonomers with high molar mass can become a problem.

In the '*grafting from*' method, a macroinitiator, *i.e.*, a polymer scaffold that carries initiation sites, is first produced. Here, the side chains are grown from the backbone initiation sites, thus avoiding the problem of steric hindrance of the already linked side chains. In order to prevent coupling of the growing chains, low radical concentrations are essential. For this reason, Nitroxide-mediated radical polymerization (NMP) as well as Atom transfer radical polymerization (ATRP) approaches are preferably used in this context. Another advantage over the other two methods is that no separation of the unlinked side chains is required, making the purification process much easier.^[80,91,92]

Finally, in the '*grafting to*' method, chain-end functionalized polymers as well as the to-be-grafted-on macromolecules are prepared and subsequently reacted. To ensure efficient grafting, often *click chemistry* reactions are employed.^[93] In similar manner, due to steric hindrance of the side chains, high graft densities can be hard to reach and unreacted side chains need to be removed upon grafting.^[94,95] In the context of this approach, especially pentafluorophenyl (PFP) esters emerged as an effective synthesis platform, as they can be easily post-polymerized with the suitable nucleophiles.^[96]

Since the described approaches allow for manifold combination of monomers, macromonomers as well as structural variations of the backbone, many different bottlebrush structures have been prepared. As an illustrative example, statistical bottlebrushes, bottlebrush block copolymers as well as core-shell bottlebrush copolymers (cs-BBCPs) are depicted in Scheme 2.9.^[14,81,84,97]

2.5 Pentafluoro Motifs in Polymer Chemistry¹

Fluorinated polymers are macromolecules, which are decorated with fluorine-carbon bonds. These bonds are considered to be the strongest covalent bonds of any other carbon-X bond ($X = \text{any other element}$).^[98] Due to this high bond strength, fluorinated polymers possess remarkable properties, such as hydrophobicity, low surface energy, high thermal stability as well as excellent chemical resistance.^[99] The combination of these advantageous properties led to their use as high-performance materials (coatings, electrical and thermal insulators, anti-adhesives), and even found their way into everyday life, with poly(tetrafluoroethylene) (PTFE) being the most known example in the form of coatings (*Teflon*) or waterproof fabric membranes (*Gore-Tex*).^[99-101] Their extreme chemical resistance however, also renders them inert to further reactions in order to tailor their properties. In contrast, a different class of fluorinated polymers allows the targeted modification of the polymer backbone, and thus of the properties: polymers possessing pentafluorobenzene moieties.

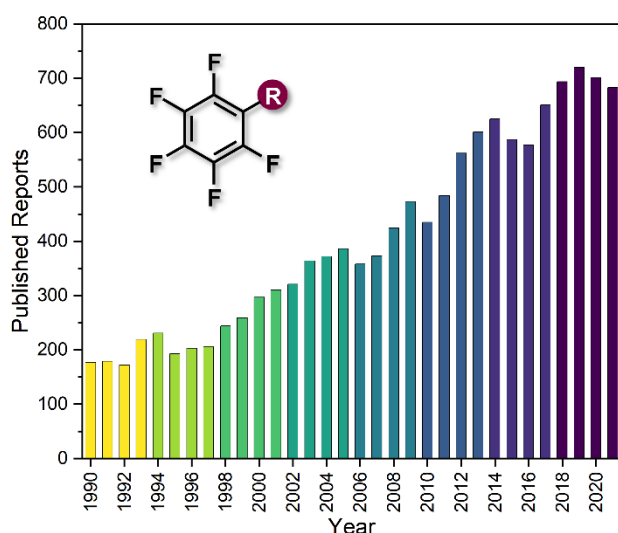


Figure 2.4: Publications containing the pentafluorobenzene motif per year from 1990 – 2021 (retrieved from SciFinderⁿ on 07.09.22).

Although the use of pentafluorobenzene motifs increased steadily in the last 20 years (Figure 2.4), their popularity in polymer science increased, when the facile modification of pentafluoro pendant groups became apparent. Here, initially the substitution of pentafluorophenyl active esters was investigated in detail and used as methodology to easily prepare polymer libraries *via* trans-esterification reaction.^[71] At a later stage, in the context of pentafluorostyrene-derived polymers, the work of HOOGENBOOM and SCHUBERT proved expedient as they reported the grafting of (macro)molecules to a polymer

scaffold through *para*-substitution of pendant pentafluorobenzene moieties.^[102] A year later, BECER *et al.* used the same strategy for the synthesis of glycopolymers and selected a thiol-glycoside for the reaction, which resulted in a full conversion at atmospheric temperatures.^[103] Thus, a new method for effective ligation with thiols was established, *i.e.*, the *para*-fluoro thiol reaction (PFTR; see following section).

¹ Parts of this subchapter - including text, figures, tables and schemes - might/will be subsequently published within a perspective article in the near future.

Since these findings, a large number of polymerizable pentafluorobenzene-derivatives emerged in the context of functional polymers.^[104] A small selection of representatives is shown in Figure 2.5.^[104] Here, the monomer structures were adjusted to fit certain polymerization techniques, such as radical polymerization (pentafluorostyrene (PFS), pentafluorofluorobenzyl acrylate (PFBA), pentafluorofluorobenzyl methacrylate (PFBMA), pentafluorofluorophenyl acrylate (PFPA), pentafluorofluorophenyl methacrylate (PFPMA)),^[61] ring-opening metathesis polymerizations (ROMP) (pentafluorofluorophenyl norbornenecarboxylate (PFPNorB))^[105] and ring-opening polymerization(perfluorophenyl methyl trioxocarboxylate (MTC-OPhF₅)).^[106]

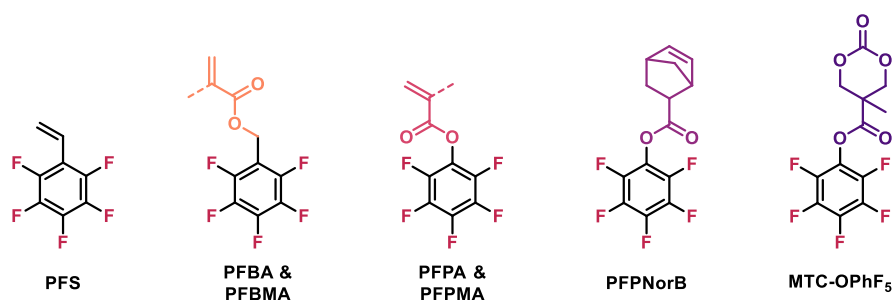
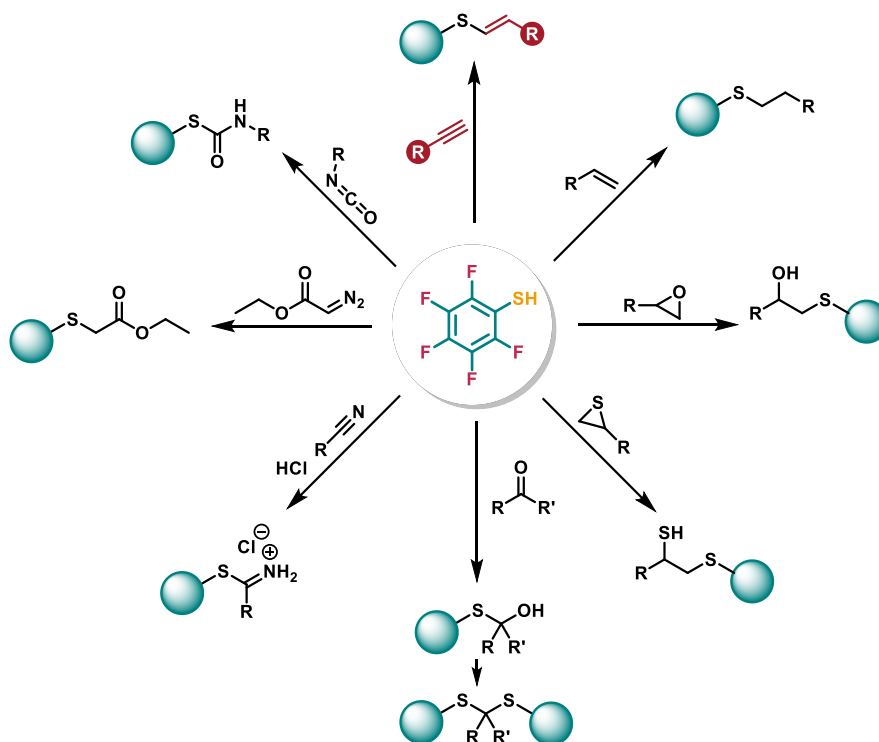


Figure 2.5: Depiction of several pentafluorobenzyl derived monomers.

Besides the grand variety of related monomers, one exception can be found: the structurally related thiol, i.e., 2,3,4,5,6-pentafluorobenzene-1-thiol or pentafluorothiophenol (**PFTP**) largely ignored in the context of polymer science and only found sporadic use as a ligand^[107,108] or was employed for the synthesis of electrolyte material additives.^[109]

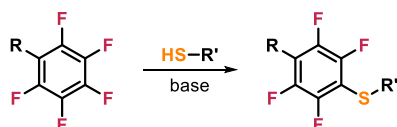


Scheme 2.10: Overview of the possible addition reactions of pentafluorothiophenol (PFTP).

However, this is in strong contrast to the synthetic potential of this compound. As early as 1975, LEONG and PEACH showed the remarkable potential of **PFTP** through addition reactions to numerous functional groups, such as alkenes, alkynes, oxiranes, thiiranes, diazo compounds, aldehydes, ketones, and nitriles (Scheme 2.10).^[110] In theory, some of corresponding products should be suitable substrates for the *para*-fluoro thiol reaction (PFTR). Since the focus of this thesis lays on the utilization of alkynes, for the first time, the chemistry of the corresponding pentafluorophenyl vinyl sulfide was investigated in the context of functional polymer synthesis (refer to Chapter 6).

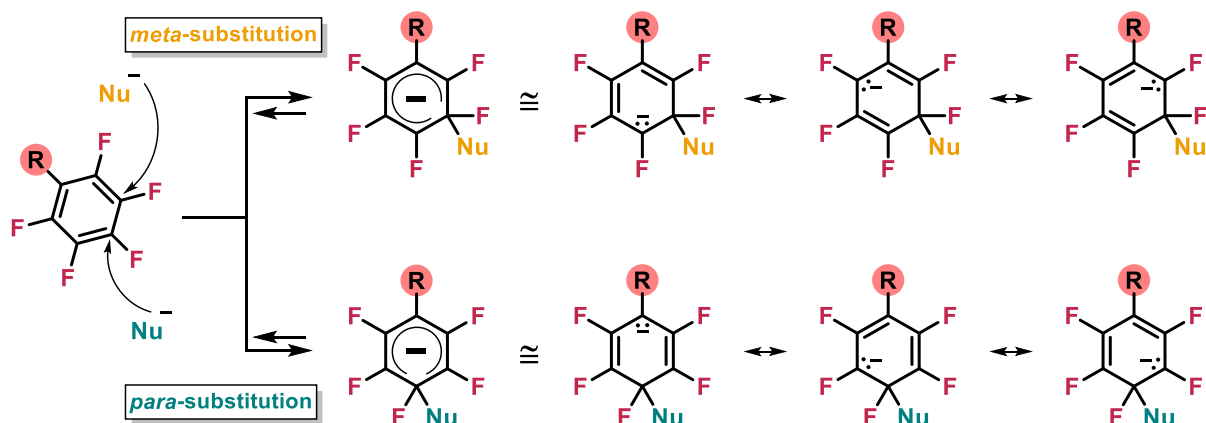
2.5.1.1 The Para-Fluoro Thiol Reaction

The *para*-fluoro thiol reaction (PFTR) is a nucleophilic aromatic substitution (S_NAr) that has found increasing application in organic chemistry, and especially polymer science, as a platform for an efficient ligation.^[73] The approach involves the reaction of a fluorinated benzene derivative with thiol substrates, resulting in the selective substitution of the *para*-positioned fluorine atom on the aromatic ring (Scheme 2.11). This remarkable selectivity is owed to the influence of the fluorine substituents; indeed, fluorinated molecules often show drastically changed chemical behavior compared to their non-fluorine counterparts.^[111]



Scheme 2.11: General reaction scheme for the *para*-fluoro thiol reaction (PFTR).

Since fluorine possesses the highest electronegativity of any element, the carbon-fluorine bond is highly polarized, which results in a formal positive charge on the carbon atom, making it vulnerable towards nucleophilic attack.^[112,113] Early studies on the displacement of fluorine atoms in such molecules were performed in the second half of the last century, when several hexafluorobenzene derivatives were obtained through the reaction of with hydroxides, alkoxides, amines, lithium organyls and others.^[114–117] However, due to the increased acidity and nucleophilicity of thiols, this class of substrates in particular, emerged as the preferred nucleophile. Here, the reactions can be performed in polar solvents, such as DMF, with weak bases, *e.g.*, triethyl amine, to yield the desired substitution products in short reaction times (minutes to hours, sometimes near instantly^[118]) at atmospheric temperatures.^[73,119] The observed selectivity of the PFTR can be elucidated *via* mechanistical considerations as discussed in detail by KVIČALA *et al.*^[120] During the nucleophilic attack on the ring, the delocalized electrons can be represented as mesomeric forms, as shown in Scheme 2.12. Here, in similar fashion as with benzene derivatives, the substituent has an influence on the regioselectivity of the reaction. With non-electron donating substituents, the *para*-substitution pathway is favored due to a better charge delocalization. This observation is also supported by computational studies.^[120]



Scheme 2.12: Depiction of resonance structures for the *meta*- and *para*-pathway of nucleophilic substitutions in monosubstituted pentafluorobenzene derivatives.

In addition, the *para*-fluoro thiol reaction features the possibility to follow the reaction *via* ^{19}F NMR. Due to the extremely broad range of shifts of fluorine resonances (up to 1300 ppm^[121]), structural changes can be easily detected. Since proton and carbon resonances are not visible in ^{19}F NMR, this allows for quick reaction monitoring without the need for prior purification.

Due to its mild conditions, regioselectivity, the commercial availability of thiols, and most importantly its efficiency, PFTR has gained increasing attention as a method for post-polymerization modification of polymer scaffolds.^[13]

3 Synthesis of α,ω -functionalized Hydrocarbons *via* Alkyne Zipper Reaction

3.1 Motivation

As mentioned in Chapter 1 the aim of the current thesis is the evaluation of possible syntheses of alkyne-functionalized PE-like materials *via* incorporation of long-chain hydrocarbon synthons in the backbone structure of polymers or as side-chains. At the core of obtaining such materials is the availability of functional long hydrocarbon molecules that can be modified accordingly to enable their polymerization. Thus, one goal was to find a suitable route towards functional hydrocarbons that can be obtained in a multi-gram fashion.

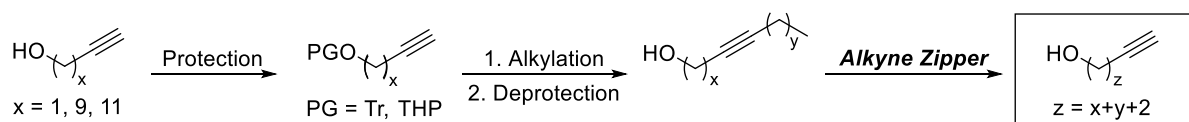
The most prominent literature-based strategies for the build-up of similar molecules usually employ long multi-step routes that are either based on the dimerization of fatty-acid derivatives with limited chain lengths *via* olefin metathesis or the connection of two alkyl chains with protected functionalities *via* GRIGNARD reaction, WURTZ coupling or WITTIG reactions.^[10,11,122,123] Both strategies have restrictions as they strongly depend on the availability of necessary precursor molecules that need to be orthogonally protected and deprotected for further use. In this manner, WAGENER *et al.* reported a procedure for the synthesis of long-chain alkenols as building blocks for ADMET monomers.^[10] Here the longest alkenol bearing 36 carbon atoms between its functional groups could be synthesized in a yield of 17 % over 16 reaction steps. Although the mentioned synthesis is claimed to be facile in nature due to minimal chromatographic purification, it still shows that the build-up of α,ω -functionalized hydrocarbons is not trivial at all and requires great synthetic efforts including lengthy multi-step syntheses.

Although α,ω -functionalized long-chain hydrocarbons can be synthesized with the previously mentioned method, their transformation from alkenes to alkynes requires two additional steps. As such, a lengthy synthesis route requires immense effort, therefore a new and more convenient methodology was greatly desired. To this end, alternative synthetic approaches were investigated and a viable possibility based on the Alkyne Zipper reaction was discovered. Here, the formation of long-chain hydrocarbons with a hydroxyl- and alkyne-moiety on the α - and ω -positioned end can be achieved through the migration of unsaturation from aliphatic internal alkynes. In order to use such building blocks for the formation of PE-like polymers or post-polymerization reactions, a substantial amount of material is necessary. Therefore, ideally a viable, short and high-yielding route towards such molecules is essential. In addition, a modular approach should enable the formation of any targeted chain length *via* the conceived strategy. Accordingly, the following chapter describes the design of such a synthesis concept.

3.2 Synthesis of long-chain Hydrocarbons *via* Alkyne Zipper Reaction

3.2.1 General Concept

To fulfill the above-mentioned criteria, a three-step synthesis starting from commercially available, short chain length α,ω -alkynols and *n*-haloalkanes was devised (Scheme 3.1).



Scheme 3.1: General three-step synthesis of long-chain alkynols *via* Alkyne Zipper reaction.

To allow future scale-up of the synthesis route, the commercial alkynol starting units were narrowed down to two substrates: propargyl alcohol and undec-10-yn-1-ol. Propargyl alcohol was chosen due to its general availability and enhanced reactivity that is anticipated at the alkylation step due to the hydroxyl group proximity to the alkyne. Furthermore, purification and isolation of the elongated alkynols is simplified, as the deprotected propargyl alcohol is water soluble and can thus be removed during aqueous purification steps, further facilitating the removal of the unreacted *n*-haloalkanes by column chromatography.

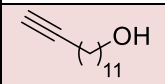
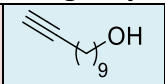
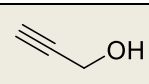
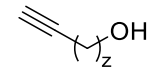
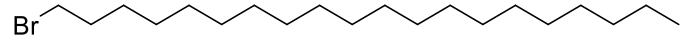
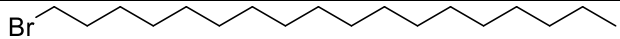
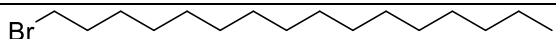
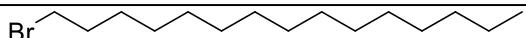
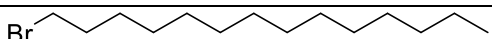
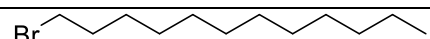
In order to ensure chain lengths above 30 carbon atoms, a suitable synthon of at least ten carbon atoms is essential. However, the commercial availability of long chain bifunctional hydrocarbons is limited, as such molecules are mostly based on a few fatty acid derivatives in milligram quantities. To overcome this substrate deficiency a simple two step synthesis of protected tridec-12-yn-1-ol **5** was devised (*vide infra*).

Considering the *n*-haloalkanes, a plethora of commercial substrates with all desirable chain lengths is available, especially for the bromide derivatives. Although *n*-iodoalkanes are preferred due to increased reactivity in S_N2 reactions, the respective lesser stability tends to limit their commercial availability. In consequence, the project was focused on the utilization of all bromo-derivatives with a chain length above ten carbons and only one *n*-iodoalkane. Notably, such haloalkanes are relatively cheap (*e.g.*, \$54 for 500 g of 1-bromotetradecane, Ambeed^[124]) compared to other substrate classes that are employed for the buildup of long-chain hydrocarbons, such as expansive fatty acids or derivatives thereof (*e.g.*, \$524 for 250 mg of tetradec-13-en-1-ol, Ambeed^[125]), and thus especially suited for upscaling.

To generate any chain length of choice, it is essential to select the suitable commercial haloalkane in accordance with the employed starting alkynol. In fact, a summary of the possible chain lengths that theoretically can be obtained upon the Alkyne Zipper reaction starting from propargyl alcohol, undecyn-1-ol or tridecyn-1-ol is shown in **Table 3.1**. For clarity

the iodoalkanes are emitted, as only one such substrate was used in the context of this work. It is also important to mention that the longest haloalkane that was considered in the context of this project is 1-bromoeicosane, as it is commercially available.

Table 3.1: Overview of the possible chain lengths after the Alkyne Zipper reaction that can be obtained from the combination of propargyl alcohol, undec-10-yn-1-ol or tridecyn-1-ol and *n*-bromoalkanes of increasing chain lengths.

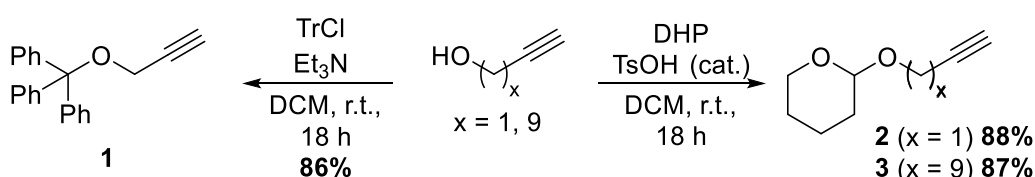
	Starting alkynols		
			
<i>n</i> -Bromoalkanes	Final chain lengths		
			
 1-Bromoeicosane (C ₂₀ H ₄₁ Br)	31	29	21
 1-Bromooctadecane (C ₁₈ H ₃₇ Br)	29	27	19
 1-Bromoheptadecane (C ₁₇ H ₃₅ Br)	28	26	18
 1-Bromohexadecane (C ₁₆ H ₃₃ Br)	27	25	17
 1-Bromopentadecane (C ₁₅ H ₃₁ Br)	26	24	16
 1-Bromotetradecane (C ₁₄ H ₂₉ Br)	25	23	15
 1-Bromododecane (C ₁₂ H ₂₅ Br)	23	21	13
 1-Bromoundecane (C ₁₁ H ₂₃ Br)	22	20	12

As can be seen in **Table 3.1**, the combination of the above mentioned alkynols with the suitable *n*-haloalkane theoretically allows the synthesis of α,ω -functionalized hydrocarbons within the range of eleven to 31 carbons between the functional moieties. Noteworthy, both even and also odd-chain lengths are easily accessible by this route, in contrast to fatty acid derivatives which are mostly limited to even-numbered chain lengths.

3.2.2 Precursor Synthesis and Alkylation

The first step in the reaction sequence consists in the protection of the alcohol group of the starting alkynols. Although the alkylation is also possible without applying protecting groups, the orthogonal protection-deprotection sequence was favored due to generally higher yields and a better reproducibility.^[126]

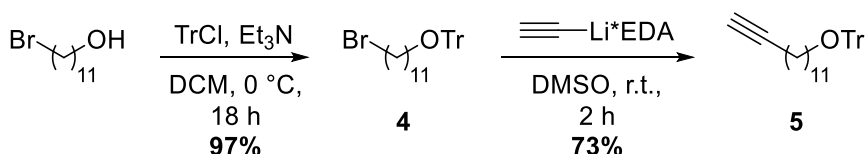
Thus, two α,ω -alkynol substrates – propargyl alcohol or undec-10-yn-1-ol – were reacted first with either trityl chloride or 3,4-dihydropyran (DHP) under basic (Et_3N) and acidic (TsOH) conditions, respectively (Scheme 3.2).



Scheme 3.2: Protection of propargyl alcohol and undec-10-yn-1-ol with trityl chloride (TrCl) and 3,4-dihydropyran (DHP).

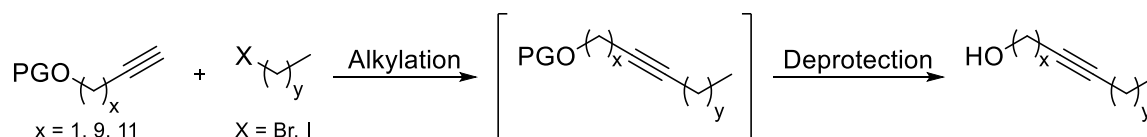
The trityl protecting group was initially chosen due to its stability under basic conditions as well as its high UV-light absorption which facilitated the efficient product purification and isolation *via* the employed automated flash purification system. However, due to its ease of deprotection, the DHP group was preferred at a later stage of the project (*vide infra*).

Besides the two above-mentioned alkynols, a third alkynol substrate was essential to enable the synthesis of chain lengths over 30 carbon atoms. Thus, trityl-protected tridecyn-1-ol was obtained *via* a two-step synthesis (Scheme 3.3). To do so, commercially available 11-bromoundecan-1-ol was first protected with trityl chloride under basic conditions, yielding almost quantitatively compound 4. Then, the trityl ether was alkynylated by lithium acetylide ethylenediamine complex resulting in the desired tridecyn-1-ol derivative 5 in a good 70% yield over both steps. The purity of the obtained products was verified *via* ^1H and ^{13}C NMR spectroscopy.



Scheme 3.3: Two-step synthesis of a trityl-protected tridecyn-1-ol (5) *via* protection with trityl chloride and subsequent alkynylation with lithium acetylide ethylenediamine complex.

The protected alkynes were alkylated with a selection of *n*-haloalkanes (Scheme 3.4). More precisely, *n*-butyl lithium was chosen for deprotonation of the terminal alkynes and DMPU was added as a polar cosolvent to help dissociating the lithium cations from the alkynyl anions and thus increasing the overall reaction reactivity (*vide infra*).^[127]



Scheme 3.4: General reaction scheme for the two-step synthesis of extended alkynols through elongation of the terminal alkynes with *n*-alkane chains.

Following the alkylation, the obtained product mixture was not directly separated, as the difference of polarity of the products after deprotection greatly facilitated the isolation of the desired products. Thus, after usual aqueous workup, the protecting group was removed in a second step by TsOH catalysis in pure methanol or with the use of THF or DCM as cosolvents. At last, the resulting product mixture was again precleaned *via* aqueous workup. In the case of the propargyl ethers, unalkylated propargyl alcohol could be removed due to its water miscibility. Furthermore, at a later stage of the project, DHP was employed as the protective group further facilitating the purification, which is discussed below in more detail.

In this manner a series of different extended alkynols were prepared and characterized by ¹H-, ¹³C NMR, SEC and IR spectroscopy. An overview of the employed starting material combinations is given in Table 3.2.

The critical step of the extended alkynols synthesis lies in the alkylation step, which strongly depend on the starting material and the reaction conditions. In consequence, different reaction conditions based on previous literature reports were evaluated to optimize those parameters and thus increase the alkylation yields.^[128–131] Firstly, *n*-butyl lithium was chosen as the base for the elongation, due to its general availability and suitable basicity ($pK_a \approx 50$)^[119] for the generation of the prerequisite acetylide anion. As longer alkynes and haloalkanes show lesser tendency to react in S_N2 reactions, additives such as tetrabutylammonium iodide (*n*Bu₄NI, Entry 2) or potassium iodide (KI, Entry 1, 3 - 5) catalyzed the displacement of the bromide towards better leaving groups, *e.g.*, iodide. To further increase the reactivity, tetramethylethylenediamine (TMEDA) was added as a deaggregation agent for the lithium-base clusters to guarantee efficient deprotonation.^[132] The obtained yields (ranging from 38 to 93%) indicate that the use of DMPU as a polar cosolvent had the crucial effect on the reaction. Possible outlier values (Entry 4) can be attributed to the varying quality of commercially available *n*BuLi batches.

Table 3.2: Overview of the used starting material combinations, the conditions and yields for the synthesis of the targeted alkylated alkynols **A1** – **A6**.

Entry	Protected Alkynol	Halo-alkane	Alkylation conditions ^{a)}	Deprotection conditions	Product	Yield [%] ^{b)}
1			<i>n</i> BuLi, 10 mol% KI, THF/DMPU, 0 °C → r.t., 18 h	5 mol% TsOH, MeOH/DCM, r.t., 2 h		93%
2			<i>n</i> BuLi, <i>n</i> Bu ₄ NI, THF, -84 °C → 70 °C, 18 h	5 mol% TsOH, MeOH/THF, 70 °C, 2 h		61%
3			<i>n</i> BuLi, TMEDA, 10 mol% KI, THF, 0 °C → r.t., 18 h	1 eq. TsOH, MeOH/THF, r.t., 3 h		38%
4			<i>n</i> BuLi, 10 mol% KI, THF/DMPU, 0 °C → r.t., 18 h	10 mol% TsOH, MeOH/DCM, reflux, 6 h		45%
5			<i>n</i> BuLi, 10 mol% KI, THF/DMPU, 0 °C → r.t., 18 h	5 mol% TsOH, MeOH/DCM, r.t., 2 h		93%
6			<i>n</i> BuLi, THF/DMPU (3:1) v/v), 0 °C → r.t., 18 h	15 mol% TsOH, MeOH/DCM, reflux, 1 h		52%

a) Usually, 1.5 equivalents of haloalkane were employed. b) Yield over two steps.

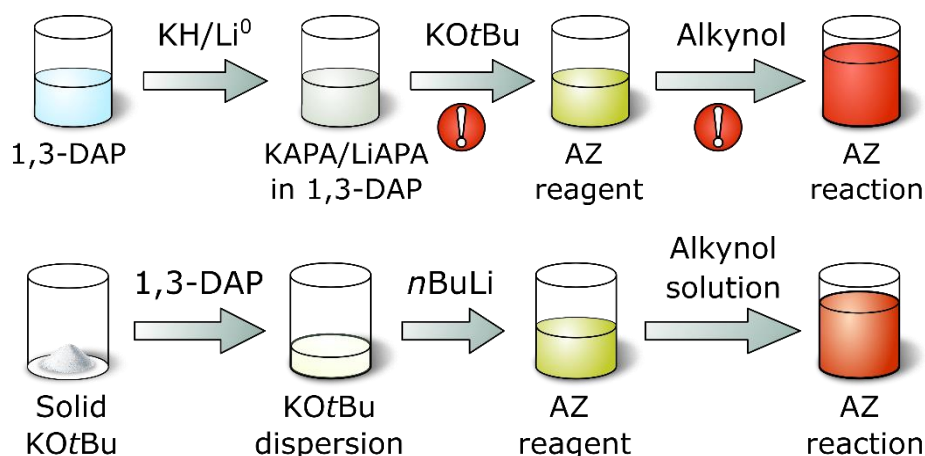
Comparing the two employed protecting groups in this strategy, it has been shown that the UV-active trityl group is more burdensome in its deprotection as it usually needed longer reaction times and higher temperatures (such as 70 °C or reflux) to reach high conversions. In contrast, the DHP group showed faster protection-deprotection kinetics as well as easier work up and side product removal, *e.g.*, water-soluble 5-hydroxypentanal after scission of the protecting group. Due to limited solubility in pure methanol additional solvents such as THF or DCM were needed for the deprotection step. By this way, alkyl-elongated internal alkynols with a total chain length of up to 33 carbon atoms were synthesized in up to 93% yield over a two-step process and in a gram-scale fashion.

Following the successful synthesis of the elongated alkynes, the next section focuses on the Alkyne Zipper reaction towards the formation of their α,ω -functionalized analogs.

3.2.3 α,ω -Alkynol Synthesis *via* Alkyne Zipper Reaction

After successful synthesis of the elongated alkynols, their isomerization into the corresponding α,ω -functionalized derivatives was investigated. As previously mentioned in Chapter 2.1 the Alkyne Zipper reaction requires a very strong base to be effective. In this regard, several different synthesis protocols and reagent combinations were reported for the *in-situ* generation of suitable reactants, with the KAPA reagent (potassium 3-aminopropylamide, KH/1,3-diaminopropane) being the most used historically. Although being very effective, potassium hydride suffers from several safety concerns, including its hazardous nature and pyrophoric propensity in air which makes it difficult to handle.^[132,133] As a result, an alternative reagent based on the combination of *n*-butyl lithium, potassium *tert*-butoxide (KOtBu) and 1,3-diaminopropane (DAP) was chosen for the alkyne isomerization within this project.

Conventional literature protocols for the lithium 3-aminopropylamide-based Alkyne Zipper reaction comprise of the preparation of the isomerization agent by reacting lithium metal with DAP at elevated temperatures (such as 70 °C) and prolonged time, *e.g.*, overnight.^[131,134] The resulting mixture of DAP and the lithium salt thus form a white dispersion. The mixture is subsequently treated with solid KOtBu, which only slowly dissolves into the reaction mixture and gives it a slightly yellow coloration. However, most reactions described in the literature involved substrates with hydrocarbon chains smaller than 12 carbon atoms, which are liquids. As a result, such substrates could be added as is to the prepared mixture, resulting in the formation of a brick-red dispersion indicating the effective alkyne-allene interconversion. A graphical abstract of such general reaction protocols is depicted in Scheme 3.5, *top*).



Scheme 3.5: Graphical depiction of the standard literature protocol for the Alkyne Zipper reaction (*top*) and adjusted method (*bottom*) for the isomerization of long-chain alkynols. Problematic steps (low solubility of KOtBu & long-chain alkynols) are denoted with an exclamation point.

Although the standard reaction protocol is suitable for the isomerization of short-chain alkynols, it is inadequate for the transformation of longer alkynols. Here the main problem arises from the lowered solubility of the solid long-chain alkynols in 1,3-diaminopropane, as well as of the corresponding alkoxides in DAP after deprotonation, as observed by BROWN.^[24] Furthermore, it has been found impractical to add the solid substrates to the reaction, as they tend to form an insoluble blanket atop the reaction mixture and thus impeding the actual transformation and harshly lowering the overall yield of the desired product.

To overcome these challenges, a novel reaction protocol for the Alkyne Zipper had to be devised. Starting at the actual *in situ* generation of the isomerization reagent, the necessary reaction conditions were first optimized. Here, the low solubility of KO^tBu was obviated through an inverse order of addition of the reagents: first, a dispersion of the base in DAP was prepared with vigorous stirring, slight heating at 50 °C and ultrasonication. After successful formation of the dispersion the ambient atmosphere was switched to argon and subsequently *n*-butyl lithium was added (as a hexane solution) under cooling with ice. The formed yellow solution indicated that the actual generation of lithium 3-aminopropylamide/KO^tBu reagent was successful. Although mechanistically the reaction should only require catalytic amounts of the isomerization reagent, an excess is usually employed in literature protocols.^[27,135,136] Thus, for the optimized protocol five equivalents of KO^tBu and *n*BuLi were used. In order to cope with the very low solubility of the long-chain hydrocarbons in DAP, the starting materials were dispersed in a small volume of the diamine, then slightly heated and placed in an ultrasonic bath for ten minutes. If solid material persisted the volume of DAP was continuously increased while the steps were repeated until a clear concentrated solution was obtained. Consequently, the warm solution was added to the reaction yielding an orange reaction mixture that was usually stirred overnight to ensure an adequate product formation. This protocol allowed for a faster and more facile reaction setup, as well as homogenous reaction mixture and thus higher yields. A graphical depiction of the optimized protocol is depicted in Scheme 3.5, *bottom*.

Upon the isomerization, a suitable purification method needed to be established, as the separation of starting materials and isomerized products was found to not be trivial due to their chemo-physical and structural similarities. In particular, the difficulty of purification was found to be proportional to the chain lengths of the internal and terminal alkynols. This is due to two factors: first, the separation via column chromatography becomes more difficult as the difference in polarity of the internal and terminal alkynes diminishes with increasing chain length and thus the separation on silica usually necessitates less polar solvent mixtures. And second, the general solubility of longer chain alkynols heavily decreases, especially with chain lengths over 20 carbons. To solubilize these molecules larger solvent volumes of chlorinated solvents such as DCM or chloroform are necessary, which further hampers purification, as the separation on silica gel is lessened. Therefore, to efficiently isolate the desired products the use of automated flash column chromatography has shown itself to be an effective

purification method. Here, after regular aqueous work up, the crude reaction mixture was deposited on Celite® 545, transferred to a dryload cartridge and separated with chloroform or DCM as the mobile phase over the course of up to 15 column volumes. In this manner, it was possible to isolate the desired α,ω -functionalized alkynols with chain-lengths up to 25 carbons in good to excellent yields. A detailed summary is given in Table 3.3.

Table 3.3: Summarized results of the Alkyne Zipper isomerization reactions of previously prepared internal alkynols **A1** – **A6**.

Entry	Internal Alkynol	Conditions	Product	Yield [%]
1		<i>n</i> BuLi/KOtBu DAP, r.t., 18 h		76 ^{b)}
2		<i>n</i> BuLi/KOtBu DAP, 50 °C, 18 h		68 ^{a)} 94 ^{b)}
3		<i>n</i> BuLi/KOtBu DAP, r.t., 18 h		76 ^{b)}
4		<i>n</i> BuLi/KOtBu DAP, 80 °C, 18 h		64 ^{a)}
5		<i>n</i> BuLi/KOtBu DAP, r.t., 20 h		70 ^{b)}
6		<i>n</i> BuLi/KOtBu DAP, r.t., 3 h		-
7		Li ⁰ /KOtBu DAP, r.t., 36 h		
8		<i>n</i> BuLi/KOtBu DAP, 0 ° → 70 °C, 18 h		

a) Literature protocol. b) Optimized protocol.

The successful transformation as well as the purity of the obtained products was verified by SEC, as well as NMR and IR spectroscopy. Exemplarily the obtained proton spectra of the alkyl ether **1**, alkylated alkynol **A1** and α,ω -alkynol **AZ1** are shown in Figure 3.1 for comparison. Here, the alkylation of the starting ether compound is clearly evidenced by the disappearance of the terminal alkyne proton triplet marked in orange (2.41 ppm/H₃) and the newly emerged alkyl chain resonances (2.21 ppm/H₂, 1.56 – 1.44 ppm/H₃ and 1.42 – 1.15 ppm/H₄), with the terminal methyl triplet marked in green (0.87 ppm/H₅). The successful alkyne isomerization is further revealed by the newly appeared alkyne triplet marked in red at 1.9 ppm. Further evidence is provided by IR spectroscopy. Here the terminal alkyne gives rise to the absorption band located at 3330 – 3260 cm⁻¹ which correspond to the stretching of the terminal C-H bond (Figure 3.1, right, grey box).

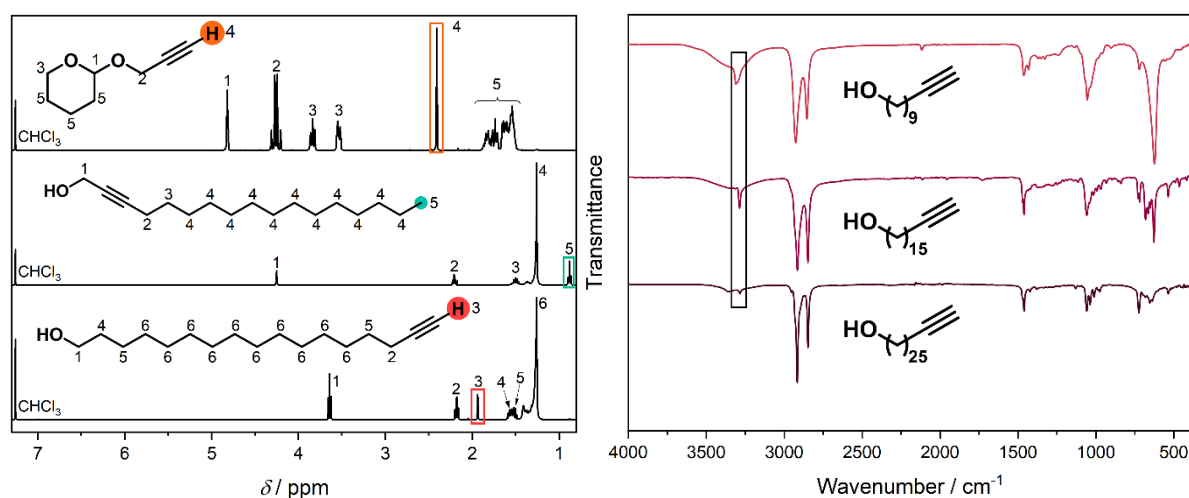


Figure 3.1: Left: Comparative ¹H NMR spectra (400 MHz, CDCl₃) of alkyl ether **1** (top), internal alkynol **A1** (middle) and α,ω -alkynol **AZ1** (bottom). Associated resonances arising from the terminal groups are colored. Right: Stacked IR spectra of undec-10-yn-1-ol (top), alkynol **AZ1** (middle) and alkynol **AZ5** (bottom). The alkyne C-H stretching band of all compounds is marked (grey box).

What can be deduced from the obtained yields given in Table 3.3 is that longer alkynols generally yield less product compared to shorter chains. This is easily rationalized from a mechanistic point of view as the reaction is actually a set of repeated transformations happening in succession. As shown in Chapter 2.1 the Alkyne Zipper reaction is the sum of several allene-alkyne isomerization steps happening successively until the chain terminus is reached and the alkyne moiety is fixated *via* the formation of a stable terminal acetylide. However, this process is for the most part statistically driven. In the case of short-chain substrates the deprotonated alcohol, *i.e.*, the alkoxide, is driving the isomerization towards the chain end by means of repulsion of the negative charges. In long-chain alkynols this effect is mostly negligible as the distance between the alkoxide and the active reaction site are largely separated by an extended number of carbon-carbon bonds and thus, the alkyne moieties tend to “move” along the chain in both directions. As this process cannot be driven towards the terminal alkyne formation, this results in a natural barrier for the overall isomerization of longer hydrocarbon chains towards terminal acetylides past a certain threshold (see Table 3.3, Entry 6 – 8).

In the case of the longest internal alkynol **A6** the reaction did not yield the desired α,ω -alkynol **AZ6** with the standard conditions/protocol (Table 3.3, Entry 6). To rule out a possibly degraded batch of *n*-butyl lithium, the reaction was repeated with elemental lithium metal for the generation the isomerization reagent and the reaction was carried out for 36 hours to ensure an adequate time for the product formation (Table 3.3, Entry 7). Unfortunately, ¹H NMR spectroscopy showed that upon workup, both crude reaction mixtures showed identical

chemical shifts, with the desired alkyne triplet at 1.9 ppm missing. Subsequently, another approach with the optimized reaction protocol was conducted and the reaction temperature raised to 70 °C for 18 hours (Table 3.3, Entry 8). This time, although the alkyne resonance was detectable *via* ^1H NMR, the overall product content in the obtained crude material was calculated to be around 5%. However, in contrast to the two previous approaches the resonance for protons adjacent to the internal alkyne moiety (2.13 ppm, Figure 3.2 *left*; marked in beige) was shifted and distorted (2.18 ppm, Figure 3.2 *left*; dark grey line). This hints a possible side reaction that damaged the alkyne bond. The resulting product could not be deduced from the spectra obtained (NMR & ATR-IR), yet an addition of the diamine or the reduction towards an alkene seems unlikely based on the proton spectrum. A reduction of the triple bond, however seems most probable. Interestingly, the recorded SEC trace of the obtained material (Figure 3.2 *right*) shows a shift of the main peak towards slightly higher molecular mass (A) and one additional peak at a molecular mass of 2.20 kg·mol⁻¹ (B). The shift of the SEC trace of **A6** corresponds to a mass change of about 80 g·mol⁻¹, which could be attributed to the molecular mass of 1,3-diaminopropane (74.1 g·mol⁻¹). However, this measurement lies within the measurement accuracy of the SEC and requires further analysis for validation. The appearance of the second peak B, indicates a possible linking of two (or more) of the original alkynol chains. And although alkyne dimerization reaction catalyzed by (non-noble) metal complexes under basic conditions were published, the reported products of these reactions do not agree with the obtained NMR results.^[137–139]

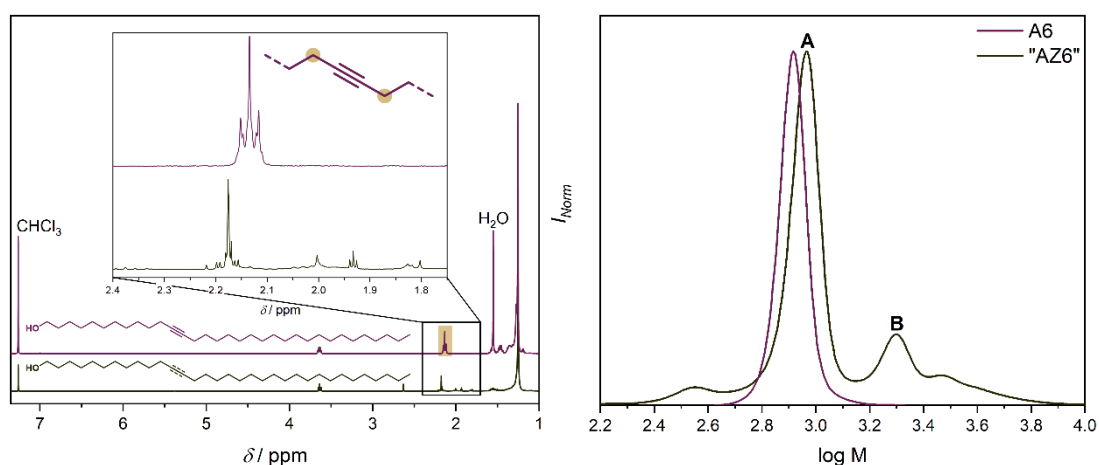


Figure 3.2: Comparative ^1H NMR (400 MHz, CDCl_3) (*left*) and SEC Traces (*right*) of alkynol **A6** (purple) and the reaction product after the isomerization attempt (dark grey) (refer to **Table 3.3**, Entry 8).

Finally, the obtained α,ω -alkynols were analyzed *via* size exclusion chromatography (SEC) and differential scanning calorimetry (DSC). As can be seen from the obtained SEC curves in Figure 3.3 the increasing chain length is directly correlated to the increasing chain size. Interestingly, already the increase of two carbon atoms in the chain is evidenced by an increase of its hydrodynamic volume.

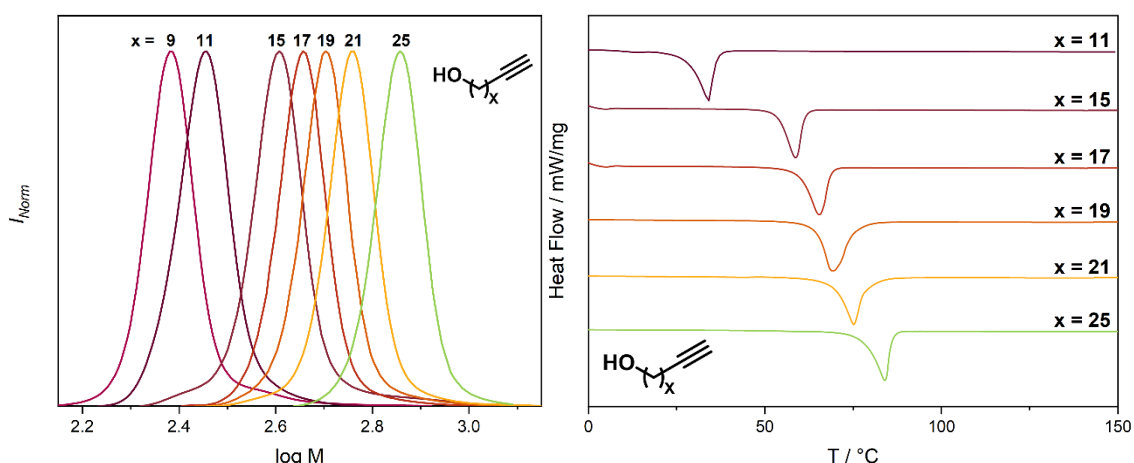


Figure 3.3: SEC curves of the synthesized α,ω -alkynols **A1** – **A5** displaying the increasing hydrocarbon chain length.

The same trend is verified by the thermal analysis of the long-chain hydrocarbons. As expected, the increasing chain length is also expressed by the rising melting temperature of the molecules from 58.7 °C (**AZ1**) to 84.0 °C (**AZ5**).

The obtained values enable the correlation of the chain length with the melting point and thereby allow the theoretical prediction of the thermal properties of even longer alkynols. However, such an interpretation is only limited towards a small range of longer chain lengths, as the melting point curve of polyethylene-like compounds should approach a plateau and flatten towards the reported melting point of high density-polyethylene at around 130 °C.^[140] The correlation of the collected data is depicted in Figure 3.4.

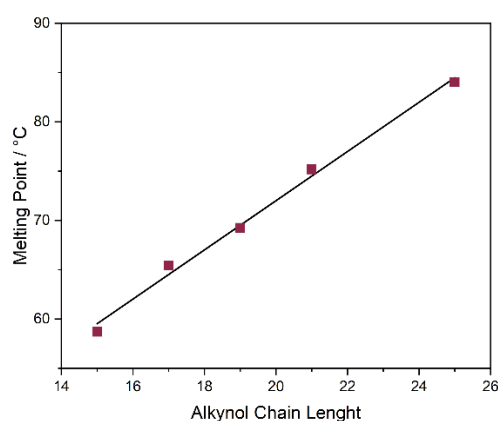
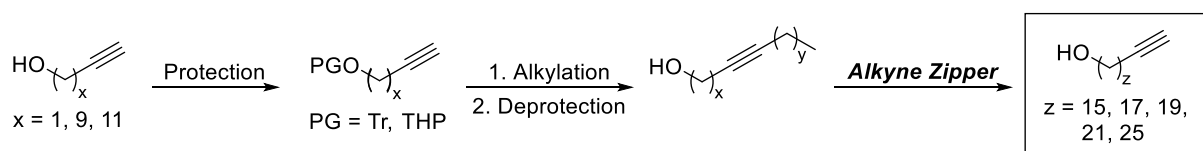


Figure 3.4: Linear fit correlation of the melting points and chain lengths of the synthesized α,ω -alkynols **A1** – **A5**.

Based on the obtained linear fit towards the peak temperatures of the obtained DSC curves, the not-obtained alkynol **AZ6** of 31-carbons length is expected to have a melting temperature around 100 °C.

3.3 Conclusion

In summary, a synthesis route towards long-chain hydrocarbons was devised and realized through the use of the Alkyne Zipper reaction (Scheme 3.6). Here, short alkynols were protected in an orthogonal manner and elongated *via* a S_N2 reaction with haloalkanes. The thus obtained hydrocarbons bear an internal alkyne moiety that was subsequently shifted to the ω -terminus of the chains. The efficiency of the Alkyne Zipper reaction was particularly increased by the optimization of the reaction protocol, where an inverse order of addition of the reagents as well as longer reaction times (up to 20 h) facilitated the isomerization of chain lengths comprising more than 20 carbon atoms. The successful conversion was verified by NMR and IR spectroscopy, as well as SEC and DSC analyses. In this way a series of five α,ω -alkynols was synthesized in gram-scale fashion.



Scheme 3.6: Schematic summary of the synthesis approach towards alkylated alkynols **A1 – A6** and subsequent formation of the α,ω -functionalized hydrocarbons **AZ1 – AZ5** *via* Alkyne Zipper reaction.

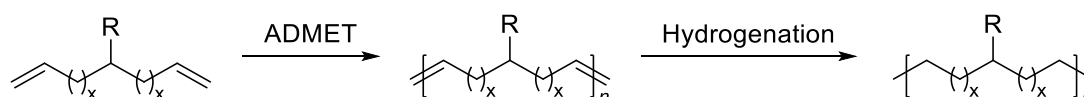
The long-chain hydrocarbons illustrated in this chapter have been further employed for the post-polymerization modification of poly(pentafluorophenol acrylate) (see Chapter 5). Furthermore, the α,ω -alkynols can be converted to the respective dialkynes for the precise poly(ethylene) *via* SONOGASHIRA reaction (refer to Chapter 4) as well as for the synthesis of fluorinated polymers *via* the *para*-fluoro thiol reaction of novel pentafluorophenyl vinyl sulfide derivatives (see Chapter 6).

4 Precise Polyethylene *via* SONOGASHIRA Polycondensation

4.1 Motivation

Precise poly(ethylene) polymers are a subclass of polyethylene polymers that are synthesized in a non-classical way, *e.g.*, without the use of ethylene gas or alkene comonomers and classical Ziegler-Natta catalysts.^[2] As the most prominent contributor to the field, WAGENER showed that polyethylenes with precisely placed functional groups along the polymer backbone can be synthesized *via* acyclic diene metathesis (ADMET) polymerization of symmetrical long chain dialkenes (Scheme 4.1).^[2,141] Here the imparted symmetry of the monomer is transferred to the polymer yielding a fixed distance between the functional groups upon a hydrogenation. In this way, a plethora of functional groups, such as alkyl groups, esters, sulfones, halides and even amino acids have been incorporated in such polymers.^[2]

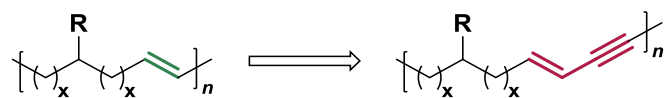
Most notably, such polymers bearing alkyl side chains have been used to study the impact of side chain branching in the conventional poly(ethylene) synthesis, as the additional branching off of the main branches has different effects (such as the crystallization behavior for instance) on the PE properties.^[76,142,143]



Scheme 4.1: General reaction scheme for the synthesis of precise poly(ethylene)s *via* ADMET polymerization.

Furthermore, through the controlled placement of the functional group along the chain as well as control over the chemical character of the introduced moiety, physical properties, such as the melting point can be tailored. The latter has been exploited impressively by WEGENER in a report with the placement of a butyl group on every 75th carbon atom along the polymer chain.^[142] Although this outstanding example shows the possibility of sequence control, the synthesis of such symmetrical long-chain monomers is extremely tiresome and usually requires a long multistep syntheses, as shown Chapter 3.1. At the core of such syntheses is the buildup of essential α,ω -functionalized hydrocarbon synthons. As shown in the previous section, such long-chain building blocks can also be synthesized *via* the Alkyne Zipper reaction, which carry a terminal alkyne moiety, accordingly. Through retrosynthetic considerations one

can conclude that the alkene group of the unsaturated ADMET polymers can be replaced with other unsaturated motifs, such as an enyne moiety for example (Scheme 4.2).



Scheme 4.2: Depiction of the conceived replacement of the alkene group in an ADMET polymer with an enyne motif.

Since the focus of this thesis lays on the utilization of alkynes in the context of polymer science, and such motifs can be generated through a combination of vinyl halides and terminal alkynes *via* the SONOGASHIRA reaction, it was of great interest to investigate the possibility of the build-up of such polymers. Accordingly, a detailed description of the general concept is given below.

4.2 General Concept for the Synthesis of unsaturated PE Precursors

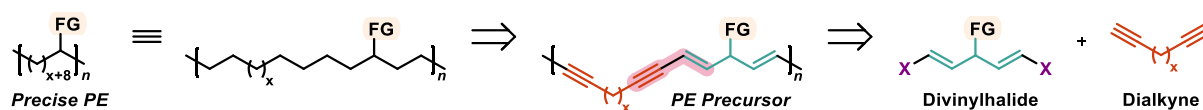
The ADMET polymerization methodology is in-depth elaborated, and, indeed, it was efficiently used for the synthesis of numerous polymers due to its efficiency.^[2,141] However, this it is not without flaws as shown in Table 4.1. Comparing the ADMET polymerization with the established SONOGASHIRA polycoupling methodology, several differences become apparent. For once, the SONOGASHIRA reaction shows a greater chemoselectivity, as unsaturated moieties are generally well tolerated, and no isomerization reactions (such as the Ru-catalyzed hydride isomerization) take place. Furthermore, even functional protic groups, such as alcohols are tolerated, and no protection is required, in contrast to ADMET polymerization. The possible side reaction in the form of Glaser coupling can be problematic but can be eliminated using oxygen-free methods or copper-free protocols.^[32,38,44] Most importantly the SONOGASHIRA reaction does not require low-pressure conditions in order to remove condensates and thus drive the polymerization.

Table 4.1 Comparison between the SONOGASHIRA polycoupling and ADMET polymerization.

Criteria	SONOGASHIRA polycondensation	Acyclic diene metathesis (ADMET)
In-chain unsaturation	✓	✗
Atm. pressure	✓	✗
No isomerization	✓	✗
Functional group tolerance	✓	✗
Side reactions	Glaser coupling	✗

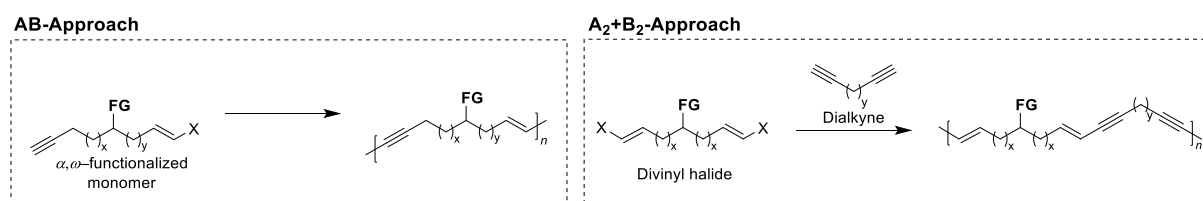
The benefits shown in Table 4.1 make the SONOGASHIRA reaction an attractive alternative for the build-up of unsaturated polymeric carbon materials. Since the present thesis is focused on the use of alkynes for the synthesis of such, a general concept for the synthesis of precise poly(ethylene)s based on the SONOGASHIRA reaction shall be introduced at this point. A retrosynthetic approach was followed for its design as shown in Scheme 4.3. As the hydrocarbon chains in precise PE can be viewed as combinations of unsaturated motifs prior the hydrogenation process, such as alkenes or alkynes for example. Thus, combinations of these motifs were retrosynthetically introduced in the carbon chain. Since the SONOGASHIRA

reaction allows the linking of alkynes and vinyl halides to enynes (*light red*), suitable precursors for this motif were found in divinyl halides and dialkynes, respectively.

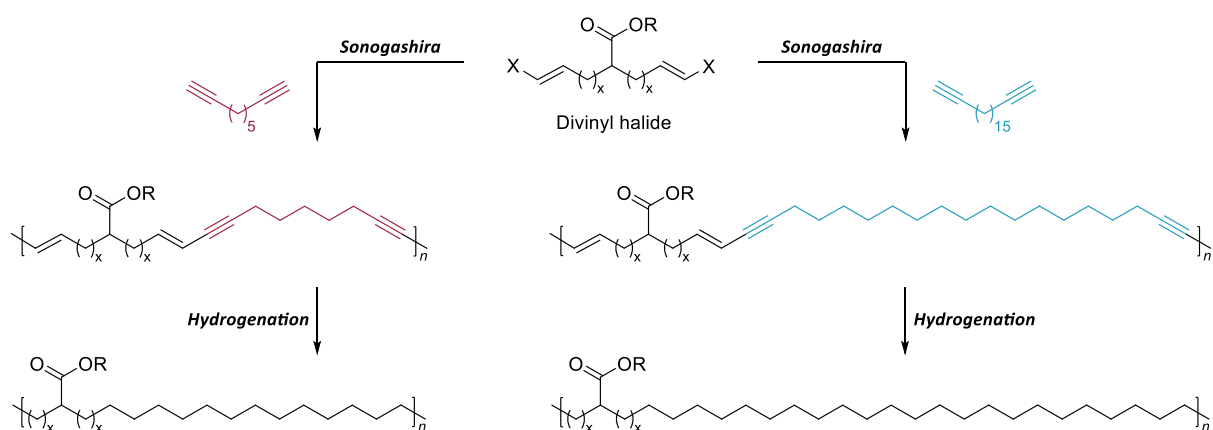


Scheme 4.3: Depiction of the retrosynthetic approach towards Precise PE based on SONOGASHIRA compatible motifs, *i.e.*, vinyl halides and alkynes (FG = functional group).

With the desired enyne-motif in mind, two approaches for the synthesis of the PE precursor polymers were devised (Scheme 4.4). Here, the AB-approach is based on the polymerization of an α,ω -functionalized monomer, *i.e.*, a monomer that carries both, the alkyne and a vinyl halide, as its terminal groups. Although AB-monomers are preferred in the context of step-growth polymerization due to the intrinsic stoichiometric balance of both reaction sites, the synthetic effort to synthesize such is grand. The A_2+B_2 -approach, however, requires the combination of a central divinyl building block and dialkynes to form the targeted enyne-linkages. Here, only the divinyl halide needs to be accordingly synthesized, as dialkynes of different chain lengths are commercially available. Accordingly, through the use of dialkynes of different chain lengths, the distance between the functional groups of the divinyl unit can be precisely set, as shown in Scheme 4.5. Here, the influence of the chain-length is exemplary demonstrated through the combination of the divinyl unit with 1,8-nonadiyne and nonadeca-1,18-diyne, respectively. Due to this modular approach the synthetic effort is less demanding compared to the ADMET-based syntheses of precise PE, especially if the functional group placement cannot be achieved with commercial substrates.^[2,10] Thus, only the A_2+B_2 -approach was investigated in the context of this thesis.

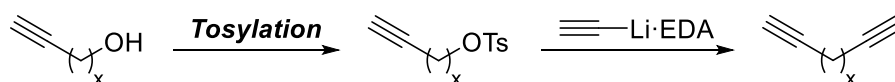


Scheme 4.4: Depiction of the AB- (*left*) and A_2+B_2 -approach (*right*) towards unsaturated PE precursor polymers based on the combination of alkynes and vinyl halides.



Scheme 4.5 Depiction of the general concept, which allows to control the functional group distance in precise PE using dialkynes with different chain lengths (*ester group added for the purpose of illustration*).

Finally, as demonstrated in the previous section, long-chain α,ω -functionalized hydrocarbons can be synthesized *via* the Alkyne Zipper reaction. Since any chain length up to 30 carbon atoms can be achieved, this methodology can be further leveraged for the conceptualized precise PE synthesis presented in this section. To this end, the α,ω -functionalized alkynols can be transformed to the respective dialkynes by a two-step process depicted in Scheme 4.6.



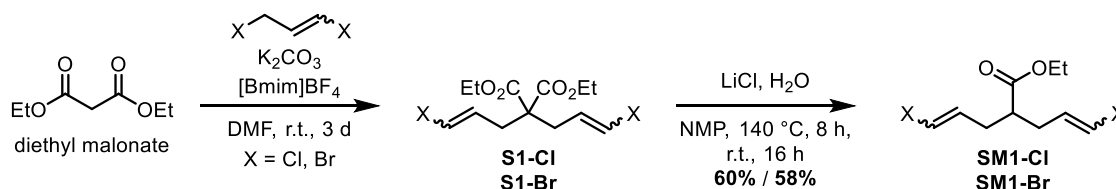
Scheme 4.6: Reaction scheme for the conversion of alkynols to dialkynes *via* tosylation and subsequent reaction with lithium acetylide ethylenediamine complex (x = varying number of methylenegroups, refer to Chapter 3).

4.3 Synthesis of modular Monomers and their Polymerization

4.3.1 Ester System

As mentioned in the previous section, the devised strategy employs a divinyl halide and a dialkyne as the monomers. As some dialkyne derivatives are commercially available, initially the focus of this chapter lay on the synthesis of the divinyl monomer unit (as shown in Scheme X). Although the coupling of chloride substrates is less explored in SONOGASHIRA reactions compared to bromides,^[36] the considerably lower price of the former justifies investigations of this reactant class, which would allow the essential scale-up. In the context of this project, the price difference is particularly noticeable for the employed chlorine- (e.g., €95.10 for 250 mL of 1,3-dichloropropene, *Sigma-Aldrich*)^[144] and bromine-bearing (e.g., €459.00 for 25 g of 1,3-dibromopropene, *Sigma-Aldrich*)^[145] monomer building blocks. For this reason, divinyl chlorine and divinyl bromine monomers should be investigated.

Here, in similar fashion to the ADMET-monomer syntheses,^[2] the initial route was based on the two-fold alkylation of diethyl malonate and subsequent KRAPCHO decarbalkoxylation^[146] as shown in Scheme 4.7.



Scheme 4.7: Reaction scheme for the two-step synthesis of divinyl monomers

The double alkylation of the employed malonate was carried out with the respective 1,3-dihalopropene in DMF in the presence of K₂CO₃ as the inorganic base in addition to 1-butyl-3-methylimidazolium hexafluorophosphate ([bmim][PF₆]) as the cosolvent and phase transfer catalyst.^[147] The obtained diester derivatives **S1-Cl** and **S1-Br** were subsequently decarbalkoxylated in NMP at 140 °C with LiCl to yield, upon an efficient column chromatography, the respective mono-ester divinyl halides **SM1-Cl** and **SM1-Br** in good yields of 58 and 60%, respectively. Exemplarily, the proton spectra of the corresponding bromo-derivatives are shown in Figure 4.1. Notably, the second step of the synthesis is verified through the appearance of the broad multiplet (3), caused by the coupling of the introduced tertiary proton towards the adjacent methylene protons. Furthermore, both products were obtained as mixtures of *E*-/*Z*-isomers, since the employed 1,3-dihalopropene starting

materials were both isomeric mixtures. In the specific case of the shown monomer the starting material ratio of *E:Z* = 40/60 was incorporated in **SM1-Cl** and thus in **SM1-Br** without change.

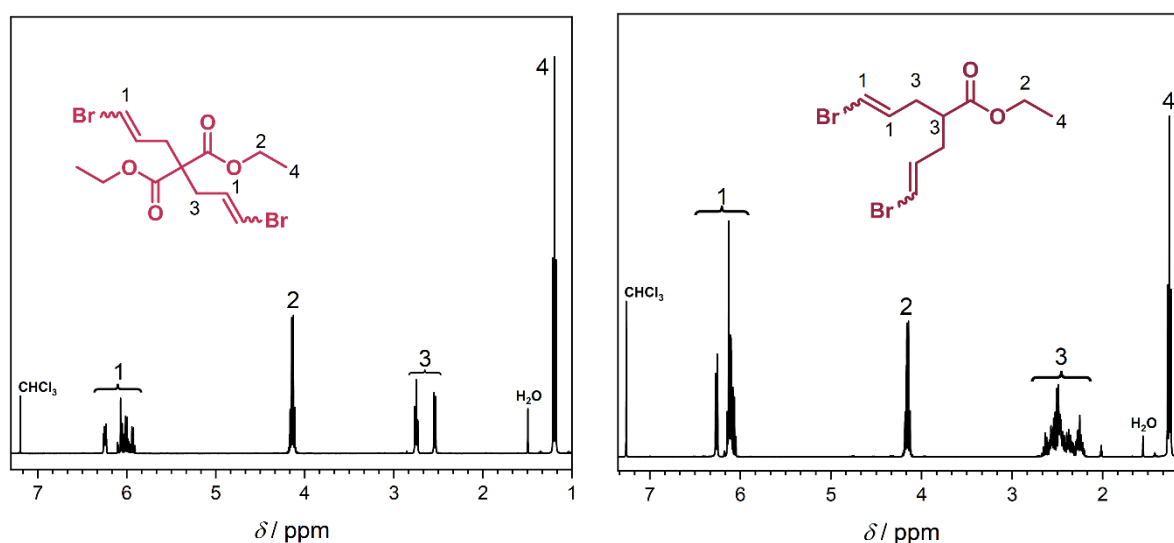
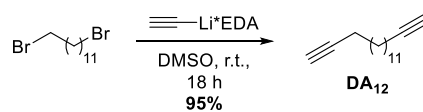


Figure 4.1: ¹H NMR (CDCl_3 , 400 MHz) spectra of **S1-Br** (left) and **SM1-Br** (right) evidencing the successful alkylation and decarbalkoxylation.

Since nona-1,8-diyne (from here on denoted as **DA₅**, with the subscript number abbreviating the number of methylene groups of the respective dialkyne) is the longest diyne, longer chain lengths were desired to compare the influence on the polymer properties. Furthermore, a solid dialkyne would facilitate the stoichiometric weigh-ins required for optimal step-growth processes. Thus, 1,12-dibromododecan was reacted with lithium acetylide to form hexadeca-1,15-diyne (**DA₁₂**) in an excellent yield of 95% (Scheme 4.8).

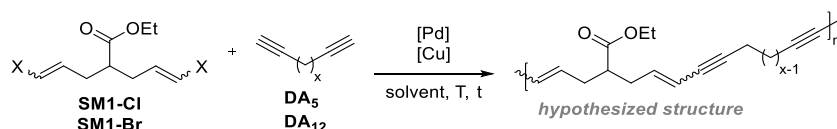


Scheme 4.8: Reaction scheme for the synthesis of hexadeca-1,15-diyne (**DA₁₅**).

With both essential components, functionalized divinyl halides and dialkynes of different lengths, in hand, the SONOGASHIRA polycoupling was investigated.

In order to obtain polymers from the synthesized building blocks, suitable reaction conditions are essential. Even more so, as high molecular weight polymers can only be reached with adequate reaction kinetics. Therefore, efficient reaction parameters were sought for the planned polymerizations. Since the SONOGASHIRA reaction allows for the tuning of multiple variables, such as solvent, concentration, employed base, temperature, additives, copper or non-copper variants and finally the catalyst source itself, it was difficult to determine an ideal

selection for the present case.^[36,148] In addition, literature protocols mostly concern coupling reactions of more reactive aryl substrates and neglect on aliphatic substrates, which is especially true for purely aliphatic coupling partners.^[36,148,149] However, LINSTRUMELLE and ALAMI published some selected works on very similar vinyl halide couplings^[150–153] and thus, the employed conditions were adapted from these reports. Concerning the employed Palladium catalysts, two species stood out in literature research: Tetrakis(triphenylphosphine)palladium(0) (**Pd(PPh₂)₄**) as a “universal” catalyst for the coupling of a broad spectrum of substrates and Bis(benzonitrile)palladium dichloride (**PdCl₂(PhCN)₂**), which is especially suited for coupling reactions of chlorine substrates due to facilitated oxidative addition through the weakly coordinating benzonitrile ligands.^[151] Thus, the monomers **SM1-Cl** and **SM1-Br** were reacted with **DA₅** and **DA₁₂** under varying conditions with **Pd(PPh₂)₄** and **PdCl₂(PhCN)₂** as catalysts (Scheme 4.9). The summarized results are given in Table 4.2.



Scheme 4.9: General reaction scheme for the SONOGASHIRA polycoupling of **SM1-Cl** and **SM1-Br**.

Table 4.2: Summarized results of the SONOGASHIRA polycoupling of **SM1-Cl** & **SM1-Br** with **DA₅** & **DA₁₂**.

Entry	Catalyst	Cocatalyst	Monomer	Alkyne	Solvent ^{a)}	T	t	Result
1	PdCl ₂ (PhCN) ₂	CuI	SM1-Br	DA ₁₂	Pyr	r.t.	24 h	No polymer
2	Pd(PPh ₂) ₄	CuI	SM1-Br	DA ₁₂	Pyr	50 °C	2 d	Insoluble material ^{b)}
3	PdCl ₂ (PhCN) ₂	CuI	SM1-Cl	DA ₁₂	Pyr	r.t.	24 h	Insoluble material ^{b)}
4	PdCl ₂ (PhCN) ₂	-	SM1-Cl	DA ₅	Pyr/DMF	70 °C	24 h	No polymer
5	Pd(PPh ₂) ₄	-	SM1-Cl	DA ₅	Pyr/DMF	70 °C	24 h	No polymer
6	PdCl ₂ (PhCN) ₂	CuI	SM1-Cl	DA ₁₂	Pyr/DMF	70 °C	18 h	Crosslinking ^{c)}
7	PdCl ₂ (PhCN) ₂	-	SM1-Cl	DA ₁₂	Pyr	70 °C	5 d	No solids/no polymer
8	Pd(PPh ₂) ₄	-	SM1-Cl	DA ₁₂	Pyr	70 °C (→ 100 °C) ^{d)}	5 d (→ 9 d) ^{d)}	5 d: No polymer 9 d: No polymer
9	PdCl ₂ (PhCN) ₂	-	SM1-Cl	DA ₁₂	Pyr	100 °C	24 h	Crosslinking
10	PdCl ₂ (PhCN) ₂	CuI	SM1-Cl	DA ₁₂	Pyr/ <i>o</i> -DCB	70 °C	15 h	Crosslinking
11	PdCl ₂ (PhCN) ₂	CuI	SM1-Cl	DA ₁₂	Pyr/ <i>o</i> -DCB	70 °C	6 h	Crosslinking during drying
12	PdCl ₂ (PhCN) ₂	CuI	SM1-Cl	DA ₁₂	Pyr	70 °C	24 h	MeHQ ^{e)} additive - Crosslinked in air during workup

^{a)} Pyr = Pyrrolidine; *o*-DCB = *ortho*-Dichlorobenzene. M = 0.15 mol·L⁻¹. ^{b)} After precipitation. ^{c)} Network formation during reaction. ^{d)} Increased T after 5 d. ^{e)} MeHQ = 4-methoxyphenol.

The polymerization reactions were conducted under the shown conditions and, if possible, an aliquot of the reaction mixture was subjected to SEC analyses after solvent removal or filtration over neutral alumina. Unfortunately, the desired polymers could not be isolated accordingly as they showed an intrinsic instability. Notably, some of the polymerization reactions led to crosslinked material that completely absorbed the solvent and thus yielded a solid mass in the reaction vessel (Entry 6, 9, 10). Furthermore, precipitation of the crude reaction mixture led to the isolation of material that was insoluble in most common solvents as well as chlorinated hydrocarbons, such as chlorobenzene, even under ultrasonication conditions (Entry 2 & 3). In one case the crosslinking occurred during drying of the crude aliquot *via* pressurized air (Entry 11). Since the crosslinking occurred at lower temperatures, i.e., r.t. or 70 °C, only in the presence of a copper source, copper-free approaches were conducted (Entry 4 & 5, 7 – 9). However, SEC analyses of the attempts showed no formation of higher molecular mass polymers. An increase in temperature however, again led to network formation (Entry 9). Interestingly, no crosslinking was observed (compare Entry 6 & 12) if a radical scavenger, i.e., 4-methoxyphenol (MeHQ) was added to the reaction mixture. During exposure to air however, the crude material inevitably crosslinked. Photographs of selected examples of the crosslinked materials are shown in Figure 4.2.



Figure 4.2: Photographs of selected crosslinked specimen from the reactions summarized in **Table 4.2**. *Top left:* Fully crosslinked material which took the shape of the reaction vessel. *Top right & bottom left:* Ring and circle shaped networks obtained during drying in vials. *Bottom right:* Rectangle cut from the circle (*bottom left*), evidencing the self-supporting nature of the crosslinked material.

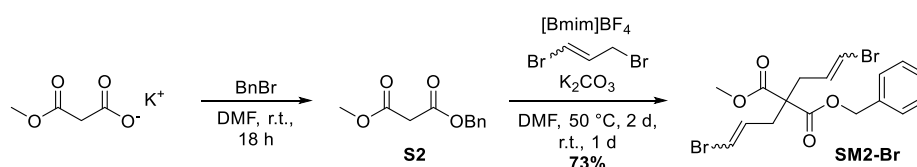
Interestingly, the reactions mixtures that crosslinked during reaction of in air, took the shape of their surrounding environments, i.e., the reaction vessel or vial. The formed materials were self-supportive and could be bend and cut. After prolonged time (weeks) the networks become increasingly brittle and broke down, if a force was applied. IR spectroscopic analyses of the crosslinked materials did not allow for conclusions about the crosslinking mechanism.

Most likely, the accumulation of unsaturated motifs led to side reactions that possibly involve the formed enyne moiety. Reports of structurally related, unsaturated substrates that underwent enyne cyclization reactions under transition metal catalysis are known to literature.^[154,155]

One of the key points in determining the success of the employed strategy is the evaluation of the degree of GLASER coupling linkages, i.e., 1,3-diyne moieties arising as a side reaction. Through the formation of such a unit, the precise placement of the functional group is disturbed and thus a “defect” in the chain occurs. To evaluate the occurrence of said defects the obtaining of pure and stable material is absolutely essential. Since the 1,3-diyne moieties do not differ in their proton resonances compared to the remaining part of the polymer structures, the linked alkynes can only be observed *via* ¹³C NMR spectroscopy measurements.^[156] To conduct these, however, the potential cross-linking side reaction must be prevented. Due to the instability of the materials, a structurally different monomer was devised, as described in the following section.

4.3.1 Diester System

Due to the unsuccessful utilization of the previously shown ester monomers owing to the inherent instability of the obtained materials, a change either in conditions or chemical motifs became apparent. Hereto, an alternative synthesis strategy was envisioned: due to the unsuccessful use of the divinyl chlorine motifs the central building block structure, only divinyl bromides were used for further reactions. Furthermore, to impart more stability in the obtained polymeric systems, the second step of the central block synthesis, *i.e.*, the KRAPCHO decarbalkoxylation, was to be conducted after the parent polymerization. In doing so, it was envisioned that the bulkier diester system would impede uncontrolled crosslinking reaction of the enyne moieties. To this end, an alternative monomer was synthesized, starting from potassium 3-methoxy-3-oxopropanoate (Scheme 4.10).



Scheme 4.10: Two-step synthesis of the **SM2-Br** monomer from potassium 3-methoxy-3-oxopropanoate.

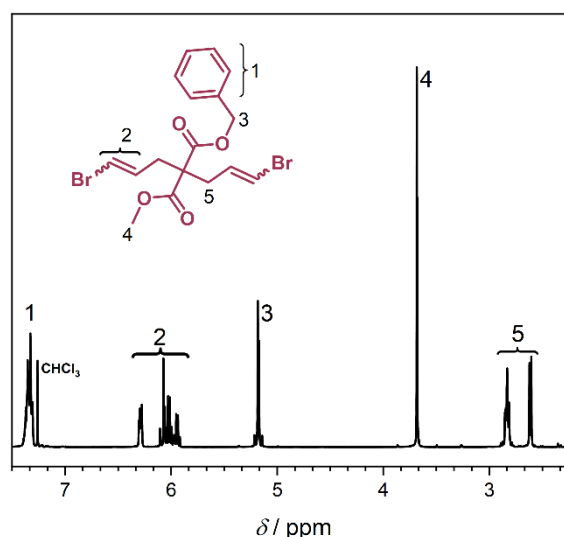
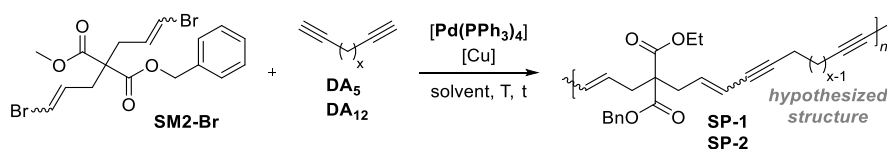


Figure 4.3: Proton NMR spectrum (CDCl₃, 400 MHz) of the diester divinyl bromide monomer **SM2-Br**.

Here, an unsymmetrical diester was considered, to facilitate the evaluation of cruder polymer mixtures *via* NMR spectroscopy. Thus, the benzyl moiety was introduced to the monomer in order to induce a steric hindrance between the enyne in the final polymers. Accordingly, the proton spectrum of the new monomer is depicted in Figure 4.3 and shows all essential resonances, such as the benzyl signals at 7.34 (1) and 5.18 ppm (2) as well as the vinyl

resonances at 6.37 – 5.88 ppm (3). As in the case for the previous monomers, the product showed a ratio of 40:60 of the *E/Z*-isomers.

In similar fashion as previously with **SM1-Cl** and **SM1-Br**, the new monomer was subjected to the polymerization conditions that are summarized in Table 4.3. Here, upon the polymerization, the reactions mixtures were precipitated in ice-cold diethyl ether and centrifuged. The obtained material was immediately subjected to SEC analyses to evaluate the obtained molecular masses. Both dialkyne derivatives (**DA₅** and **DA₁₂**) were tested in this manner to reveal if the different chain lengths of the monomers have an influence on the obtained results (Entry 1 and 2), if the remaining parameters are held constant.



Scheme 4.11: General reaction scheme for the SONOGASHIRA polycondensation of **SM2-Br**.

Table 4.3: Summarized results of the SONOGASHIRA polycondensation of **SM2-Br** with **DA₅** & **DA₁₂**.

Entry	Polymer	Catalyst	Cocatalyst	Alkyne	Solvent	T	t	M_n [kg·mol ⁻¹] ^{a)}	M_w [kg·mol ⁻¹] ^{a)}	\bar{D} (M_w/M_n)
1	SP-1	Pd(PPh ₂) ₄	CuI	DA₅	Pyr	r.t.	19 h	9.64	13.9	1.44
2	SP-2	Pd(PPh ₂) ₄	CuI	DA₁₂	Pyr	r.t.	19 h	19.1	30.8	1.61
3	-	Pd(PPh ₂) ₄	-	DA₁₂	Pyr/DMF	r.t.	48 h	-	-	-

^{a)} Determined by THF-SEC with PS standards. Evaluation based on respective SEC peak traces (Figure 4.4).

To further proof the presence of the proposed polymer structure, a crude NMR sample was taken, subsequently subjected to vacuum and analyzed by ensuring the exclusion of air under any circumstances (**SP-1**, Entry 1). As shown in Figure 4.4 (*left*), the respective proton NMR shows the magnetic resonances of the desired polymer structure (benzyl moiety – resonance 1 & 3; vinyl moiety – resonance 2; alkyl chain – resonances 6, 7 & 8). Notably, a broadening of the signals at is observed, which in turn is characteristic for polymers. Most importantly however, the presence of the vinyl group is evidenced through the resonances at 5.98 – 5.39 ppm, which corresponds to an upfield shift of the signals compared to the monomer (6.37 – 5.88 ppm), caused by the displacement of the electronegative bromide atoms. Furthermore, the assigned signals also show the expected integration values corresponding to the proposed structure, thus indicating that the formation of the polymer essentially occurs.

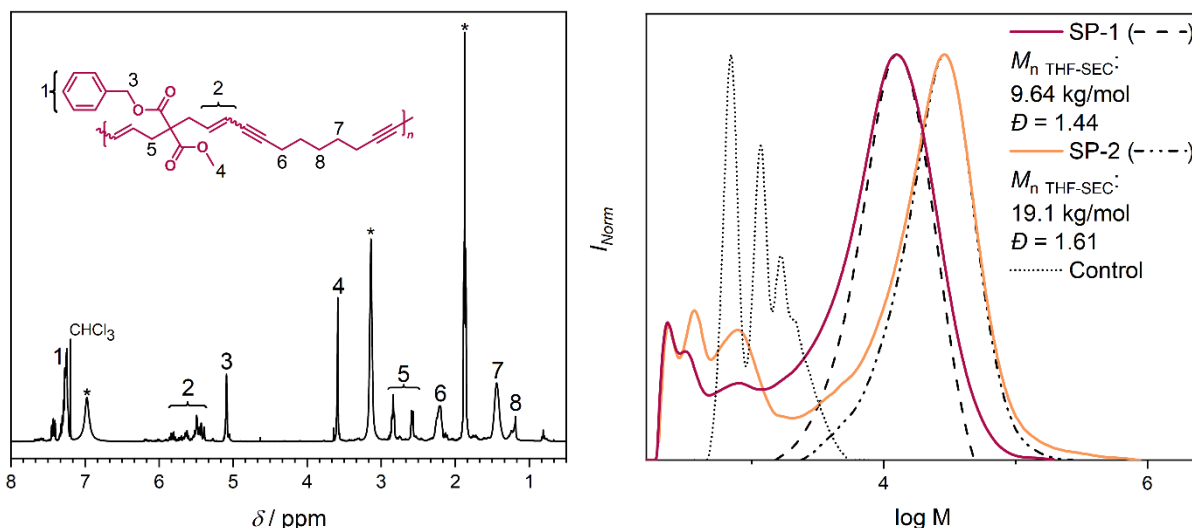
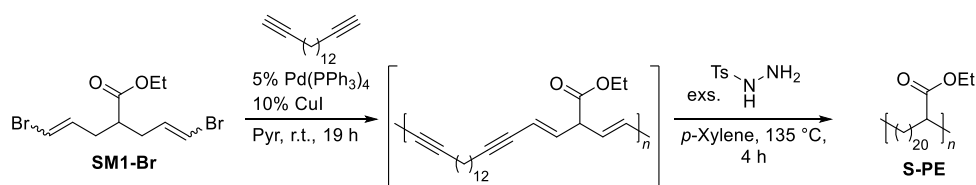


Figure 4.4: Crude proton NMR spectrum (CDCl_3 , 400 MHz) corresponding to the experiment shown in **Table 4.3** Entry 1 (*left*) and the SEC traces corresponding to Entry 1 and 2, respectively.

Unfortunately, the structural change in the monomer imparted only partial stability to the desired polymers as they still crosslinked after several minutes after precipitation. However, at least an immediate SEC measurement of the obtained materials was possible. The corresponding SEC measurements showed low-intensity traces in the molecular mass areas of 5 to 25 $\text{kg}\cdot\text{mol}^{-1}$. Although the results cannot be regarded as fully meaningful due to possible partial crosslinking, the samples were evaluated to have molar masses of 9.64 $\text{kg}\cdot\text{mol}^{-1}$ (Table 4.3, Entry 1) and 19.1 $\text{kg}\cdot\text{mol}^{-1}$ and dispersity values of $D = 1.44$ and $D = 1.61$ (Table 4.3, Entry 2), respectively (evaluation based on the respective dashed SEC peak traces). A comparative control experiment (Table 4.3, Entry 3; Figure 4.4 *right* – dotted line) did not show comparable traces.

In a final attempt, in other words, as a proof of concept, a polymerization and subsequent *in-situ* hydrogenation reaction was conducted (Scheme 4.12). Here, the contents of the polymerization reaction were transferred to a second vessel containing *p*-toluenesulfonyl hydrazide, which is decomposed to the hydrogenation agent, *i.e.*, diimide, *in-situ* at 135 °C.



Scheme 4.12: Reaction scheme for the polymerization and *in-situ* hydrogenation.

After purification *via* precipitation, the obtained black material was analyzed *via* ^1H NMR, SEC and TGA (Figure 4.5).

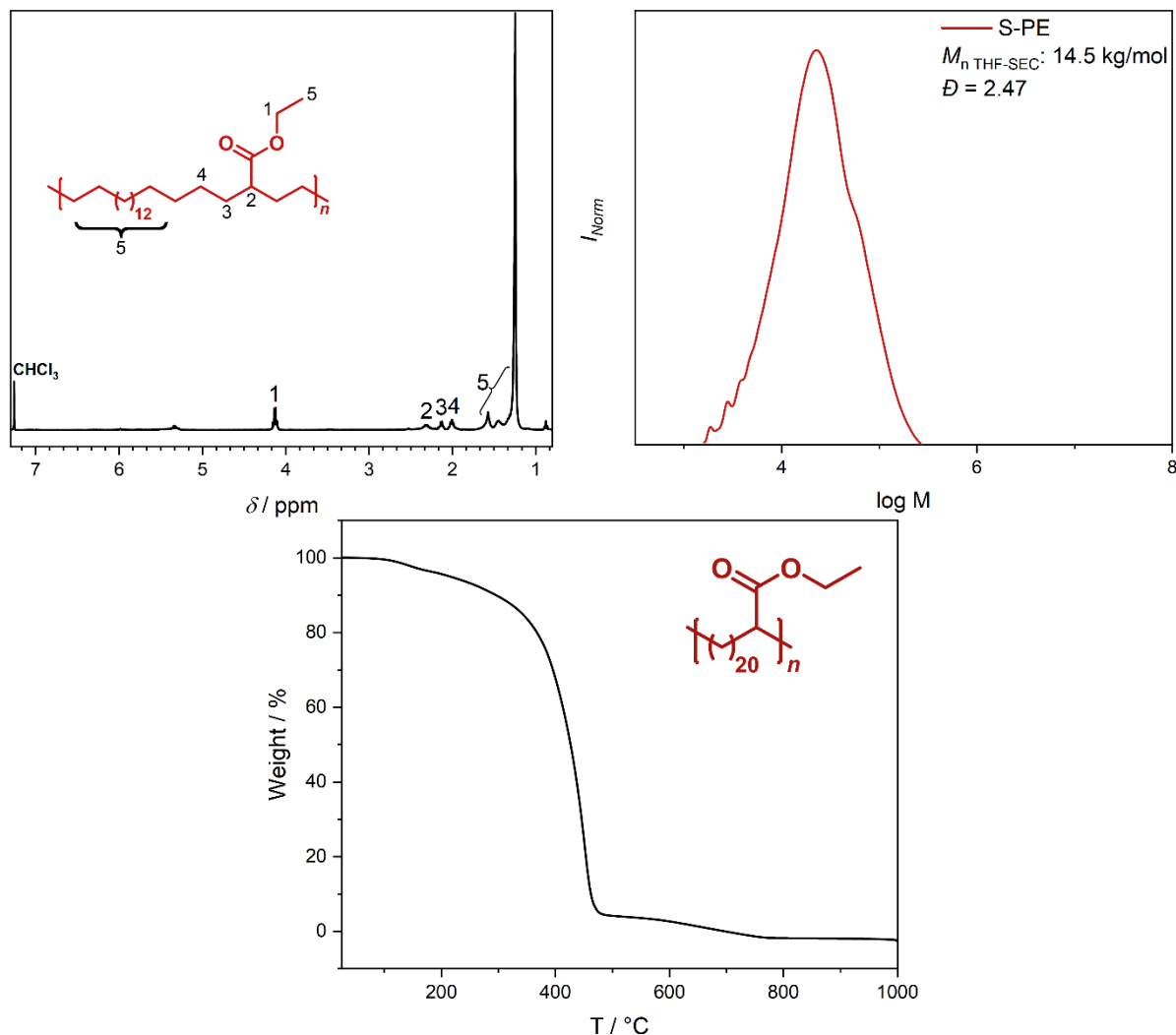


Figure 4.5: Depiction of the conducted ^1H NMR (*top left*), SEC (*top right*) and TGA analyses (*bottom*) of the hydrogenated polymer **S-PE**.

Fortunately, the *in-situ* hydration reaction has yielded the desired aliphatic polymer **S-PE**, which could be analyzed via SEC (Figure 4.5 *top right*) without problems. The respective SEC trace revealed a polymer with a molar mass of $14.5 \text{ kg}\cdot\text{mol}^{-1}$ and a dispersity of $D = 2.47$, which is expected for a step-growth process. NMR spectroscopy (Figure 4.5 *top left*) evidenced the incorporation and respective stability of the ester group through the resonances 1 – 4 (4.13, 2.31, 2.13 and 2.00 ppm, respectively) as well as the overall aliphatic nature of the obtained polymer (lacking the vinyl resonances at 5.98 – 5.39 ppm). Interestingly, the TGA trace of **S-PE** showed a steady decomposition pattern starting from 100 °C to 470 °C. This can be attributed to the continuous degradation of the incorporated ester group, which is accelerated above 300 °C.

4.4 Conclusion

In this section, the conceptualization and synthesis of functionalized (precise) poly(ethylene) polymers *via* SONOGASHIRA polycondensation was depicted. According to the general concept (shown in Scheme 4.5), two suitable divinyl halide monomers carrying an ester group were synthesized. To investigate a possible scale-up of the envisioned synthesis not only bromine but also chlorine-bearing monomers were considered (**SM1-Cl** and **SM1-Br**). Subsequently, both monomers were subjected to SONOGASHIRA reactions with two dialkynes of different chain lengths (**DA₅** and **DA₁₂**). Unfortunately, several challenges were encountered with the employed conditions, such as crosslinking during the polymerization reaction or while the precipitation process, in addition to the drying process at atmospheric environment. Due to a possible involvement of a copper in these events, copper-free SONOGASHIRA protocols were employed, which however did not yield polymeric material.

To circumvent the hurdles, a structurally bulkier monomer (**SM2-Br**) was synthesized and subsequently polymerized under similar conditions as stated before. Here, only a slight improvement in the synthesis was achieved, as the isolated material crosslinked marginally slower, whereas still allowed for immediate SEC measurements that hinted towards high molar mass species of 10 – 20 kg·mol⁻¹. Crude NMR analyses under strict air exclusion conditions further hinted to the successful build-up of polymer through broadened magnet resonances as well as upfield shifted vinyl resonances at 5.98 – 5.39 ppm, indicating successful formation of enyne linkages. Finally, one attempt was undertaken to hydrate the presumably unsaturated polymer *in-situ* with thermally released diimide. In doing so, the respective polymer **S-PE** could be obtained, and its aliphatic character was verified *via* proton NMR. The respective SEC trace of the hydrogenated polymer revealed a molar mass of 14.5 kg·mol⁻¹ and a dispersity of $\bar{D} = 2.47$.

Thus, the general concept for the synthesis of a functionalized poly(ethylene) *via* SONOGASHIRA polycondensation was proven.

5 Bottlebrush Architectures *via* PPM of Poly(Pentafluorophenol acrylate) with long-chain α,ω -Alkynols

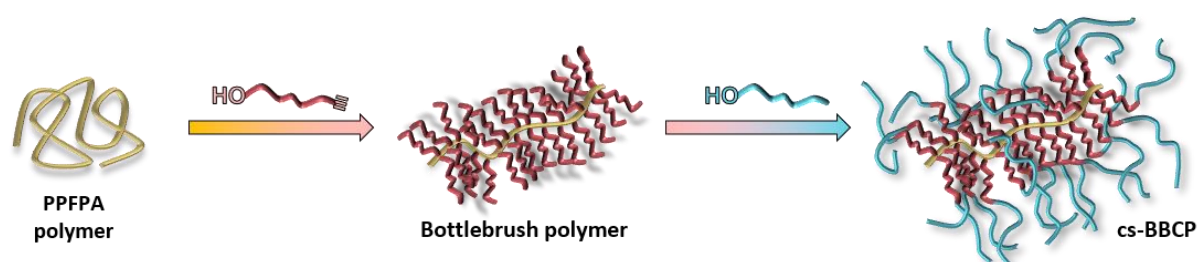
5.1 Motivation

Several different techniques have emerged in polymer science that allow the synthesis of diverse polymer architectures that deviate from “classical” linear polymers. In this regard, block copolymers, dendrimers,^[82] star polymers,^[78,86] rings^[83] and even 3-D cage-shaped polymers^[86,87,157] have been reported. Here, especially macromolecules with controlled three-dimensional topologies stand out, as they mimic the architectonic complexity of protein architectures on a basic level.^[158,159] One famous example of architectonical control is the synthesis of polyethylene (PE), as the properties of the final polymer, *i.e.*, low-density PE *vs.* high-density PE, depend on the employed reaction conditions that control the degree of branching.^[76,160] To gain control over the branching degree several approaches for the synthesis of graft polymers were devised, as described in Chapter 2.4.1. If (polymer) chains are tethered to a parent linear macromolecule, so called comb or bottlebrush polymers architectures are obtained, depending on the graft density, respectively.^[161] The latter exhibit interesting properties and therefore were utilized as sensors,^[162] pH-probes^[163] or drug delivery systems.^[164] Recently, the grafting of radically polymerized active esters, and especially pentafluorophenyl esters, became a popular method for the synthesis of such polymers.^[72,96] Notably, this approach allows the attachment of pendant groups that are incompatible with radical polymerization, *e.g.*, unsaturated moieties such as alkenes or alkynes.

As described in Chapter 3 long-chain alkynols were successfully synthesized *via* the Alkyne Zipper reaction. The two terminal functionalities of these hydrocarbons, *i.e.*, the (α -)hydroxy group and the terminal (ω -)alkyne, furthermore allow orthogonal reaction control through the varied chemistry available to them. The α -hydroxy group for example can be used as a nucleophile while the ω -alkyne offers prospects for metal-catalyzed coupling reactions, cycloadditions or thiol-yne reactions. However, the radical polymerization of monomers derived from these alkynols is not possible, as the alkyne moiety is not compatible with the radical process. However, a “graft-to”-approach should circumvent this problem and make the corresponding bottlebrush polymers with pendant alkyne-terminal hydrocarbons accessible.

To this end, through a post-polymerization process with long-chain alkynols of known lengths, bottlebrush polymers with precisely controllable side-chain dimensions should be

synthesized. Accordingly, a polymeric precursor carrying active ester groups with a narrow molecular weight distribution shall be synthesized. In the second step of the synthesis, the obtained polymer shall be modified through the attachment of long-chain alkynols, thus yielding bottlebrush polymers with precise side-chain length. Spectroscopical analyses, SEC as well as DSC measurements should be carried out in order to provide information about the property dependence of the side-chain lengths of the new materials and give insights into the thermal behavior. Since the employed alkynols carry an alkyne at the terminal chain end, further chemical derivatization is possible and should be investigated in order to access more complex architectures, such as core-shell bottlebrush copolymer (cs-BBCPs). The general project concept is depicted in Scheme 5.1.

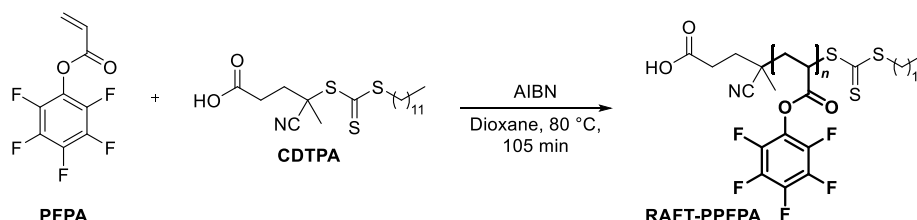


Scheme 5.1: Depiction of the general concept for the synthesis of bottlebrush polymers *via* transesterification of PFP esters with previously synthesized long-chain alkynols and subsequent derivatization with alcohols to core-shell bottlebrush copolymers (cs-BBCSs).

5.2 Polymer Synthesis and Post-Polymerization Reactions with α,ω -Alkynols

To investigate the post-polymerization reaction with the previously synthesized long-chain α,ω -alkynols (refer to Chapter 3.2.3), a suitable parent polymer was needed. To this end, a polymer with active ester moieties should be synthesized.

To enable better comparison of the final bottle-brush polymers, a precursor with a uniform molecular weight distribution was essential. Hence, pentafluorophenyl acrylate (PFPA) was polymerized *via* reversible-addition-fragmentation chain-transfer (RAFT) polymerization to ensure a predictable chain lengths and narrow molecular weight distribution (Scheme 5.2). Here, 4-Cyano-4-[(dodecylsulfanylthiocarbonyl)sulfanyl]pentanoic acid (CDTPA) was the RAFT agent of choice, as it allows excellent control over the polymerization of acrylates.^[55] As the aim of the subsequent reactions were the employment of previously synthesized long-chain alkynols for the synthesis of precise bottlebrush structures, the molecular weight changes should be easily evidenced *via* SEC. Thus, a molecular weight below $10 \text{ kg}\cdot\text{mol}^{-1}$ was targeted and the polymerization was run for a relatively short time of 105 minutes in 1,4-dioxane at $80 \text{ }^\circ\text{C}$. After purification, the controlled nature of the polymerization was evidenced *via* SEC indicating a low polydispersity index $\mathcal{D} = 1.13$ and a molecular weight M_n of around $7.10 \text{ kg}\cdot\text{mol}^{-1}$. The purity of the polymer was validated by ^1H and ^{19}F NMR (Figure 5.1) and DSC analysis (Figure 5.4).



Scheme 5.2: Synthesis of the active-ester polymer **RAFT-PPFPA** *via* controlled radical polymerization with chain-transfer agent **CDTPA**.

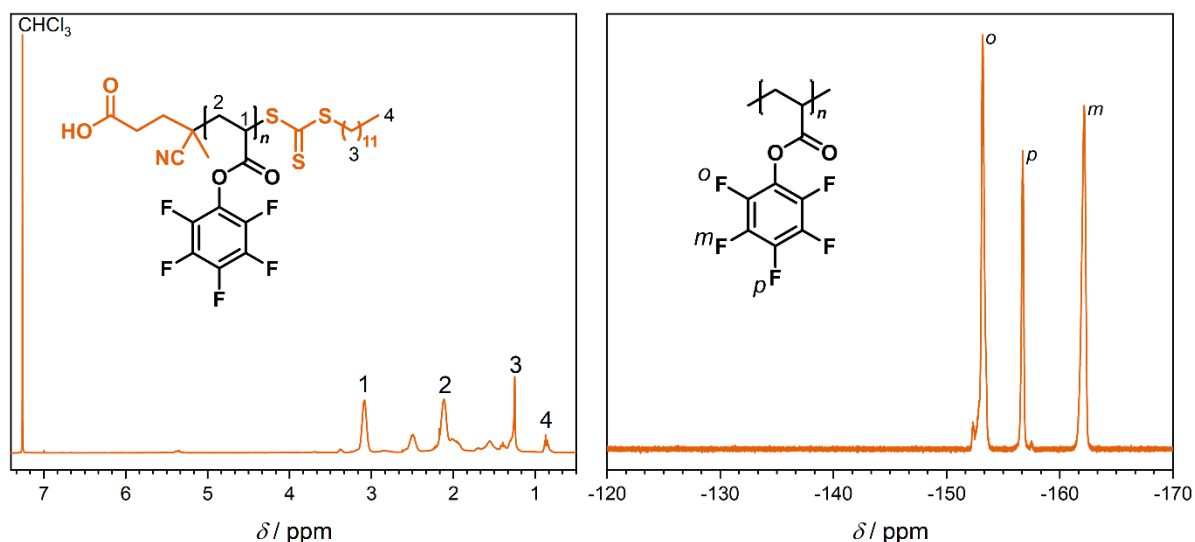
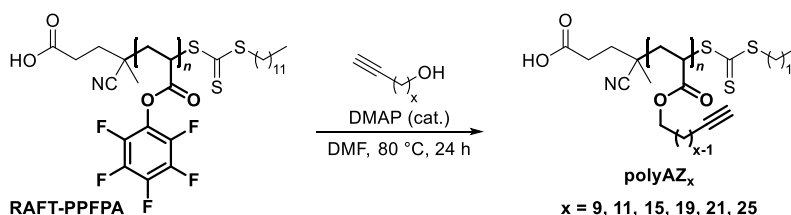


Figure 5.1: NMR spectroscopic analyses of **RAFT-PPFPA** showing the polymeric backbone as well as additional chain-transfer agent resonances (*left*) and broadened pentafluoro phenol resonances (*right*).

After the synthesis of a suitable precursor polymer, the nucleophilic substitution of the active-ester moieties was investigated. As reported previously by THÉATO *et al.* in 2015, pentafluorophenol esters can be effectively substituted with various alcohols in the presence of catalytical amounts of 4-dimethylaminopyridine (DMAP) at elevated temperatures in DMF.^[96] Since these conditions covered not only low molecular weight molecules but also a poly(ethylene glycol) methyl ether specimen of similar molecular weight as the to-be employed long-chain alkynols, the reported experimental procedure was adapted. Thus, **RAFT-PPFPA** was trans-esterified with the previously synthesized **AZ1**, **AZ2** – **AZ5** with 0.2 equivalents of DMAP at 80 °C in DMF for 24 hours towards the respective graft polymers denoted as **polyAZ_x** (with **x** abbreviating the number of methylene groups of the respective alkynols) (Scheme 5.3). To ensure better comparison of grafted bottlebrush polymers with shorter side chains, the reaction was also performed with undec-10-yn-1-ol and tridecyn-1-ol as nucleophiles.



Scheme 5.3: Reaction scheme for the trans-esterification of **RAFT-PPFPA** with undec-10-yn-1-ol, tridecyn-1-ol **AZ1**, **AZ3** – **AZ5**.

Through careful choice of solvents for the precipitation of the polymers, all polymers could be accordingly purified and were subsequently analyzed *via* NMR, SEC, DSC and IR spectroscopy.

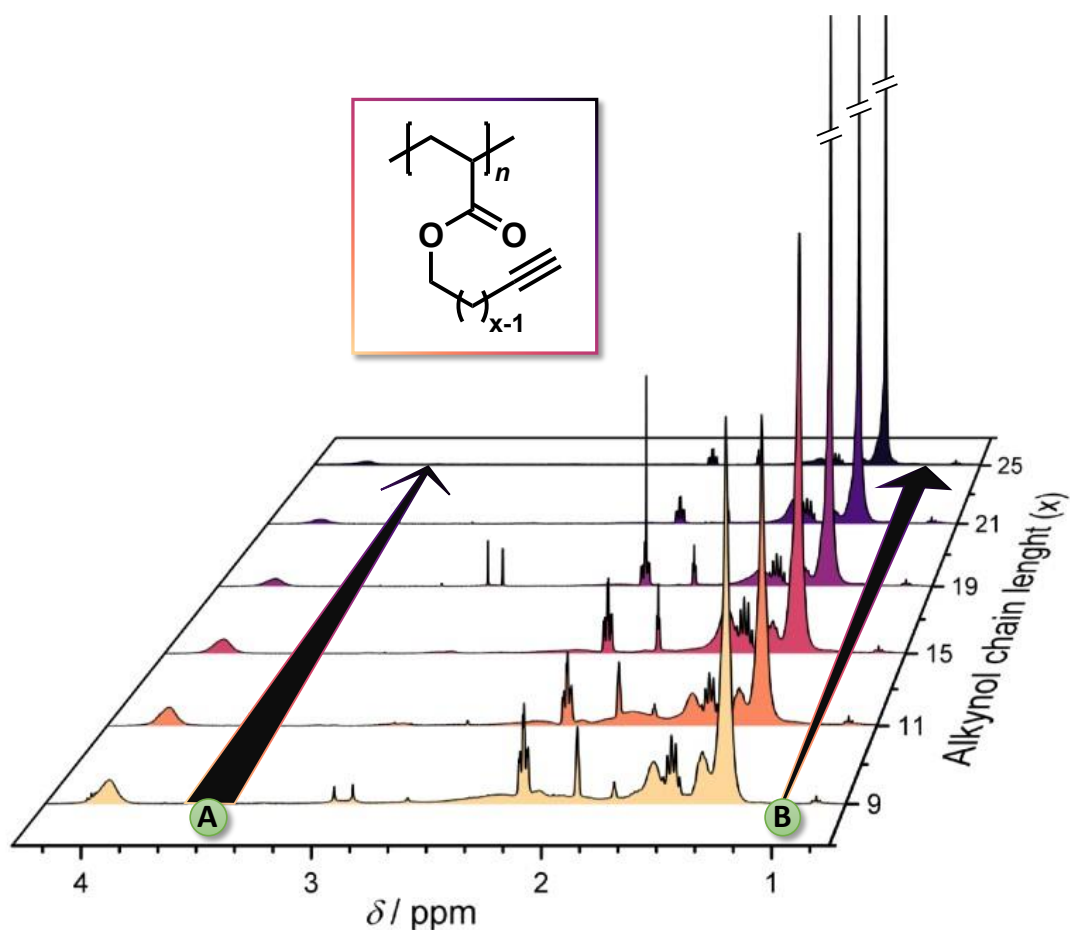


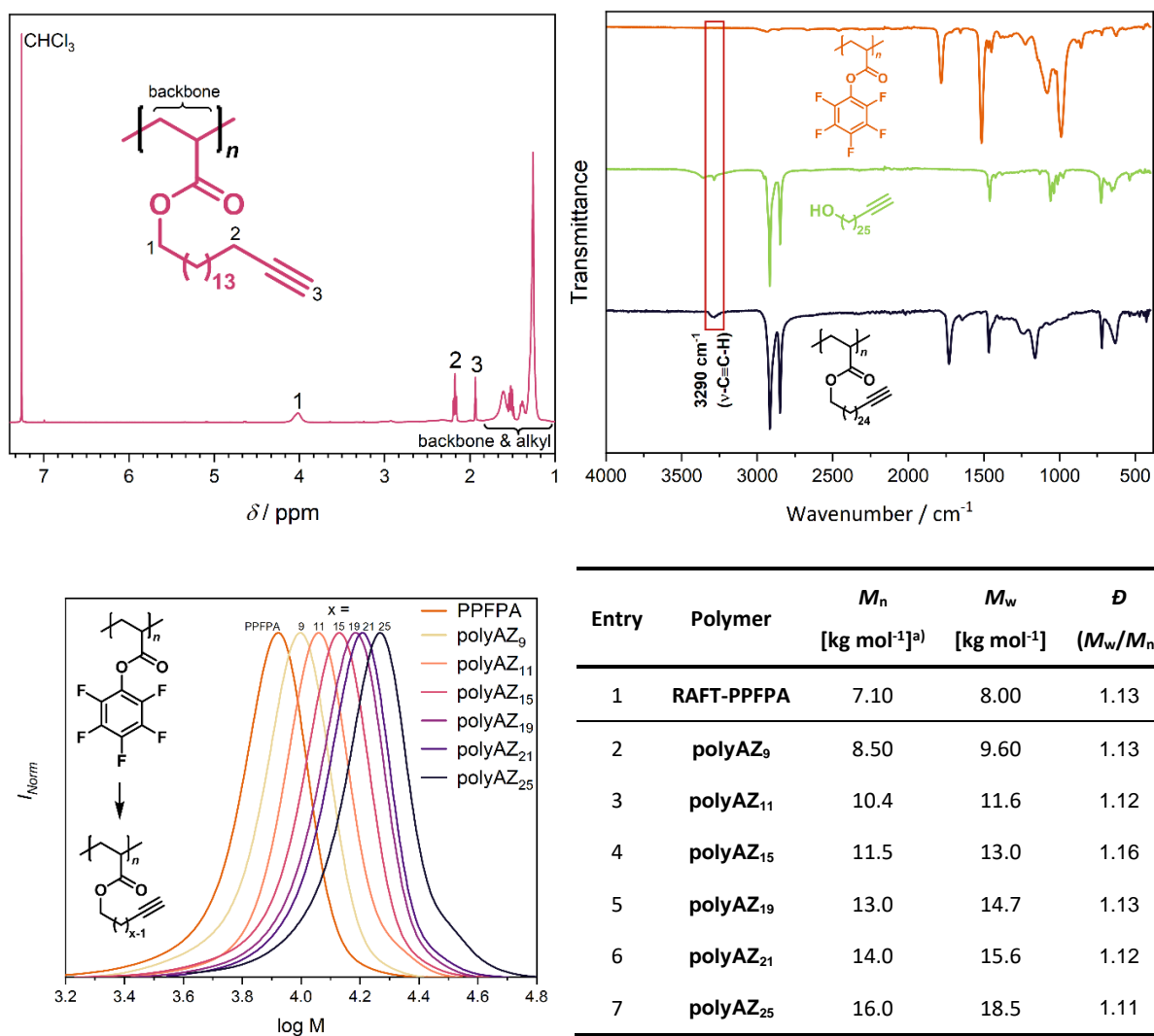
Figure 5.2: Depiction of arranged ^1H NMR measurements (cutout in CDCl_3 , 400 MHz) of **polyAZ_x** ($x = 9, 11, 15, 19, 21, 25$) evidencing the successful trans-esterification with all alkynols.

Fortunately, all substitution reactions showed full conversion for all employed alkynols, as is confirmed through the absence of any resonances in the fluorine NMR spectra. Thus, a complete grafting to the main-chain is affirmed. Respectively, ^1H NMR revealed new magnetic resonances corresponding to the now-attached alkynols. Exemplarily, the proton spectrum of **polyAZ₁₅** is depicted in Figure 5.3 for more detail. Here, the alkynol resonances appear most evidently as the broadened signal at 4.02 ppm (singlet, 1), the triplet of doublet at 2.18 ppm (2) and the triplet at 1.93 ppm (3), which corresponds to the terminal alkyne proton (for comparison, see Figure 5.1 *left*). Generally, the proton spectra of all polymers are similar in appearance as shown in Figure 5.2. Here, the relative ratio of the ester-adjacent protons (4.02 ppm, denoted as 1 in Figure 5.3 *left*) to the alkyl resonances (at 1.27 ppm) is continuously lowered (*arrow A*) as alkynols with increasing chain lengths (*arrow B*) are employed for the post-polymerization reaction. The successful trans-esterification is further proven by IR

spectroscopy as shown in Figure 5.3 (*top right*). Here, for example the presence of the terminal alkyne of **AZ5** is evidenced by the present C-H stretching band at 3290 cm^{-1} in **polyAZ₂₅**.

Most notably, the successful reaction with the individual alkynols is demonstrated *via* the SEC graphs of the grafted polymers (Figure 5.3 *bottom left*). In similar fashion as already shown for the long-chain hydrocarbons in Figure 3.3, a difference of only two carbon atoms in the chain is already expressed through a shifted SEC trace towards higher molecular weights. The obtained values are summarized in Figure 5.3 (*bottom right*). As expected, the apparent molecular masses of the bottlebrush polymers increase accordingly to the lengths of the employed alkynols. In the case of **polyAZ₂₅**, a number average molecular mass of 16.0 kg mol^{-1} was obtained, which corresponds to an increase of more than twice of the parent polymer mass value (7.10 kg mol^{-1}). Based on the degree of polymerization of the precursor polymer **RAFT-PPFPA** ($DP \sim 30$) the molar mass of **polyAZ₂₅** is calculated to be approximately 13.3 kg mol^{-1} , which is roughly 3 kg mol^{-1} lower than the obtained value from the SEC analysis. This difference can be attributed to an architectural change of the grafted polymer compared to the precursor. Through the graft process, the backbone of the previously folded **PPFPA** globule is uncoiled due to the steric repulsion of the grafted chains, resulting in a persistent, cylindrical shape, which is expressed through an increased hydrodynamic radius r_H , and in consequence, a higher molecular mass in the SEC measurement.^[161,165,166]

The thermal analysis of the grafted polymers shows a strong dependance of the thermal behavior to the chain length of the used alkynol. Most striking is the T_g change for the reaction towards **polyAZ₉**. Here a change of the glass transition temperature of 101 K towards a lower value is observed. Interestingly, the two-carbon extended alkynol, *i.e.*, tridecyn-1-ol, yields a polymer with a complex thermal response at $-26.4\text{ }^\circ\text{C}$. Both materials were obtained as brown honey-like oils, respectively. Further increasing the side-chain length from 11 to 15 carbon atoms as in **polyAZ₁₅** already yields a solid polymer with a T_m slightly above room temperature and further side chain elongations yield higher melting temperatures up to $77.4\text{ }^\circ\text{C}$ for the 25-carbon side chain. The trend of these thermal responses can be explained by the possibility of the side chains to form semi-crystalline areas. The grafted polymers with lower side-chain lengths (**polyAZ₉** and **polyAZ₁₁**) lack the necessary overlap of methylene groups to properly align and thus the formation of crystalline areas is suppressed. This however, is possible for longer side-chain lengths. Interestingly, only a four-carbon difference in side-chain length lay between the amorphous and semi-crystalline polymers.



^{a)} Determined by THF-SEC with PMMA standards.

Figure 5.3: Top left: Depiction of the proton NMR spectrum (CDCl_3 , 400 MHz) of **polyAZ₁₅** with assigned resonances. Top right: Stacked IR spectra of **AZ5** and its trans-esterification product **polyAZ₁₅**. Bottom: Comparative SEC traces (left) and corresponding result values (right) for the precursor polymer PPFPA and all PPM products.

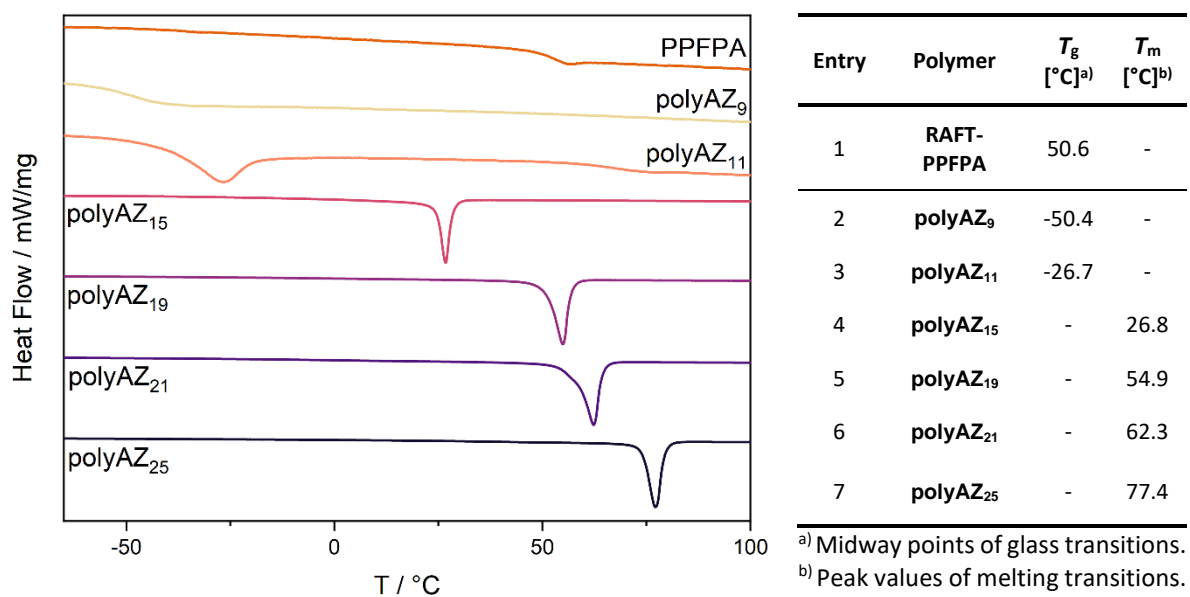
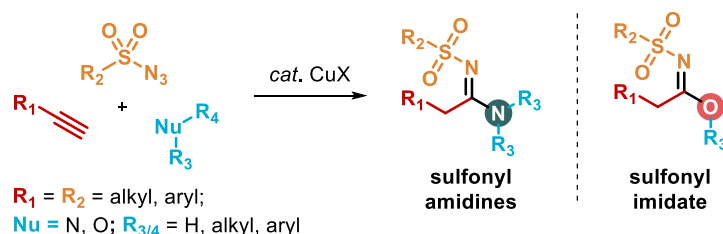


Figure 5.4: Stacked DSC traces of PPFPA and the trans-esterification products **polyAZ_x** (*left*). The corresponding data is shown in the table (*right*).

5.3 Derivatization of precise Bottlebrush Polymers

Upon the successful synthesis of the grafted polymers further derivatization should be investigated. As the tethered hydrocarbon chains carry an alkyne moiety at its ω -chain end, a plethora of chemical transformations is available for further derivatization.^[167] Ideally, such post-polymerization reactions should proceed in quantitative fashion as the final polymer properties are dependent on the degree of functionalization. To this end, versatile “click” chemistry strategies have been developed that allow the chemo-selective and highly efficient chemical transformations of polymers.^[168] Concerning alkynes in this context, two prominent reactions have emerged as the tools of choice: copper(I)-catalyzed alkyne-azide cycloaddition (CuAAC)^[65,168] and thiol-yne (alkyne hydrothiolation).^[69,70,169] However, one of the drawbacks of these strategies are the set constraints on the structural necessities of the to-be-attached molecules. That means, the desired attachment needs to be suitably functionalized with an azide or thiol functionality, respectively, in order to be reacted with an alkyne. Although several substrate classes are commercially available, in specialized cases the chemical synthesis of derivatives becomes necessary which is sometimes accompanied by other difficulties, such as functional group intolerance, tedious work-up procedures or simply a very high price. For this reason, alternative reactions that circumvent the need for derivatization and allow direct reaction of commercial substrates are sought after. One such method is the three-component reactions (3-CR) of sulfonyl azides, terminal alkynes and nucleophiles, such as amines or alcohols (Scheme 5.4).



Scheme 5.4: Schematic representation of the copper-catalyzed three-component reactions (3CR) of sulfonyl azides, terminal alkynes and nucleophiles.

This copper-catalyzed multicomponent reaction yields *N*-sulfonylamidines with amines and *N*-sulfonylimidates with alcohols, respectively, and thus allows the synthesis of complex molecules in a straightforward one-pot fashion.^[170,171] Due to its high efficiency, this reaction was also employed as a polymerization technique for biodegradable polymers.^[172,173] Most importantly, it allows the attachment of variable nucleophiles towards alkynes, without the need to transform them into suitable derivatives for the alkyne-azide cycloaddition or thiol-yne reaction, respectively.

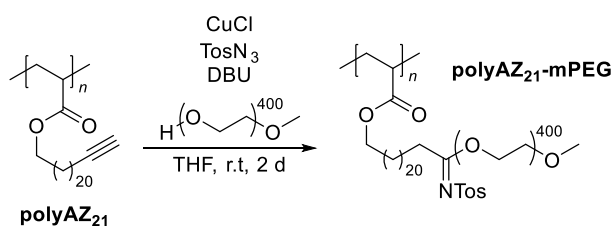
With this methodology established, a suitable nucleophile for the 3-CR was essential. As the graft-to approach described in the previous section proved to be very effective for the synthesis of bottle-brush polymers, the attachment of a suitable nucleophile with known

length and molecular weight would allow for the synthesis of core-shell bottlebrush copolymers (cs-BBCPs), which have interesting properties such as large molecular size and cylindrical “worm”-like shapes, high density in addition to bulk phase separation characteristics.^[80,90,174,175] Moreover, this approach would expand the possible syntheses of such macromolecular architectures, as they usually require the tedious synthesis of a suitable polymerizable monomer^[90] (graft-through approach) or a multi-step synthesis including a total of three polymerization reactions^[97] (main-chain polymerization and 1st and 2nd graft-from reactions) (graft-from approach). In the latter case, the approach carries one severe downside associated with polymerization reactions: the appearance of distributions in each step.

Due to the possibility to use amines and alcohols for the three-component reaction, one class of alcohols was of particular interest due to its intensive use in battery science: polyethylene glycols (PEGs). Interestingly, ROSENBACH *et al.* found that poly(methacrylate) bottlebrushes carrying PEG sidechains exhibited good ($\sim 0.13 \text{ mS}\cdot\text{cm}^{-1}$ at 30 °C) ionic conductivities when used as polymer electrolytes for lithium batteries.^[176] However, the T_g of such PEG-carrying polymers is low ($\ll 0 \text{ °C}$) and thus, they have lessened dimensional stability, which in turn is suboptimal for the application as electrolytes.^[176,177] Since the obtained bottlebrush polymers **polyAZ_x** (see previous section) show high T_m values (up to 77 °C), it was of interest to investigate their PEGylated bottlebrush derivatives, as these could be applied as polymer electrolytes.

Accordingly, **polyAZ₂₁**, should be reacted with a suitable PEG-derivative in a 3-component reaction (3-CR) in the presence of a sulfonyl azide. To prevent the coupling of two bottlebrush polymers during reaction a mono-functionalized alcohol of similar molar mass relative to the grafted alkynol was chosen: methoxy polyethylene glycol with an average molecular weight of $400 \text{ g}\cdot\text{mol}^{-1}$ or mPEG 400, for short. The necessary sulfonyl azide component was synthesized in one step from tosyl chloride with sodium azide according to a literature procedure.^[178]

Finally, with all components in hand, **polyAZ₂₁**, mPEG 400 and tosyl azide were reacted under copper catalysis and DBU as base in THF (Scheme 5.5).



Scheme 5.5 Reaction scheme for the 3-component reaction of **polyAZ₂₁**, mPEG 400 and tosyl azide.

To ensure adequate product formation, the reaction was conducted for two days and subsequently quenched by precipitation in diethyl ether. After further purification *via* precipitation in ethanol, the obtained material was analyzed *via* NMR and IR spectroscopy, in addition to SEC and DSC.

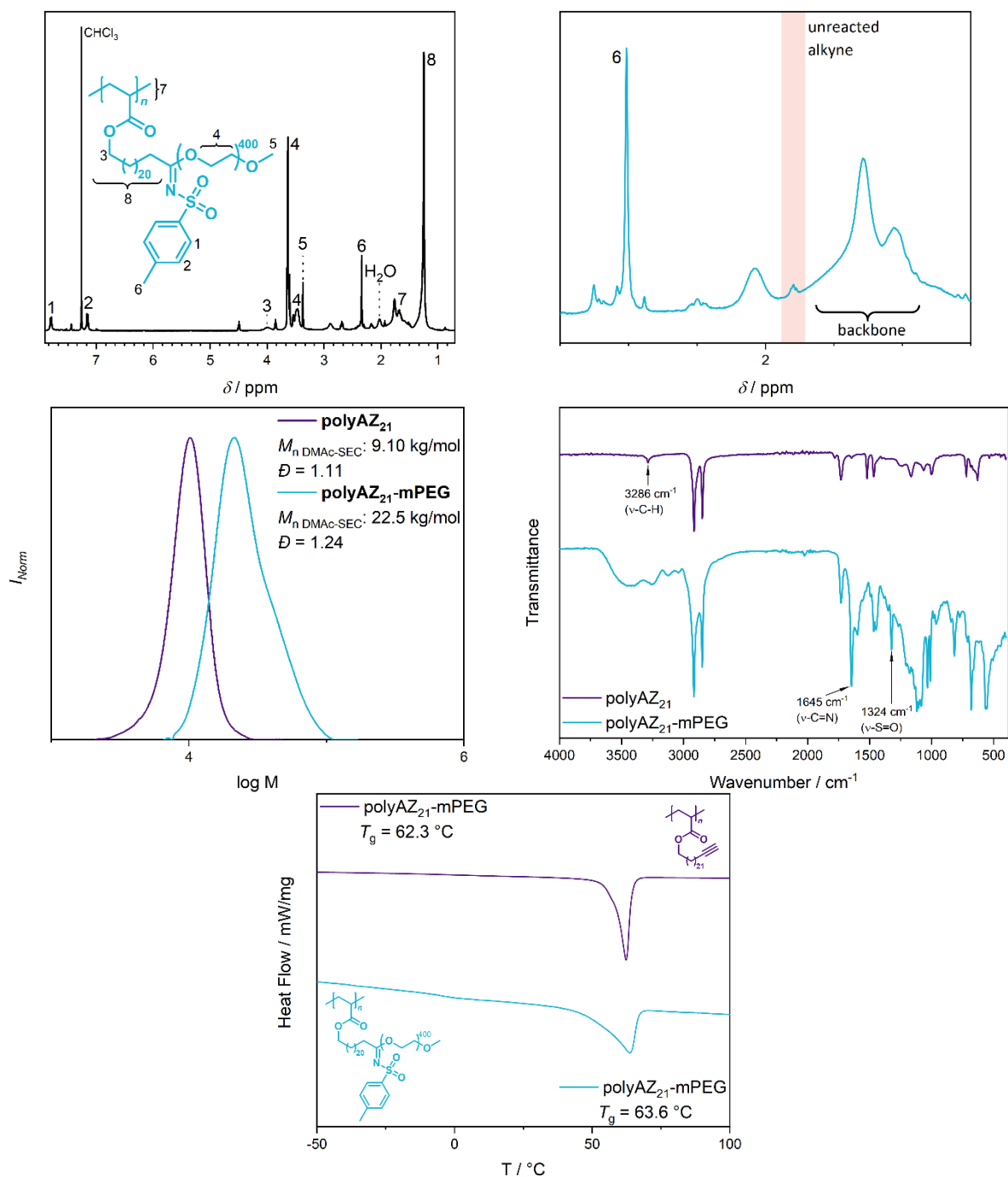


Figure 5.5: Top: ^1H NMR (CDCl_3 , 400 MHz) of **polyAZ₂₁-mPEG** (left) and a zoom-in (1.50 ppm – 2.50 ppm) (right) showing the remaining alkyne resonance. Middle: Comparative DMAC-SEC traces (left) and IR spectra (right) before and after the 3-CR. Bottom: Comparative DSC analyses of **polyAZ₂₁** and **polyAZ₂₁-mPEG**.

NMR analysis of the obtained polymer revealed the successful attachment of mPEG 400 chains to the terminal alkynes through the appearance of the respective polyethylene glycol resonances at 3.76 – 3.4 ppm (4) and 3.37 ppm (5) (Figure 5.5 *top left*). Additionally, the incorporation of the sulfonyl azide component is evidenced by the appearance of the resonances at 7.79 and 7.15 ppm (1 and 2), as well as at 2.34 ppm (6), corresponding to the *p*-tolyl moiety. As can be seen from the enlarged section of the proton spectrum shown in Figure 5.5 (*top right*), the conversion of the alkyne moiety was not quantitative as the terminal alkyne proton is still present. However, an accurate calculation of the conversion is hindered through the large overlap with the resonances of the polymer backbone. An approximate calculation based on the resonances 1 and 3 resulted in a conversion ratio of about 70%. This moderate value can be attributed to the relatively low nucleophilicity of the methoxy polyethylene glycol and could be possibly improved through an increase in reaction temperature, as shown in literature.^[96] SEC analysis further evidenced the successful 3-CR through a strong shift of the traces from 9.1 kg mol⁻¹ (**polyAZ₂₁**) towards a higher molecular mass of 22.5 kg mol⁻¹ for the PEGylated polymer (Figure 5.5 *middle left*). In similar manner to the previous results, the mass change exceeds a doubling due to further conformational change of the bottlebrush architecture as discussed in the previous section (*vide supra*). In contrast to the bottlebrush synthesis, the 3-CR also resulted in a slight increase of the dispersity from $\mathcal{D} = 1.11$ to $\mathcal{D} = 1.24$. The newly introduced functional motifs, *i.e.*, the sulfonyl imidates, are also expressed as new absorption bands in the respective IR spectra (Figure 5.5 *middle right*). Here, the especially the S=O stretching band at 1324 cm⁻¹ and the C=N stretching band at 1645 cm⁻¹ are of importance, as they represent the link between the aliphatic and PEG chains. Finally, the thermal properties of the newly-synthesized core-shell bottlebrush copolymers were investigated *via* DSC (Figure 5.5 *bottom*). Compared to the parent polymer, a change in the thermal response is recorded in the thermogram of **polyAZ₂₁-mPEG**. Here, a melting transition is observed from 57.8 to 64.5 °C with a peak temperature of 62.3 °C. Interestingly, the integrals of both melting transitions greatly differ: the calculated enthalpy of fusion for **polyAZ₂₁-mPEG** (20.2 J/g) is a fifth as large as the value for the parent polymer **polyAZ₂₁** (93.3 J/g). The lessened energy requirements for the melting transition can be attributed to the suppression of crystallization behavior of the amphiphilic chains. Notably, although the melting process proceeds over a temperature range of nearly 13 K (57.8 – 64.5 °C), the still very high values itself are evidence for the stability-providing nature of the long hydrocarbon branches. Thus, the presented strategy indeed allows the synthesis of suitable materials for application as polymer electrolytes, provided that the PEG chains provide a good enough solubility for respective lithium salts.

5.4 Conclusion

In this section the successful synthesis of core-shell bottlebrush polymers was shown. First, an active-ester polymer (PPFPA) with a narrow dispersity was synthesized *via* RAFT polymerization and characterized. Subsequently, this polymer was reacted with a series of long-chain alkynols (refer to Chapter 3) to yield hydrocarbon bottlebrush polymers with varying side-chain lengths. The obtained polymers were characterized *via* NMR, SEC, DSC and IR spectroscopy. Notably, fluorine NMR analysis revealed that transesterification reactions showed no remaining fluorine resonances, thus evidencing full conversion and a high grafting density. Both SEC and DSC analyses showed a strong side chain length-dependance in their curves and thermograms, respectively. The obtained SEC molar mass values indicate a change in architecture towards less folded polymer particles due to increasing steric demand of the grafted hydrocarbons, *i.e.*, the formation of a cylindrical structure. The thermal behavior of the polymers changed with increasing side-chain length and melting transitions were observed above a threshold of 13 carbon atoms (including the alkyne moiety). With the longest employed alkynol for the grafting, a high melting temperature T_m of 77.4 °C for the corresponding bottlebrush polymer was observed.

As the obtained polymers carried a terminal alkyne moiety on their side-chains, further derivatization of the polymers was investigated, based on this group. Deviating from the standard alkyne-focused reactions, such as copper(I)-catalyzed alkyne-azide cycloadditions (CuAAC) or thiol-yne reactions, a three-component reaction (3-CR) was chosen to enable the attachment of broader substrate scopes such as alcohols. In order to examine the possible synthesis of core-shell bottlebrush copolymers (cs-BBCPs) a low molar mass alcohol, *i.e.*, methoxy polyethylene glycol (MW \sim 400 g mol⁻¹) was reacted in the 3-CR with tosyl azide as the third component. The successful attachment of the PEG chains was evidenced *via* NMR and IR spectroscopy as well as SEC and DSC. The collected NMR data showed all anticipated resonances, but also revealed a moderate conversion of roughly 70%. The linkage *via* the sulfonyl imidate motif was further proven through the appearance of the S=O (sulfonyl) and C=N (imine) absorption bands. Notably, the SEC trace showed a strong shift to a higher molar mass of 22.4 kg mol⁻¹ and the thermogram revealed a still high melting temperature (62.3 °C) and a lowered enthalpy of fusion compared to the parent polymer brush. Thus, an application of this material as a polymer electrolyte was deemed applicable.

6 Pentafluorophenyl Vinyl Sulfides and their Polymerization²

6.1 Motivation

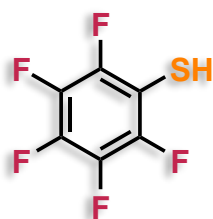


Figure 6.1: The chemical structure of PFTP.

Fluorinated polymers are a subclass of polymers that contain fluorine atoms in their structure. Due to the extremely stable carbon-fluorine bond these polymers exhibit remarkable properties such as hydrophobicity, low surface energy, high thermal stability and excellent chemical resistance.^[99] While “classical” fluoropolymers such as Teflon (polytetrafluoroethylene, PTFE), poly(vinylidene difluoride) (PVDF) were extensively investigated in the last century, more recently pentafluoro-derivatives emerged as viable building-blocks in polymer science.^[72,99,179,180] As described in Chapter 2.4.1, different pentafluoro derivatives were used in the context of polymer science. For example, the post-polymerization reaction *via* substitution of pentafluorophenyl (PFP) active esters or *para*-fluoro substitution of fluorinated poly(acrylates)s have been extensively studied.^[180,181] Furthermore, the *para*-fluoro thiol reaction (PFTR) has been used not only for ligation chemistry, but also for the synthesis of polymeric networks through the use of linkers carrying multiple PFP moieties.^[182] To this end, pentafluorobenzene-derived motifs such as PFP esters or pentafluorostyrene remain the most commonly employed in polymer science.^[180,183] However, the structurally related thiol, *i.e.*, 2,3,4,5,6-pentafluorobenzene-1-thiol or pentafluorothiophenol (**PFTP**) (Figure 6.1) only found sporadic use as a ligand in coordination chemistry^[107] or as precursor for electrolyte material additives^[109] and remains unused in the realm of polymer science. This is in strong contrast to the available chemistry of this molecule.

In 1975, LEONG and PEACH reported a series of addition reactions of **PFTP** to a broad range of substrates such as alkenes, alkynes, aldehydes, ketones, oxiranes, diazo compounds, nitriles and others.^[110] In the context of the previously mentioned *para*-fluoro thiol reaction, the products of these addition reactions should be suitable substrates for the selective nucleophilic aromatic substitution. As the focus of this thesis is laid on the use of alkynes, their reaction with **PFTP** should be tested and subsequently evaluated whether the product obtained can undergo a *para*-fluoro thiol reaction. Through the use of aliphatic dialkynes, this strategy should yield a symmetric monomer that can be polymerized *via* PFTR with dithiols (Scheme 6.1).

² Parts of this subchapter - including text, figures, tables and schemes - will be subsequently published in the near future.

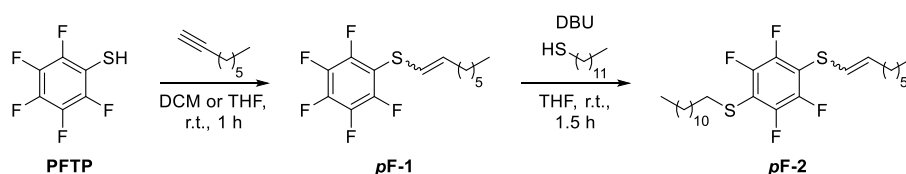


Scheme 6.1: Depiction of the general concept for the synthesis of a symmetrical monomer based on PFTP and dialkynes and subsequent polymerization via *para*-fluoro thiol reaction with dithiols.

6.2 PFPT Hydrothiolation & Monomer Synthesis

As mentioned above, pentafluorothiophenol can undergo addition reactions to unsaturated substrates such as alkenes and alkynes. In the case of alkynes, the resulting structural motif, pentafluorophenyl vinyl sulfide, has several potential sites for further modification. For example, the fluorinated ring should allow for (*para*-)substitution reactions with nucleophiles and the vinyl group can be addressed *via* alkene chemistry.^[184–186] Prerequisite for the successful use of the *para*-fluoro thiol reaction on such a substrate is its stability under the employed conditions, as further substitutions on the neighboring fluorine atoms are theoretically possible. As no reports of such structural motifs under similar conditions exist, a model compound was synthesized to validate productive reaction parameters and ensure the stability of this structural motif.

Thus, first the reaction of pentafluorothiophenol (**PFPT**) with terminal alkynes and the subsequent fluorine substitution was investigated. For this purpose, **PFPT** was reacted with 1-octyne to obtain a model substrate for the to-be-investigated *para*-fluoro thiol reaction. The obtained pentafluoro vinyl sulfide **pF-1** was then reacted with 1-dodecanthiol in the presence of DBU as a base (Scheme 6.2).



Scheme 6.2: Reaction scheme for the hydrothiolation of 1-octyne with PFPT towards pentafluoro vinyl sulfide **pF-1** and subsequent *para*-fluoro thiol reaction with 1-dodecanthiol in THF.

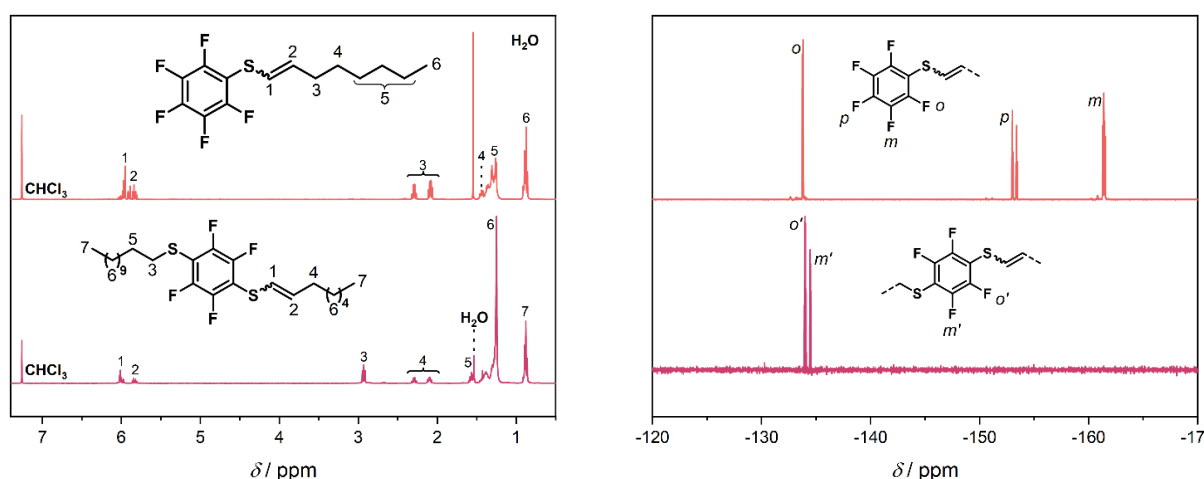
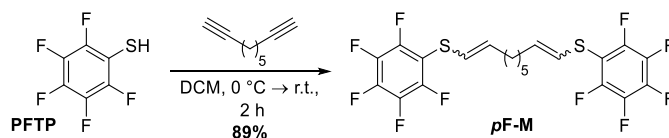


Figure 6.2: Comparative ¹H (left, 400 MHz) and ¹⁹F (right, 377 MHz) spectra of pentafluoro vinyl sulfide **pF-1** (top) and *para*-fluoro thiol reaction product **pF-2** (bottom) evidencing successful mono-substitution with no apparent side-reactions.

As can be seen in the ^1H and ^{19}F NMR spectra in Figure 6.2 both reactions were successful under the employed reaction conditions (DCM/THF, r.t., 1 – 1.5 h). First, the hydrothiolation with **PFTP** is evidenced by the appearance of the vinyl proton resonances (Figure 6.2, *left*, denoted as 1 and 2) and their adjacent methylene protons (denoted as 3). As expected, the reaction yielded a mixture of isomers which is reflected in the splitting of the allylic proton resonances (5.96 & 5.87 ppm), with the further downfield shifted which is attributed to the *E*-isomer. From the integration values of these resonances, no apparent isomer is favored in the reaction, independent of the employed reaction solvent (THF or DCM). Notably, only the *anti*-MARKOVNIKOV product was spectroscopically observed. Second, the employed conditions for the *para*-fluoro thiol reaction were compatible with the desired product. 1-Dodecanthiol was the choice of nucleophile due to lessened odor, and DBU as the base, as it is known to be an efficient promotor for the PFTR.^[118,187] The successful incorporation of the dodecyl chain is evidenced by the newly appeared proton resonances (Figure 6.2, *bottom left*, denoted as 3, 5 and 6). Satisfactorily, no reaction occurred on the vinyl moiety as the corresponding resonances remained intact, although a slight excess (0.1 eq) of the thiol was used. The nucleophilic aromatic substitution was particularly evident from the collected ^{19}F NMR spectra (Figure 6.2, *right*). Here, the complete disappearance of the *para*-fluorine as well as a shift of the *meta*-resonance from -161 ppm (Figure 6.2, *top right, m*) to -134 ppm (Figure 6.2, *top right, m'*) confirmed the formation of the desired mono-substituted product. Thus, it was concluded that the new structural motif of a pentafluoro vinyl sulfide is a suitable candidate for the polymerization reactions under the employed conditions.

With these results in hand, subsequently a suitable monomer for the polymerization *via* the *para*-fluoro thiol reaction was synthesized. For this purpose, a commercially available diyne, i.e. 1,8-nonadiyne, was reacted with **PFTP** under the same conditions as before (*vide supra*), yielding the symmetrical di(pentafluoro vinyl sulfide) monomer **pF-M**, which was obtained in 89% yield as a mixture of isomers that could not be separated. 1,8-Nonadiyne was chosen as the initial dialkyne, as it provides a long enough spacer between the two reaction sites during hydrothiolation, thus preventing a possible loss of yield due to steric hindrance of the bulky fluorinated rings. Repeated syntheses of **pF-M** in THF gave similar yields (*e.g.*, 86 – 89%), successfully even on multi-gram scale. In similar manner, the purity of the product was assessed by proton and fluorine NMR (Figure 6.3). Similar to **pF-1**, the spectrum of **pF-M** reveals the newly formed vinyl (5.95 and 5.82 ppm) as well as the desired fluorine resonances (-133, -153 and -161 ppm; *ortho*-, *para*- and *meta*-fluorine, respectively).



Scheme 6.3: Reaction scheme for the hydrothiolation of 1,8-nonadiyne with **PFTP** towards the difunctional monomer **pF-M** in DCM.

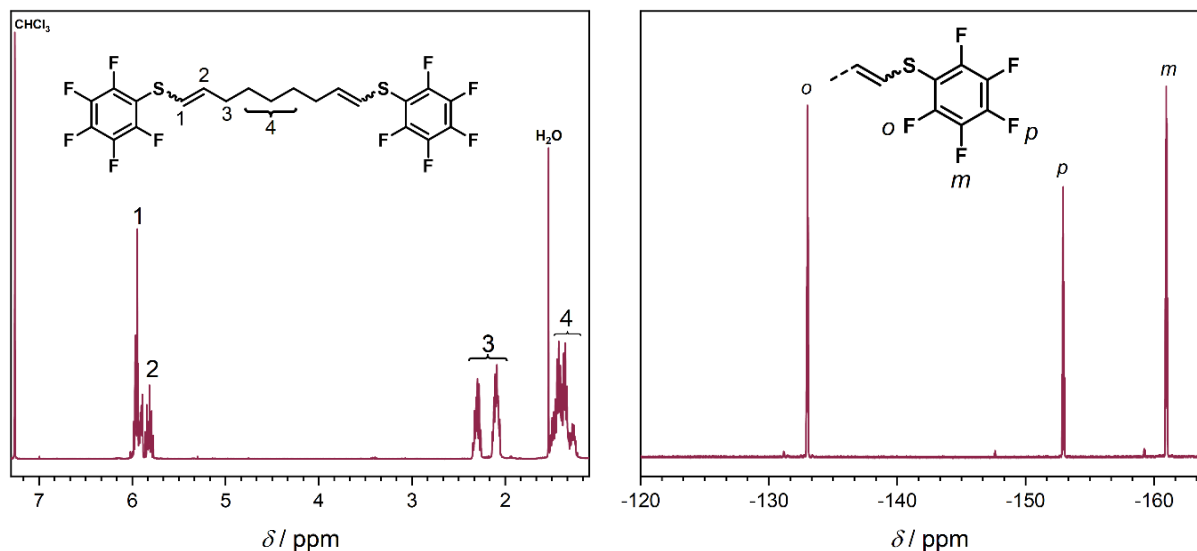
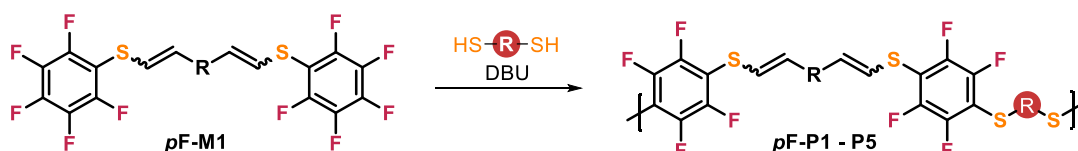


Figure 6.3: ^1H NMR (left, 400 MHz) and ^{19}F NMR (right, 377 MHz) spectra of **pF-M** showing the characteristic vinyl as well as fitting fluorine resonances for the desired symmetrical monomer.

Thus, the relevant di(pentafluoro vinyl sulfide) monomer **pF-M** could be synthesized in one step by a hydrothiolation reaction starting from commercially available substrates in excellent yield (89%). Subsequently, polymerization reactions with different dithiols were conducted in a systematic manner. The synthesis and characterization of targeted polymers as well as further post-polymerization reactions are described in the following section.

6.3 Polymerization *via para*-Fluoro Thiol Reaction

Upon the successful synthesis of the new difunctional monomer **pF-M**, its polymerizability with various dithiol derivatives should be investigated. To demonstrate the versatility of the employed strategy and show the ability to fine-tune the final polymer properties, a series of structurally diverse dithiols was selected.



Scheme 6.4: General reaction scheme for the synthesis of fluorinated polymers *via para*-fluoro thiol reaction of the difunctional pentafluoro vinyl sulfide monomer **pF-M** and a series of dithiols.

The chosen commercially available dithiols comprise a variety of structural motifs, thus mimicking other common polymer classes. These thiols include an aliphatic dithiol (**DT2**) representing generic polymer backbones, an ether-linked dithiol (**DT1**) mimicking PEG-ylated chains, dithiothreitol (**DT3**) representing functional, hydroxy-decorated polymers, a polyester-like thiol (**DT4**) and an aromatic specimen (**DT5**) as shown in Figure 6.4

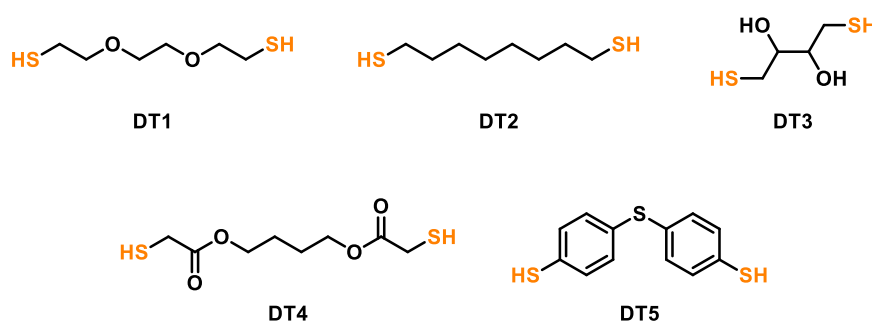


Figure 6.4: Depiction of the series of dithiols used for the *para*-fluoro thiol polymerization.

As only few synthetic procedures for the build-up of polymers *via para*-fluoro thiol reaction have been reported in the literature, initial conditions were adopted from those reports.^[118,188,189] To this end, for the first investigations **DT1** was chosen as the dithiol component. To ensure efficient deprotonation 1,8-diazabicyclo(5.4.0)undec-7-ene (DBU) was used as the base. Furthermore, 2.2 equivalents of base were employed as it was shown, that less-than-stoichiometric amounts have a negative effect on the maximum attainable molecular mass.^[188] First, the kinetics of the devised polymerization was investigated. Hence, a screening of the polymerization in different solvents was conducted first. For better comparison of the reactivity of the different dithiols (based on the literature), in the initial phase of the project, the polymerization time was set to 15 minutes. Thus, a number of different polar and nonpolar

solvents was tested for the polymerization, and the obtained polymers were subsequently analyzed by SEC. The results are summarized in Table 6.1. The corresponding SEC curves are shown in **Figure 9.3** in the Appendix.

Table 6.1: Summary of the solvent screening of **pF-M** with dithiol **DT1** under standard conditions.

Entry	Solvent	Concentration [mol·L ⁻¹]	M_n [kg·mol ⁻¹] ^{a)}	M_w [kg·mol ⁻¹] ^{a)}	\mathcal{D} (M_w/M_n)
1	Toluene ^{b)}	~0.2	42.1	275	7.3
2	MeCN ^{b)}	~0.2	50.2	214	4.3
3	Dioxane	~0.2	38.4	264	6.8
4	DMac	~0.2	31.7	245	7.7
5	DMF	~0.2	22.2	90.1	4.0
6	DMF	0.5	26.5	76.7	2.8
7	DCM	0.5	15.7	29.6	1.9
8	THF	0.5	29.7	141	4.7
9	THF	~0.2	27.3	93.4	3.4
10	THF ^{c)}	1	-	-	-
11	THF ^{d)}	0.5	14.3	27.9	1.9
12	THF ^{d,e)}	0.2	29.5	47.1	1.6
13	THF ^{d,f)}	0.2	33.8	67.4	1.9

Standard conditions: r.t., 15 min. ^{a)} Determined by THF-SEC with PS standards; ^{b)} Resulted in coagulation. Results correspond to soluble fraction. ^{c)} Instant crosslinking. ^{d)} Performed at 0 °C. ^{e)} Runtime: 3h. ^{f)} Runtime: 6h.

It was possible to obtain polymeric material in both polar and nonpolar solvents with a broad distribution of number average molecular masses ranging from 14 to 50 kg·mol⁻¹ with expected dispersity (\mathcal{D}) values for step growth polymerizations. In some solvents (such as acetonitrile and toluene), gelation or crosslinking occurred, and thus only the soluble fractions could be analyzed, which showed very broad distributions (Table 6.1, Entry 1 – 3). The latter could be attributed to possible side reactions, involving additional fluorine substitutions on the aromatic ring, which lead to potential crosslinking. Judging from the SEC curves, DCM and THF appeared to be the most promising solvents, as they resulted in the formation of polymers with monomodal distributions (shown in Figure 6.5). Due to its higher boiling point compared to the other solvents, THF appeared to be the favored solvent.

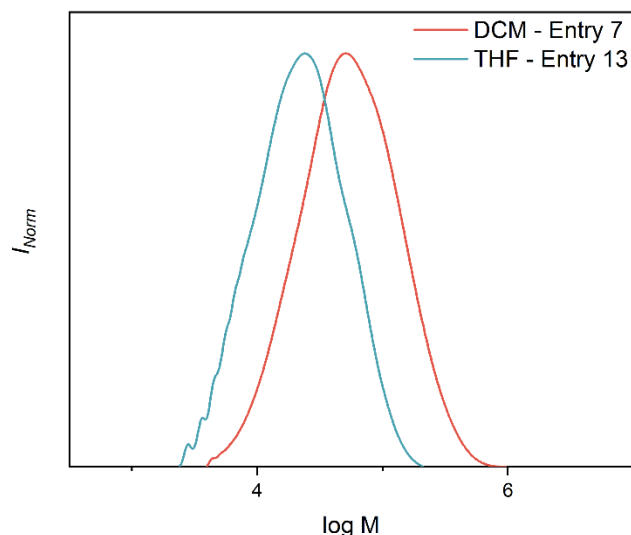


Figure 6.5: SEC traces of **pF-M** with dithiol **DT1** in DCM and THF yielding monomodal distributions.

A detrimental effect was observed in DMF, as crosslinking was often observed in this solvent. Increasing the concentration from around 0.2 mol L^{-1} to 0.5 mol L^{-1} slightly improved the obtained values. A further increase towards concentrations of 1 M (Table 6.1, Entry 10) however, resulted in the instant formation of crosslinked material upon the addition of the base, *i.e.*, DBU. One possible reason for this is the slight exothermic reaction is released at the point of base addition. In high concentrations the dissipation of heat is hindered and thus side reactions resulting in crosslinking are favored. However, a control experiment (0.5 mol L^{-1} in DMF; *not shown*) with dropwise base addition did not yield improved results compared to Entry 6 in Table 6.1. On the contrary, lowering the temperature towards $0 \text{ }^{\circ}\text{C}$ resulted in narrower distributions, however, accompanied with lower molecular masses (Table 6.1, Entry 11 – 13). Interestingly, at this temperature ($0 \text{ }^{\circ}\text{C}$) the concentration as well the prolongation of polymerization time to three or six hours only had a small effect on the obtained masses. Based on these results, the optimum conditions were determined to be THF or DCM as the solvent with a concentration of either 0.2 mol L^{-1} or 0.5 mol L^{-1} and a reaction time of 15 minutes.

Based on the above conditions, the polymerizations with the remaining dithiols **DT2** – **DT5** were conducted in a similar fashion. Due to the deviating nucleophilicities of the employed dithiols (*e.g.*, less reactive **DT3** to very reactive **DT5**), the employed conditions were adjusted in order to minimize crosslinking and assure monomodal distributions. Accordingly, the remaining polymerization results are summarized in Table 6.2 with Entry 1 as a reference for **DT1**.

Table 6.2: Overview of the polymerization results of **pF-M** with selected dithiols **DT2 – DT5**.

Entry	Monomer	Solvent	Concentration [mol·L ⁻¹]	T [°C]	M _n [kg·mol ⁻¹] ^{a)}	M _w [kg·mol ⁻¹] ^{a)}	Đ (M _w /M _n)
1	DT1	THF	~0.2	r.t.	27.3	93.4	3.4
2	DT2	DCM	0.5	r.t.	38.1	147	3.8 ^{b)}
3	DT2	DCM	0.5	0	41.2	226	5.4 ^{b)}
4	DT2	DMF	0.5	0	-	-	- ^{c)}
5	DT2	THF	0.2	-40	37.8	143	3.7
6	DT2	THF	0.5	-40	58.8	193	3.2
7	DT3	THF	0.5	r.t.	39.4	110	2.7 ^{d)}
8	DT4	THF	0.5	r.t.	15.6	59.4	3.7
9	DT5	THF	0.5	r.t.	49.7	399	8.0 ^{b)}
10	DT5	THF	0.5	0	38.9	134.1	3.4 ^{e)}
11	DT5	THF	0.2	r.t.	6.51	9.33	1.4 ^{f)}
12	DT5	THF	0.2	r.t.	13.0	27.8	2.1 ^{g)}

Standard runtime: 15 min. ^{a)} Determined by THF-SEC with PS standards; ^{b)} Resulted in coagulation. Results correspond to soluble fraction. ^{c)} Instant crosslinking. ^{d)} Determined by DMAc-SEC with PS standards. ^{e)} Gelation observed within 5 min; reaction quenched. ^{f)} Obtained oligomers. ^{g)} Reaction time: 3 h.

As can be seen from the summary shown in Table 6.2, the successful polymerization could be achieved with all dithiols yielding molecular masses in the range of 6 to 58 kg mol⁻¹. Interestingly, the differences in reactivity of the chosen nucleophiles became apparent, as it was essential to lower the reaction temperature to 0 °C (compare Entry 3 vs. Entry 5 and Entry 9 vs. Entry 10). The more nucleophilic dithiols **DT2** and **DT5** tended towards crosslinking (Entry 2, 3, 9) while the less reactive **DT3** and **DT4** yielded polymers at room temperature in a homogenous fashion. Once more, the latter can be attributed to additional fluorine substitution reactions on the fluorinated moieties. In the case of **DT2**, it was even necessary to lower the temperature to -40 °C to obtain near monomodal distributions. Similarly, the polymerizations with **DT5** coagulated at 0.5 molar concentrations, even at 0 °C after 5 minutes (Entry 9 & 10). The SEC analyses of the associated soluble fractions showed polymers with high number average molecular masses of 49.7 kg mol⁻¹ (Entry 9) and 38.9 kg mol⁻¹ (Entry 10), but with substantially high dispersity values (*e.g.*, Đ = 8.0 and 3.4, respectively). With a reduced concentration of 0.2 mol L⁻¹ however, after 15 minutes the obtained SEC curve showed only an oligomeric composition of the material. With a prolonged runtime of three hours, polymeric material with a molecular mass of 13.0 kg mol⁻¹ (Entry 12) could be obtained.

Thus, it was evidenced that the employed strategy for the synthesis of polymers *via* the *para*-fluoro thiol reaction is expedient. The obtained polymers were analyzed by means of ^1H -, ^{19}F NMR and IR spectroscopy, as well as SEC, DSC and TGA.

In an exemplary manner, Figure 6.6 shows the obtained proton and fluorine spectra with the resonance assignments.

As can be seen from Figure 6.6, the proton spectra for all obtained polymers evidence the successfully incorporated dithiol monomers, as can be seen from the newly appeared chemical shifts corresponding to their respective structures, *e.g.*, the aromatic resonances denoted as **1** (at 7.24 ppm) in the proton spectrum of **pF-P5**. Furthermore, the stability of **pF-M** under the employed polymerization conditions is again proven. First, the proposed structure is confirmed through the chemical shifts of the vinyl resonances around 6 ppm (compare with Figure 6.3). Second, all recorded fluorine spectra show the disappearance of the *para*-fluorine atom of the monomer (-153 ppm; compare Figure 6.3 *right*) and the desired characteristic shift of the *meta*-positioned atom on the aromatic rings. Interestingly, the high sensitivity of the ^{19}F NMR shows slightly different shaped resonances depending on the electronic nature of the employed dithiol.

Furthermore, ATR-IR spectroscopic analyses confirmed the previous results, as the presence of characteristic functional groups is evidenced by the appearance of the corresponding absorption bands. Exemplarily, the most meaningful spectra are depicted in Figure 6.7. Here, the IR spectra of the monomer **pF-M** (*top*), **pF-P3** (*middle*) and **pF-P4** are compared. Most notably, the absorptions for the C=C bending vibrations (*orange box*) around 1000 cm^{-1} , corresponding to the vinyl group, are present in all polymer spectra, which again proves that the vinyl group is stable under the employed conditions and also no further thiol addition takes place. Functional groups relevant to the polymer structure, such as the hydroxyl groups in the case of **pF-P3** are represented by the broad absorption at 3350 cm^{-1} (*blue box*). Similarly, the ester groups of **pF-P4** (*green box*) are clearly represented at 1730 cm^{-1} .

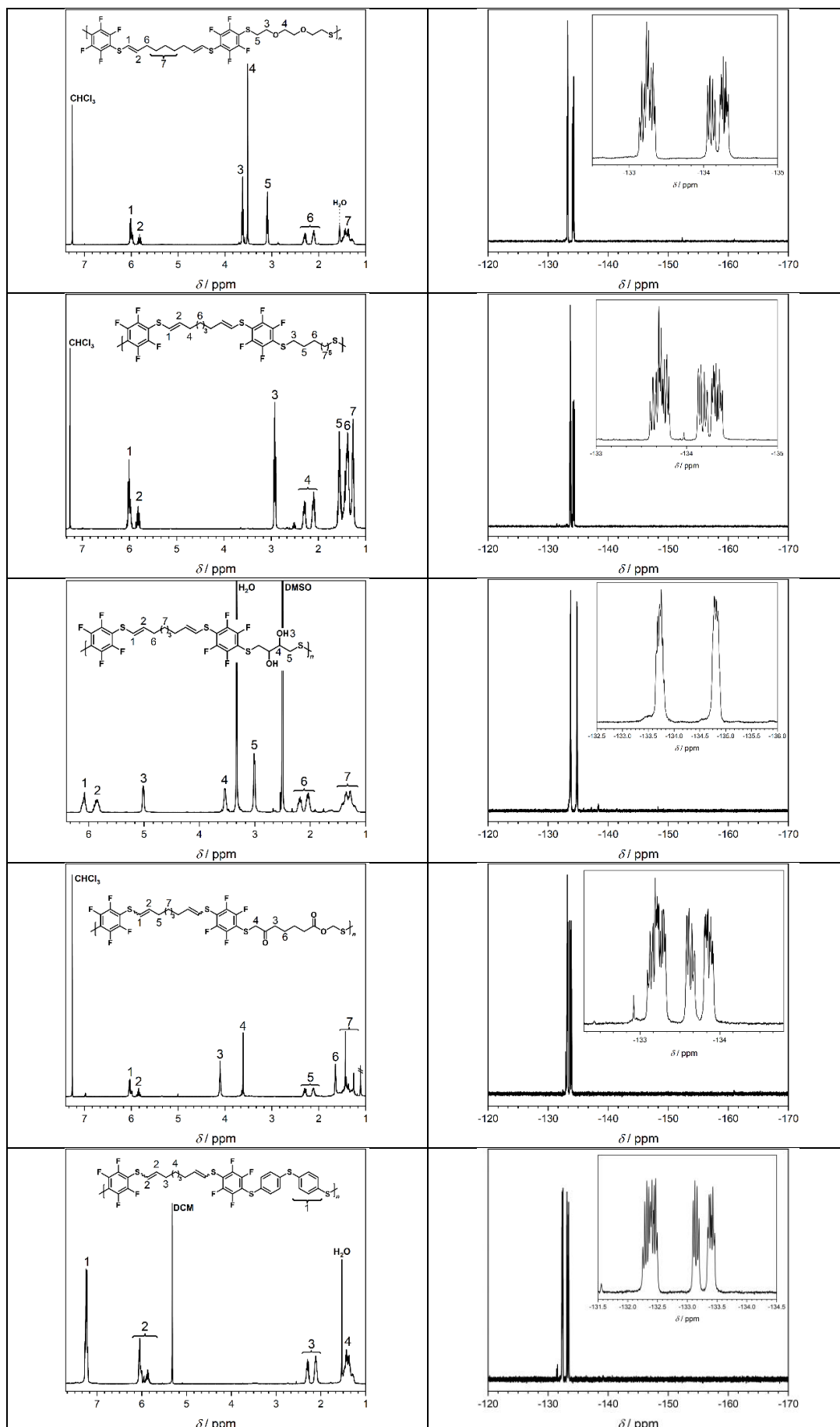


Figure 6.6: Depiction of the ^1H (left) and ^{19}F NMR (right) spectroscopic investigations of **pF-P1** – **pF-P5** (descending order) and their respective signal assignments.

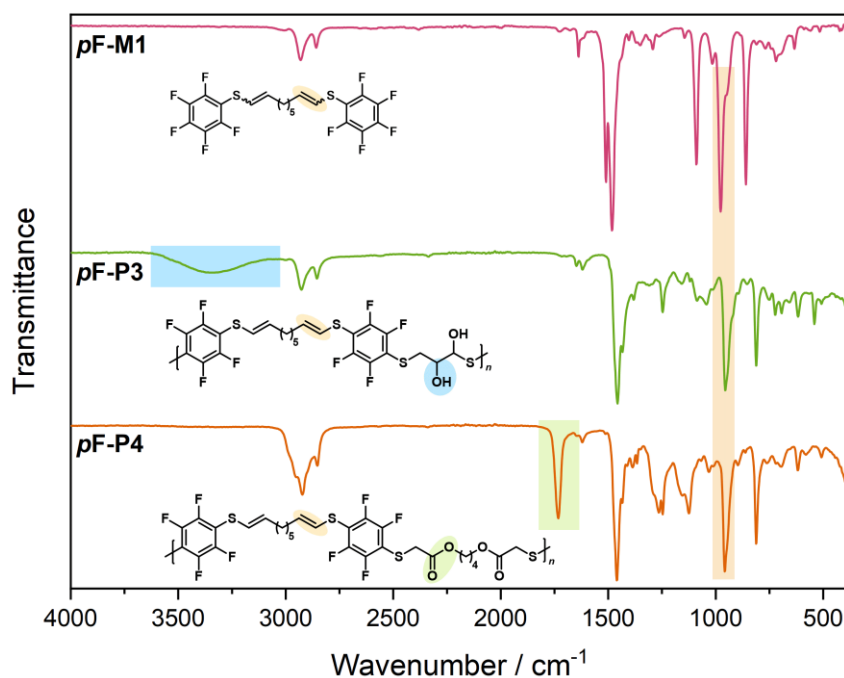


Figure 6.7: Stacked IR-Spectra of monomer **pF-M** (top), **pF-P3** (middle) and **pF-P4** (bottom). The polymer-characteristic IR bands are color coded: **pF-P3**: hydroxyl group – blue; **pF-P4**: ester group – green).

Finally, the thermal properties of the obtained polymers were investigated by differential scanning calorimetry (DSC) and thermogravimetric analysis (TGA). The obtained results are summarized in Table 6.3. As can be seen from Figure 6.8, the obtained DSC heating curves of the polymers differ, depending on what structural motif was introduced into the polymer backbone through the respective dithiol. All obtained polymers only show glass transition temperatures and no discrete melting points, and are thus in an amorphous state. Notably, the polymers with linear methylene chains, *i.e.*, **pF-P1**, **pF-P2** and **pF-P4**, show a similar heating response with a low glass transition temperatures ranging from -30 to -18 °C. Whereas the shorter and more rigid dithiols, such as **DT3** and **DT5** yielded polymers with a much higher T_g around 20 °C. Interestingly, the incorporation of oxygen atoms in the repeating unit, instead of a bare methylene chain, only marginally increased the glass transition temperature, while the incorporation of hydroxy groups on the chain drastically impacted the thermal behavior through the formation of hydrogen bonds. In the case of **pF-P5** the planar aromatic rings enabled π - π stacking between the chains and thus a higher energy is necessary to induce the state transition. Considering the general thermal stability of the obtained materials, the deviations within the series are only minor as the onset temperatures of the thermal degradations begin at around 300 °C and increase up to 328 °C. This stands in strong contrast

to the facile degradation of these polymers that can be easily triggered by means of oxidative or radical treatment (refer to Chapter 6.4.2).

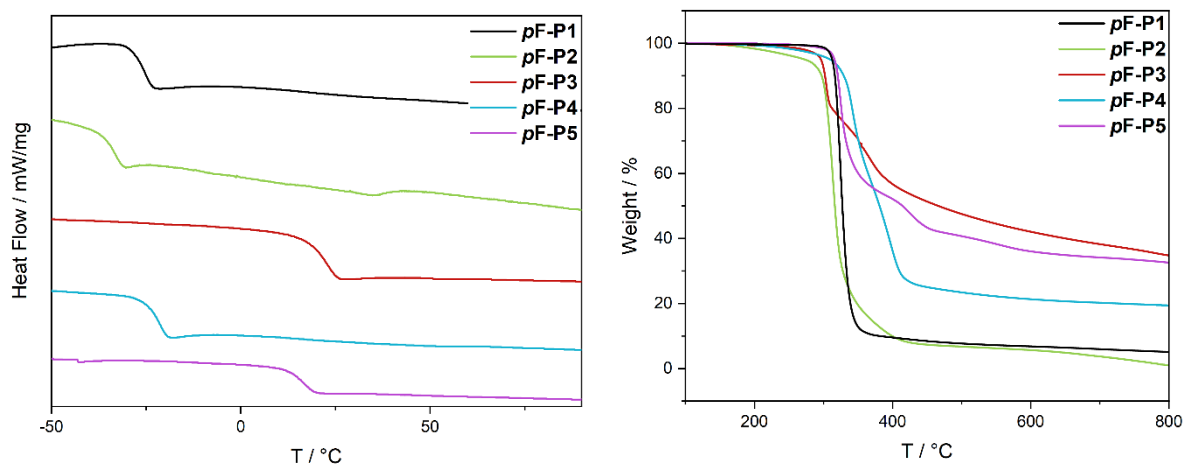


Figure 6.8: Comparative depiction of the DSC (*left*) and TGA curves (*right*) of polymers **pF-P1 - pF-P5**.

Table 6.3: Summary of the thermal properties obtained *via* DSC and TGA analyses.

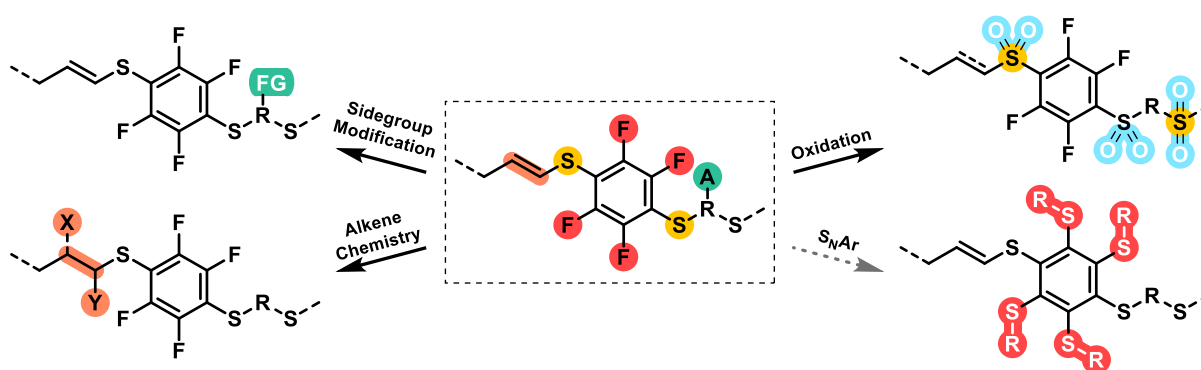
Polymer		T_g [°C]	T_o [°C] ^{a)}
pF-P1		-29.6	317
pF-P2		-33.2	302
pF-P3		21.4	297
pF-P4		-22.1	328
pF-P5		16.0	317

^{a)} Onset temperature of thermal decomposition.

6.4 Post-Polymerization Modification

As mentioned in the previous chapter, the general polymer structure that is obtained from the pentafluoro vinyl sulfide monomers should be susceptible to a series of different post-polymerization functionalization reactions that are derived from the incorporated functional groups. Following a post-polymerization approach, three distinct functional groups can be identified that possibly allow for further derivatization of the polymer structure. The devised strategies are depicted in Scheme 6.5. Beginning with the dithiol, such substrates can be selected that carry further functional groups, which can be chemically accessed for derivatization (*top left*). Next, the ring-adjacent sulfur atoms can be oxidized to the corresponding sulfoxides, thus changing the polymer properties (*top right*).^[190] Furthermore, the internal double bond opens up possibilities to use well-investigated alkene chemistry for transformations on the polymer backbone (*bottom left*). The often-employed thiol-ene reaction as well as halogenation reactions stand out in particular in this context.^[191,192] Lastly, the remaining tetrafluorobenzene-motif offers the possibility to further derivatize the aromatic ring *via* nucleophilic aromatic substitution reactions (S_NAr) (*bottom right*).^[193]

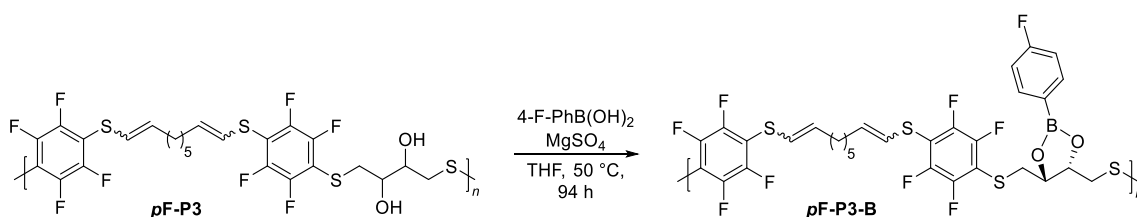
However, since the nucleophilic aromatic substitutions of *para*-substituted tetrafluorobenzene moieties have been covered intensively in literature,^[193–198] investigations for the derivatization on this part of the structure were excluded from this project. Thus, the synthetic potential of the first three mentioned functional moieties shall be investigated.



Scheme 6.5: Schematic depiction of the theoretically possible PPM strategies based on the available functional groups/atoms embedded in the polymer structures.

6.4.1 Derivatization based on the Dithiol Functional Groups

The use of different nucleophiles for the polymerization enables further chain modification by employment of functional dithiols, such as dithiothreitol, *i.e.*, **DT3**. After polymerization, these functional groups can be addressed for further reactions. In the case of **pF-P3** the two hydroxy groups of dithiothreitol can be used for the formation of acetals,^[199] (silyl) ethers^[200,201] or (boronic) esters^[202,203] among others. Recently, the condensation of diols with boronic acid or their derivatives was increasingly employed for the synthesis of stimuli-responsive biomedical materials, such as dynamic covalent networks or boronic ester-based hydrogels.^[204] Thus, the formation of boronic esters on the glycol motifs in the backbone of **pF-P3** was investigated.



Scheme 6.6: Reaction scheme of the boronic ester formation of **pF-P3** with

The ester formation was carried out with 4-fluorophenylboronic acid, as the additional fluorine atom allows facile tracking of the reaction progress *via* ¹⁹F NMR and **pF-P3** is lacking any aromatic protons whose resonances could overlap with the employed substrate. After a reaction time of four days, the esterified polymer **pF-P3-B** could be obtained upon a basic aqueous workup and precipitation in cold petrol ether, and was characterized by NMR and SEC. The obtained results are depicted in Figure 6.9.

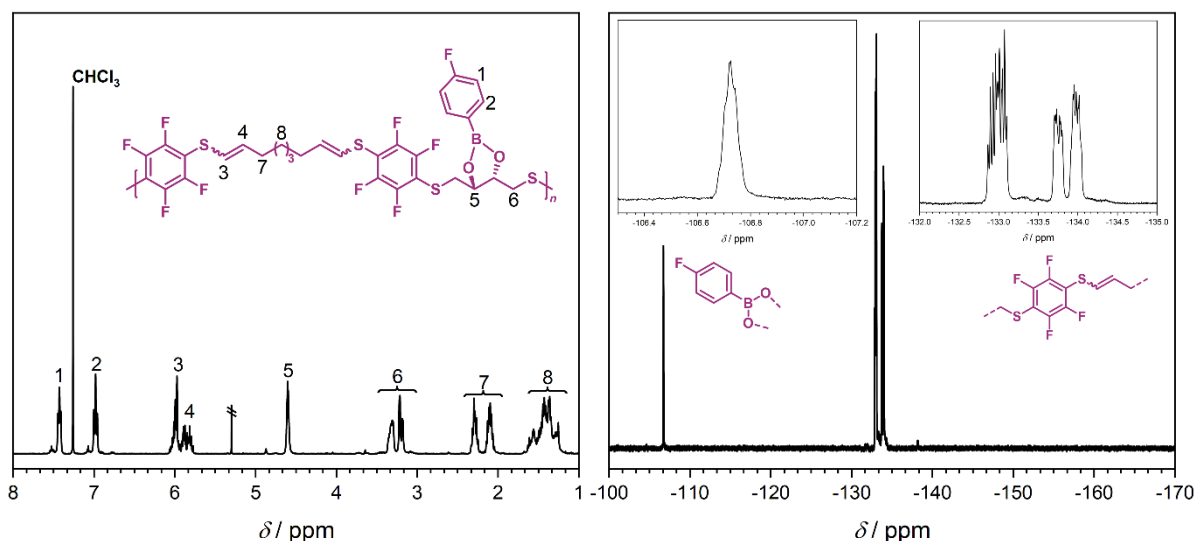


Figure 6.9: Analysis of polymer **pF-P3-B** *via* ¹H and ¹⁹F NMR, depicting the newly appeared aromatic protons as well as the additional fluorine resonance.

Proton NMR analysis revealed that the obtained polymer showed full conversion of the hydroxyl groups, which is indicated by the shifted resonances of the tertiary protons at 4.60 ppm. The incorporation of the phenyl moiety is furthermore evidenced by the appearance of the aromatic proton resonances at 7.43 and 6.98 ppm in addition to the ^{19}F NMR spectrum at -106 ppm. The successful transformation is also confirmed *via* SEC analysis (Figure 6.10). Here however, the obtained SEC trace is shifted towards a lower molecular mass compared to the parent polymer. This phenomenon can be possibly explained through the ability of the introduced 4-fluoropheny groups to form π - π -stacking interactions. This would in return stabilize a more compact folded polymer globule, which is expressed in a lower hydrodynamic radius r_{H} and thus an apparent lower molecular mass in the SEC measurement. Interestingly, Weck *et al.* employed a combination of structurally similar phenyl and 2,3,4,5,6-pentafluorophenyl groups on a triblock polymer to force in-chain folding *via* π - π -stacking interactions, thus further validating the observed phenomenon as a compaction event.^[205] A depiction of a hypothesized folding motif is shown in Figure 6.10.

In summary, this example showed that free functionalities in the polymer backbone, brought in through careful choice of the employed dithiol, can be further used for post-polymerization functionalization reactions, which can lead to possibly interesting property changes of the final polymers.

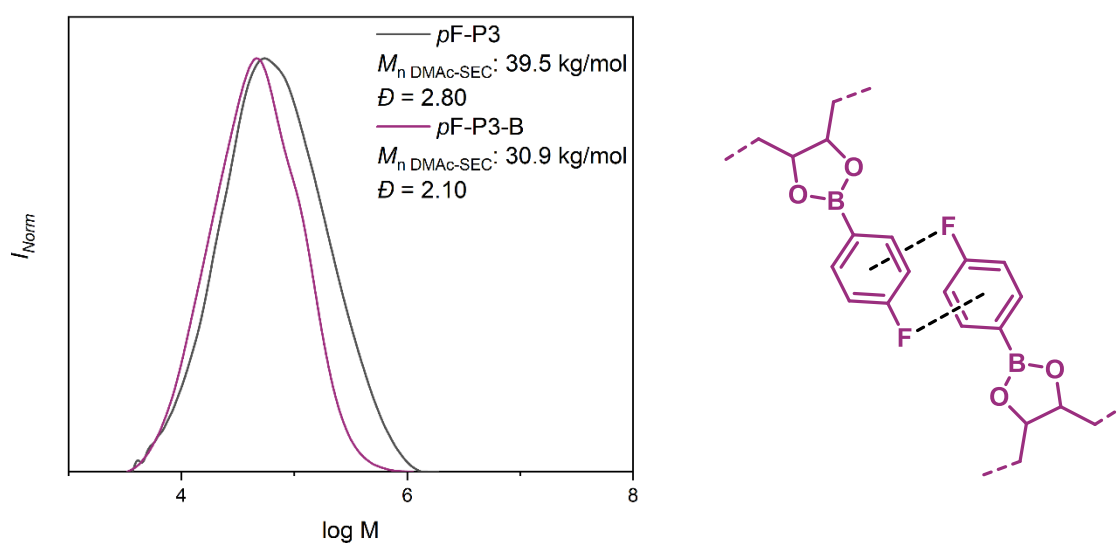
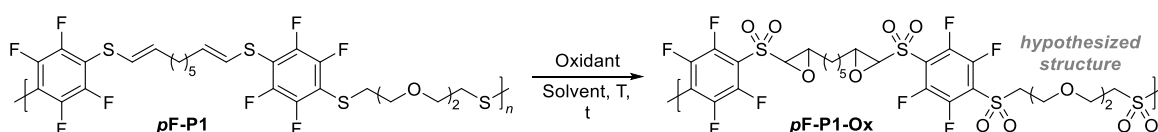


Figure 6.10: SEC analyses of **pF-P3-B** and its parent polymer **pF-P3** (*left*) and a simplified drawing of the hypothesized π - π -stacking interactions.

6.4.2 Derivatization based on Oxidation

One of the most common post-polymerization modifications of polymers decorated with thioether linkages is the oxidation towards their respective polysulfone derivatives.^[190,192,206] This transformation is usually facile and quantitative, and yields polymers with drastically altered thermal characteristics compared to their unoxidized precursors. As the polymers presented in Chapter 6.3 carry sulfur atoms in their backbone linking not only aromatic with aliphatic motifs, but additionally also aromatic groups with vinyl groups, it was of great interest to investigate the oxidation behavior of these materials (Scheme 6.7).



Scheme 6.7: General reaction scheme for the oxidation of **pF-P1** with the originally assumed structure of the oxidized polymer **pF-P1-Ox**.

As several literature protocols for the oxidation of thioethers towards sulfoxides exist, three sets of different conditions were adapted. Potassium peroxymonosulfate (KMPS, *Oxone*[®]) and *meta*-chloroperoxybenzoic acid (*m*CPBA) were initially chosen as oxidants, since both are solid materials and thus easy to handle. Additionally, *Oxone*[®] is water soluble, which facilitates the respective purification. Finally, one approach was carried out with hydrogen peroxide as the adapted literature protocol previously proved to be efficient for the oxidation of polythioethers.^[206] The summarized reaction conditions are depicted in Table 6.4. The reactions were carried out with three different batches of previously synthesized **pF-P1** stemming from the polymerization solvent screening described in Table 6.1.

Table 6.4: Summary of the reaction conditions for the oxidation of **pF-P1**.

Entry	Oxidant	Solvent	Reaction time	Temperature [° C]
1	<i>Oxone</i> [®]	MeCN/DMF	5 d	60
2	<i>m</i> CPBA	DCM	2 d	r.t.
3	H ₂ O ₂	AcOH/THF (2.5:1)	15 min	80

The previously synthesized polymers were dissolved in the respective solvents and treated with the oxidizing agents for the respective time listed in Table 6.4. Depending on the employed reagents, usually an aqueous workup step was conducted to purify the oxidized

materials, and subsequently SEC and NMR analyses were conducted. As can be seen from the SEC traces depicted in Figure 6.11, every oxidation approach led to the degradation of the polymers. The recorded SEC traces indicate that the reaction time directly correlates with the degree of degradation, as the 5 d-long oxidation with *Oxone*[®] yielded smaller oligomers than the 2 d-long *mCPBA* treatment. Interestingly, even the very short reaction time of the hydrogen peroxide reaction led to drastically reduced molecular mass compared to the parent polymer.

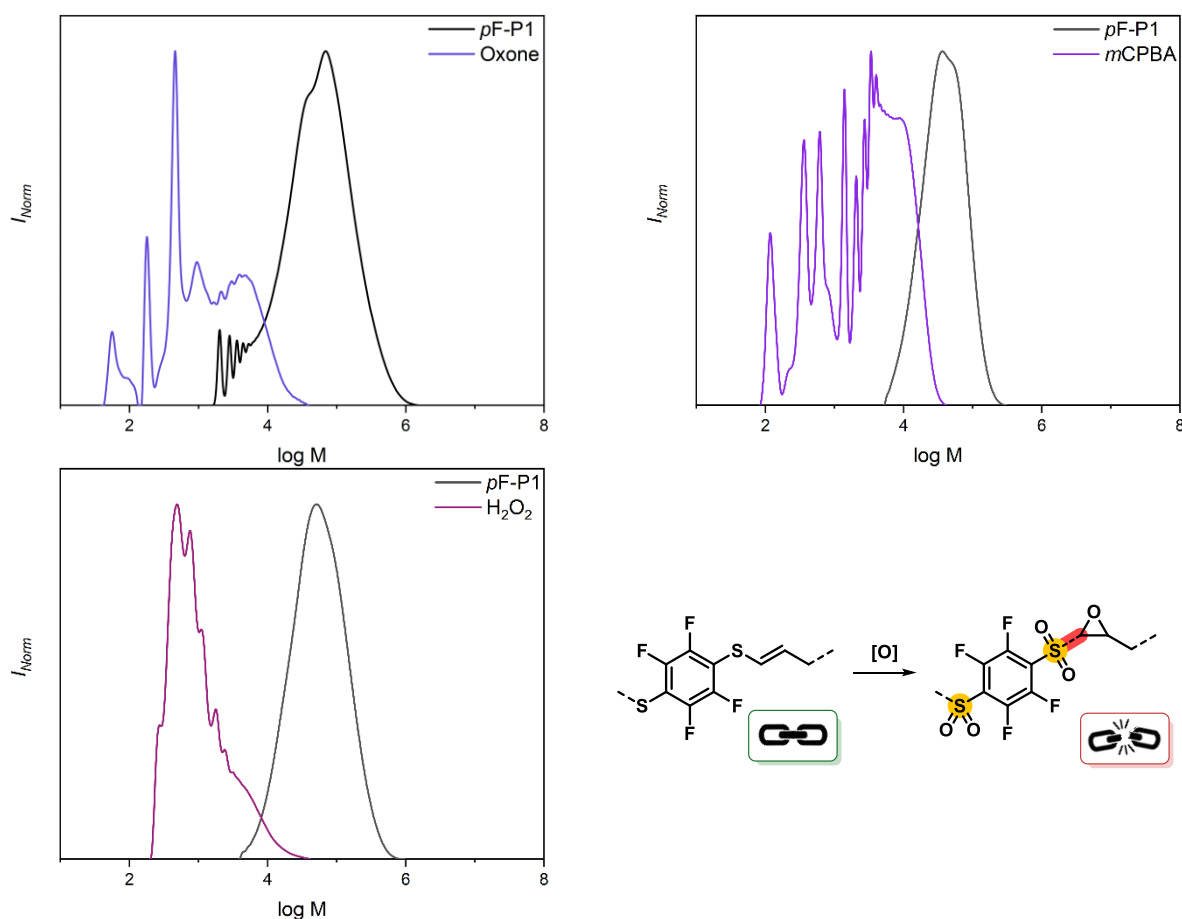
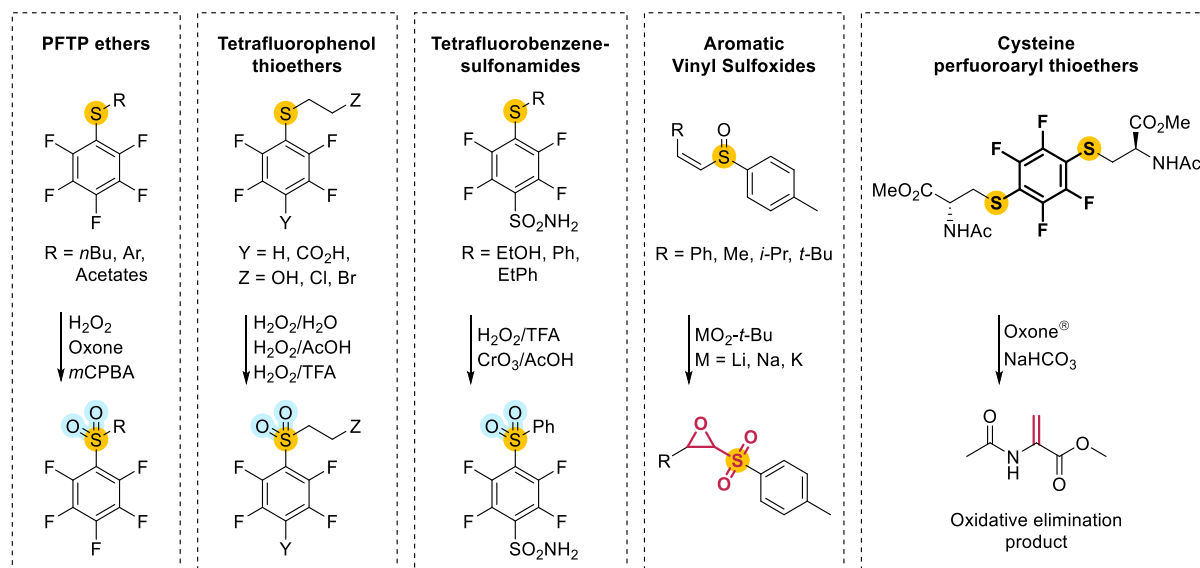


Figure 6.11: Comparative SEC traces of the different batches of **pF-P1** and the obtained oxidized materials after reaction with *Oxone*[®] (*top left*), *mCPBA* (*top right*) and H_2O_2 (*bottom left*). The hypothesized structural breaking point in the polymer backbone is depicted in red (*bottom right*).

In the case of the hydrogen peroxide-oxidation, ^{19}F NMR analysis showed no remaining fluorine resonances in the purified material. This indicates that the linkage towards the aromatic group is degraded and that a polar, water-soluble product is formed which potentially has been removed during the aqueous workup step.

To better understand the mechanism of the oxidative degradation of the polymers, literature research was conducted to find similar structural motifs that were oxidized in similar conditions (Scheme 6.8). To this end it was found that pentafluorothiophenol ethers,^[207–209]

aliphatic tetrafluorophenol thioethers (with and without *para*-substituents),^[210] and 4-thiophenyl-2,3,5,6-tetrafluorobenzenesulfonamides^[211] were oxidized under very similar conditions as the ones employed in the context of this project. Interestingly, DE LA PRADILLA *et al.* reported a protocol for the epoxidation of *cis*-vinyl sulfoxides, albeit not with fluorinated substrates, indicating that an epoxide moiety adjacent to a sulfoxide group is stable under atmospheric conditions.^[212] Unfortunately, no such fluorinated structural motif is reported in literature, indicating the possible instability of such a group.



Scheme 6.8: Summary of literature reports covering oxidation reactions of structurally similar motifs as in **pF-P1**.

Finally, GAVENONIS *et al.* reported the oxidation-elimination of a symmetrical tetrafluorobenzene dithioether which was obtained after reacting a protected cysteine with hexafluorobenzene. Here interestingly, similar conditions were employed as shown in Table 6.4, Entry 1, which resulted in the oxidative elimination of the fluorinated moiety in 42%. No further information, however, was provided on the reaction products or a plausible mechanism and thus a comparison with the observed reaction outcomes in this project is hindered. Finally, partially fluorinated poly(aryl thioether)s carrying the 2,3,5,6-tetrafluorophenyl-motif could be oxidized with H_2O_2 in acetic acid at $100\text{ }^\circ\text{C}$, as reported by KIMURA *et al.*^[213] Although no aliphatic dithiol was used in this study, it seems that the absence of a vinyl sulfide group enables the degradation-free oxidation of such polymers.

Based on the obtained results for the three oxidation reactions, as well as from the literature research, it can be concluded that a polymer degradation is probably occurring at the pentafluoro vinyl sulfide moiety (a depiction is shown in Figure 6.11, *bottom right*), as

numerous reports describe the oxidation of penta- and tetrafluoro (di)thio ethers with the same oxidants as shown in Table 6.4.

Mechanistically the degradation is most plausibly explained by the weakening of the sulfur-carbon bond caused through the oxidation processes of both the sulfur and the adjacent double bond. The resulting structure, comprising of an electron-deficient tetrafluoro(sulfonyl)phenyl sulfonyl-oxirane is unknown to literature which indicates the impossibility of isolation of such motifs. Unfortunately, the resulting oxidation products could not be elucidated in the course of this thesis.

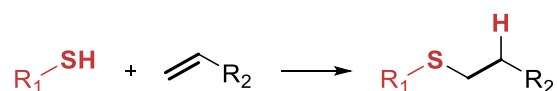
Interestingly, the results described in this chapter stand in strong contrast to the thermal stability of the polymers observed by the TGA measurements described in Chapter 6.3. There, all polymers proved to be stable up to temperatures of 300 °C independent of the employed dithiol for the polymerization. In contrast, it was shown in this chapter that the same polymers can be degraded *via* oxidative treatment using common oxidizing agents such as hydrogen peroxide, *m*CPBA or *Oxone*® under mild conditions.

These results prove that the obtained polymers, although thermally stable under inert atmosphere, carry an oxidation-sensitive handle that enables their breakdown in mild conditions. In the context of ever-increasing accumulation of polymer wastes in nature, structural motifs such as tetrafluorophenyl vinyl sulfides could pose an interesting possibility for natural polymer degradation, especially through Iron-oxidizing bacteria.^[214]

6.4.3 Derivatization based on the Vinyl Group

6.4.3.1 Modification based on the Thiol-ene Reaction

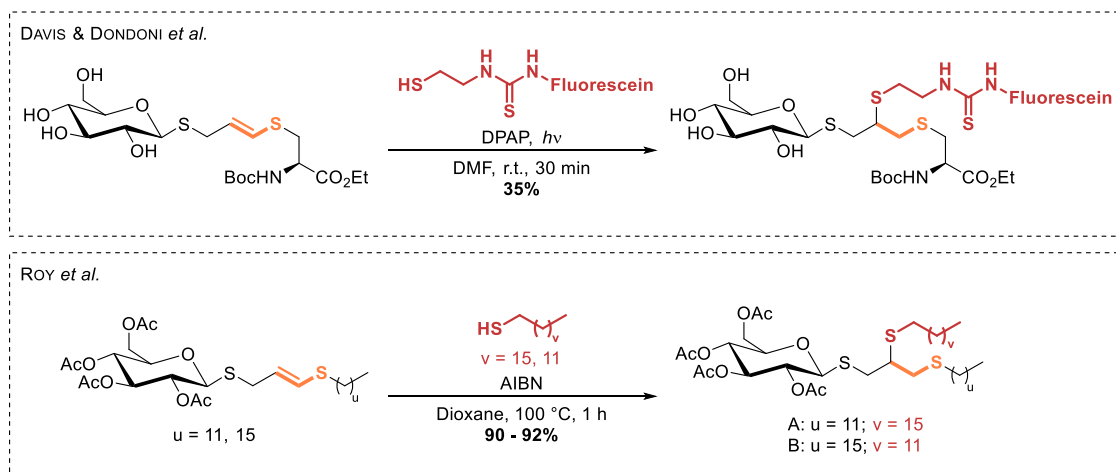
As mentioned previously, the thiol-ene reaction is one of the most employed methods for the transformation of unsaturated substrates.^[191] Here, a thiol is reacted with an alkene, usually with a radical initiator, to form a thioether in *anti*-MARKOVNIKOV fashion.



Scheme 6.9: General reaction scheme for the thiol-ene reaction yielding a thioether.

Due to this regioselectivity, as well as high yields and fast addition rate, the reaction fulfils the “click chemistry” criteria, which justifies its popularity.^[68,191,215] In the context of polymer science, it has been employed for the synthesis of monomers, (photo) thiol-ene polymerization and post-polymerization reactions, covering the entire bandwidth of polymer synthesis and modification.^[191,216,217]

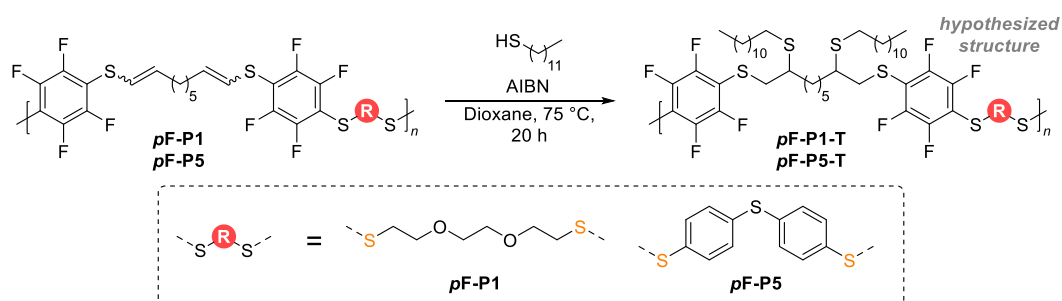
Since the thiol-ene reaction is usually performed with terminal alkenes, examples of reactions with vinyl sulfide substrates are less often reported. Still, DAVIS and DONDONI reported the successful hydrothiolation of a cysteine-carbohydrate vinyl sulfide with a fluorescein-derived thiol under UV irradiation with 2,2-dimethoxy-2-phenylacetophenone (DPAP) as photoinitiator.^[218] Furthermore, Roy *et al.* presented the synthesis of unsymmetrical neoglycolipids by reacting an alkyne-carrying carbohydrate with two different aliphatic thiols successively. In their study, the vinyl sulfide was reacted under thermal conditions with AIBN as the radical source (Scheme 6.10).^[219]



Scheme 6.10: Reported examples of hydrothiolation reactions of vinyl sulfides under UV irradiation (*top*) and thermal conditions (*bottom*) (adapted from ^[218] and ^[219], respectively).

In both cases however, the vinyl sulfide moieties are enclosed by aliphatic groups. As no thiol-ene reaction on pentafluorophenyl vinyl sulfides is reported in literature, the reaction conditions for the post-polymerization reaction were loosely adapted from Roy *et al.*^[219] Here, the thermally activated thiol-ene reaction was preferred over the UV induced variant due to extensively higher yields and facilitated reaction setup. However, the temperature was lowered to 75 °C to obviate possible side reactions.

Thus, **pF-P1** and **pF-P5** were reacted with 1-dodecanthiol in 1,4-dioxane at 75 °C and AIBN as the radical initiator (Scheme 6.2). These two structurally different polymers were chosen due to their very different glass transition temperatures T_g as shown in Figure 6.8. Through the attachment of the aliphatic chain the impact on the thermal properties should be investigated.



Scheme 6.11: Reaction scheme for the thiol-ene reaction of 1-dodecanthiol with **pF-P1** and **pF-P5**.

In similar fashion as described in Chapter 6.4.2, the reacted polymers were precipitated and subsequently analyzed *via* ^1H and ^{19}F NMR as well as SEC. Interestingly, a similar reaction outcome was observed as with the previously described oxidation reactions (*vide supra*). SEC analysis revealed that the original polymer had degraded into lower molecular mass chains (Figure 6.12 *top left & right*). To further investigate the observed phenomenon, the precipitation supernatant of **pF-P5** was also subjected to SEC analysis revealing that smaller chain fragments solubilized during precipitation and were removed from the precipitate. However, although the SEC analyses of both reaction products showed no trace of 1-dodecanthiol (soluble in the precipitation solvent)^[220] in the precipitate the magnetic resonance of the terminal methyl group appears in the corresponding proton spectra, which also shows complete removal of vinyl proton resonances (see Appendix, Figure 9.1). This indicates, that the radically induced hydrothiolation of the polymers was partially successful and either a side or follow-up reaction led to the breaking of the polymer chains. Also, the recorded fluorine spectra showed that chemical shifts changed (Figure 6.12). Notably, for **pF-P1-T** the fluorine resonances at -134.2 ppm vanished, indicating that the previously unsymmetrical structure of the pentafluorophenyl vinyl sulfides is changed towards a more symmetrical one. In the case of **pF-P1-T** a similar change is observed: the multiplet at -132.4 is drastically reduced and instead a resonance at -131 ppm appeared. Although the obtained

resonances cannot be assigned to a particular structural motif, they indicate strong change in the chemical environment of the fluorine atoms.

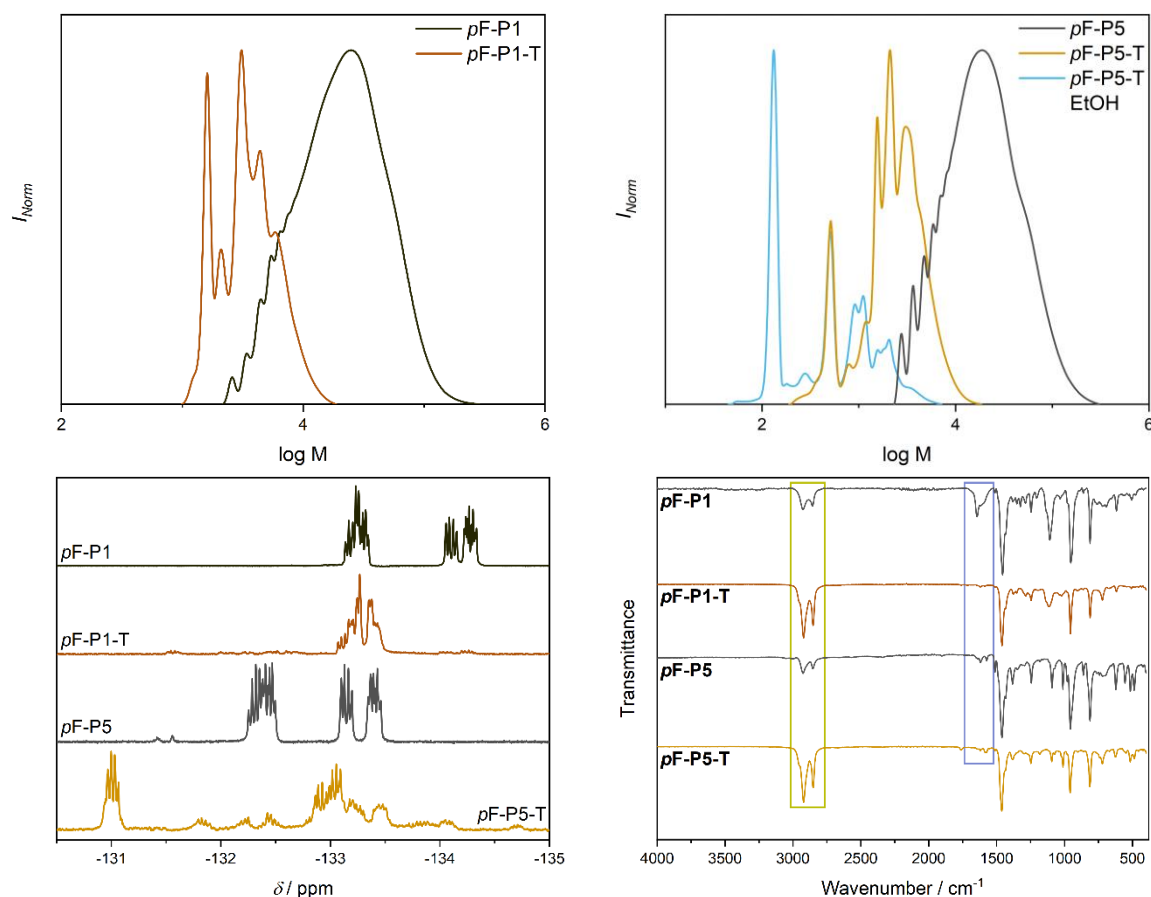


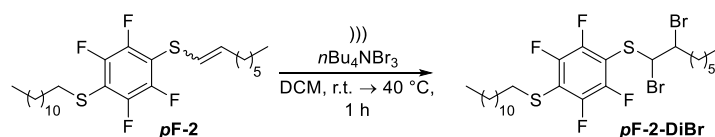
Figure 6.12: SEC analyses of the attempted thiol-ene reactions with $\rho\text{F-P1}$ (top left) and $\rho\text{F-P5}$ (top right). Comparative fluorine NMR (bottom left) and IR spectra (bottom right) of the parent polymers and the reaction products.

Two observations stand out from the obtained IR spectra of the reaction products. On one hand, the absorbance of the C-H stretching band ranging from 2800 – 2990 cm^{-1} increased in both cases (Figure 6.12 bottom right; green box). On the other hand, the vinylidene $\text{C}=\text{C}$ stretching band at 1640 cm^{-1} nearly vanished (Figure 6.12 bottom right; blue box). These results support the hypothesis that a reaction of the vinyl group took place, either *via* hydrothiolation or a side reaction, respectively.

6.4.3.2 Modification based on Halogenation

Halogenation is one of the oldest reported reactions for unsaturated substrates and commonly used for the production of flame-retardant materials or intermediates in chemical synthesis.^[221] Literature protocols for the halogenation of aryl vinyl sulfides or derivatives date back to as early as 1912.^[222] Since then, protocols for the chlorination,^[223] bromination^[224] and fluorination^[225] were reported. Although the halogenation of the particular fluorinated aryl vinyl sulfide motif, which is dealt with in this thesis, is unknown to literature, structurally similar aryl vinyl sulfide halogenations were reported (*vide supra*) and thus allow a rough estimation of reactivity for the present case. Here, the electronegative fluorine atoms on the ring should exert an electron withdrawing effect on the double bond, which should thus have lessened reactivity in halogenation reactions compared to non-fluorinated vinyl sulfide counterparts, respectively. In contrast to chlorinations and fluorinations, bromination reactions are easiest to carry out on a laboratory scale and thus this reaction was chosen in the context of this work.

For the investigation of the bromination of the tetrafluorophenyl vinyl sulfide moiety the model compound **pF-2** was employed for preliminary studies. To evade the health risks associated with the use of elemental bromide, a chemical substitute in the form of tetrabutylammonium bromide ($n\text{Bu}_4\text{NBr}_3$, TBAT) was used for the halogenation. This solid reagent is easily weighed in and allows precise balancing of the desired equivalents of bromine, which is provided in the form of a $[\text{Br}_3]^-$ ion. Furthermore, as reported by BERTHELOT *et al.*, TBAT very effectively brominates alkenes under ultrasonic irradiation.^[226] Thus, **pF-2** was reacted with the tribromide in DCM under ultrasonic irradiation (Scheme 6.12).



Scheme 6.12: Reaction scheme for the bromination of **pF-2** with $n\text{Bu}_4\text{NBr}_3$ (TBAT).

Delightfully, fluorine NMR showed a complete shift of the magnetic resonances from -134.1 to -132.5 ppm indicating full conversion of the vinyl bond (Figure 6.13 *right*). Accordingly, also proton NMR showed the successful transformation of the vinyl bond towards the vicinal dibromide. As expected, the product was obtained as a mixture of *threo*- and *erythro* forms in equal ratios, which is indicated by the splitting of the proton resonances at 5.55 ppm and 4.34 ppm (denoted as **1** and **2** in Figure 6.13 *left*), respectively.

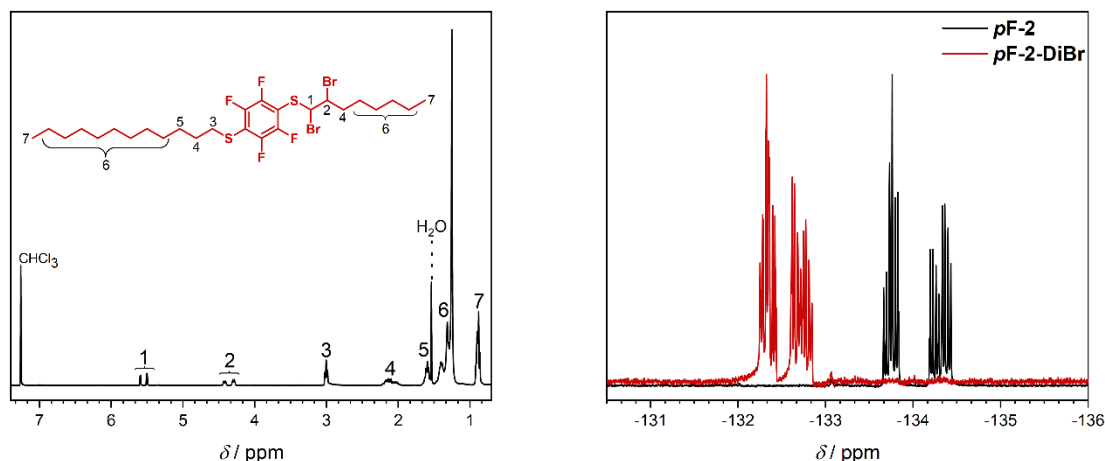
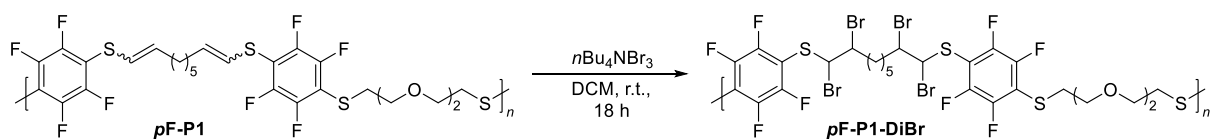


Figure 6.13: Proton (*left*) and fluorine NMR (*right*) analyses of the bromination product **pF-2-DiBr** evidencing the successful halogenation of the vinyl sulfide moiety of **pF-2**.

Upon the successful halogenation of the model compound, the halogenation of the polymer **pF-P1** was investigated. The reaction was conducted under the same conditions as previously, *i.e.*, under ultrasonic irradiation for one hour. Consecutively after the halogenation, the polymers were subjected to aqueous workup to remove the ammonium salts and then precipitated. The obtained material was analyzed *via* SEC, NMR and IR spectroscopy, TGA and DSC.

In contrast to the small molecule reaction however, the ultrasonication led to a side reaction on the polymer as was evidenced by proton NMR analysis (see Appendix, Figure 9.2). Most likely, an addition of the *tert*-butyl ammonium unit to the polymer occurred since a methyl group resonance appeared in the corresponding proton spectrum. To circumvent this side reaction, the same reaction was repeated with conventional stirring for 20 hours at ambient temperature. Luckily these conditions suppressed the side reaction nearly completely as shown in the recorded proton spectrum (Figure 6.14 *top left*). To circumvent the side reaction altogether the halogenation was also once conducted with a different batch of **pF-P1** and elemental bromine as the halogenation agent. Interestingly, these conditions led to a degradation of the polymer which is confirmed *via* SEC (Figure 6.14, *bottom left*). Possibly, an oxidative follow-up reaction caused by excess bromine took place after the halogenation and led to chain deterioration, similarly as described previously with other oxidants (refer to Chapter 6.4.2).



Scheme 6.13: Reaction scheme for the halogenation of **pF-P1** with $n\text{Bu}_4\text{NBr}_3$.

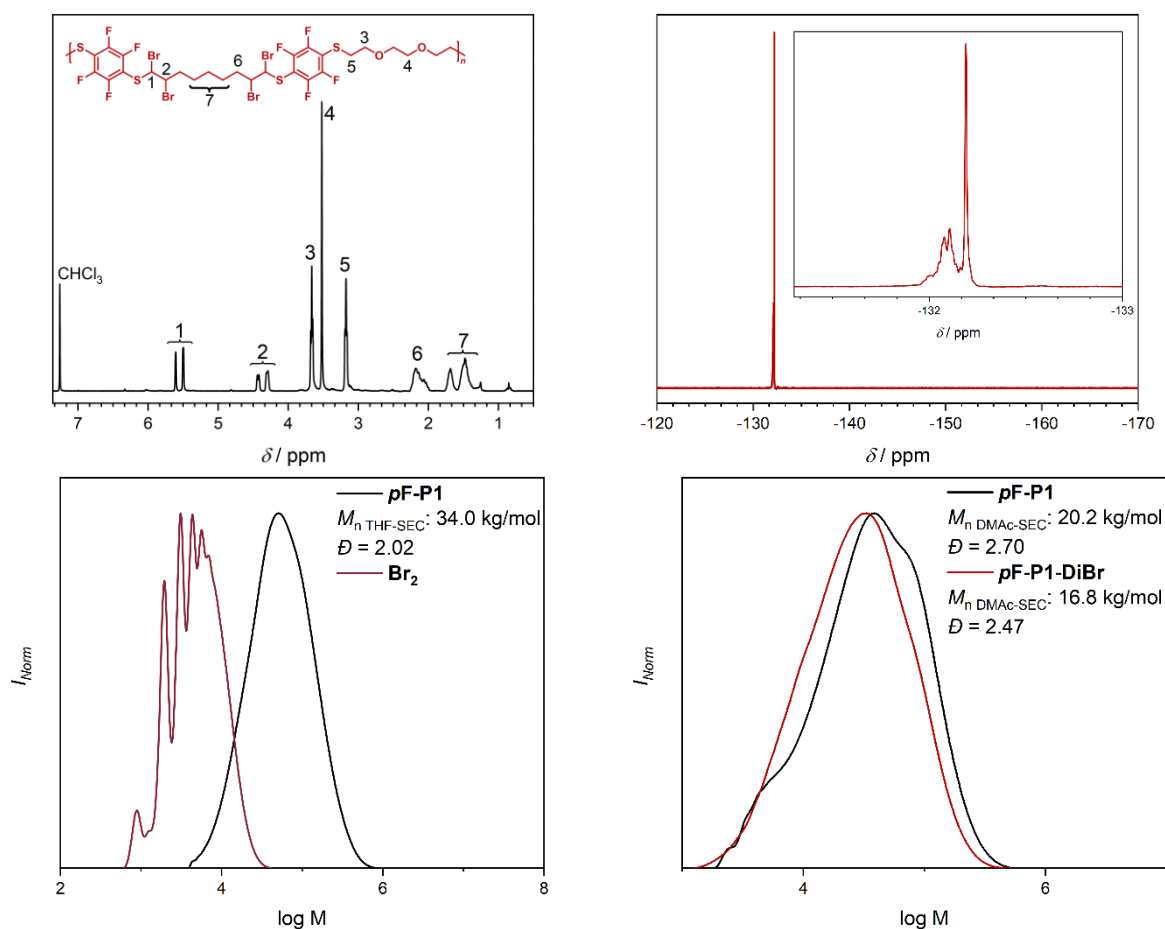


Figure 6.14: Proton (*top left*) and fluorine (*top right*) NMR analyses of the halogenated polymer ***pF-P1***. SEC traces for the halogenation reaction with bromine (*bottom left*) and nBu_4NBr_3 (*bottom right*) confirm the polymer stability in the latter case.

As seen in the case for ***pF-2-DiBr***, the polymer proton spectrum of ***pF-P1-DiBr*** shows *threo*- and *erythro* motifs in the backbone. Interestingly, the corresponding fluorine resonance is shifted to -132 ppm and distorted compared to the fluorine spectrum of the model compound or the parent polymers (*vide supra*), hinting towards a different chemical environment of the polymer globule compared to previous polymers. The chemical change is further evidenced *via* a shift in the SEC trace compared to the precursor. Interestingly, the shift implies a change towards lower molecular mass from $20 \text{ kg}\cdot\text{mol}^{-1}$ (***pF-P1***) towards nearly $17 \text{ kg}\cdot\text{mol}^{-1}$ (***pF-P1-DiBr***). This observation can be possibly explained by the fact that sulfur and bromine atoms can form so-called halogen bonds (*X*-bonds). *i.e.*, $S\cdots Br$ bonds in this case, which are non-covalent attraction forces similar to the well-known hydrogen binding motifs.^[227] Switching the SEC eluent to THF yielded the same shift towards lower molecular weights, thus verifying the previous results.

Finally, the thermal properties of the halogenated polymer ***pF-P1-DiBr*** were investigated via DSC and TGA and compared to the precursor polymer (Figure 6.15). The DSC thermogram revealed a shift of nearly 45K of the glass transition temperature T_g from -29.6 °C (***pF-P1***) to

15.1 °C for the halogenated derivative, indicating amorphous behavior of the new material. Interestingly, the TGA curve shows a strong change after the post-polymerization modification: a two-step degradation pattern for the halogenated polymer is observed with onset-temperatures of 197 °C for the first and 308 °C for the second step. Most likely, the first degradation step consists of the deterioration of the vicinal dibromides as it corresponds to 27% weight loss, which is close to the calculated value of 32%.

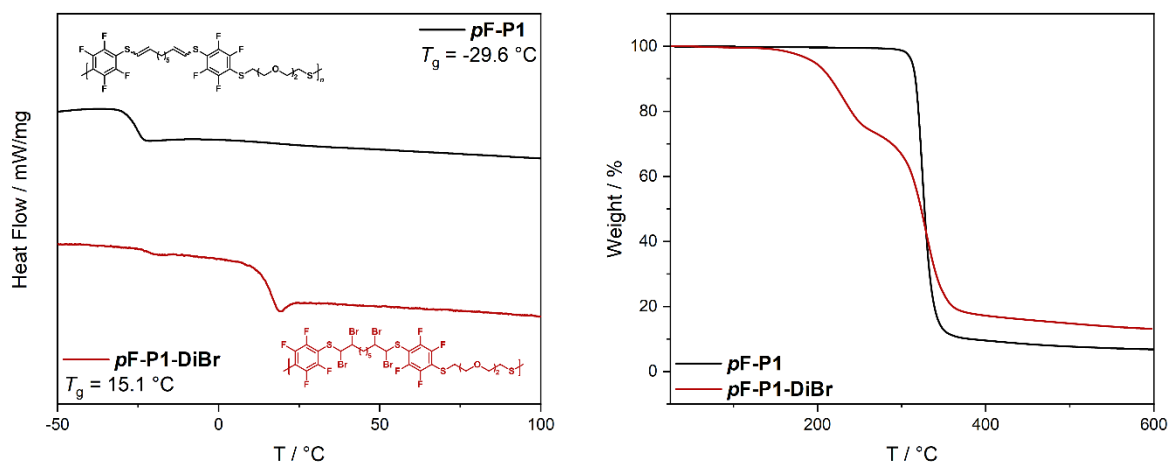


Figure 6.15: Comparative DSC (*left*) and TGA (*right*) traces of **pF-P1** and **pF-P1-DiBr**.

Thioethers with adjacent vicinal dibromide groups can undergo regioselective elimination reactions towards halo-vinyl sulfides^[224,228,229] or complete eliminations to alkynes.^[230] Thus, the halogenated polymer **pF-P1-DiBr** has further synthetic potential *via* these reactions.

6.5 Conclusion

In this chapter, the synthesis and characterization of new fluorinated polymers on the basis of **PFTP** hydrothiolation and subsequent *para*-fluoro thiol reaction was shown. First, preliminary studies were conducted where 2,3,4,5,6-pentafluorobenzene-1-thiol (**PFTP**) was reacted with alkynes to yield fluorinated aryl vinyl sulfides. It was then tested in a *para*-fluoro thiol reaction (PFTR) and successfully yielded the desired *para*-substituted product. Based on these results the reaction was repeated with a commercial dialkyne to yield a symmetrical monomer **pP-M**, which was subsequently polymerized with a series of (functional) dithiols **DT2 – DT5**. The set of structurally different polymers was characterized *via* NMR and IR spectroscopy, SEC, DSC and TGA. Proton NMR analysis revealed the incorporation of all desired structural functionalities and fluorine NMR confirmed their attachment in the *para*-position through disappearance of the *para*-fluorine signal and shift of the *ortho*- and *meta*-fluorine resonances. The obtained SEC traces evidenced molecular masses in the range of 6 to 58 kg·mol⁻¹ with dispersity values that are expected for step-growth polymerizations. Thermal analysis *via* TGA revealed a thermal stability of all polymers ranging from 300 °C to 330 °C, depending on the employed structural motifs of the employed dithiol. Similarly, the structural differences were noticeable in the SEC thermograms through a range of glass transition temperatures T_g from -33 °C to 21 °C, indicating the amorphous state of all polymers.

Subsequently, several post-polymerization modification approaches for were investigated. The chemical transformations of the synthesized polymers were structured according to the targeted structural motifs in the polymer, including the functional dithiol, the thioether linkages and the vinyl bonds. The reaction products were analyzed accordingly *via* NMR, SEC, IR spectroscopy and TGA and DSC where applicable. To this end, the modification of the hydroxy functionalities of the dithiol unit in **pF-P3**, *i.e.*, dithiothreitol were investigated. The successful boronic ester formation of these units was evidenced by SEC and more importantly by ¹H and ¹⁹F NMR, as the employed boronic acid carried a fluorine atom. Investigations of the oxidation reaction on the polymers yielded interesting results, as their degradation was easily triggered by different oxidants in acidic and basic conditions in short reactions times, possibly again through involvement of the tetrafluorophenyl vinyl sulfide moiety, as was shown through a comparison of reactions on similar structures in literature. Finally, the vinyl group was targeted for the modification *via* thiol-ene and halogenation reactions. In the first case, the employed radical conditions led to polymer degradation, which was proven by ¹⁹F NMR, SEC and IR spectroscopy. In the latter, the halogenated polymer could be obtained *via* careful choice of the halogenating agent, *i.e.*, TBAT instead of elemental bromine. The halogenated polymer showed greatly changed properties compared to the precursor, such as *threo*- and *erythro* motifs in the backbone, a much higher T_g and a two-step thermal degradation which was revealed by NMR, DSC and TGA analyses, respectively.

7 Conclusion and Outlook

The present thesis demonstrated the use of aliphatic alkynes for the synthesis of structurally diverse macromolecules, such as precisely functionalized poly(ethylene) (Chapter 4), core-shell bottlebrush copolymers (Chapter 5) and alkyne-derived polymers based on pentafluorophenyl vinyl sulfide monomers (Chapter 6).

Accordingly, Chapter 3 addressed the need for a straightforward approach for the synthesis of α,ω -functionalized hydrocarbons through the Alkyne Zipper reaction. To this end, commercially available short alkynols were elongated *via* alkylation with haloalkanes. In a second step the internal alkyne groups were isomerized to the ω -terminus of the chains, yielding the desired α,ω -functionalized derivatives. In this manner, five long-chain alkynols with up to 25 methylene spacers could be obtained in gram-scale. They were further employed for the synthesis of bottlebrush polymers, which were elaborated in Chapter 5.

To leverage the described method for the build-up of long hydrocarbons, the polymerization of their structural relatives, i.e., aliphatic dialkynes, was investigated in Chapter 4. Here, an alternative route towards precise poly(ethylene) through the linking of dialkynes and symmetric divinyl halide monomers towards enyne moieties *via* the SONOGASHIRA reaction was investigated. Although the conceived strategy was hindered by an intrinsic instability of the final materials, as they tended to crosslink, subsequent studies with a sterically more demanding monomer led to the verification of the actual formation of the desired polymer structure by SEC and NMR spectroscopy, respectively. In a final proof-of-concept experiment, the instability of the enyne-containing polymers was circumvented by *in-situ* hydrogenation, which led to the successful isolation and characterization of the desired precise poly(ethylene) derivative.

The project in Chapter 5, presented the use of long-chain α,ω -alkynols for the synthesis of bottlebrush polymers *via* a 'grafting to' approach with poly(pentafluorophenyl acrylate) (PPFPA). The active-ester decorated parent polymer was initially synthesized *via* RAFT polymerization, and subsequently reacted with a series of alkynol derivatives of different chain lengths. The full conversion of the PFP moieties was revealed by ^{19}F NMR, thus proving a high grafting density. Expectedly, both SEC and DSC results showed a strong dependency on the employed chain length of the alkynols. Notably, the obtained SEC results further indicated an unfolding of the polymer globule towards a more cylindrical structure. Subsequently, further derivatization of one bottlebrush polymers was investigated by the means of a three-component reaction (3-CR) involving the alkyne moiety at the terminal chain ends in the presence of a sulfonyl azide and an alcohol. Thus, methoxy polyethylene glycol (MW $\sim 400 \text{ g mol}^{-1}$) was tethered *via* the 3-CR, yielding in sulfonyl imidate linkages with a 70% conversion. In this way, a non-trivial synthesis of core-shell bottlebrush copolymers (cs-BBCPs) was achieved.

Finally, in Chapter 6, a new fluorinated motif for polymerizations *via* the *para*-fluoro thiol reaction (PFTR) was introduced for the first time. Here, anew, an aliphatic dialkyne was reacted with pentafluorothiophenol (PFTP) yielding a difunctional pentafluorophenyl vinyl sulfide monomer, which was subsequently polymerized with a series of structurally diverse dithiols *via* PFTR. The successful incorporation of the thiols was evidenced by ^1H -, ^{19}F NMR and IR spectroscopy, as well as TGA and DSC analyses. The two latter methods revealed a strong dependence of the thermal properties to the incorporated structural motifs of the dithiols and showed thermal stability up to 330 °C. Since the tetrafluorophenyl vinyl sulfide moiety in the final polymers displayed a great synthetic potential, several post-polymerization methods were investigated. The respective PPMs were applied on the dithiol functionalities, the thioether linkages and the vinyl group. In the first case, the vicinal dithiothreitol hydroxyl groups were successfully converted to a fluorinated boronic ester, which was evidenced by NMR spectroscopy and SEC. The modification of the thioether linkages was examined through oxidation reactions, which led to the degradation of the polymers in basic and acidic conditions, respectively. Finally, the vinyl group should be modified through thiol-ene and halogenation reactions. In the first case, again polymer degradation was observed, while the latter yielded a halogenated polymer with *threo*- and *erythro* motifs in the backbone and a two-step thermal degradation pattern.

The logical extension of the herein presented projects would envision the combination of the developed methods for the synthesis of new polymers based on the molecules shown in the individual chapters. In this regard, the three-component reaction (3-CR) described in Chapter 5 in combination with the synthesized α,ω -alkynols (Chapter 3) should yield PE-like polymers with sulfonyl imidate motifs in the backbone. This would also further establish the use of the Alkyne Zipper reaction in polymer science, since it can be considered pioneering in the field of macromolecular chemistry as shown in this thesis. In a similar manner, the hydrothiolation reaction of pentafluorothiophenol (**PFTP**) can be applied as a post-polymerization reaction, for instance on polymers with alkyne-pendant sidechains as the ones presented in Chapter 5, thus yielding fluorinated bottlebrush polymers. This would further enable structural deviation of said polymers through multiple nucleophilic fluorine substitutions on the pentafluoro phenyl vinyl moiety. Finally, the intrinsic instability of the unsaturated polymers described in Chapter 4 could be addressed through an alternative coupling methodology. Here, an alternative linking motif, i.e., a change from enynes to 1,3-diynes, should impart the desired stability and allow in-depth characterization of unsaturated PE precursor polymers. Indeed, a suitable protocol for the straight-forward polymerization of symmetrical dialkynes *via* a nickel(II)-based Glaser-Hay reaction was reported very recently by REINEKE and HOYE.^[231]

Thus, the results presented in this work can be considered as an advance towards new ways for the synthesis of novel (fluorinated or PE-like) functional materials for future applications.

8 Experimental Part

8.1 Materials

Used chemicals were obtained from ABCR, ACROS ORGANICS (THERMO FISHER), ALFA AESAR, CARL ROTH, MERCK, SIGMA ALDRICH, TCI and VWR in the highest possible purity but at least in “for synthesis”-grade. Liquid chemicals were stored in a fridge, radical initiators in a freezer at -20 °. 1,3-Dichloropropene was distilled prior to use. Commercially redistilled compounds as well as air- and water-sensitive chemicals were handled *via* common SCHLENK line techniques under argon atmosphere and reactions were performed in dry solvents. Common solvents were obtained from VWR CHEMICALS with AnalaR NORMAPUR purity grade and were used as received.

NMR samples were prepared with deuterated solvents from EURISO-TOP.

8.2 Instrumentation

8.2.1 Nuclear Magnetic Resonance (NMR) Spectroscopy

^1H NMR, $^{13}\text{C}\{\text{H}\}$ NMR and $^{19}\text{F}\{\text{H}\}$ NMR measurements were performed on a Bruker Avance III 400 MHz spectrometer with a frequency of 400 MHz, 101 MHz and 377 MHz for proton, carbon and fluorine spectra, respectively. Samples were dissolved in CDCl_3 or deuterated $\text{DMSO}-d_6$. Chemical shifts are reported relative to the solvent residual peaks (^1H NMR: δ 7.26 for CDCl_3 ; δ 2.50 for $\text{DMSO}-d_6$, ^{13}C NMR: δ 77.16 for CDCl_3 ; δ 39.52 for $\text{DMSO}-d_6$). Abbreviations for the multiplicity of signals are: s (singlet), d (doublet), t (triplet), q (quartet) and m (multiplet) or combinations thereof, for example dt (duplet of triplet). Assignments are based on COSY, HSQC and HMBC 2D NMR measurements. The obtained spectra were analyzed with the software MestReNova 14.

8.2.2 Liquid Flash Chromatography Purification

Liquid Flash chromatography was performed on an Interchim *puriFlash*[®] XS520 Plus with Interchim *puriFlash*[®] SI-HP 30 μm columns. If soluble, the crude materials were deposited on the purification column as a concentrated solution in a suitable solvent, usually mixtures of cyclohexane. Crude materials with insufficient solubility in the main eluent or mixtures thereof were deposited on Celite 545 prior to purification with *puriFlash*[®] Dry-Load cartridges (PF-DLE-

F0012, PF-DLE-F0025 or PF-DLE-F0040). If possible automated UV-detection was used for fraction collection.

8.2.3 Size Exclusion Chromatography (SEC)

Due to changing analytics devices, two THF SEC systems were used in the context of this thesis. For individual projects, measurements were always conducted using the same system, to enable comparison. Samples insoluble in THF or incompatible with the employed THF systems were measured in DMAc.

The following calibrations were used for the respective projects:

Chapter 3: PMMA Calibration

Chapter 4: PS Calibration

Chapter 5: PMMA Calibration

Chapter 6: PS Calibration

8.2.3.1 THF Systems

System 1:

Agilent Technologies 1200 Series System, comprising an autosampler, a guard column followed by three PLgel 5 μm Mixed - C (300 \times 7.5 mm) and one PLgel 3 μm Mixed - E columns (300 \times 7.5 mm) and a differential refractive index detector (RID) as well as a UV detector (DAD) using THF (HPLC grade + 0,55g/2,5L BHT) as the eluent at 40 °C with a flow rate of 1 mL \cdot min⁻¹.

System 2:

Agilent Technologies 1260 Infinity II System, comprising an autosampler, a guard column followed by a PSS SDV Lux 1000A 5 μm (300 \times 8 mm) and one PSS SDV Lux 100.000A 5 μm (300 \times 8 mm) column and a differential refractive index detector (RID) as well as a UV detector (VWD) using THF (HPLC grade + 0,55g/2,5L BHT) as the eluent at 40 °C with a flow rate of 1 mL \cdot min⁻¹. The SEC system was calibrated using ReadyCal Standards:

Both SEC systems were calibrated using ReadyCal Standards:

- PS standards S3 ranging from 370 to 2.25 \cdot 10⁶ Da
- PMMA standards S3 ranging from 800 to 2.2 \cdot 10⁶ Da

Calculation of the molecular weight proceeded via the Mark-Houwink parameters for polystyrene, *i.e.*, $K = 14.1 \cdot 10^{-5} \text{ dL} \cdot \text{g}^{-1}$, $\alpha = 0.70$. The samples were filtered through polytetrafluorethylene (PTFE) membranes with a pore size of 0.2 μm prior to injection.

8.2.3.2 DMAc System

Agilent Technologies 1260 Infinity II System, comprising an autosampler, a guard column followed by two PSS GRAM Lux 1000A 5 μ m (300 \times 8 mm) and one PSS GRAM Lux 30A 5 μ m (300 \times 8 mm) column, a differential refractive index detector (RID) as well as a UV detector (VWD) using DMAc (HPLC grade + 0,79g/2,5L LiBr) as the eluent at 40 °C with a flow rate of 1 mL \cdot min⁻¹. The SEC system was calibrated using the same ReadyCal Standards as for the THF systems.

8.2.4 Thermogravimetric Analysis (TGA)

TGA was performed on a TGA Q5000 from TA Instruments or on a TGA/SDTA851e instrument by Mettler Toledo. Pre-dried samples were measured in nitrogen atmosphere up to at least 600 °C with a heating rate of 10 K/min.

8.2.5 Differential Scanning Calorimetry (DSC)

DSC measurements were performed on a DSC 214 *Polyma* by Netzsch. Samples were prepared with 3–7 mg of sample material with a pierced lid crucible. The measurements were done with the following sequence:

- 1.) 25 °C \rightarrow 150 °C, 5 K/min
- 2.) 150 °C \rightarrow -80 °C, 5 K/min
- 3.) Isothermal at -80 °C for 10 min
- 4.) -80 °C \rightarrow 150 °C, 10 °C / min

All graphs of DSC traces are depicted as “exo up”.

8.2.6 IR Spectroscopy

IR spectra were recorded on a Bruker ALPHA II Spectrometer in the frequency range from 400 to 4000 cm⁻¹ employing ATR technology.

8.2.7 Centrifuge

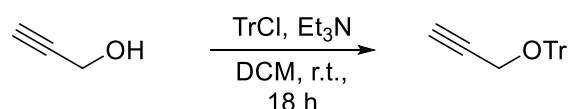
For centrifugation, Sigma 2-7 and Sigma 2-16P centrifuges were used. Usual centrifugation time was four minutes at maximum RPM settings.

8.3 Synthesis Procedures

8.3.1 Experimental Procedures for Chapter 3

8.3.1.1 Synthesis of precursor molecules

8.3.1.1.1 Propargyl trityl ether (**1**)



In an oven-dried 100 mL flask 2 g of propargyl alcohol (35,7 mmol, 1.3 eq.) and 67 mg of DMAP (0.548 mmol, 2 mol%) were dissolved in 8 mL dry DCM and treated with 7.66 mL Et₃N (55.9 mmol, 5.55 g, 2 eq.). The mixture was stirred for 15 minutes and 7.65 g Trityl chloride (27.4 mmol, 1 eq.) was added in portions at atmospheric temperature. The reaction was stirred at atmospheric temperature for 18 h and subsequently quenched by the addition of water and ethyl acetate. The phases were separated and the aq. phase was extracted once with DCM. The combined organic phases were washed with brine, dried with MgSO₄ and the solvent was removed *in vacuo*. The obtained crude solids were purified by Flash column chromatography (CH/DCM = 4:1).

Yield: 6.07 g, 86%.

¹H-NMR (400 MHz, DMSO-*d*₆): δ / ppm = 7.45 – 7.21 (m, 15H, H₁), 3.66 (d, *J* = 2.4 Hz, 2H, H₂), 3.40 (t, *J* = 2.4 Hz, 1H, H₃).

¹³C-NMR (100 MHz, DMSO-*d*₆): δ / ppm = 143.5 (3C), 128.5 (8C), 127.7 (3C), 87.3, 80.6, 77.1, 52.9.

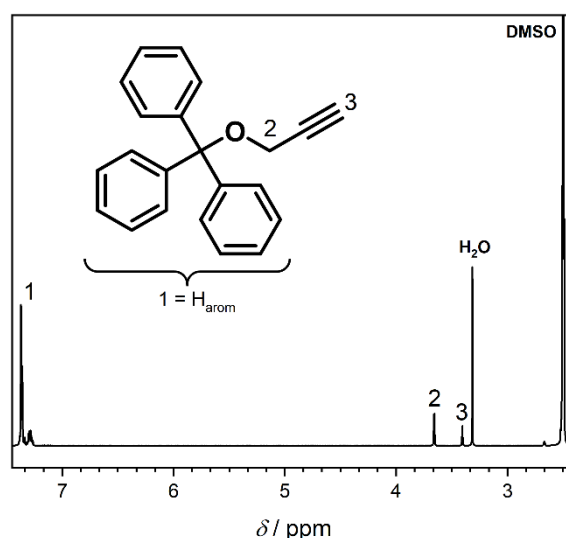
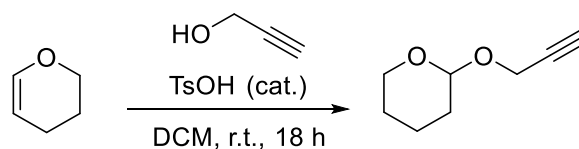


Figure 8.1: Proton NMR spectrum of **1** (DMSO-*d*₆).

8.3.1.1.2 2-(Prop-2-yn-1-yloxy)tetrahydro-2H-pyran (2)



In an oven-dried 50 mL flask 5.00 g propargyl alcohol (89.2 mmol, 1.10 eq.) and 140 mg of *p*-toluenesulfonic acid (0.811 mmol, 0.01 eq.) were dissolved in 15 mL DCM and cooled to 0 °C. Subsequently, 7.13 g of 3,4-dihydropyran (7.69 mL, 84.8 mmol, 1.00 eq.) were added dropwise and the mixture was stirred for 18 hours at atmospheric temperature. To quench the reaction saturated Na₂CO₃ solution was added and the phases were separated. The aqueous phase was extracted once with DCM and the combined organic phases were washed twice with water, once with brine, dried with MgSO₄ and the solvent was removed in *vacuo*. The material was obtained as a slightly yellow liquid and was pure according to ¹H NMR spectroscopy.

Yield: 9.97 g, 88%.

¹H-NMR (400 MHz, CDCl₃): δ / ppm = 4.82 (t, *J* = 3.5 Hz, 1H, H₁), 4.34 – 4.18 (m, 2H, H₂), 3.90 – 3.78 (m, 1H, H₃), 3.59 – 3.49 (m, 1H, H₃), 2.41 (t, *J* = 2.4 Hz, 1H, H₄), 1.92 – 1.44 (m, 4H, H₅).

The obtained spectroscopic data is in agreement with the literature.^[232]

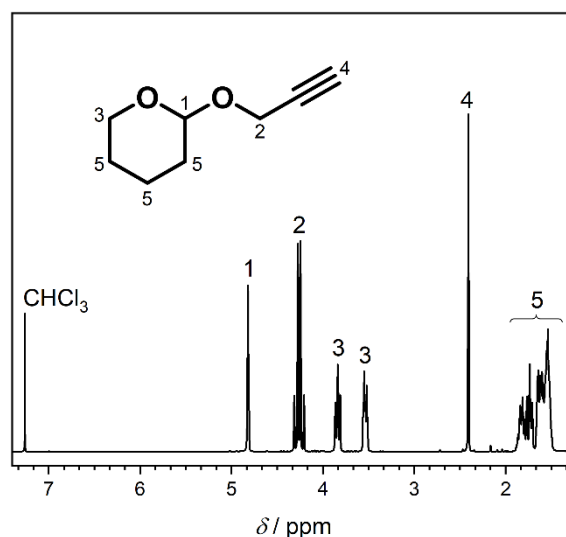
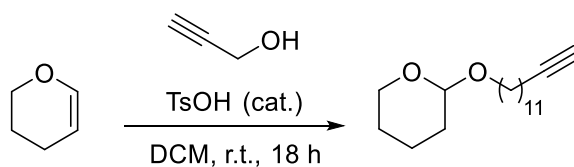


Figure 8.2: Proton NMR spectrum of **2** (CDCl₃).

8.3.1.1.3 2-(undec-10-yn-1-yloxy)tetrahydro-2H-pyran (3)



In an oven-dried 50 mL flask 1.50 g undec-10-yn-1-ol (8.91 mmol, 1.00 eq.) and 30.2 mg of *p*-toluenesulfonic acid (0.178 mmol, 0.02 eq.) were dissolved in 15 mL DCM and cooled to 0 °C. Subsequently, 1.21 mL of 3,4-dihydropyran (1.21 g, 13.4 mmol, 1.50 eq.) were added dropwise and the mixture was stirred for 18 hours at atmospheric temperature. To quench the reaction saturated Na₂CO₃ solution was added and the phases were separated. The aqueous phase was extracted once with DCM and the combined organic phases were washed twice with water, once with brine, dried with MgSO₄ and the solvent was removed in *vacuo*. The material was obtained as a slightly yellow liquid and was pure according to ¹H NMR spectroscopy.

Yield: 1.95 g, 87%.

¹H-NMR (400 MHz, CDCl₃): δ / ppm = 4.57 (dd, J = 4.4, 2.7 Hz, 1H, H₁), 3.87 (ddd, J = 11.2, 7.4, 3.5 Hz, 1H, H₂), 3.73 (dt, J = 9.6, 6.9 Hz, 1H, H₃), 3.50 (dtd, J = 10.7, 4.9, 4.0, 2.4 Hz, 1H, H₂), 3.38 (dt, J = 9.6, 6.6 Hz, 1H, H₃), 2.18 (td, J = 7.1, 2.7 Hz, 2H, H₄), 1.93 (t, J = 2.6 Hz, 1H, H₅), 1.83 (qt, J = 8.5, 3.7 Hz, 1H, H₆), 1.77 – 1.66 (m, 1H, H₆), 1.65 – 1.45 (m, 8H, H₆ & H₇), 1.44 – 1.22 (m, 10H, H₈).

¹³C-NMR (100 MHz, CDCl₃): δ / ppm = 98.87, 84.81, 68.05, 67.69, 62.37, 30.81, 29.76, 29.43, 29.06, 28.75, 28.49, 26.23, 25.53, 19.73, 18.41.

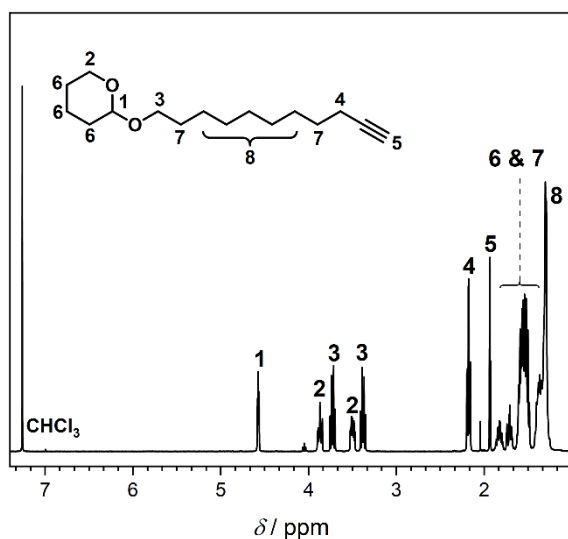
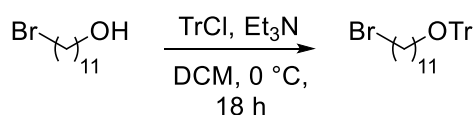


Figure 8.3: Proton NMR spectrum of **3** (CDCl₃).

8.3.1.1.4 Synthesis of (((11-Bromoundecyl)oxy)methanetriyl)tribenzene (**4**)



In an oven-dried 250 mL flask 4.65 g 11-bromoundecan-1-ol (18.5 mmol, 1 eq.) and 5.16 mL Et₃N (3.75 g, 37.0 mmol, 2 eq.) were dissolved in 20 mL dry THF and 20 mL dry DCM. The solution was cooled to 0 °C and 6.45 g TrCl (23.1 mmol, 1.25 eq.) was added in portions. After stirring for 15 min the ice bath was removed and the reaction was stirred at room temperature for 3d. Subsequently, sat. NH₄Cl solution and ethyl acetate was added to quench the reaction, which was then transferred to a separation funnel. Additional brine was required to enable separation of the aq. and organic phase. The aq. phase was extracted with DCM until the organic phase was colorless. The combined organics were dried with MgSO₄ and the solvent was removed in *vacuo*. The crude product was obtained as a yellow oil. Toluene was added and partial precipitation was observed. The precipitate was suspended with ultrasonication and filtered off leaving a clear solution. The solvent was removed in *vacuo* yielding an orange viscous oil. The product was dried in high vacuum overnight.

Yield: quant.

¹H-NMR (400 MHz, DMSO-*d*₆): δ / ppm = 7.45 – 7.17 (m, 15H), 3.61 (t, *J* = 6.7 Hz, 1H), 3.51 (t, *J* = 6.7 Hz, 1H), 2.95 (t, *J* = 6.4 Hz, 2H), 1.72 (ddt, *J* = 34.0, 14.2, 7.0 Hz, 2H), 1.54 (p, *J* = 6.7 Hz, 2H), 1.26 (m, 16H).

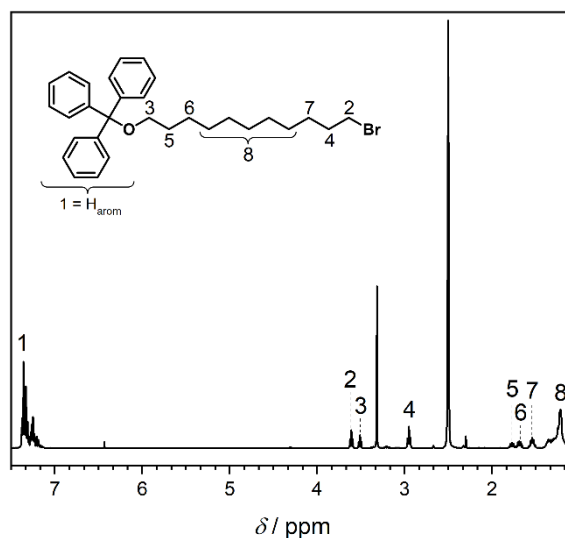
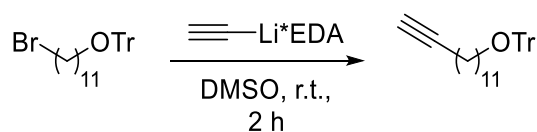


Figure 8.4: Proton NMR spectrum of **4** (DMSO-*d*₆).

8.3.1.1.5 Synthesis of ((Tridec-12-yn-1-yloxy)methanetriyl)tribenzene (5)



To a solution of 3.03 g (90%, 29.6 mmol, 1.5 eq.) lithium acetylide ethylenediamine complex in 20 mL dry DMSO was added a 20 mL THF solution of 9.75 g of **AZ-28** in a portion wise manner in two hours. The reaction was stirred for two hours at room temperature and then carefully quenched by addition of water. The mixture was transferred to a separation funnel with 100 mL additional water and was extracted three times with ethyl acetate. The combined organic phases were washed with 1 M HCl solution and dried with MgSO_4 . The solvent was removed in *vacuo*. The crude product was purified by flash chromatography (cyclohexane/ethyl acetate, gradient 100:0 \rightarrow 70:30 v/v).

Yield: 6.34 g, 73%.

$^1\text{H-NMR}$ (400 MHz, $\text{DMSO-}d_6$): δ / ppm = 7.43 – 7.19 (m, 15H), 2.95 (t, J = 6.5 Hz, 2H), 2.72 (t, J = 2.6 Hz, 1H), 2.13 (td, J = 7.0, 2.7 Hz, 2H), 1.54 (p, J = 6.7 Hz, 2H), 1.48 – 1.08 (m, 16H).

$^{13}\text{C-NMR}$ (100 MHz, $\text{DMSO-}d_6$): δ / ppm = 144.58, 128.64, 128.31, 127.38, 86.22, 63.34, 29.74, 29.34, 29.13, 28.93, 28.58, 26.12, 18.13.

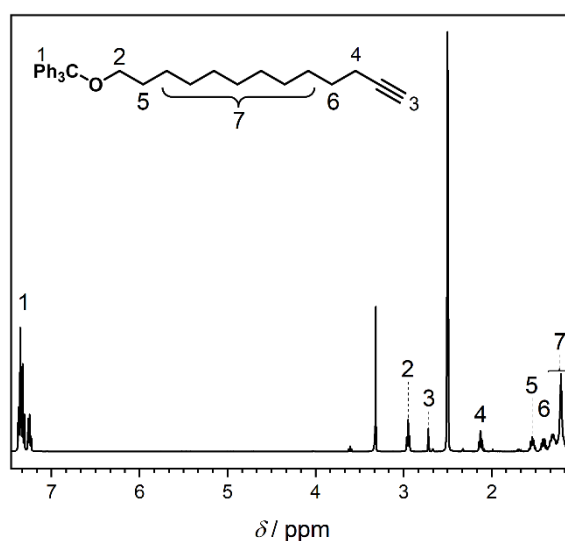


Figure 8.5: Proton NMR spectrum of **5** ($\text{DMSO-}d_6$).

8.3.1.2 General procedure for the alkylation of terminal alkynes

In an oven-dried flask the protected alkynol was dissolved in dry THF. The solution was purged with Argon for 5 minutes and cooled to 0 °C. Subsequently, a 2.5M *n*BuLi solution was added dropwise. The reaction mixture was warmed up to atmospheric temperature and the respected additive (*n*Bu₄NI; KI; TMEDA) if desired. Subsequently, the bromoalkane was added to the reaction as a DMPU solution (full dissolution was ensured *via* slight heating or ultrasonication). The reaction was stirred for the indicated time and subsequently quenched by addition of sat. NH₄Cl solution. The phases were separated and the aq. phase was extracted multiple times with ethyl acetate or DCM, depending on the solubility of the products. The combined organic extracts were washed with brine, dried with MgSO₄ and concentrated *in vacuo*. The crude products were dissolved in MeOH (or MeOH/DCM for **A3-A6**) and TsOH was added in one portion. After the indicated reaction times, the reaction was quenched by addition of water. The organic phase was washed twice with water and the aq. phases were extracted thrice with DCM. The combined organic phases were dried with MgSO₄ and the solvent was removed in *vacuo* yielding a white solid material. The crude products were purified by flash chromatography with cyclohexane/ethyl acetate mixtures or DCM as the eluent. The employed reaction conditions are summarized in Table 3.2

8.3.1.2.1.1 Synthesis of Heptadec-2-yn-1-ol (A1)



¹H-NMR (400 MHz, CDCl₃): δ / ppm = 4.25 (t, J = 2.2 Hz, 2H, H₁), 2.21 (tt, J = 7.2, 2.2 Hz, 2H, H₂), 1.56 – 1.44 (m, 2H, H₃), 1.42 – 1.15 (m, 22H, H₄), 0.92 – 0.84 (m, 3H, H₅).

¹³C-NMR (100 MHz, CDCl₃): δ / ppm = 86.75, 78.25, 51.49, 31.94, 30.95, 29.71, 29.69, 29.67, 29.64, 29.54, 29.37, 29.16, 28.90, 28.62, 22.71, 18.75, 14.13.

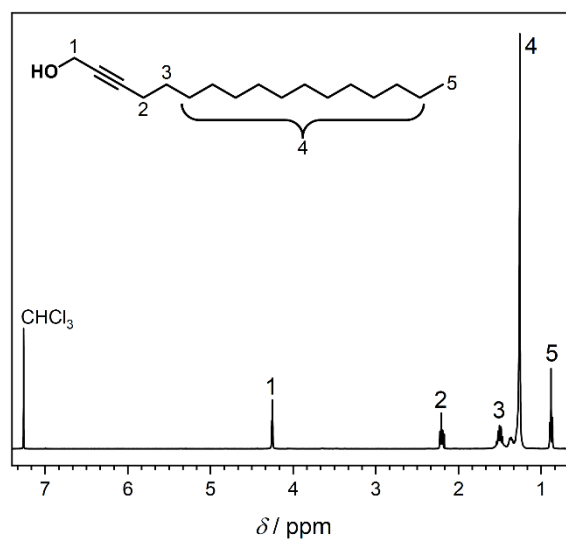


Figure 8.6: Proton NMR spectrum of **A1** (CDCl₃).

8.3.1.2.1.2 Synthesis of Nonadec-2-yn-1-ol (A2)



¹H-NMR (400 MHz, DMSO-*d*₆): δ / ppm = 5.00 (t, J = 5.8 Hz, 1H, H₁), 4.01 (dt, J = 5.7, 2.2 Hz, 2H, H₂), 2.16 (tt, J = 7.0, 2.2 Hz, 2H, H₃), 1.24 (s, 25H), 0.89 – 0.81 (m, 3H, H₆).

¹³C-NMR (100 MHz, DMSO-*d*₆): δ / ppm = 84.58, 80.79, 49.60, 31.76, 29.50, 29.42, 29.17, 29.01, 28.73, 28.69, 22.56, 18.47, 14.43.

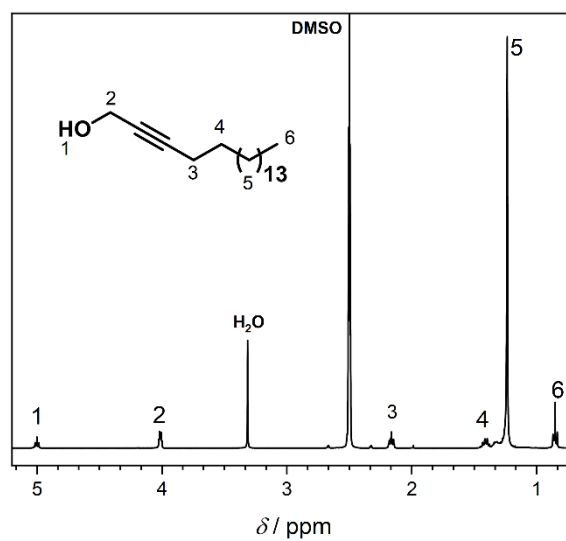
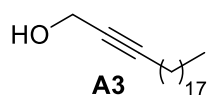


Figure 8.7: Proton NMR spectrum of **A2** (DMSO-*d*₆).

8.3.1.2.1.3 Synthesis of Henicos-2-yn-1-ol (A3)



¹H-NMR (400 MHz, DMSO-*d*₆): δ / ppm = 4.25 (dt, *J* = 6.1, 2.2 Hz, 2H, H₁), 2.21 (tt, *J* = 7.2, 2.2 Hz, 2H, H₂), 1.54 – 1.45 (m, 2H, H₃), 1.25 (s, 30H, H₄ – aliphatic chain), 0.92 – 0.83 (m, 3H, H₅).

¹³C-NMR (100 MHz, DMSO-*d*₆): δ / ppm = 86.72, 78.26, 51.47, 31.93, 30.92, 29.68 (d, *J* = 3.6 Hz), 29.53, 29.37, 29.15, 28.89, 28.62, 22.70, 18.74, 14.12.

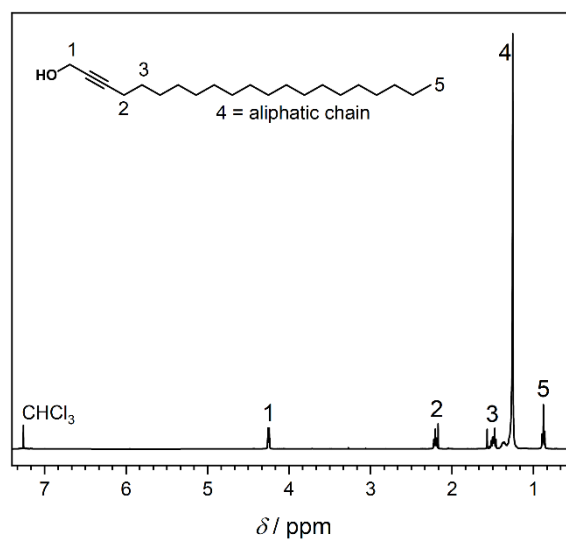


Figure 8.8: Proton NMR spectrum of **A3** (CDCl₃).

8.3.1.2.1.4 Synthesis of Tricos-2-yn-1-ol (A4)



¹H-NMR (400 MHz, DMSO-*d*₆): δ / ppm = 4.25 (dt, J = 6.0, 2.2 Hz, 2H, H₁), 2.21 (tt, J = 7.2, 2.2 Hz, 2H, H₂), 1.53 – 1.43 (m, 2H, H₃), 1.25 (s, 34H, H₄ – aliphatic chain), 0.92 – 0.84 (m, 3H, H₅).

¹³C-NMR (100 MHz, DMSO-*d*₆): δ / ppm = 86.87, 78.39, 51.62, 32.08, 29.83 (d, J = 3.3 Hz), 29.68, 29.51, 29.30, 29.04, 28.76, 22.84, 18.89, 14.27.

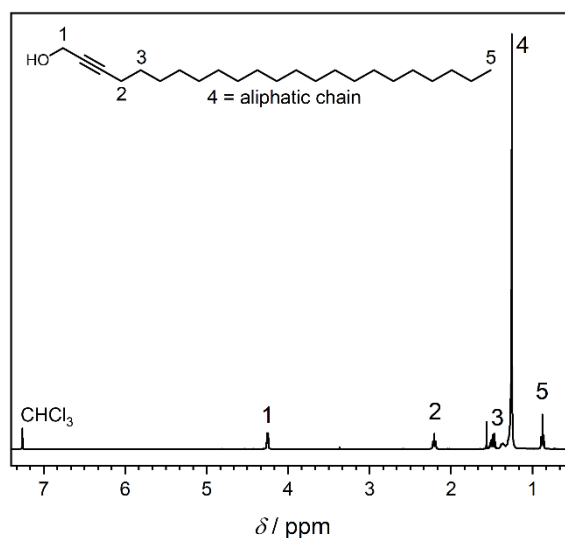
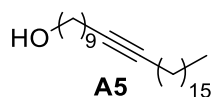


Figure 8.9: Proton NMR spectrum of **A4** (CDCl₃).

8.3.1.2.1.5 Synthesis of Heptacos-10-yn-1-ol (A5)



¹H-NMR (400 MHz, CDCl₃): δ / ppm = 3.64 (t, J = 6.6 Hz, 2 H, H₁), 2.17 – 2.09 (m, 4 H, H₂), 1.56 (q, J = 7.4 Hz, 2 H, H₁), 1.52 – 1.42 (m, 6 H, H₄), 1.41 – 1.15 (m, 34 H, H₅), 0.92 – 0.84 (m, 3 H, H₆).

¹³C-NMR (100 MHz, DMSO-*d*₆): δ / ppm = 63.11, 32.83, 31.94, 29.72, 29.70, 29.68, 29.59, 29.51, 29.40, 29.38, 29.20, 29.17, 29.11, 28.90, 28.85, 25.74, 22.71, 18.78.

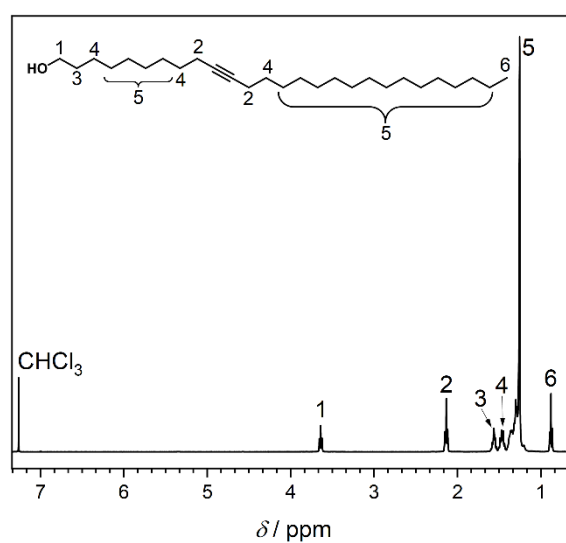


Figure 8.10: Proton NMR spectrum of **A5** (CDCl₃).

8.3.1.2.1.6 Synthesis of Tritriacont-12-yn-1-ol (A6)



$^1\text{H-NMR}$ (400 MHz, CDCl_3): δ / ppm = 3.57 (t, J = 6.6 Hz, 1H), 2.11 – 2.02 (m, 2H), 1.48 (s, 7H), 1.39 (q, J = 7.1 Hz, 1H), 1.19 (d, J = 7.3 Hz, 19H), 0.85 – 0.77 (m, 1H).

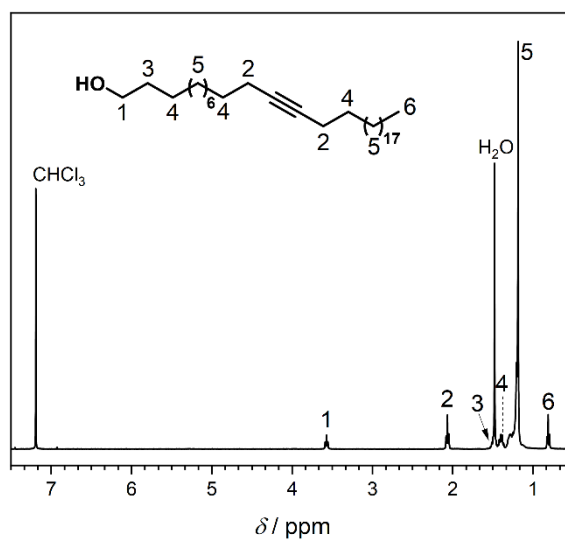


Figure 8.11: Proton NMR spectrum of **A6** (CDCl_3).

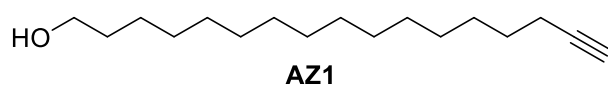
8.3.1.3 General procedure for the Alkyne Zipper reaction

The improved reaction protocol is stated here, for the standard procedure refer to the literature.^[28]

In a 250 mL flask 5.00 eq. KO^tBu are dispersed in 10 mL 1,3-diaminopropane (DAP) with slight heating (heat gun) or ultrasonication. The dispersion is cooled to 0°C and purged with argon for 10 minutes. Subsequently, a *n*BuLi solution (5.00 eq.) is added to the mixture and stirred for 30 minutes. The white dispersion slowly changes color to yellow, indicating successful formation of the isomerization reagent. The starting materials are dispersed in a small volume of the diamine, then slightly heated and placed in an ultrasonic bath for ten minutes. If solid material persisted the volume of DAP was continuously increased while the steps were repeated until a clear concentrated solution was obtained. Consequently, the warm solution was added to the reaction yielding an orange reaction mixture that was usually stirred overnight to ensure an adequate product formation. The reaction is quenched by precipitation into ice-cold water.

Purification of the isomerized alkynols was achieved *via* Flash column chromatography (CH/Ea = 9:1 or pure chloroform).

8.3.1.3.1.1 Synthesis of Heptadec-16-yn-1-ol (AZ1)



¹H-NMR (400 MHz, CDCl₃): δ / ppm = 3.64 (t, J = 6.6 Hz, 2H, H₁), 2.18 (td, J = 7.1, 2.6 Hz, 2H, H₂), 1.94 (t, J = 2.6 Hz, 1H, H₃), 1.54 (dddd, J = 17.9, 15.0, 9.8, 4.5 Hz, 4H H₄), 1.44 – 1.19 (m, 24H, H₅ – aliphatic chain).

ATR-IR: $\tilde{\nu}$ / cm⁻¹: 3354, 3286, 2915, 2848, 1461, 1059, 680, 629.

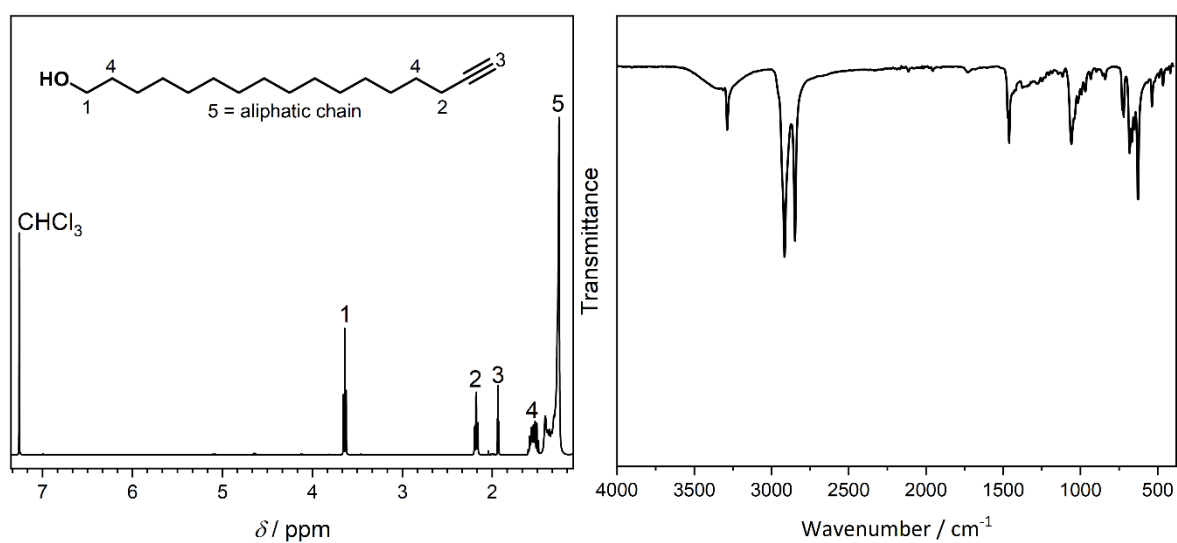
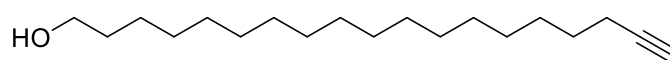


Figure 8.12: Proton NMR (CDCl₃) (*left*) and IR spectrum of **AZ1**.

8.3.1.3.1.2 Synthesis of Nonadec-18-yn-1-ol (AZ2)



AZ2

¹H-NMR (400 MHz, DMSO-*d*₆): δ / ppm = 4.30 (t, J = 5.2 Hz, 1H, H₁), 3.36 (td, J = 6.5, 5.1 Hz, 2H, H₂), 2.72 (t, J = 2.7 Hz, 1H, H₃), 2.13 (td, J = 7.0, 2.7 Hz, 2H, H₄), 1.24 (s, 30H, H₅).

ATR-IR: $\tilde{\nu}$ / cm⁻¹: 3338, 3286, 2915, 2848, 1461, 1059, 682, 629.

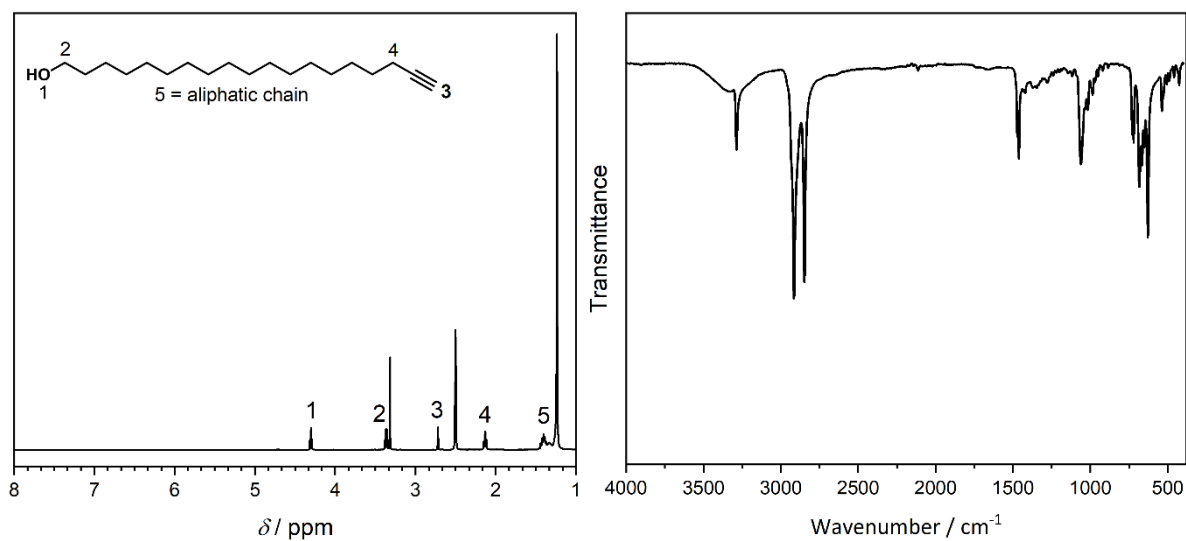
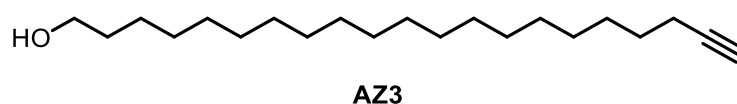


Figure 8.13: Proton NMR (DMSO-*d*₆) (*left*) and IR spectrum of **AZ2**.

8.3.1.3.1.3 Synthesis of Henicos-20-yn-1-ol (AZ3)



¹H-NMR (400 MHz, CDCl₃): δ / ppm = 3.64 (q, J = 6.1 Hz, 2H, H₁), 2.22 – 2.13 (m, 2H, H₂), 1.93 (d, J = 3.1 Hz, 1H, H₃), 1.67 – 1.45 (m, 4H, H₄), 1.26 (d, J = 6.9 Hz, 28H, H₅).

ATR-IR: $\tilde{\nu}$ / cm⁻¹: 3348, 3286, 2914, 2846, 1462, 1057, 682, 627.

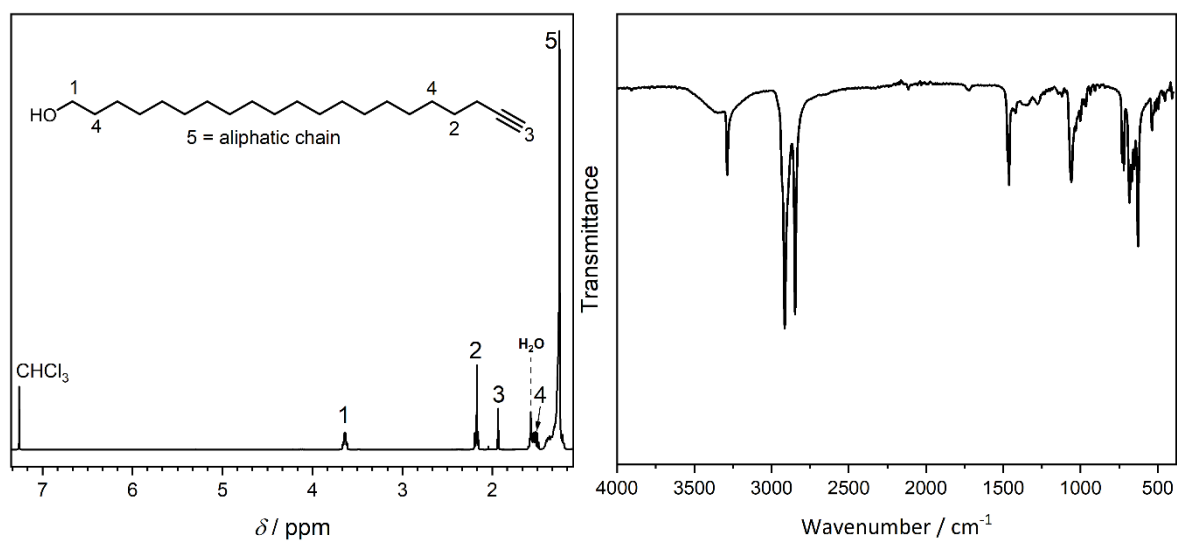
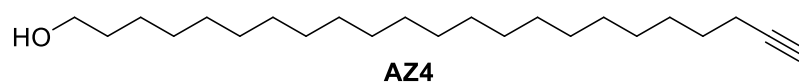


Figure 8.14: Proton NMR (CDCl₃) (*left*) and IR spectrum of **AZ3**.

8.3.1.3.1.4 Synthesis of Tricos-22-yn-1-ol (AZ4)



¹H-NMR (400 MHz, CDCl₃): δ / ppm = 3.64 (q, J = 6.1 Hz, 2H, H₁), 2.22 – 2.13 (m, 2H, H₂), 1.93 (d, J = 3.1 Hz, 1H, H₃), 1.67 – 1.45 (m, 4H, H₄), 1.26 (d, J = 6.9 Hz, 34H, H₅).

ATR-IR: $\tilde{\nu}$ / cm⁻¹: 3334, 3286, 2914, 2846, 1462, 1061, 719, 684, 627.

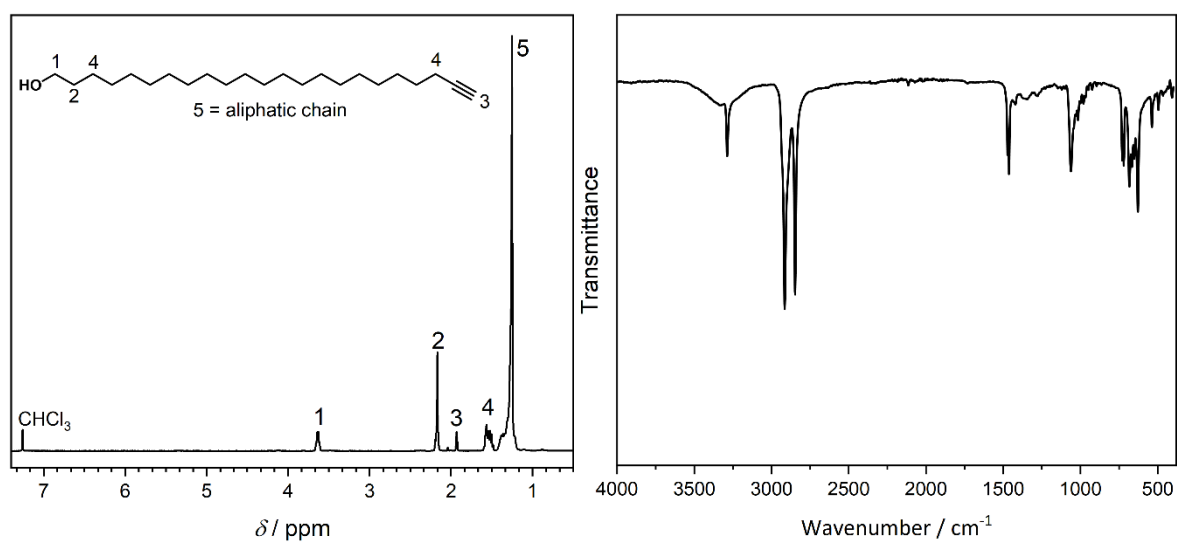
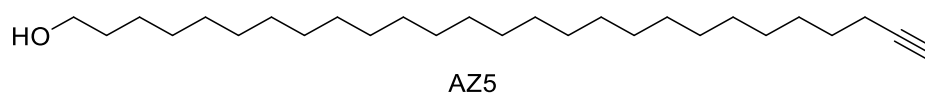


Figure 8.15: Proton NMR (CDCl₃) (*left*) and IR spectrum of **AZ4**.

8.3.1.3.1.5 Synthesis of Heptacos-26-yn-1-ol (AZ5)



$^1\text{H-NMR}$ (400 MHz, CDCl_3): δ / ppm = 3.64 (t, J = 6.6 Hz, 2H, H_1), 2.18 (td, J = 7.1, 2.7 Hz, 2H, H_2), 1.93 (t, J = 2.6 Hz, 1H, H_3), 1.62 – 1.46 (m, 4H, H_4), 1.25 (s, 42H, H_5).

$^{13}\text{C-NMR}$ (100 MHz, CDCl_3): δ / ppm = 68.02, 63.14, 32.84, 29.71, 29.63, 29.45, 29.13, 28.79, 28.52, 25.75, 18.42.

ATR-IR: $\tilde{\nu}$ / cm^{-1} : 3354, 3284, 2915, 2848, 1461, 1059, 725, 653.

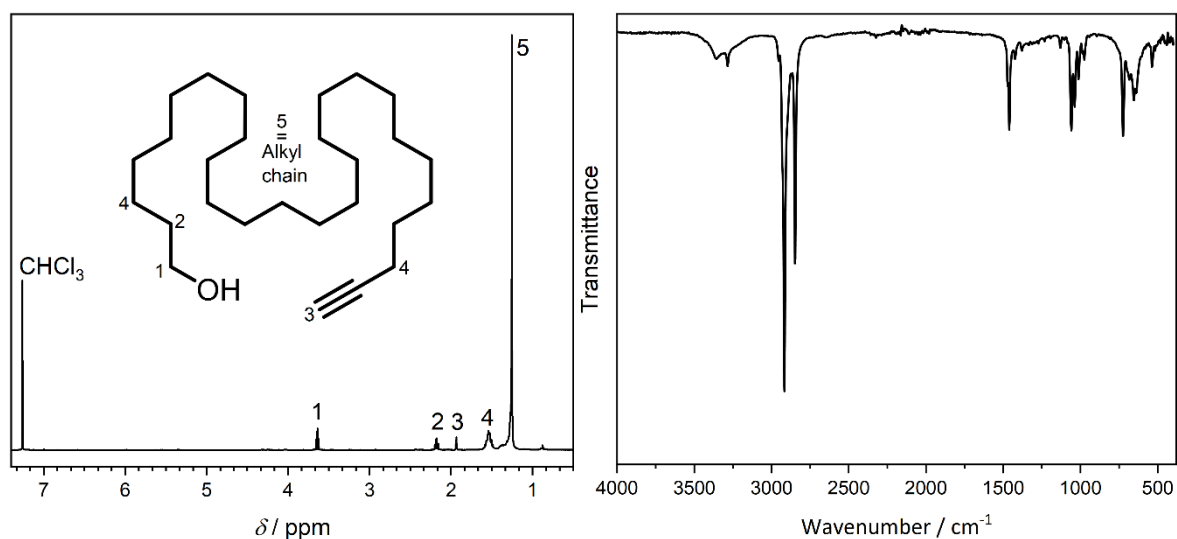
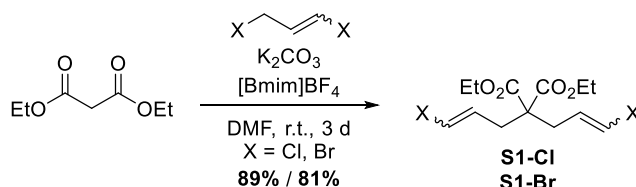


Figure 8.16: Proton NMR (CDCl_3) (*left*) and IR spectrum of **AZ4**.

8.3.1 Experimental Procedures for Chapter 4

8.3.1.1 Monomer Synthesis

8.3.1.1.1 Synthesis of Diethyl 2,2-bis(3-haloallyl)malonate (S1-Cl & S1-Br)



General procedure:

In an oven-dried 100 mL flask K₂CO₃ (2.50 eq.) was weighed in, dispersed in 20 mL DMF and cooled to 0 °C. Diethyl malonate (1.00 eq.) is added *via* syringe and the reaction is stirred for 15 minutes at 0 °C. The respective 1,3-dihalopropene (2.20 eq.) was added in portions over 10 minutes. Subsequently, [Bmim]PF₄ (0.10 eq.) was added *via* syringe and the reaction was stirred for three days. Subsequently, the reactions mixture was filtered into a separatory funnel and the solids were rinsed with ethyl acetate. Water was added and the aqueous phase was extracted thrice with ethyl acetate. The combined organic phases were washed with brine, dried with MgSO₄ and the solvent was removed *in vacuo*. The obtained crude oils were purified by Flash column chromatography (CH/Ea = 9:1).

Diethyl 2,2-bis(3-chloroallyl)malonate (S1-Cl)

Yield: 2.43 g, 89%.

¹H-NMR (400 MHz, CDCl₃): δ / ppm = 6.03 (dt, *J* = 13.2, 1.3 Hz, 2H, H₁), 5.76 (dt, *J* = 13.2, 8.0 Hz, 2H, H₂), 4.20 (q, *J* = 7.1 Hz, 4H, H₃), 2.61 (dd, *J* = 7.9, 1.3 Hz, 4H, H₄), 1.25 (t, *J* = 7.1 Hz, 6H, H₅).

¹³C-NMR (100 MHz, DMSO-*d*₆): δ / ppm = 170.06, 127.65, 121.11, 61.86, 57.05, 34.50, 14.24.

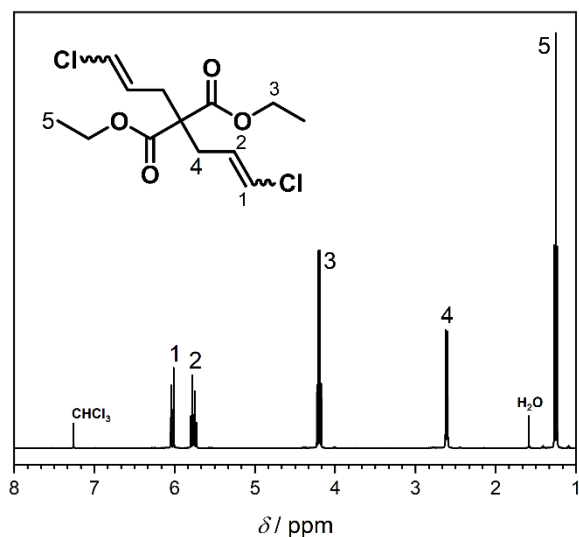


Figure 8.17: Proton NMR (CDCl₃) of S1-Cl.

Diethyl 2,2-bis(3-bromoallyl)malonate (S1-Br)

Yield: 5.42 g, 81%.

¹H-NMR (400 MHz, CDCl₃): δ / ppm = 6.36 – 5.93 (m, 4H, H₁), 4.20 (q, J = 7.2 Hz, 4H, H₂), 2.90 – 2.53 (m, 4H, H₃), 1.26 (t, J = 7.1 Hz, 6H, H₄).

¹³C-NMR (100 MHz, DMSO-*d*₆): δ / ppm = 84.82, 68.01, 63.10, 32.83, 29.67, 29.61, 29.51, 29.44, 29.12, 28.77, 28.51, 25.75, 18.41.

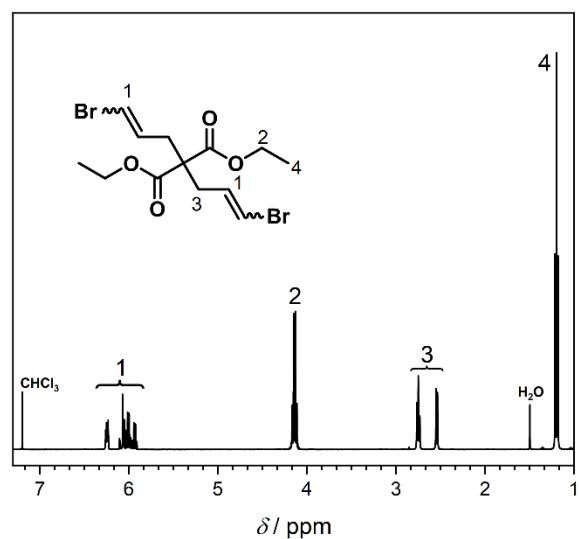
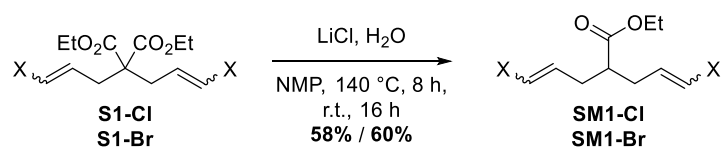


Figure 8.18: Proton NMR (CDCl₃) of S1-Br.

8.3.1.1.2 Synthesis of Ethyl 5-halo-2-(3-bromoallyl)pent-4-enoate (SM1-Cl & SM1-Br)



General procedure:

In a 2-neck 250 mL flask LiCl (3.00 eq.) and H₂O (2.00 eq.) were weighed in. 10 mL of dry NMP were added and the flask was equipped with a waterless condenser. The solution was purged with argon for 5 minutes and the condenser was sealed with a septum and an argon balloon. **S1-X** (1.00 eq.) was dissolved in 5 mL NMP and another 5 mL were used to rinse the flask. The NMP solution was added to the reaction mixture under argon and the flask was placed in a 140 °C preheated oil bath. The reaction mixture was stirred 8 h at 140 °C, then the heating was stopped and the reaction was left stirring in the hot oil bath for another 16 hours. Ethyl acetate was added and the mixture was transferred to a separation funnel. Saturated NH₄Cl solution was added and the phases were separated. The aq. phase was extracted with ethyl acetate and the combined organics were washed with 1M HCl and brine, dried with MgSO₄. Removal of the solvent *in vacuo* yielded yellow oils. Purification was performed *via* flash column chromatography (CH 100% → CH/EA = 95:5). The products were obtained as yellowish oils.

Ethyl 5-bromo-2-(3-chloroallyl)pent-4-enoate (SM1-Cl)

Yield: 7.20 g, 50%.

¹H-NMR (400 MHz, CDCl₃): δ / ppm = 6.01 (dt, J = 13.2, 1.3 Hz, 2H, H₁), 5.82 (dt, J = 13.2, 7.6 Hz, 2H, H₂), 4.15 (q, J = 7.1 Hz, 2H, H₃), 2.49 (tt, J = 7.8, 6.0 Hz, 1H, H₄), 2.43 – 2.17 (m, 4H, H₅), 1.26 (t, J = 7.1 Hz, 3H, H₆).

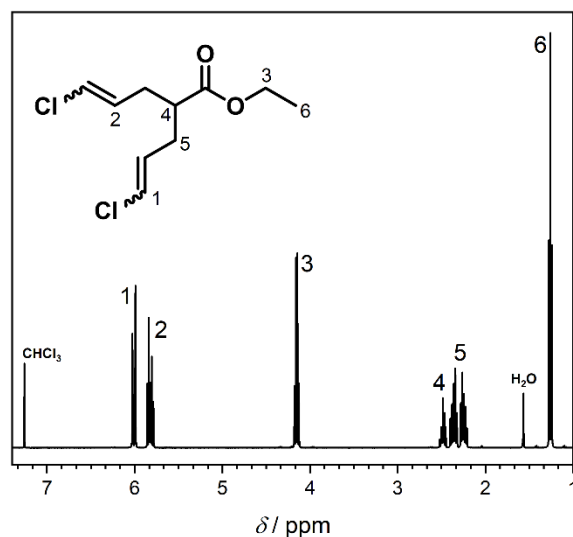


Figure 8.19: Proton NMR (CDCl_3) of **SM1-Cl**.

Ethyl 5-bromo-2-(3-bromoallyl)pent-4-enoate (**SM1-Br**)

Yield: 1.37 g, 58%.

$^1\text{H-NMR}$ (400 MHz, CDCl_3): δ / ppm = 6.31 – 6.01 (m, 4H, H_1), 4.25 – 4.09 (m, 2H, H_2), 2.76 – 2.15 (m, 5H, H_3), 1.26 (ddt, J = 8.1, 7.3, 1.0 Hz, 3H, H_4).

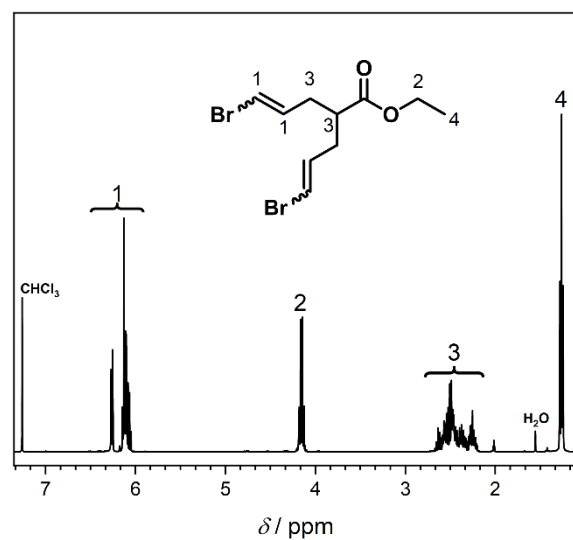


Figure 8.20: Proton NMR (CDCl_3) of **SM1-Br**.

8.3.1.1.3 Synthesis of Hexadeca-1,15-diyne (DA₁₅)



To a dispersion of 0.655 g lithium acetylide ethylenediamine complex (90%, 6.40 mmol, 2.10 eq.) in 10 mL dry DMSO was added a 10 mL DMSO solution of 1 g 1,12-dibromododecan (3.05 mmol, 1.00 eq.) in a portion wise manner. After full addition, the reaction was stirred overnight at room temperature and then carefully quenched by the addition of water. The mixture was transferred to a separation funnel with 100 mL additional water and was extracted three times with petrol ether. The combined organic phases were washed with 1 M HCl solution and dried with MgSO_4 . The solvent was removed in *vacuo*. Purification was performed *via* flash column chromatography (PE 100% \rightarrow PE/EA = 95:5).

Yield: 0.631 g, 95%.

¹H-NMR (400 MHz, CDCl_3): δ / ppm = 2.18 (td, J = 7.1, 2.6 Hz, 4H, H₁), 1.94 (t, J = 2.7 Hz, 2H, H₂), 1.58 – 1.46 (m, 4H, H₃), 1.43 – 1.34 (m, 4H, H₄), 1.32 – 1.23 (m, 12H, H₅).

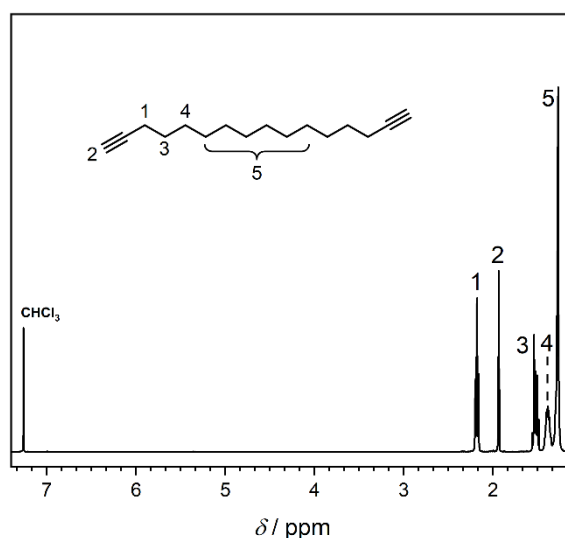
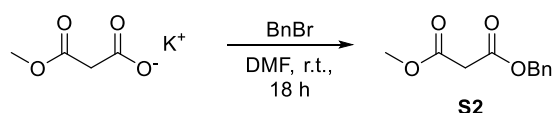


Figure 8.21: Proton NMR (CDCl_3) of DA₁₂.

8.3.1.1.4 Synthesis of Benzyl methyl malonate (S2)



A dispersion of 5 g (32.0 mmol, 1 eq.) of methyl potassium malonate in 70 mL dry DMF was purged with argon for ten minutes. Subsequently, 3.61 mL (5.20 g, 30.4 mmol, 0.95 eq.) of benzyl bromide was added slowly (first dropwise, then faster) to the mixture. The reaction was stirred for 21 hours at atmospheric temperature and quenched by addition of water. Ethyl acetate was added and the phases were separated. The aqueous phase was once extracted with ethyl acetate and the combined organic phases were washed three times with water. After drying with MgSO₄ and removal of the solvent *in vacuo* the crude oil was purified by passing it through a silica plug (CH/Ea = 9:1). The product was obtained as a yellow oil.

Yield: 5.42 g, 81%.

¹H-NMR (400 MHz, CDCl₃): δ / ppm = 7.43 – 7.27 (m, 5H, H₁), 5.19 (s, 2H, H₂), 3.74 (s, 3H, H₃), 3.44 (s, 2H, H₄).

¹³C-NMR (100 MHz, CDCl₃): δ / ppm = 167.00, 166.48, 135.37, 128.74, 128.59, 128.42, 67.40, 52.67, 41.47.

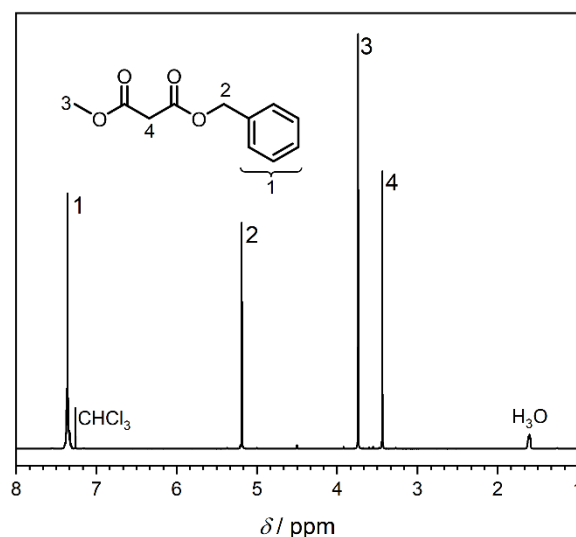
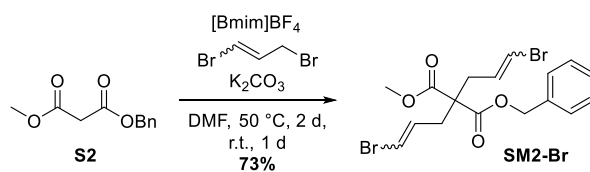


Figure 8.22: Proton NMR (CDCl₃) of S2.

8.3.1.1.5 Synthesis of 1-Benzyl 3-methyl 2,2-bis(3-bromoallyl)malonate (SM2-Br)



The synthesis was conducted in similar manner as for SM1-X (see 8.3.1.1.1).

Yield: 3.15 g, 73%.

¹H-NMR (400 MHz, CDCl₃): δ / ppm = 7.34 (dtt, J = 11.9, 7.3, 1.9 Hz, 5H, H₁), 6.37 – 5.88 (m, 4H, H₂), 5.18 (d, J = 4.6 Hz, 2H, H₃), 3.68 (d, J = 1.6 Hz, 3H, H₄), 2.90 – 2.55 (m, 4H, H₅).

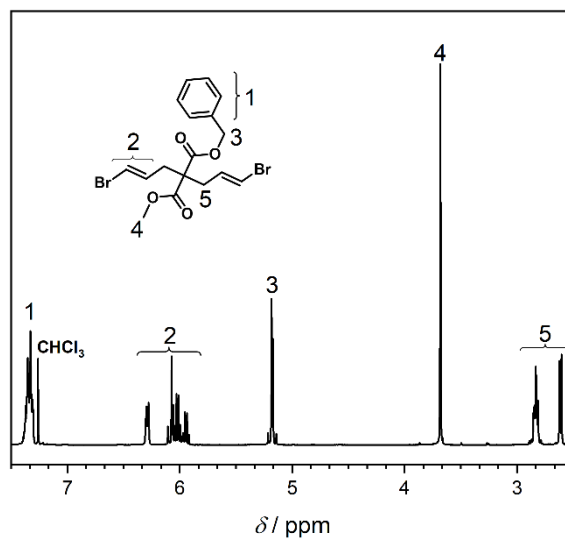
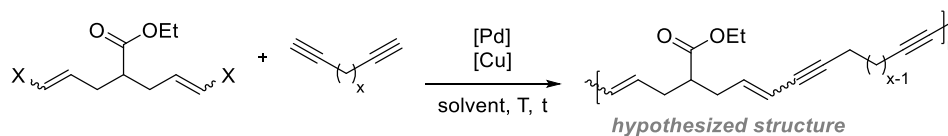


Figure 8.23: Proton NMR (CDCl₃) of SM2-Br.

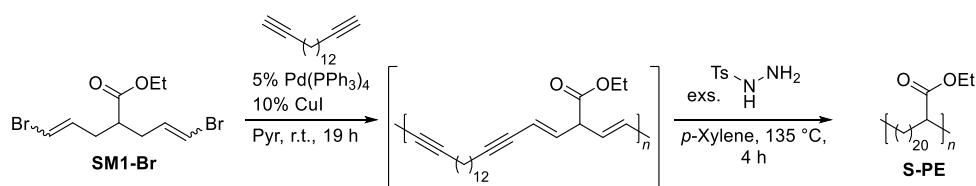
8.3.1.2 General Procedure for SONOGASHIRA Polycondensation reactions



In an oven-dried crimp vial both monomers (dialkyne and divinyl halide) were weighed in, dissolved in dry pyrrolidine (or pyrrolidine/solvent mixtures) mixtures, purged carefully with argon for ten minutes and stirred at room temperature. In a second crimp vial the palladium and copper catalysts were weighed in, dissolved in dry pyrrolidine and purged with argon for ten minutes. Subsequently, the catalyst solution was injected into the reaction mixture at once and placed in a vial block at the desired temperature. The reaction was stirred for the indicated time, filtered through neutral aluminum oxide and precipitated in MeOH or Et₂O.

Stoichiometric calculations were performed with respect to 100 mg of the dihalide monomer, with one equivalent of dialkyne. 5 mol% of palladium catalyst and 10 mol% of copper iodine. Solvent (pyrrolidine) volumes were calculated to be 50:50 mixtures and yield a final concentration of $M = 0.15 \text{ mol}\cdot\text{L}^{-1}$.

8.3.1.3 Procedure for the *in-situ* hydration (S-PE)



The polymerization was conducted as described in the previous section prior to hydrogenation.

In a 250 mL flask equipped with a waterless condenser 2 g of *p*-toluenesulfonyl hydrazide (10.7 mmol) were dissolved in 10 mL *p*-xylene, 3 mL of triethyl amine were added and the mixture was purged with argon for 10 minutes. After 19 h of polymerization time, under argon, the polymerization mixture was transferred to the flask, which was immediately placed in a 135 °C preheated oil bath. The previously white mixture slowly darkened and gas evolution was observed. After one hour, the solution turned grey and heating was stopped. After the mixture reached room temperature, again 3 mL of triethyl amine and 2 g of *p*-toluenesulfonyl hydrazide were added under argon and the process was repeated. The thus obtained grey mixture was subsequently precipitated in 250 mL of MeOH, which was acidified with a few drops of conc. HCl. The mixture was left to settle and excess MeOH was decanted. The remaining mixture was centrifuged, upon which black solids were obtained. The material was precipitated two more times in MeOH and dried *in vacuo*.

¹H-NMR (400 MHz, CDCl₃): δ / ppm = 4.13 (q, J = 7.1 Hz, H₁), 2.46 – 2.20 (m, H₂), 2.13 (q, J = 7.6 Hz, H₃), 2.08 – 1.93 (m, J = 6.8 Hz, H₄), 1.70 – 1.14 (m, H₅).

THF-SEC: 14.5 kg/mol, \bar{D} = 2.45.

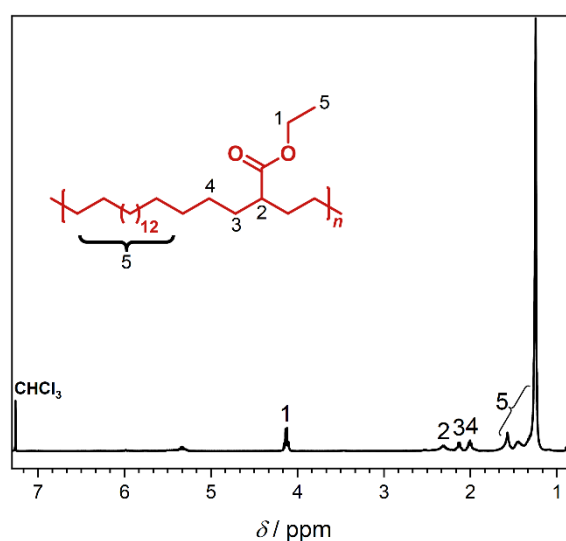
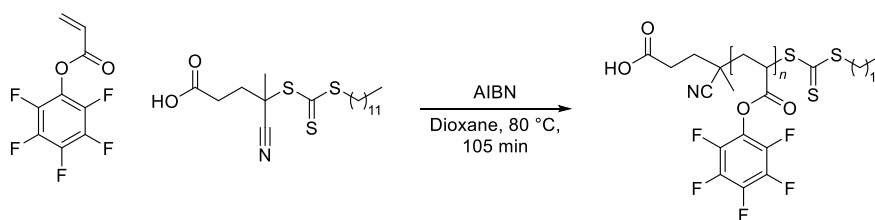


Figure 8.24: Proton NMR (CDCl₃) of S-PE.

8.3.2 Experimental Procedures for Chapter 5

8.3.2.1 RAFT Polymerization of Pentafluoro acrylate (RAFT-PPFPA)



In an oven-dried 5 mL flask 0.681 mL pentafluorophenyl acrylate (0.9858 g, 4.33 mmol, 48 eq.), 0.35 mg CDTA (0.086 mmol, 1 eq.) and 2.6 mg AIBN (0.016 mmol) were dissolved in 1.3 mL dioxane and the solution was purged with argon for 10 minutes in a water bath. Subsequently, the flask was lowered in a preheated 80 °C warm oil bath and stirred for 105 minutes. The reaction was quenched by opening it to air and cooling in an ice bath. The yellow solution was precipitated twice in cold methanol and dried overnight in *vacuo* at 40 °C to yield a slightly yellow powder.

¹H-NMR (400 MHz, CDCl₃): δ / ppm = 3.09 (s, H₁ - backbone), 2.28 – 1.84 (m, H₂ - backbone), 1.46 – 1.16 (m, H₃ – dodecyl chain), 0.87 (t, J = 6.5, 3.1 Hz, H₄ – dodecyl methyl).

¹⁹F-NMR (377 MHz, CDCl₃): δ / ppm = -153.17 (d, J = 36.4 Hz), -156.73, -162.12.

THF-SEC: 7.11 kg/mol, $D = 1.1$.

ATR-IR: $\tilde{\nu}$ / cm⁻¹: 1782, 1516, 1079, 989.

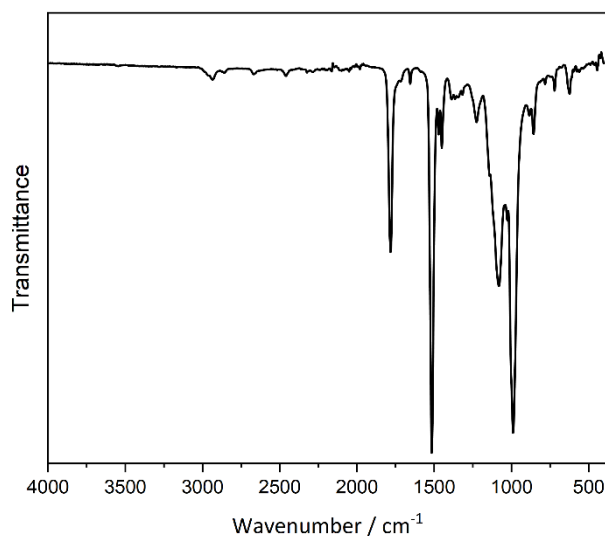
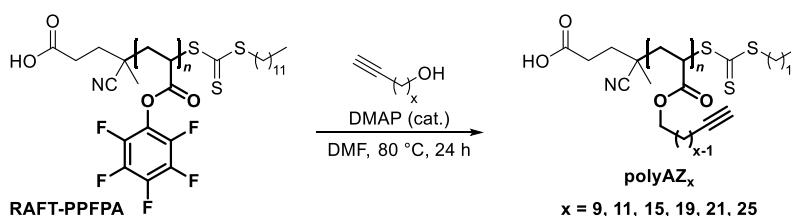


Figure 8.25: ATR-IR spectrum of RAFT-PPFPA.

Corresponding NMR spectra are depicted in Figure 5.1, IR spectrum and DSC thermogram in Figure 5.3.

8.3.2.2 General procedure for the trans-esterification of RAFT-PPFPA



In an oven-dried crimp vial 100 mg of **RAFT-PPFPA** (7.11 kg/mol, $\bar{D} = 1.1$), 10.3 mg DMAP (0.083 mmol, 0.2 eq.) and the specific alkyne (1.2 eq.) were dissolved in 1 mL DMF (final concentration of 420 μM) and stirred at 80 $^\circ\text{C}$ for 24 h. After cooling to room temperature, the reaction was quenched by addition of saturated NaHCO_3 solution and ethyl acetate. The phases were separated, the organic phase was washed once with brine, dried with MgSO_4 and concentrated *in vacuo*. The obtained crude material was purified by precipitation in cold PE (**polyAZ₉** & **polyAZ₁₁**), MeOH (**polyAZ₁₅**, **polyAZ₁₉**, **polyAZ₂₁**) or EtOH (**polyAZ₂₅**) and dried *in vacuo* at 40 $^\circ\text{C}$. The products were obtained as brown oils (**polyAZ₉** & **polyAZ₁₁**) or beige solids (**polyAZ₁₅**, **polyAZ₁₉**, **polyAZ₂₁** & **polyAZ₂₅**).

The corresponding SEC traces of all polymers are shown in Figure 5.3.

Table 8.1: Summarized SEC results for the trans-esterification reactions.

Entry	Polymer	M_n [kg mol ⁻¹] ^{a)}	M_w [kg mol ⁻¹]	\bar{D} (M_w/M_n)
1	RAFT-PPFPA	7.10	8.00	1.13
2	polyAZ ₉	8.50	9.60	1.13
3	polyAZ ₁₁	10.4	11.6	1.12
4	polyAZ ₁₅	11.5	13.0	1.16
5	polyAZ ₁₉	13.0	14.7	1.13
6	polyAZ ₂₁	14.0	15.6	1.12
7	polyAZ ₂₅	16.0	18.5	1.11

Table 8.2: Summarized DSC results for the polymers in Chapter 5.

Entry	Polymer	T_g [°C] ^{a)}	T_m [°C] ^{b)}
1	RAFT-PPFPA	50.6	-
2	polyAZ ₉	-50.4	-
3	polyAZ ₁₁	-26.7	-
4	polyAZ ₁₅	-	26.8
5	polyAZ ₁₉	-	54.9
6	polyAZ ₂₁	-	62.3
7	polyAZ ₂₅	-	77.4

8.3.2.3 polyAZ₉

¹H-NMR (400 MHz, CDCl₃): δ / ppm = 4.06 (d, J = 31.5 Hz, H₁), 2.18 (td, J = 7.2, 2.6 Hz, H₂), 1.94 (p, J = 1.7 Hz, H₃ - alkyne), 1.73 – 1.15 (m, alkyl chain & backbone).

ATR-IR: $\tilde{\nu}$ / cm⁻¹: 3290, 2927, 2854, 1518, 1162, 1003, 625.

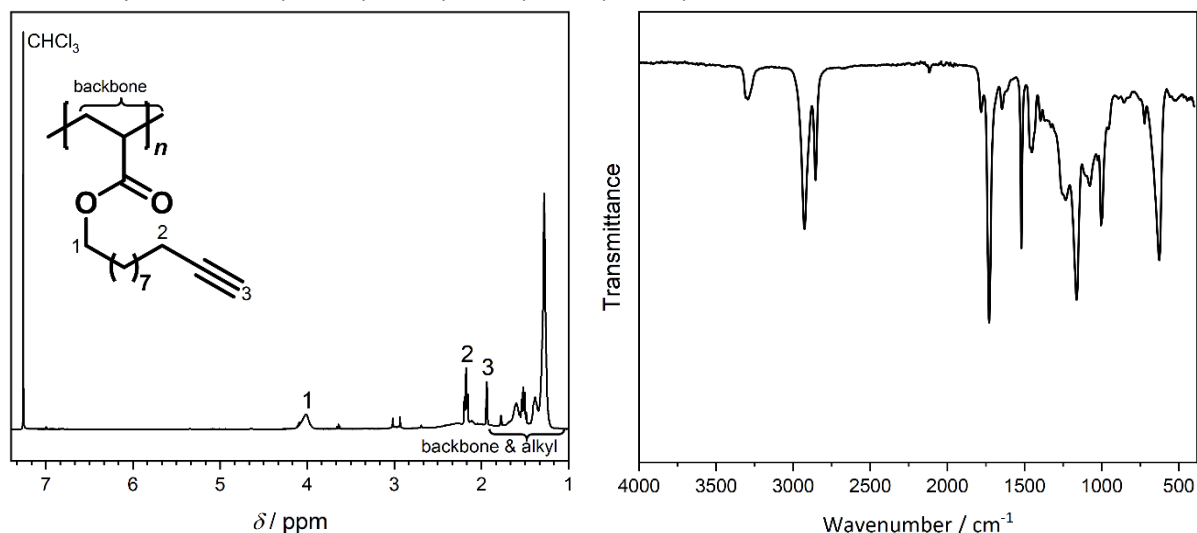


Figure 8.26: Proton NMR (CDCl₃) (left) and ATR-IR spectrum (right) of polyAZ₉.

8.3.2.4 polyAZ₁₁

¹H-NMR (400 MHz, CDCl₃): δ / ppm = 4.02 (s, H₁), 2.18 (td, J = 7.1, 2.6 Hz, H₂), 1.94 (td, J = 2.8, 1.3 Hz, H₃), 1.67 – 1.15 (m, alkyl chain & backbone).

ATR-IR: $\tilde{\nu}$ / cm⁻¹: 3305, 2922, 2852, 1729, 1520, 1454, 1164, 1064, 1003, 625.

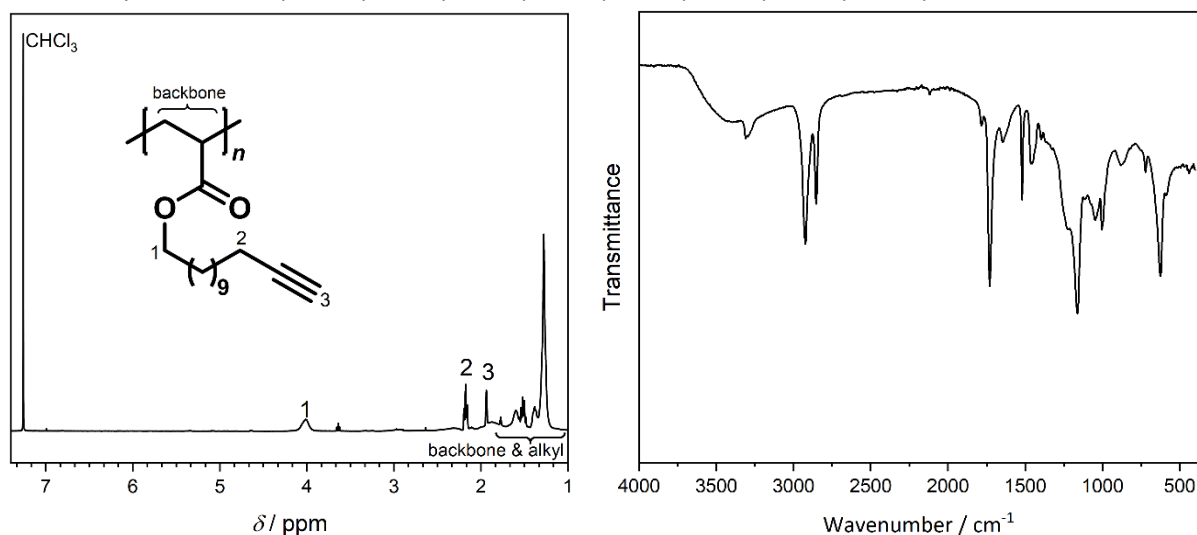


Figure 8.27: Proton NMR (CDCl₃) (left) and ATR-IR spectrum (right) of polyAZ₁₁.

8.3.2.5 polyAZ₁₅

¹H-NMR (400 MHz, CDCl₃): δ / ppm = 4.02 (s, H₁), 2.18 (td, J = 7.1, 2.7 Hz, H₂), 1.93 (t, J = 2.7 Hz, H₃), 1.77 – 1.11 (m, alkyl chain & backbone).

ATR-IR: $\tilde{\nu}$ / cm⁻¹: 3292, 2930, 2859, 1520, 1160, 1013, 632.

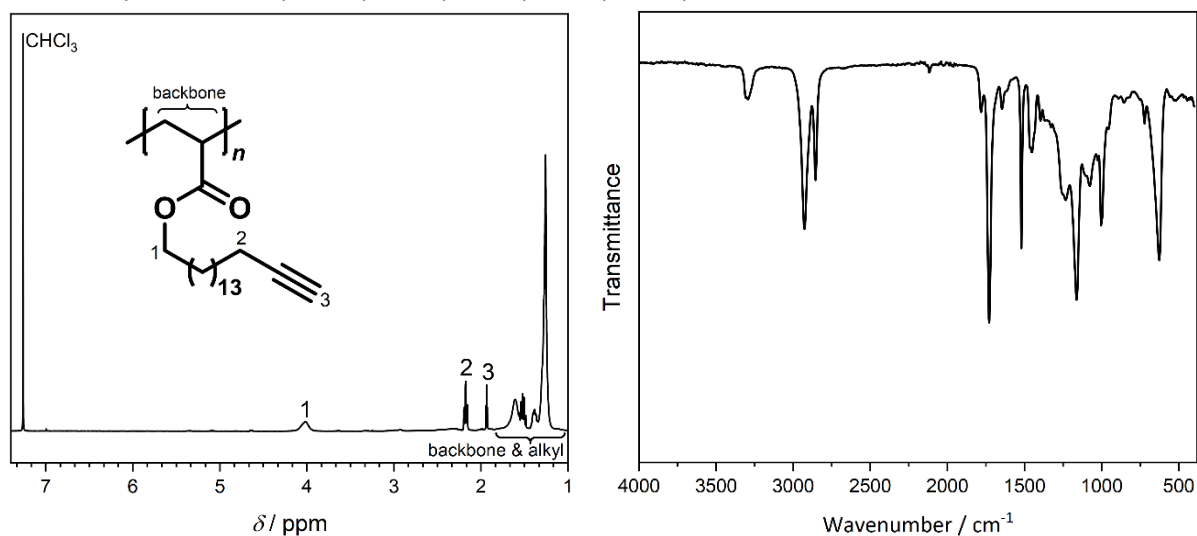


Figure 8.28: Proton NMR (CDCl₃) (left) and ATR-IR spectrum (right) of polyAZ₁₅.

8.3.2.6 polyAZ₁₉

¹H-NMR (400 MHz, CDCl₃): δ / ppm = 4.02 (s, H₁), 2.24 – 2.13 (m, H₂), 1.94 (d, J = 2.8 Hz, H₃), 1.72 – 1.13 (m, alkyl chain & backbone).

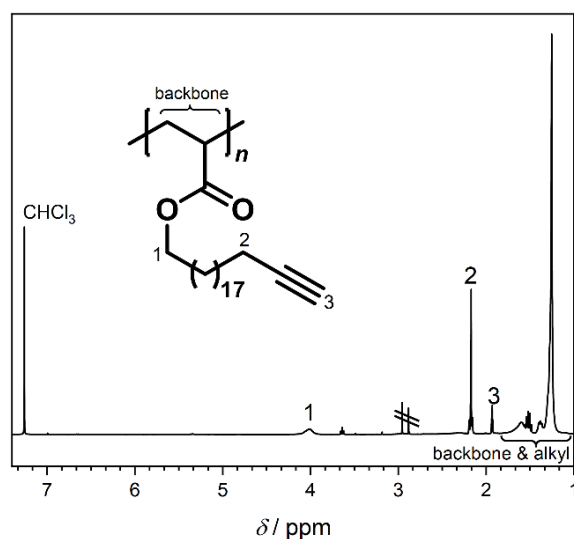


Figure 8.29: Proton NMR (CDCl₃) of polyAZ₁₉.

8.3.2.7 polyAZ₂₁

¹H-NMR (400 MHz, CDCl₃): δ / ppm = 4.03 (s, H₁), 2.17 (td, J = 7.1, 2.6 Hz, H₂), 1.96 – 1.90 (m, H₃), 1.73 – 1.05 (m, alkyl chain & backbone).

ATR-IR: $\tilde{\nu}$ / cm⁻¹: 3286, 2916, 2848, 1729, 1520, 1464, 1162, 995, 719, 629.

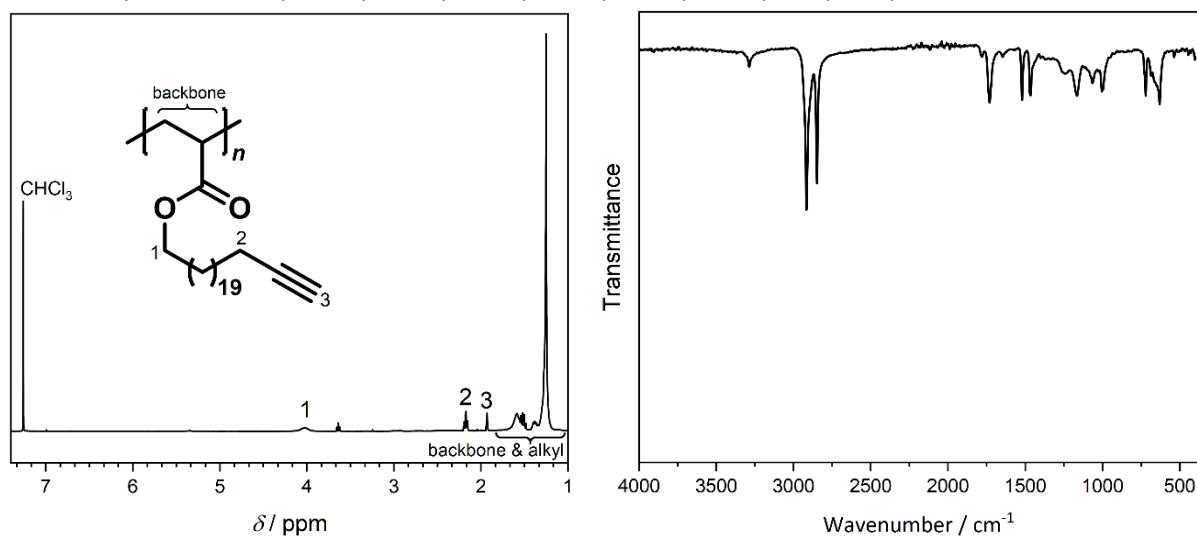


Figure 8.30: Proton NMR (CDCl₃) (left) and ATR-IR spectrum (right) of polyAZ₂₁.

8.3.2.8 polyAZ₂₅

¹H-NMR (400 MHz, CDCl₃): δ / ppm = 4.02 (s, H₁), 2.17 (td, J = 7.1, 2.7 Hz, H₂), 1.93 (t, J = 2.7 Hz, H₃), 1.81 – 1.11 (m, alkyl chain & backbone).

ATR-IR: $\tilde{\nu}$ / cm⁻¹: 3282, 2915, 1731, 1467, 1161, 719, 631.

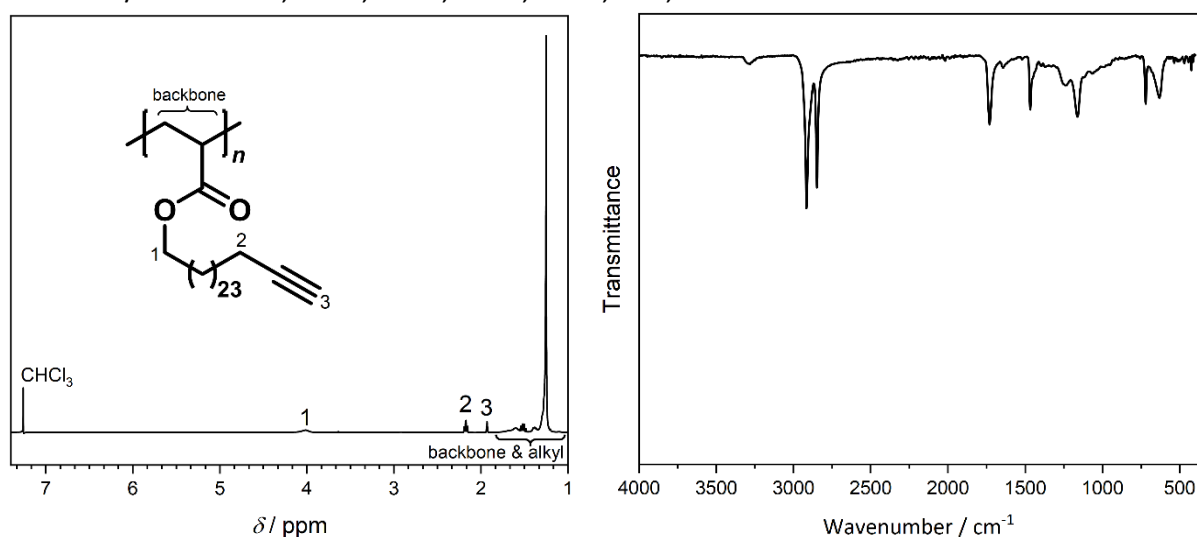
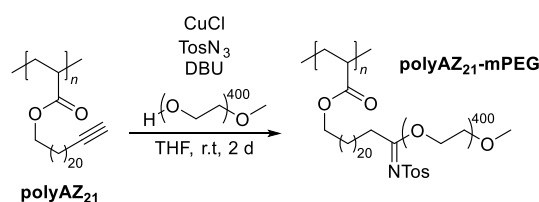


Figure 8.31: Proton NMR (CDCl₃) (left) and ATR-IR spectrum (right) of polyAZ₂₅.

8.3.2.9 3-Component reaction (3-CR) with polyAZ₂₁ (polyAZ₂₁-mPEG)



In an oven-dried crimp vial 60 mg of **polyAZ₂₁** (0.154 mmol of repeating unit, 1 eq.), 5 mg of copper(I) chloride (0.05 mmol, 0.33 eq.) and 78.9 mg of mPEG-400 (0.184 mmol, 1.20 eq.) were dissolved in 2 mL of THF, purged with argon for 5 minutes and stirred at atmospheric temperature. In a second oven-dried crimp vial 90.8 mg tosyl azide (0.460 mmol, 3.00 eq.) were dissolved in 1 mL THF, purged with argon for 5 minutes and added to the previous reaction mixture, yielding a yellow solution. Finally, 0.115 mL DBU (117 mg, 0.768 mmol, 5 eq.) was added *via* syringe to the reaction mixture which then slowly turned brown. NMR spectroscopy revealed nearly full conversion of the alkyne moiety after two days and the reaction was subsequently dried in *vacuo*. The crude material was dissolved in a small volume of THF and precipitated twice into cold Et₂O yielding a dark brown, slightly sticky material that was dried in *vacuo* at 40 °C. Further purification was done *via* precipitation in room-temperature warm EtOH and subsequent drying in *vacuo* at 40 °C for three days.

The respective ¹H NMR and IR spectrum, SEC curve and DSC thermogram are depicted in Scheme 5.5.

¹H-NMR (400 MHz, CDCl₃): δ / ppm = 7.79 (d, J = 7.9 Hz, 2H, H₁), 7.15 (d, J = 7.8 Hz, 2H, H₂), 3.99 (s, 2H, H₃), 3.76 – 3.40 (m, 36H, H₄ – PEG chain), 3.37 (s, 3H, H₅), 2.34 (s, 3H, H₆), 1.96 – 1.06 (m, H₇ & H₈ – backbone and alkyl chain).

DMAc-SEC: 22.5 kg/mol, D = 1.24.

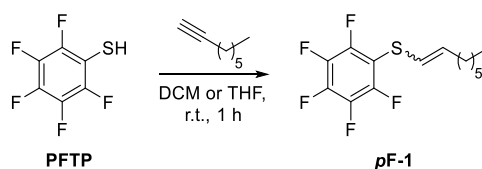
DSC: T_g = 63.6 °C.

ATR-IR: $\tilde{\nu}$ / cm⁻¹: 3435 (broad), 3554, 2916, 2848, 1729, 1645 (C=N), 1468, 1445, 1324(S=O), 1118 (broad), 1032, 1009, 816, 680, 555.

8.3.3 Experimental Procedures for Chapter 6

8.3.3.1 Experimental Procedures for the Synthesis of Small Molecules

8.3.3.1.1 Synthesis of Oct-1-en-1-yl(perfluorophenyl)sulfane (*p*F-1)



In a 50 mL flask, 700 mg of 1-octyne (6.35 mmol, 1.10 eq.) were dissolved in 3 mL of THF and purged with argon for 10 minutes. Subsequently, a solution of 1.16 g of pentafluorothiophenol (5.77 mmol, 1.00 eq) in 2 mL of THF was added and the mixture was stirred for 1 hour. The solvent was removed and the obtained crude oil was purified by flash column chromatography (PE).

Yield: 1.44 g, 80%.

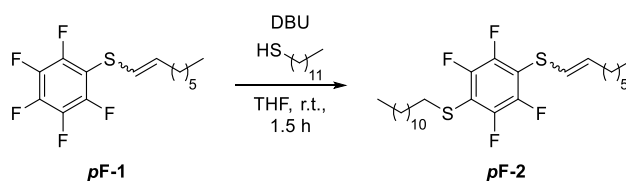
¹H-NMR (400 MHz, DMSO-*d*₆): δ / ppm = 6.15 – 6.05 (m, 1H, H₁), 5.91 – 5.78 (m, 1H, H₂), 2.26 – 2.01 (m, 2H, H₃), 1.40 (q, *J* = 7.1 Hz, 2H, H₄), 1.38 – 1.16 (m, 6H, H₅), 0.86 (dt, *J* = 9.6, 6.9 Hz, 3H, H₆).

¹⁹F-NMR (377 MHz, CDCl₃): δ / ppm = -133.70 – -133.87 (m), -153.20 (dt, *J* = 144.4, 22.2 Hz), -161.23 – -161.63 (m).

¹³C-NMR (100 MHz, DMSO-*d*₆): δ / ppm = 136.02, 134.13, 121.19, 118.84, 32.46, 31.48, 31.43, 28.76, 28.63, 28.51, 28.46, 22.52, 22.48, 14.37, 14.32.

The respective ¹H and ¹⁹F NMR spectra are shown in Figure 6.2.

8.3.3.1.2 Synthesis of Dodecyl(tetrafluoro-4-(oct-1-en-1-ylthio)phenyl)sulfane (**pF-2**)



In an oven-dried crimp vial 800 mg **pF-1** (2.58 mmol, 1.00 eq.) was dissolved in 2 mL THF and 574 mg dodecane-1-thiol (2.84 mmol, 1.10 eq.) was added. The mixture was stirred at atmospheric temperature for 5 minutes. In a second vial 471 mg of DBU were weighed in, dissolved in 2 mL of THF and subsequently slowly added to the reaction mixture. After complete addition the reaction was stirred for 1.5 hours and the solvent was removed in vacuo. The obtained oil was taken up in a few mL cyclohexane and directly subjected to flash chromatography (CH). The product was obtained as a clear oil (1.17 g, 92%).

Yield: 1.17 g, 92%.

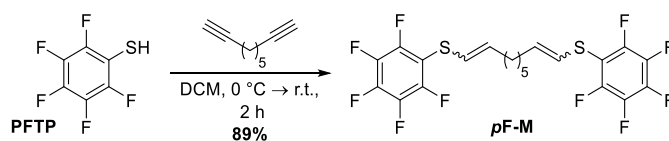
¹H-NMR (400 MHz, CDCl₃): δ / ppm = 6.08 – 5.94 (m, 1H, H₁), 5.83 (dt, J = 9.0, 7.3 Hz, 1H, H₂), 2.93 (t, J = 7.4 Hz, 2H, H₃), 2.34 – 2.06 (m, 2H, H₃), 1.62 – 1.50 (m, 2H, H₅), 1.48 – 1.18 (m, 26H, H₆), 0.88 (dd, J = 7.3, 6.3 Hz, 6H, H₇).

¹⁹F-NMR (377 MHz, CDCl₃): δ / ppm = -133.75 (td, J = 24.8, 11.5 Hz), -134.17 – -134.46 (m).

¹³C-NMR (100 MHz, CDCl₃): δ / ppm = 138.21, 138.06, 135.03, 134.91, 120.55 (d, J = 7.7 Hz), 118.48, 32.80 (d, J = 3.1 Hz), 28.85, 28.79, 28.72, 28.63, 28.57, 28.49.

The respective ¹H and ¹⁹F NMR spectra are shown in Figure 6.2.

8.3.3.1.3 Synthesis of Dodecyl(tetrafluoro-4-(oct-1-en-1-ylthio)phenyl)sulfane (pF-2)



In a 50 mL flask, 1.5 g pentafluorothiophenol (7.27 mmol, 2.10 eq.) was weighed in and dissolved in 10 mL DCM. The solution was cooled to 0 °C, purged with argon for 10 minutes and 0.521 mL 1,8-nonadiyne (3.46 mmol, 416 mg, 1.00 eq.) was added *via* syringe. The reaction was stirred for two hours at atmospheric temperature and was subsequently quenched with saturated NaHCO₃ solution. The phases were separated and the aq. phase was extracted once with DCM. The combined organic phases were dried with MgSO₄ and the solvent was removed *in vacuo*. Purification was performed *via* flash chromatography with cyclohexane. The product was obtained as a yellow oil (1.61 g, 89%).

Yield: 1.61 g, 89%.

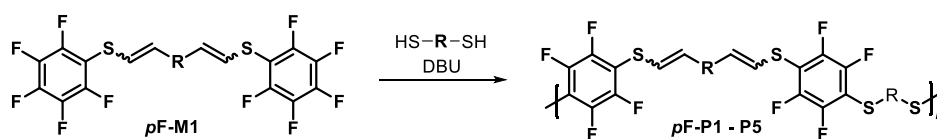
¹H-NMR (400 MHz, CDCl₃): δ / ppm = 6.03 – 5.88 (m, 2H, H₁), 5.82 (ddt, J = 11.2, 9.0, 7.2 Hz, 2H, H₂), 2.37 – 2.03 (m, 4H, H₃), 1.53 – 1.24 (m, 6H, H₄).

¹⁹F-NMR (377 MHz, CDCl₃): δ / ppm = -132.99 (m), -152.93 (m), -160.95 (m).

¹³C-NMR (100 MHz, CDCl₃): δ / ppm = 138.21, 138.06, 135.03, 134.91, 120.55 (d, J = 7.7 Hz), 118.48, 32.80 (d, J = 3.1 Hz), 28.85, 28.79, 28.72, 28.63, 28.57, 28.49.

The respective ¹H and ¹⁹F NMR spectra are shown in Figure 6.3.

8.3.3.2 Polymerization Procedures

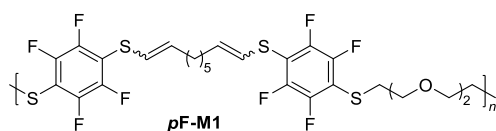


General procedure:

In an oven-dried crimp-vial **pF-M1** and the respective dithiol (**DT1 – DT5**) weighed in in stoichiometric amounts (100 mg of **pF-M1** was targeted during weighing of the oil). Subsequently, 2.50 eq. of Ph_3P was added to prevent disulfide formation. The desired solvent was weighed in and the mixture was stirred at the indicated temperature. The base **DBU** (2.20 eq.) was weighed in a second vial and dissolved in the same solvent. Both solvent volumes were calculated to give a final monomer concentration of either 1M, 0.5M or $\sim 0.2\text{M}$ solutions (the final solvent weight was calculated before reaction and allotted to $3/4^{\text{th}}$ for the monomer solution and $1/4^{\text{th}}$ to the base solution). The base solution was injected to the monomer mixture under vigorous stirring and the polymerization was run for the indicated time. Subsequently, the polymerization was quenched with a drop of acetic acid and the materials were subjected to aqueous workup to remove the formed **DBU** salts. **DCM** or ethyl acetate was added to extract the polymers. The phases were separated and the organic phase as washed once with 1 M **HCl** solution, dried with MgSO_4 and concentrated *in vacuo*. The obtained crude polymers were dissolved in small amounts of **THF** or **DCM** and precipitated in petrol ether. This process was repeated once more and the polymers were subsequently isolated *via* centrifugation and dried *in vacuo*.

The respective ^1H and ^{19}F NMR spectra are shown in Figure 6.6. The DSC and TGA thermograms are shown in Figure 6.8 and the associated results are summarized in Table 6.3.

8.3.3.2.1 *p*F-P1 - Polymerization with 2,2'-(Ethane-1,2-diylbis(oxy))bis(ethane-1-thiol)



¹H-NMR (400 MHz, CDCl₃): δ / ppm = 6.08 – 5.94 (m, H₁), 5.89 – 5.76 (m, H₂), 3.62 (t, *J* = 6.4 Hz, H₃), 3.52 (s, H₄), 3.10 (td, *J* = 6.4, 1.9 Hz, H₅), 2.38 – 2.03 (m, H₆), 1.52 – 1.21 (m, H₇).

¹⁹F-NMR (377 MHz, CDCl₃): δ / ppm = -133.23 (ddq, *J* = 32.7, 25.0, 9.1, 8.5 Hz), -134.01 – -134.38 (m).

ATR-IR: $\tilde{\nu}$ / cm⁻¹: 2927, 2855, 1644, 1456, 1246, 1108, 953, 811, 618.

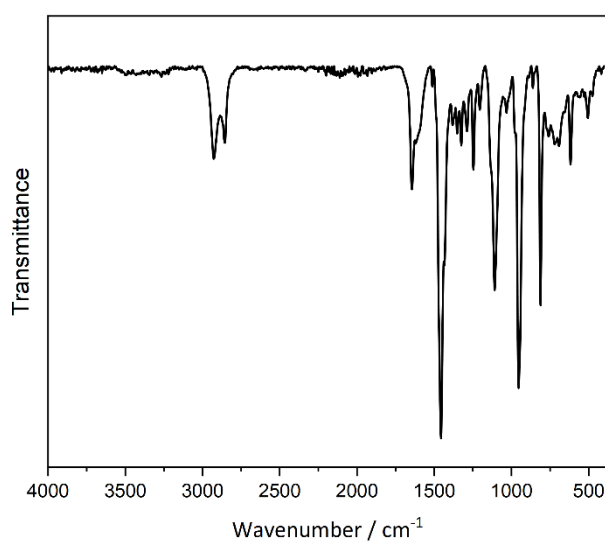
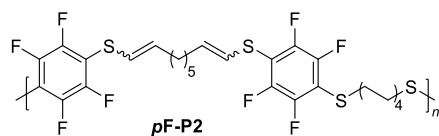


Figure 8.32: IR spectrum of *p*F-P1.

8.3.3.2.2 *p*F-P2 - Polymerization with Octane-1,8-dithiol



¹H-NMR (400 MHz, CDCl₃): δ / ppm = 6.07 – 5.94 (m, H₁), 5.82 (ddt, J = 10.4, 9.1, 7.3 Hz, H₂), 2.92 (t, J = 7.3 Hz, H₃), 2.37 – 2.01 (m, H₄), 1.56 (p, J = 7.4 Hz, H₅), 1.45 – 1.34 (m, H₆), 1.26 (d, J = 4.1 Hz, H₇).

¹⁹F-NMR (377 MHz, CDCl₃): δ / ppm = -133.70 (dddd, J = 36.8, 24.6, 11.3, 5.7 Hz), -134.05 – -134.44 (m).

ATR-IR: $\tilde{\nu}$ / cm⁻¹: 2922, 2852, 1618, 1456, 1244, 954, 812, 719, 617.

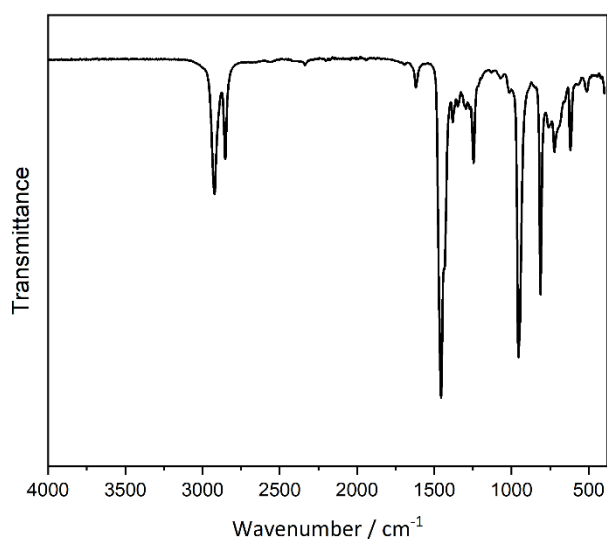
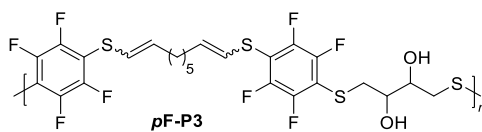


Figure 8.33: IR spectrum of *p*F-P2.

8.3.3.2.3 *p*F-P3 - Polymerization with Dithiothreitol



$^1\text{H-NMR}$ (400 MHz, CDCl_3): δ / ppm = 6.08 (q, $J = 8.2$ Hz, H_1), 5.95 – 5.76 (m, H_2), 5.02 (s, H_3), 3.54 (d, $J = 5.5$ Hz, H_4), 3.01 (d, $J = 6.2$ Hz, H_5), 2.25 – 2.11 (m, H_6), 2.11 – 1.97 (m, H_6), 1.50 – 1.10 (m, H_7).

$^{19}\text{F-NMR}$ (377 MHz, CDCl_3): δ / ppm = -133.61 – -133.86 (m), -134.70 – -134.94 (m).

ATR-IR: $\tilde{\nu}$ / cm^{-1} : 3344 (broad), 2924, 2852, 1618, 1456, 1246, 1083, 1040, 956, 810, 540.

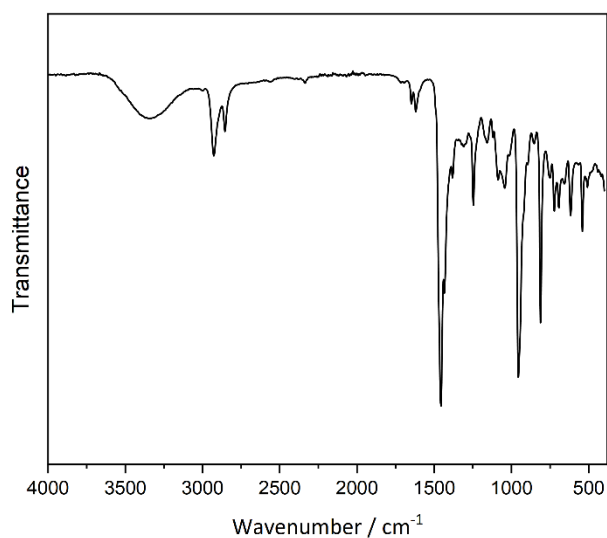
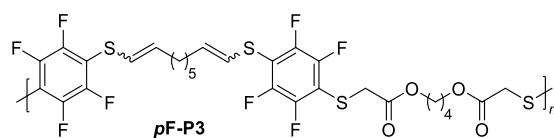


Figure 8.34: IR spectrum of *p*F-P3.

8.3.3.2.4 *p*F-P4 - Polymerization with Butane-1,4-diyl bis(2-mercaptoacetate)



¹H-NMR (400 MHz, CDCl₃): δ / ppm = 6.07 – 5.96 (m, H₁), 5.91 – 5.78 (m, H₂), 4.10 (d, J = 5.4 Hz, H₃), 3.67 – 3.59 (m, H₄), 2.42 – 1.99 (m, H₅), 1.64 (s, H₆), 1.57 – 1.16 (m, H₇).

¹⁹F-NMR (377 MHz, CDCl₃): δ / ppm = -133.05 – -133.36 (m), -133.55 – -133.72 (m), -133.74 – -133.95 (m).

ATR-IR: $\tilde{\nu}$ / cm⁻¹: 2924, 2850, 1731, 1460, 1246, 1125, 958, 812.

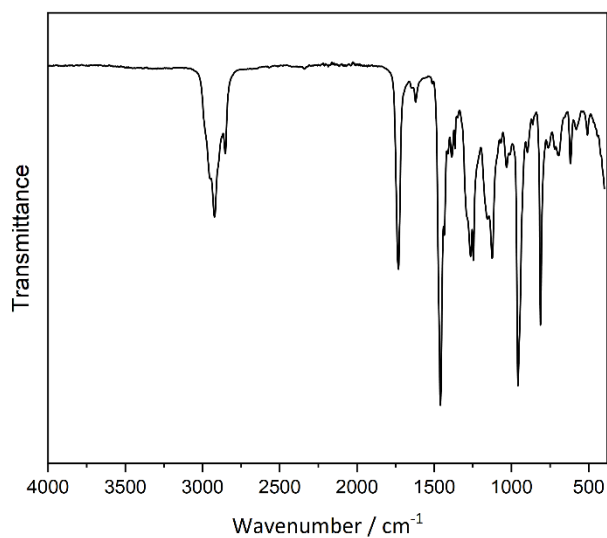
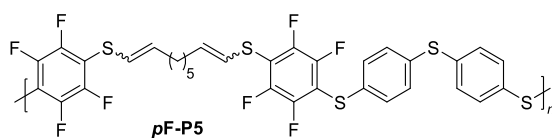


Figure 8.35: IR spectrum of *p*F-P4.

8.3.3.2.5 *p*F-P4 - Polymerization with 4,4'-Thiodibenzenethiol



¹H-NMR (400 MHz, CDCl₃): δ / ppm = 7.29 – 7.18 (m, H₁), 6.10 – 5.79 (m, H₂), 2.34 – 2.24 (m, H₃), 2.18 – 2.04 (m, H₃), 1.50 – 1.22 (m, H₄).

¹⁹F-NMR (377 MHz, CDCl₃): δ / ppm = -132.21 – -132.53 (m), -132.98 – -133.23 (m), -133.31 – -133.50 (m).

ATR-IR: $\tilde{\nu}$ / cm⁻¹: 2924, 2852, 1620, 1460, 1382, 1244, 1092, 1011, 956, 812, 621, 555, 516, 487.

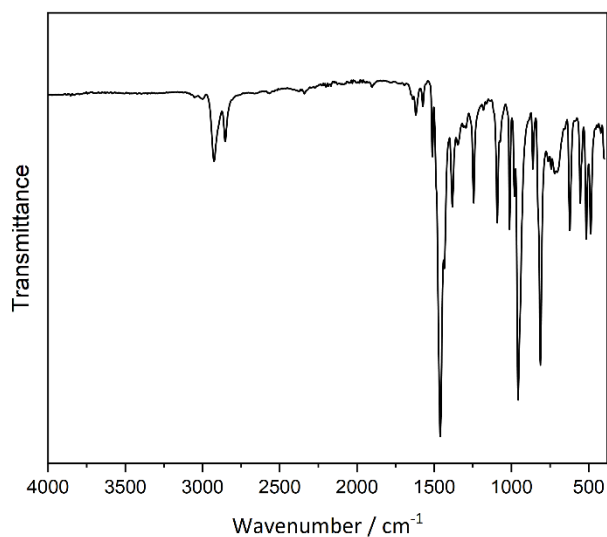
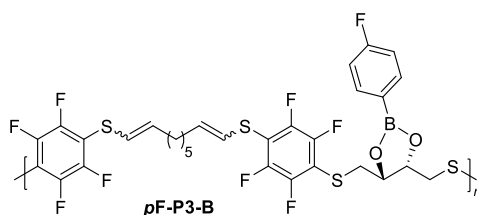


Figure 8.36: IR spectrum of *p*F-P5.

8.3.3.3 Post-Polymerization Reactions

8.3.3.3.1 Boronic ester formation



In a crimp-vial, 116 mg of polymer (**pF-P3**, 39.5k g/mol, $\bar{D} = 2.79$) were dissolved in 5 mL THF. Subsequently, 386 mg of (4-fluorophenyl)boronic acid (2.76 mmol, 15 eq.) and 663.93 mg of dried magnesium sulfate (5.52 mmol, 30 eq.) were added. The solution was stirred at atmospheric temperature for 2d, then the temperature was increased to 50 °C stirring continued for four more days. After cooling down the solids were filtered off and the solvent was removed *in vacuo*. The solids were dissolved in ethyl acetate and washed with Na₂CO₃. The organic phase was dried with MgSO₄ and removed *in vacuo*. Only little amounts of product were obtained.

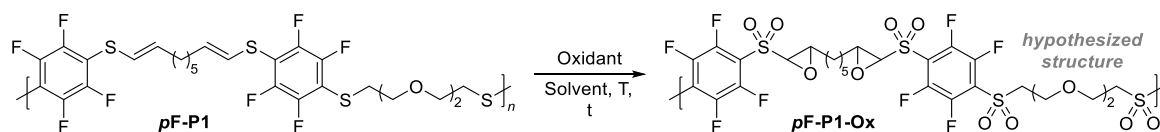
¹H-NMR (400 MHz, CDCl₃): δ / ppm = 7.47 – 7.39 (m, H₁), 7.03 – 6.94 (m, H₂), 6.08 – 5.93 (m, H₃), 5.93 – 5.77 (m, H₄), 4.63 – 4.57 (m, H₅), 3.39 – 3.14 (m, H₆), 2.36 – 2.23 (m, H₇), 1.67 – 1.17 (m, H₈).

¹⁹F-NMR (377 MHz, CDCl₃): δ / ppm = 106.72 (q, $J = 8.0$ Hz), -132.80 – -133.14 (m), -133.62 – -133.84 (m), -133.84 – -134.09 (m).

THF-SEC: 7.11 kg/mol, $\bar{D} = 1.1$.

The respective ¹H and ¹⁹F NMR spectra as well as the SEC trace are shown in Figure 6.9 and Figure 6.10, respectively.

8.3.3.3.2 Oxidation procedures



The respective SEC traces are shown in Figure 6.11

Oxidation with Oxone:

In an oven-dried crimp vial 30 mg of **pF-P1** and 287 mg Oxone (18 eq. in relation to the monomer unit) and 76 mg NaHCO_3 were weighed in, dissolved in 2.5 mL MeCN and stirred for five days at 60 °C. The reaction was quenched by addition of water and DCM. The phases were separated, the organic phase was dried with MgSO_4 and the solvent was removed *in vacuo*.

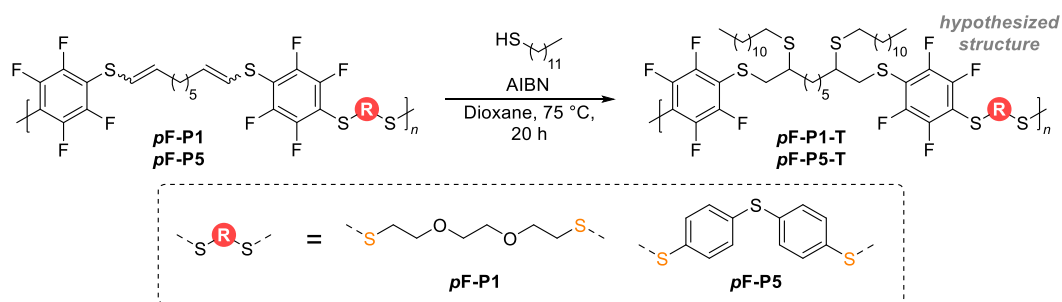
Oxidation with *m*CPBA:

In an oven-dried crimp vial 105 mg of **pF-P1** and 492 mg of 3-chloroperbenzoic acid (18 eq. in relation to the monomer unit) were weighed in, dissolved in 5 mL DCM and stirred for five days at ambient temperature. The reaction was quenched by addition of saturated sodium sulfite to remove unreacted *m*CPBA and the aqueous phase was extracted twice with DCM. The combined organic phases were washed with 1M NaOH solution, dried and the solvent was removed *in vacuo*.

Oxidation with H_2O_2 :

Weighed in 50 mg of **pF-P1** in a crimp-vial and dissolved in 2.5 mL AcOH and 2 mL THF. Added 1 mL 35% H_2O_2 solution dropwise while stirring. After complete addition the vial was closed and immediately placed in a preheated 80 °C vialblock for 15 minutes. Subsequently, the reaction was quenched by addition of ethyl acetate and Na_2CO_3 solution. The phases were separated, the organic phase was dried with MgSO_4 and the solvent was removed *in vacuo*.

8.3.3.3 Thiol-ene reactions



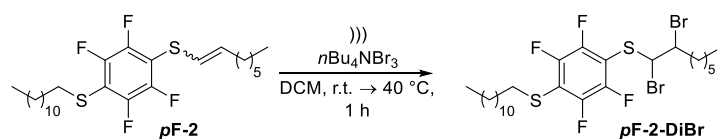
In a crimp-vial, 70 mg of polymer (**pF-P5**, 13k g/mol, $\bar{D} = 2.14$), 32 mg of AIBN (0.194 mmol, 2 eq) and 157.7 mg of dodecane-1-thiol (0.779 mmol, 8 eq) were weighed in and dissolved in 2 mL of 1,4-dioxane. The solution was purged with argon for 15 minutes and then placed in a 75 °C vialblock for 20h. Subsequently, the reaction was cooled with cold water, precipitated in cold ethanol and centrifuged. The supernatant was discarded and the obtained yellow solids were dried *in vacuo* at 40 °C.

The same procedure was used for the reaction with **pF-P5**.

The respective SEC traces, ¹⁹F NMR and IR spectra are shown in Figure 6.12.

8.3.3.3.4 Halogenation reactions

8.3.3.3.4.1 Synthesis of pF-2-Br



In an oven-dried crimp vial 308.8 mg (0.627 mmol, 1.00 eq.) of **pF-2** and 340 mg of tetrabutylammonium tribromide (1.25 mmol, 2.00 eq) were weighed in and dissolved in 5 mL DCM. The vial was closed with a septum cap equipped with a balloon for overpressure release and placed in an ultrasonic bath. After 1 hour of sonication the reaction mixture was washed twice with aqueous $\text{Na}_2\text{S}_2\text{O}_3$ solution, dried with MgSO_4 and concentrated *in vacuo*.

Yield: quant.

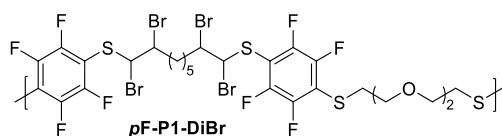
$^1\text{H-NMR}$ (400 MHz, CDCl_3): δ / ppm = 5.63 – 5.46 (m, 1H, H_1), 4.47 – 4.24 (m, 1H, H_2), 3.00 (t, J = 7.4 Hz, 2H), 2.26 – 1.92 (m, 1H), 1.59 (p, J = 7.4 Hz, 3H), 1.47 – 1.16 (m, 31H), 0.94 – 0.84 (m, 7H).

$^{19}\text{F-NMR}$ (377 MHz, CDCl_3): δ / ppm = -132.23 – -132.46 (m), -132.58 – -132.87 (m).

$^{13}\text{C-NMR}$ (100 MHz, CDCl_3): δ / ppm = 138.21, 138.06, 135.03, 134.91, 120.55 (d, J = 7.7 Hz), 118.48, 32.80 (d, J = 3.1 Hz), 28.85, 28.79, 28.72, 28.63, 28.57, 28.49.

The respective ^1H and ^{19}F NMR spectra are shown in Figure 6.13.

8.3.3.3.4.2 Synthesis of *pF*-1-DiBr



In an oven-dried crimp vial 152.70 mg of ***pF*-P1** (230 μmol of repeating unit) and 555.5 mg of tetrabutylammonium tribromide (TBAT, 1.15 mmol) were weighed in and dissolved in 5 mL DCM. The reaction mixture was stirred for 21 h at atmosphere temperature and was subsequently washed thrice with aqueous $\text{Na}_2\text{S}_2\text{O}_3$ solution and seven times with 1M HCl. The organic phase was dried with MgSO_4 and the solvent was removed. The obtained polymer was dissolved in DCM and precipitated twice in petrol ether and dried *in vacuo*, yielding a beige solid.

$^1\text{H-NMR}$ (400 MHz, CDCl_3): δ / ppm = 5.61 (d, J = 2.9 Hz, H_1), 5.50 (d, J = 3.9 Hz, H_1), 4.43 (d, J = 9.7 Hz, H_2), 4.30 (d, J = 9.1 Hz, H_2), 3.66 (t, J = 6.3 Hz, H_3), 3.52 (s, H_4), 3.22 – 3.14 (m, H_5), 2.26 – 1.97 (m, H_6), 1.77 – 1.35 (m, H_7).

$^{19}\text{F-NMR}$ (377 MHz, CDCl_3): δ / ppm = -131.92 – -132.26 (m).

The respective ^1H and ^{19}F NMR spectra and SEC curve are shown in Figure 6.14.

9 Appendix

Appendix Spectra for Chapter 6

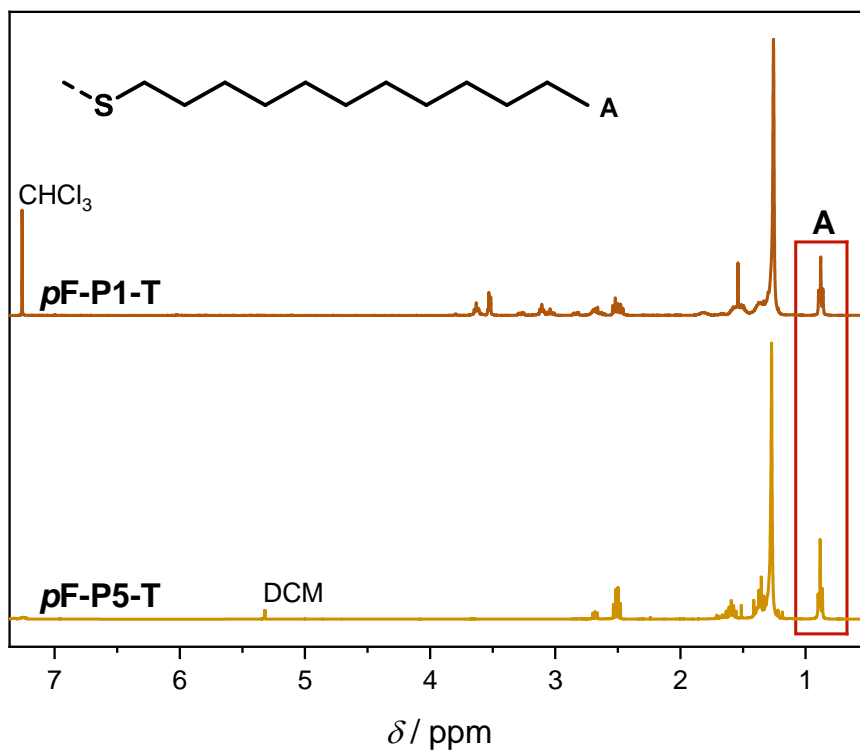


Figure 9.1: Comparative ^1H NMR spectra of **pF-P1-T** and **pF-P5-T** evidencing the addition of 1-dodecanethiol to the polymers.

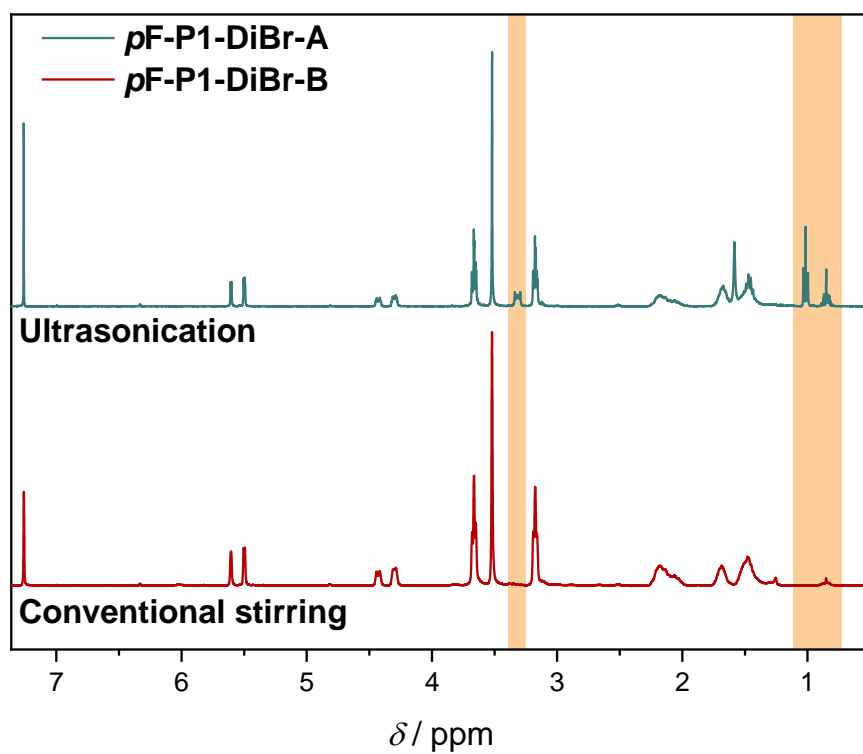


Figure 9.2: Comparative ¹H NMR spectra for the bromination reaction of **pF-P1** under ultrasonication conditions (*top*) and conventional stirring (*bottom*) evidencing the addition of *n*-butyl chains of TBAT to the polymer in the first case.

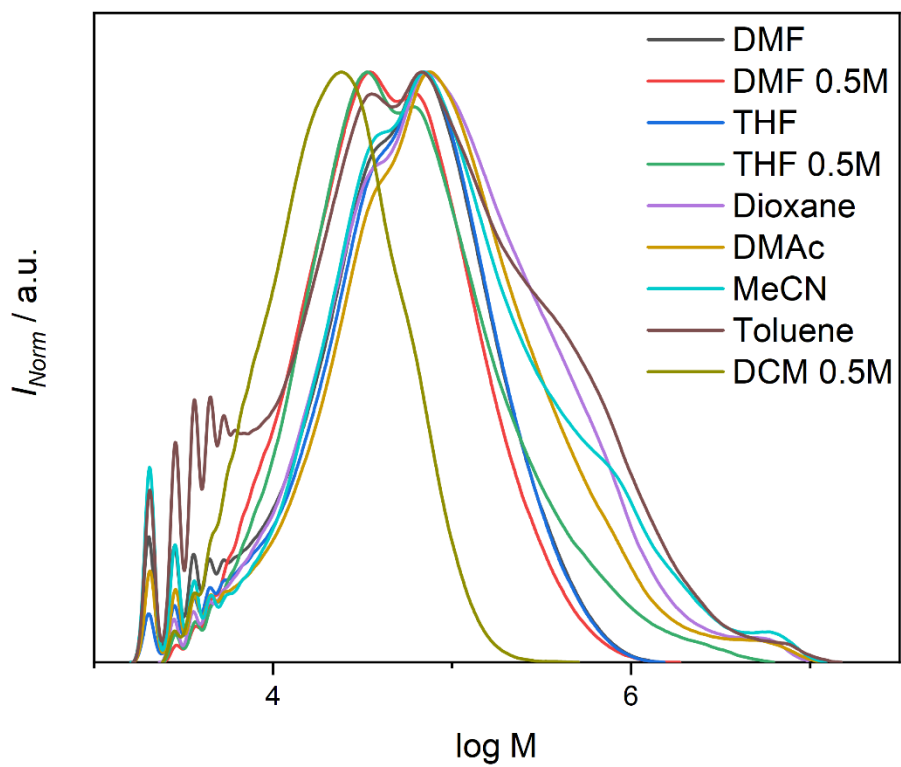


Figure 9.3: SEC traces of the solvent screening for the polymerization of **pF-M** and **DT1**.

List of Schemes, Figures and Tables

List of Schemes

<i>Scheme 2.1: Top: First example of the isomerization of a longer alcohol (hexadec-7-yn-1-ol) in the presence of potassium 3-aminopropylamide (KAPA). Bottom: Mechanism of the Alkyne Zipper reaction.</i>	4
<i>Scheme 2.2: Synthesis of Tricolorin A via the Alkyne Zipper reaction employed in the third step of the sequence.</i>	4
<i>Scheme 2.3: Depiction of the isomerization of 1,3-diynes, which leads towards vicinal alkynes at the same chain end.</i>	5
<i>Scheme 2.4: General representation of the SONOGASHIRA reaction (top) and relative reactivities of sp^2-carbon substrates bearing different halides (halides).</i>	6
<i>Scheme 2.5: Depiction of multiple reaction mechanisms of copper- and copper-free variants of the SONOGASHIRA reaction. Left: Textbook mechanism for the Pd/Cu catalyzed coupling. Middle: Textbook mechanism for the Cu-free variant. Right: Recently reported Pd-Pd transmetallation mechanism.^[39] OA – oxidative addition; TM – transmetallation; Isom. – cis–trans isomerization.</i>	7
<i>Scheme 2.6: Depiction of three different examples for the use of the SONOGASHIRA reaction in the field of polymer and material science.</i>	8
<i>Scheme 2.7: General reaction scheme (top) and mechanism of the RAFT process.</i>	11
<i>Scheme 2.8: Depiction of the varied post-polymerization chemistries that are available to RAFT-polymers.</i>	12
<i>Scheme 2.9: Depiction of different grafting methods for the synthesis of bottlebrush polymers (which can vary as statistical, block and core-shell): grafting through (left), grafting to (middle) and grafting from (right).</i>	16
<i>Scheme 2.10: Overview of the possible addition reactions of pentafluorothiophenol (PFTP).</i>	20
<i>Scheme 2.11: General reaction scheme for the para-fluoro thiol reaction (PFTR).</i>	21
<i>Scheme 2.12: Depiction of resonance structures for the meta- and para-pathway of nucleophilic substitutions in monosubstituted pentafluorobenzene derivatives.</i>	22
<i>Scheme 3.1: General three-step synthesis of long-chain alkynols via Alkyne Zipper reaction.</i>	24
<i>Scheme 3.2: Protection of propargyl alcohol and undec-10-yn-1-ol with trityl chloride (TrCl) and 3,4-dihydropyran (DHP).</i>	26
<i>Scheme 3.3: Two-step synthesis of a trityl-protected tridecyn-1-ol (5) via protection with trityl chloride and subsequent alkynylation with lithium acetylide ethylenediamine complex.</i>	26
<i>Scheme 3.4: General reaction scheme for the two-step synthesis of extended alkynols through elongation of the terminal alkynes with <i>n</i>-alkane chains.</i>	27
<i>Scheme 3.5: Graphical depiction of the standard literature protocol for the Alkyne Zipper reaction (top) and adjusted method (bottom) for the isomerization of long-chain alkynols. Problematic steps (low solubility of KOtBu & long-chain alkynols) are denoted with an exclamation point.</i>	29
<i>Scheme 3.6: Schematic summary of the synthesis approach towards alkylated alkynols A1 – A6 and subsequent formation of the α,ω-functionalized hydrocarbons AZ1 – AZ5 via Alkyne Zipper reaction.</i>	35
<i>Scheme 4.1: General reaction scheme for the synthesis of precise poly(ethylene)s via ADMET polymerization.</i>	36
<i>Scheme 4.2: Depiction of the conceived replacement of the alkene group in an ADMET polymer with an enyne motif.</i>	37
<i>Scheme 4.3: Depiction of the retrosynthetic approach towards Precise PE based on SONOGASHIRA compatible motifs, i.e., vinyl halides and alkynes (FG = functional group).</i>	39
<i>Scheme 4.4: Depiction of the AB- (left) and A_2+B_2-approach (right) towards unsaturated PE precursor polymers based on the combination of alkynes and vinyl halides.</i>	39
<i>Scheme 4.5: Depiction of the general concept, which allows to control the functional group distance in precise PE using dialkynes with different chain lengths (ester group added for the purpose of illustration).</i>	40

Scheme 4.6: Reaction scheme for the conversion of alkynols to dialkynes via tosylation and subsequent reaction with lithium acetylide ethylenediamine complex ($x =$ varying number of methylenegroups, refer to Chapter 3).	40
Scheme 4.7: Reaction scheme for the two-step synthesis of divinyl monomers	41
Scheme 4.8: Reaction scheme for the synthesis of hexadeca-1,15-diyne (DA_{15}).....	42
Scheme 4.9: General reaction scheme for the SONOGASHIRA polycoupling of SM1-Cl and SM1-Br.	43
Scheme 4.10: Two-step synthesis of the SM2-Br monomer from potassium 3-methoxy-3-oxopropanoate.....	47
Scheme 4.11: General reaction scheme for the SONOGASHIRA polycondensation of SM2-Br.....	48
Scheme 4.12: Reaction scheme for the polymerization and in-situ hydrogenation.	49
Scheme 5.1: Depiction of the general concept for the synthesis of bottlebrush polymers via trans-esterification of PFP esters with previously synthesized long-chain alkynols and subsequent derivatization with alcohols to core-shell bottlebrush copolymers (cs-BBCSs).....	53
Scheme 5.2: Synthesis of the active-ester polymer RAFT-PPFPA via controlled radical polymerization with chain-transfer agent CDTPA.....	54
Scheme 5.3: Reaction scheme for the trans-esterification of RAFT-PPFPA with undec-10-yn-1-ol, tridecyn-1-ol AZ1, AZ3 – AZ5.	55
Scheme 5.4: Schematic representation of the copper-catalyzed three-component reactions (3CR) of sulfonyl azides, terminal alkynes and nucleophiles.	60
Scheme 5.5 Reaction scheme for the 3-component reaction of polyAZ ₂₁ , mPEG 400 and tosyl azide.	61
Scheme 6.1: Depiction of the general concept for the synthesis of a symmetrical monomer based on PFTP and dialkynes and subsequent polymerization via para-fluoro thiol reaction with dithiols.	66
Scheme 6.2: Reaction scheme for the hydrothiolation of 1-octyne with PFTP towards pentafluoro vinyl sulfide pF-1 and subsequent para-fluoro thiol reaction with 1-dodecanthiol in THF.	67
Scheme 6.3: Reaction scheme for the hydrothiolation of 1,8-nonadiyne with PFTP towards the difunctional monomer pF-M in DCM.....	69
Scheme 6.4: General reaction scheme for the synthesis of fluorinated polymers via para-fluoro thiol reaction of the difunctional pentafluoro vinyl sulfide monomer pF-M and a series of dithiols.	70
Scheme 6.5: Schematic depiction of the theoretically possible PPM strategies based on the available functional groups/atoms embedded in the polymer structures.....	78
Scheme 6.6: Reaction scheme of the boronic ester formation of pF-P3 with.....	79
Scheme 6.7: General reaction scheme for the oxidation of pF-P1 with the originally assumed structure of the oxidized polymer pF-P1-Ox.....	81
Scheme 6.8: Summary of literature reports covering oxidation reactions of structurally similar motifs as in pF-P1.	83
Scheme 6.9: General reaction scheme for the thiol-ene reaction yielding a thioether.	85
Scheme 6.10: Reported examples of hydrothiolation reactions of vinyl sulfides under UV irradiation (top) and thermal conditions (bottom) (adapted from ^[218] and ^[219] , respectively).	85
Scheme 6.11: Reaction scheme for the thiol-ene reaction of 1-dodecanthiol with pF-P1 and pF-P5.....	86
Scheme 6.12: Reaction scheme for the bromination of pF-2 with nBu_4NBr_3 (TBAT).	88
Scheme 6.13: Reaction scheme for the halogenation of pF-P1 with nBu_4NBr_3	89

List of Figures

Figure 2.1: Depiction of the general RAFT agent structure as well as selected examples for the class of thioesters (A), trithiocarbamates (B), dithiocarbamates (C) and xanthate esters (D).	11
Figure 2.2: Overview over the most common PPM reactions: Diels-Alder, CuAAC, thiol-ene & thiol-yne, trans-esterification and amidation of active-esters in addition to the para-Fluoro Thiol reaction (PFTR).	14
Figure 2.3: Depiction of various polymer architectures that can be generated via modern polymerization techniques.	15
Figure 2.4: Publications containing the pentafluorobenzene motif per year from 1990 – 2021 (retrieved from SciFinder ⁿ on 07.09.22).	18
Figure 2.5: Depiction of several pentafluorobenzyl derived monomers.	19
Figure 3.1: Left: Comparative ¹ H NMR spectra (400 MHz, CDCl ₃) of alkyl ether 1 (top), internal alkynol A1 (middle) and α,ω -alkynol AZ1 (bottom). Associated resonances arising from the terminal groups are colored. Right: Stacked IR spectra of undec-10-yn-1-ol (top), alkynol AZ1 (middle) and alkynol AZ5 (bottom). The alkyne C-H stretching band of all compounds is marked (grey box).	32
Figure 3.2: Comparative ¹ H NMR (400 MHz, CDCl ₃) (left) and SEC Traces (right) of alkynol A6 (purple) and the reaction product after the isomerization attempt (dark grey) (refer to Table 3.3, Entry 8).	33
Figure 3.3: SEC curves of the synthesized α,ω -alkynols A1 – A5 displaying the increasing hydrocarbon chain length.	34
Figure 3.4: Linear fit correlation of the melting points and chain lengths of the synthesized α,ω -alkynols A1 – A5.	34
Figure 4.1: ¹ H NMR (CDCl ₃ , 400 MHz) spectra of S1-Br (left) and SM1-Br (right) evidencing the successful alkylation and decarbalkoxylation.	42
Figure 4.2: Photographs of selected crosslinked specimen from the reactions summarized in Table 4.2. Top left: Fully crosslinked material which took the shape of the reaction vessel. Top right & bottom left: Ring and circle shaped networks obtained during drying in vials. Bottom right: Rectangle cut from the circle (bottom left), evidencing the self-supporting nature of the crosslinked material.	45
Figure 4.3: Proton NMR spectrum (CDCl ₃ , 400 MHz) of the diester divinyl bromide monomer SM2-Br.	47
Figure 4.4: Crude proton NMR spectrum (CDCl ₃ , 400 MHz) corresponding to the experiment shown in Table 4.3 Entry 1 (left) and the SEC traces corresponding to Entry 1 and 2, respectively.	49
Figure 4.5: Depiction of the conducted ¹ H NMR (top left), SEC (top right) and TGA analyses (bottom) of the hydrogenated polymer S-PE.	50
Figure 5.1: NMR spectroscopic analyses of RAFT-PPFPA showing the polymeric backbone as well as additional chain-transfer agent resonances (left) and broadened pentafluoro phenol resonances (right).	55
Figure 5.2: Depiction of arranged ¹ H NMR measurements (cutout in CDCl ₃ , 400 MHz) of polyAZ _x (x = 9, 11, 15, 19, 21, 25) evidencing the successful trans-esterification with all alkynols.	56
Figure 5.3: Top left: Depiction of the proton NMR spectrum (CDCl ₃ , 400 MHz) of polyAZ ₁₅ with assigned resonances. Top right: Stacked IR spectra of AZ5 and its trans-esterification product polyAZ ₁₅ . Bottom: Comparative SEC traces (left) and corresponding result values (right) for the precursor polymer PPFPA and all PPM products.	58
Figure 5.4: Stacked DSC traces of PPFPA and the trans-esterification products polyAZ _x (left). The corresponding data is shown in the table (right).	59
Figure 5.5: Top: ¹ H NMR (CDCl ₃ , 400 MHz) of polyAZ ₂₁ -mPEG (left) and a zoom-in (1.50 ppm – 2.50 ppm) (right) showing the remaining alkyne resonance. Middle: Comparative DMAc-SEC traces (left) and IR spectra (right) before and after the 3-CR. Bottom: Comparative DSC analyses of polyAZ ₂₁ and polyAZ ₂₁ -mPEG.	62
Figure 6.1: The chemical structure of PFTP.	65

Figure 6.2: Comparative ^1H (left, 400 MHz) and ^{19}F (right, 377 MHz) spectra of pentafluoro vinyl sulfide pF-1 (top) and para-fluoro thiol reaction product pF-2 (bottom) evidencing successful mono-substitution with no apparent side-reactions.	67
Figure 6.3: ^1H NMR (left, 400 MHz) and ^{19}F NMR (right, 377 MHz) spectra of pF-M showing the characteristic vinyl as well as fitting fluorine resonances for the desired symmetrical monomer.	69
Figure 6.4: Depiction of the series of dithiols used for the para-fluoro thiol polymerization.	70
Figure 6.5: SEC traces of pF-M with dithiol DT1 in DCM and THF yielding monomodal distributions.	72
Figure 6.6: Depiction of the ^1H (left) and ^{19}F NMR (right) spectroscopic investigations of pF-P1 – pF-P5 (descending order) and their respective signal assignments.	76
Figure 6.7: Stacked IR-Spectra of monomer pF-M (top), pF-P3 (middle) and pF-P4 (bottom). The polymer-characteristic IR bands are color coded: pF-P3: hydroxyl group – blue; pF-P4: ester group –green).	76
Figure 6.8: Comparative depiction of the DSC (left) and TGA curves (right) of polymers pF-P1 - pF-P5.	77
Figure 6.9: Analysis of polymer pF-P3-B via ^1H and ^{19}F NMR, depicting the newly appeared aromatic protons as well as the additional fluorine resonance.	79
Figure 6.10: SEC analyses of pF-P3-B and its parent polymer pF-P3 (left) and a simplified drawing of the hypothesized π - π -stacking interactions.	80
Figure 6.11: Comparative SEC traces of the different batches of pF-P1 and the obtained oxidized materials after reaction with Oxone [®] (top left), mCPBA (top right) and H_2O_2 (bottom left). The hypothesized structural breaking point in the polymer backbone is depicted in red (bottom right).	82
Figure 6.12: SEC analyses of the attempted thiol-ene reactions with pF-P1 (top left) and pF-P5 (top right). Comparative fluorine NMR (bottom left) and IR spectra (bottom right) of the parent polymers and the reaction products.	87
Figure 6.13: Proton (left) and fluorine NMR (right) analyses of the bromination product pF-2-DiBr evidencing the successful halogenation of the vinyl sulfide moiety of pF-2.	89
Figure 6.14: Proton (top left) and fluorine (top right) NMR analyses of the halogenated polymer pF-P1. SEC traces for the halogenation reaction with bromine (bottom left) and $n\text{Bu}_4\text{NBr}_3$ (bottom right) confirm the polymer stability in the latter case.	90
Figure 6.15: Comparative DSC (left) and TGA (right) traces of pF-P1 and pF-P1-DiBr.	91
Figure 8.1: Proton NMR spectrum of 1 ($\text{DMSO}-d_6$).	98
Figure 8.2: Proton NMR spectrum of 2 (CDCl_3).	99
Figure 8.3: Proton NMR spectrum of 3 (CDCl_3).	100
Figure 8.4: Proton NMR spectrum of 4 ($\text{DMSO}-d_6$).	101
Figure 8.5: Proton NMR spectrum of 5 ($\text{DMSO}-d_6$).	102
Figure 8.6: Proton NMR spectrum of A1 (CDCl_3).	104
Figure 8.7: Proton NMR spectrum of A2 ($\text{DMSO}-d_6$).	105
Figure 8.8: Proton NMR spectrum of A3 (CDCl_3).	106
Figure 8.9: Proton NMR spectrum of A4 (CDCl_3).	107
Figure 8.10: Proton NMR spectrum of A5 (CDCl_3).	108
Figure 8.11: Proton NMR spectrum of A6 (CDCl_3).	109
Figure 8.12: Proton NMR (CDCl_3) (left) and IR spectrum of AZ1.	111
Figure 8.13: Proton NMR ($\text{DMSO}-d_6$) (left) and IR spectrum of AZ2.	112
Figure 8.14: Proton NMR (CDCl_3) (left) and IR spectrum of AZ3.	113
Figure 8.15: Proton NMR (CDCl_3) (left) and IR spectrum of AZ4.	114
Figure 8.16: Proton NMR (CDCl_3) (left) and IR spectrum of AZ4.	115
Figure 8.17: Proton NMR (CDCl_3) of S1-Cl.	117
Figure 8.18: Proton NMR (CDCl_3) of S1-Br.	117
Figure 8.19: Proton NMR (CDCl_3) of SM1-Cl.	119
Figure 8.20: Proton NMR (CDCl_3) of SM1-Br.	119
Figure 8.21: Proton NMR (CDCl_3) of DA ₁₂	120

Figure 8.22: Proton NMR (CDCl ₃) of S2.....	121
Figure 8.23: Proton NMR (CDCl ₃) of SM2-Br.....	122
Figure 8.24: Proton NMR (CDCl ₃) of S-PE.	124
Figure 8.25: ATR-IR spectrum of RAFT-PPFPA.	125
Figure 8.26: Proton NMR (CDCl ₃) (left) and ATR-IR spectrum (right) of polyAZ ₉	128
Figure 8.27: Proton NMR (CDCl ₃) (left) and ATR-IR spectrum (right) of polyAZ ₁₁	128
Figure 8.28: Proton NMR (CDCl ₃) (left) and ATR-IR spectrum (right) of polyAZ ₁₅	129
Figure 8.29: Proton NMR (CDCl ₃) of polyAZ ₁₉	129
Figure 8.30: Proton NMR (CDCl ₃) (left) and ATR-IR spectrum (right) of polyAZ ₂₁	130
Figure 8.31: Proton NMR (CDCl ₃) (left) and ATR-IR spectrum (right) of polyAZ ₂₅	130
Figure 8.32: IR spectrum of pF-P1.	136
Figure 8.33: IR spectrum of pF-P2.	137
Figure 8.34: IR spectrum of pF-P3.	138
Figure 8.35: IR spectrum of pF-P4.	139
Figure 8.36: IR spectrum of pF-P5.	140
Figure 9.1: Comparative ¹ H NMR spectra of pF-P1-T and pF-P5-T evidencing the addition of 1-dodecanethiol to the polymers.....	146
Figure 0.2: Comparative ¹ H NMR spectra for the bromination reaction of pF-P1 under ultrasonication conditions (top) and conventional stirring (bottom) evidencing the addition of n-butyl chains of TBAT to the polymer in the first case.	147
Figure 0.3: SEC traces of the solvent screening for the polymerization of pF-M and DT1.....	148

List of Tables

<i>Table 3.1: Overview of the possible chain lengths after the Alkyne Zipper reaction that can be obtained from the combination of propargyl alcohol, undec-10-yn-1-ol or tridecyn-1-ol and n-bromoalkanes of increasing chain lengths.....</i>	<i>25</i>
<i>Table 3.2: Overview of the used starting material combinations, the conditions and yields for the synthesis of the targeted alkylated alkynols A1 – A6.</i>	<i>28</i>
<i>Table 3.3: Summarized results of the Alkyne Zipper isomerization reactions of previously prepared internal alkynols A1 – A6.</i>	<i>31</i>
<i>Table 4.1 Comparison between the SONOGASHIRA polycoupling and ADMET polymerization.</i>	<i>38</i>
<i>Table 4.2: Summarized results of the SONOGASHIRA polycoupling of SM1-Cl & SM1-Br with DA₅ & DA₁₂.</i>	<i>44</i>
<i>Table 4.3: Summarized results of the SONOGASHIRA polycondensation of SM2-Br with DA₅ & DA₁₂.</i>	<i>48</i>
<i>Table 6.1: Summary of the solvent screening of pF-M with dithiol DT1 under standard conditions.....</i>	<i>71</i>
<i>Table 6.2: Overview of the polymerization results of pF-M with selected dithiols DT2 – DT5.</i>	<i>73</i>
<i>Table 6.3: Summary of the thermal properties obtained via DSC and TGA analyses.</i>	<i>77</i>
<i>Table 6.4: Summary of the reaction conditions for the oxidation of pF-P1.....</i>	<i>81</i>
<i>Table 8.1: Summarized SEC results for the trans-esterification reactions.....</i>	<i>126</i>
<i>Table 8.2: Summarized DSC results for the polymers in Chapter 5.</i>	<i>127</i>

Abbreviations

AFM	Atomic-Force Microscopy
AIBN	Azo-bis-(isobutyronitrile)
at%	Atomic percent
bs	Broad singlet
CVD	Chemical vapour deposition
CuAAC	Copper-catalyzed azide-alkyne cycloaddition
d	Day
DCM	Dichloromethane
DLS	Dynamic light scattering
DMAA	N,N-Dimethylacrylamide
DMAP	4-Dimethylaminopyridin
DMF	<i>N,N</i> -Dimethylformamide
DNA	Deoxyribonucleic acid
EDC	1-Ethyl-3-(3-dimethylaminopropyl)carbodiimide
FTIR	Fourier transform infrared spectroscopy
GPC	Gel permeation chromatography
h	Hour
HDA	Hetero-Diels-Alder
i.e.	Lat.: id est (that is to say)
m	Multiplet
NMR	Nuclear Magnetic Resonance Spectroscopy
NMP	Nitroxide mediated polymerization
RI	Refractive index
rt	Room temperature
s	Singlet
SCNP/s	Single-chain nanoparticle/s
SEC	Size Exclusion Chromatography
TEM	Transmission electron microscopy
TEMPO	2,2,6,6-Tetramethylpiperidinyloxy
THF	Tetrahydrofuran
XPS	X-Ray Photoelectron Spectroscopy

Bibliography

- [1] N. A. Danilkina, A. A. Vasileva, I. A. Balova, *Russ. Chem. Rev.* **2020**, *89*, 125–171.
- [2] J. Pribyl, K. B. Wagener, G. Rojas, *Mater. Chem. Front.* **2021**, *5*, 14–43.
- [3] H. Namazi, *Bioimpacts* **2017**, *7*, 73.
- [4] Y. Shi, B. Yu, X. Wang, A. C. Y. Yuen, *Front. Mater.* **2021**, *8*, 195.
- [5] P. M. Hergenrother, *High Perform. Polym.* **2003**, *15*, 3–45.
- [6] N. Li, *Adv. Mater. Res.* **2014**, *1028*, 337–340.
- [7] M. G. Wiesli, M. Özcan, *Implant Dent.* **2015**, *24*.
- [8] A. Kowalska, J. Sokolowski, K. Bociog, *Polym. 2021, Vol. 13*, **2021**, *13*, 470.
- [9] D. Hansen, S. Zajforoushan Moghaddam, J. Eiler, K. Hansen, E. Thormann, *ACS Appl. Polym. Mater.* **2020**, *2*, 1535–1542.
- [10] N. F. Sauty, H. Li, L. C. Da Silva, K. B. Wagener, *Synth. Commun.* **2014**, *44*, 2409–2415.
- [11] J. Trzaskowski, D. Quinzler, C. Bährle, S. Mecking, *Macromol. Rapid Commun.* **2011**, *32*, 1352–1356.
- [12] C. A. Brown, A. Yamashita, *J. Am. Chem. Soc.* **1975**, *97*, 891–892.
- [13] G. Delaittre, L. Barner, *Polym. Chem.* **2018**, *9*, 2679–2684.
- [14] Z. Li, M. Tang, S. Liang, M. Zhang, G. M. Biesold, Y. He, S.-M. Hao, W. Choi, Y. Liu, J. Peng, Z. Lin, *Prog. Polym. Sci.* **2021**, *116*, 101387.
- [15] L. Claisen, *Berichte der Dtsch. Chem. Gesellschaft* **1912**, *45*, 3157–3166.
- [16] A. C. Cope, E. M. Hardy, *J. Am. Chem. Soc.* **1940**, *62*, 441–444.
- [17] M. F. Carroll, *J. Chem. Soc.* **1940**, 704–706.
- [18] A. Faworsky von, *J. für Prakt. Chemie* **1888**, *37*, 382–395.
- [19] E. R. H. Jones, G. H. Whitham, M. C. Whiting, *J. Chem. Soc.* **1954**, 3201–3207.
- [20] J. C. Craig, M. Moyle, *J. Chem. Soc.* **1963**, 4402–4408.
- [21] J. H. Wotiz, P. M. Barelski, D. F. Koster, *J. Org. Chem.* **1973**, *38*, 489–493.
- [22] J. H. Wotiz, W. E. Billups, D. T. Christian, *J. Org. Chem.* **1966**, *31*, 2069–2073.
- [23] C. A. Brown, *J. Chem. Soc. Chem. Commun.* **1975**, 222–223.
- [24] C. A. Brown, A. Yamashita, *J. Chem. Soc. Chem. Commun.* **1976**, *0*, 959–960.

- [25] R. J. Bushby, *Q. Rev. Chem. Soc.* **1970**, *24*, 585–600.
- [26] S. R. Abrams, D. D. Nucciarone, W. F. Steck, *Can. J. Chem.* **1983**, *61*, 1073–1076.
- [27] S. R. Abrams, *Can. J. Chem.* **1984**, *62*, 1333–1334.
- [28] S. R. Abrams, A. C. Shaw, *Org. Synth.* **1988**, *66*, 127.
- [29] I. A. Balova, S. N. Morozkina, D. W. Knight, S. F. Vasilevsky, *Tetrahedron Lett.* **2003**, *44*, 107–109.
- [30] I. A. Balova, S. N. Morozkina, V. N. Sorokoumov, O. V. Vinogradova, S. F. Vasilevskii, *Russ. J. Org. Chem.* **2003**, *39*, 1613–1617.
- [31] K. Sonogashira, Y. Tohda, N. Hagihara, *Tetrahedron Lett.* **1975**, *16*, 4467–4470.
- [32] L. Cassar, *J. Organomet. Chem.* **1975**, *93*, 253–257.
- [33] H. A. Dieck, F. R. Heck, *J. Organomet. Chem.* **1975**, *93*, 259–263.
- [34] K. Sonogashira, *J. Organomet. Chem.* **2002**, *653*, 46–49.
- [35] B. M. Andresen, M. Couturier, B. Cronin, M. D’Occhio, M. D. Ewing, M. Guinn, J. M. Hawkins, V. J. Jasys, S. D. LaGreca, J. P. Lyssikatos, G. Moraski, K. Ng, J. W. Raggon, A. M. Stewart, D. L. Tickner, J. L. Tucker, F. J. Urban, E. Vazquez, L. Wei, *Org. Process Res. Dev.* **2004**, *8*, 643–650.
- [36] R. Chinchilla, C. Nájera, *Chem. Rev.* **2007**, *107*, 874–922.
- [37] Y. Liang, Y. X. Xie, J. H. Li, *J. Org. Chem.* **2006**, *71*, 379–381.
- [38] F. Mohajer, M. M. Heravi, V. Zadsirjan, N. Poormohammad, *RSC Adv.* **2021**, *11*, 6885–6925.
- [39] M. Gazvoda, M. Virant, B. Pinter, J. Košmrlj, *Nat. Commun.* **2018**, *9*, 4814.
- [40] A. Soheili, J. Albaneze-Walker, J. A. Murry, P. G. Dormer, D. L. Hughes, *Org. Lett.* **2003**, *5*, 4191–4194.
- [41] A. M. Mak, Y. H. Lim, H. Jong, Y. Yang, C. W. Johannes, E. G. Robins, M. B. Sullivan, *Organometallics* **2016**, *35*, 1036–1045.
- [42] M. García-Melchor, M. C. Pacheco, C. Nájera, A. Lledós, G. Ujaque, *ACS Catal.* **2012**, *2*, 135–144.
- [43] L. B. Sessions, B. R. Cohen, R. B. Grubbs, *Macromolecules* **2007**, *40*, 1926–1933.
- [44] M. Trunk, A. Herrmann, H. Bildirir, A. Yassin, J. Schmidt, A. Thomas, *Chem. – A Eur. J.* **2016**, *22*, 7179–7183.
- [45] H. Staudinger, *Berichte der Dtsch. Chem. Gesellschaft* **1920**, *53*, 1073–1085.
- [46] G. Odian, *Princ. Polym. Wiley sons* **2004**, 128–130.

- [47] W. H. Carothers, *Chem. Rev.* **1931**, *8*, 353–426.
- [48] W. H. Carothers, *J. Am. Chem. Soc.* **1929**, *51*, 2548–2559.
- [49] M. Zhang, S. M. June, T. E. Long, in (Eds.: K. Matyjaszewski, M.B.T.-P.S.A.C.R. Möller), Elsevier, Amsterdam, **2012**, pp. 7–47.
- [50] W. H. Carothers, *Trans. Faraday Soc.* **1936**, *32*, 39–49.
- [51] J. Chiefari, Y. K. (Bill) Chong, F. Ercole, J. Krstina, J. Jeffery, T. P. T. Le, R. T. A. Mayadunne, G. F. Meijs, C. L. Moad, G. Moad, E. Rizzardo, S. H. Thang, *Macromolecules* **1998**, *31*, 5559–5562.
- [52] S. Perrier, *Macromolecules* **2017**, *50*, 7433–7447.
- [53] M. H. Stenzel, L. Cummins, G. E. Roberts, T. P. Davis, P. Vana, C. Barner-Kowollik, *Macromol. Chem. Phys.* **2003**, *204*, 1160–1168.
- [54] N. Yeole, *Synlett* **2010**, 1572–1573.
- [55] L. G. Williams, K. Sullivan, J. Tsanaktsidis, “RAFT Agents for Making Well-Defined Functionalized Polymers” can be found under <https://www.sigmaaldrich.com/DE/en/technical-documents/technical-article/materials-science-and-engineering/polymer-synthesis/raft-agents-for-functionalized-polymers> (accessed 07.09.2022).
- [56] A. J. Inglis, S. Sinnwell, T. P. Davis, C. Barner-Kowollik, M. H. Stenzel, *Macromolecules* **2008**, *41*, 4120–4126.
- [57] C. Boyer, A. Granville, T. P. Davis, V. Bulmus, *J. Polym. Sci. Part A Polym. Chem.* **2009**, *47*, 3773–3794.
- [58] H. Willcock, R. K. O’Reilly, *Polym. Chem.* **2010**, *1*, 149–157.
- [59] A. J. Inglis, M. H. Stenzel, C. Barner-Kowollik, *Macromol. Rapid Commun.* **2009**, *30*, 1792–1798.
- [60] A. Nguyen, E. Dallerba, A. B. Lowe, *Macromol. Rapid Commun.* **2022**, *43*, 2200096.
- [61] P. Theato, H. A. Klok, *Functional Polymers by Post-Polymerization Modification: Concepts, Guidelines, and Applications*, Wiley, **2013**.
- [62] W. A. Cunningham, *J. Chem. Educ.* **1935**, *12*, 120.
- [63] R. E. Oesper, *J. Chem. Educ.* **1929**, *6*, 677.
- [64] K. Matyjaszewski, K. Matyjaszewski, *Adv. Mater.* **2018**, *30*, 1706441.
- [65] W. H. Binder, R. Sachsenhofer, *Macromol. Rapid Commun.* **2007**, *28*, 15–54.
- [66] L. Liang, D. Astruc, *Coord. Chem. Rev.* **2011**, *255*, 2933–2945.

- [67] C. E. Hoyle, C. N. Bowman, C. N. Bowman, C. E. Hoyle, *Angew. Chemie Int. Ed.* **2010**, *49*, 1540–1573.
- [68] W. Zhang, K. Chen, G. Chen, *Click React. Org. Synth.* **2016**, 255–285.
- [69] A. B. Lowe, J. W. Chan, in *Funct. Polym. by Post-Polymerization Modif.*, **2012**, pp. 87–118.
- [70] A. B. Lowe, C. E. Hoyle, C. N. Bowman, *J. Mater. Chem.* **2010**, *20*, 4745–4750.
- [71] A. Das, P. Theato, *Macromolecules* **2015**, *48*, 8695–8707.
- [72] M. Eberhardt, R. Mruk, R. Zentel, P. Théato, *Eur. Polym. J.* **2005**, *41*, 1569–1575.
- [73] S. Agar, E. Baysak, G. Hizal, U. Tunca, H. Durmaz, *J. Polym. Sci. Part A Polym. Chem.* **2018**, *56*, 1181–1198.
- [74] M. Rubinstein, R. H. Colby, *Polymer Physics*, OUP Oxford, **2003**.
- [75] A. D. Jenkins, R. F. T. Stepto, P. Kratochvíl, U. W. Suter, *Pure Appl. Chem.* **1996**, *68*, 2287–2311.
- [76] S. L. Aggarwal, O. J. Sweeting, *Chem. Rev.* **1957**, *57*, 665–742.
- [77] N. Hadjichristidis, A. Hirao, Y. Tezuka, F. Du Prez, *Complex Macromolecular Architectures: Synthesis, Characterization, and Self-Assembly*, Wiley, **2011**.
- [78] J. M. Ren, T. G. McKenzie, Q. Fu, E. H. H. Wong, J. Xu, Z. An, S. Shanmugam, T. P. Davis, C. Boyer, G. G. Qiao, *Chem. Rev.* **2016**, *116*, 6743–6836.
- [79] M. Abbasi, L. Faust, M. Wilhelm, *Adv. Mater.* **2019**, *31*, 1806484.
- [80] J. Rzayev, *ACS Macro Lett.* **2012**, *1*, 1146–1149.
- [81] J. Moon, Y. Huh, S. Kim, Y. Choe, J. Bang, *Chinese J. Polym. Sci.* **2021**, *39*, 1626–1633.
- [82] E. Abbasi, S. F. Aval, A. Akbarzadeh, M. Milani, H. T. Nasrabadi, S. W. Joo, Y. Hanifehpour, K. Nejati-Koshki, R. Pashaei-Asl, *Nanoscale Res. Lett.* **2014**, *9*, 1–10.
- [83] R. Liénard, J. De Winter, O. Coulembier, *J. Polym. Sci.* **2020**, *58*, 1481–1502.
- [84] M. Schappacher, A. Deffieux, *Science (80-.)*. **2008**, *319*, 1512–1515.
- [85] Z. Deng, S. Liu, *Polymer (Guildf)*. **2020**, *207*, 122914.
- [86] M. Gauthier-Jaques, P. Theato, *ACS Macro Lett.* **2020**, *9*, 700–705.
- [87] M. Gauthier-Jaques, H. Mutlu, P. Theato, *Macromol. Rapid Commun.* **2022**, *43*, 2100760.
- [88] M. Zhang, A. H. E. Müller, *J. Polym. Sci. Part A Polym. Chem.* **2005**, *43*, 3461–3481.

- [89] J. R. Boyce, D. Shirvanyants, S. S. Sheiko, D. A. Ivanov, S. Qin, H. Börner, K. Matyjaszewski, *Langmuir* **2004**, *20*, 6005–6011.
- [90] K. Kawamoto, M. Zhong, K. R. Gadelrab, L. C. Cheng, C. A. Ross, A. Alexander-Katz, J. A. Johnson, *J. Am. Chem. Soc.* **2016**, *138*, 11501–11504.
- [91] D. Zehm, A. Laschewsky, H. Liang, J. P. Rabe, *Macromolecules* **2011**, *44*, 9635–9641.
- [92] Q. Li, J. Imbrogno, G. Belfort, X. L. Wang, *J. Appl. Polym. Sci.* **2015**, *132*, 41781.
- [93] A. C. Engler, H. Lee, P. T. Hammond, *Angew. Chemie Int. Ed.* **2009**, *48*, 9334–9338.
- [94] D. Gromadzki, *Rev. Environ. Sci. Bio/Technology* **2010**, *9*, 301–306.
- [95] J. C. Foster, S. C. Radzinski, J. B. Matson, *J. Polym. Sci. Part A Polym. Chem.* **2017**, *55*, 2865–2876.
- [96] A. Das, P. Theato, *Macromolecules* **2015**, *48*, 8695–8707.
- [97] Y. Yang, S. Lin, X. Feng, Q. Pan, *ChemistrySelect* **2022**, *7*, e202201040.
- [98] S. J. Blanksby, G. B. Ellison, *Acc. Chem. Res.* **2003**, *36*, 255–263.
- [99] G. G. Hougham, P. E. Cassidy, K. Johns, T. Davidson, *Fluoropolymers 1: Synthesis*, Springer US, **2006**.
- [100] W. E. Hanford, R. M. Joyce, *J. Am. Chem. Soc.* **1946**, *68*, 2082–2085.
- [101] G. J. Puts, P. Crouse, B. M. Ameduri, *Chem. Rev.* **2019**, *119*, 1763–1805.
- [102] C. Ott, R. Hoogenboom, U. S. Schubert, *Chem. Commun.* **2008**, 3516–3518.
- [103] C. R. Becer, K. Babiuch, D. Pilz, S. Hornig, T. Heinze, M. Gottschaldt, U. S. Schubert, *Macromolecules* **2009**, *42*, 2387–2394.
- [104] Y. Du, Q. Zeng, L. Yuan, L. He, *J. Macromol. Sci. Part A* **2021**, *58*, 521–538.
- [105] N. Vogel, P. Théato, *Macromol. Symp.* **2007**, *249–250*, 383–391.
- [106] D. P. Sanders, K. Fukushima, D. J. Coady, A. Nelson, M. Fujiwara, M. Yasumoto, J. L. Hedrick, *J. Am. Chem. Soc.* **2010**, *132*, 14724–14726.
- [107] H. Torrens, *Coord. Chem. Rev.* **2000**, *196*, 331–352.
- [108] F. Blank, H. Scherer, J. Ruiz, V. Rodríguez, C. Janiak, *Dalt. Trans.* **2010**, *39*, 3609–3619.
- [109] T. Aoki, A. Konno, T. Fujinami, *J. Power Sources* **2005**, *146*, 412–417.
- [110] T. S. Leong, M. E. Peach, *J. Fluor. Chem.* **1975**, *6*, 145–159.
- [111] D. G. Holland, G. J. Moore, C. Tamborski, *J. Org. Chem.* **1964**, *29*, 1562–1565.
- [112] T. A. Unzner, T. Magauer, *Tetrahedron Lett.* **2015**, *56*, 877–883.

- [113] S. Chowdhury, E. P. Grimsrud, T. Heinis, P. Kebarle, *J. Am. Chem. Soc.* **1986**, *108*, 3630–3635.
- [114] L. A. Wall, W. J. Pummer, J. E. Fearn, J. M. Antonucci, *J. Res. Natl. Bur. Stand. Sect. A, Phys. Chem.* **1963**, *67A*, 481.
- [115] C. Tamborski, E. J. Soloski, *J. Org. Chem.* **1966**, *31*, 746–749.
- [116] R. Filler, N. R. Ayyangar, W. Gustowski, H. H. Kang, *J. Org. Chem.* **1969**, *34*, 534–538.
- [117] J. Burdon, W. B. Hollyhead, J. C. Tatlow, *J. Chem. Soc.* **1965**, 5152–5156.
- [118] N. H. Park, G. Dos Passos Gomes, M. Fevre, G. O. Jones, I. V. Alabugin, J. L. Hedrick, *Nat. Commun.* **2017**, *8*, 1–7.
- [119] M. B. Smith, J. March, *March's Advanced Organic Chemistry Reactions, Mechanisms, and Structure.*, Wiley, Chicester, **2007**.
- [120] J. Kvičala, M. Beneš, O. Paleta, V. Král, *J. Fluor. Chem.* **2010**, *131*, 1327–1337.
- [121] J. Mason, *Multinuclear NMR*, Springer US, **1987**.
- [122] T. Witt, M. Häußler, S. Kulpa, S. Mecking, *Angew. Chemie Int. Ed.* **2017**, *56*, 7589–7594.
- [123] F. Stempfle, P. Ortmann, S. Mecking, *Chem. Rev.* **2016**, *116*, 4597–4641.
- [124] Ambeed Inc., “1-Bromotetradecane”, can be found under <https://www.ambeed.com/products/112-71-0.html> (accessed 06.09.2022).
- [125] Ambeed Inc., “Tetradec-13-en-1-ol” can be found under <https://www.ambeed.com/products/67400-04-8.html> (accessed 07.09.2022).
- [126] Y. Du, J. F. Zheng, Z. G. Wang, L. J. Jiang, Y. P. Ruan, P. Q. Huang, *J. Org. Chem.* **2010**, *75*, 4619–4622.
- [127] T. Mukhopadhyay, D. Seebach, *Helv. Chim. Acta* **1982**, *65*, 385–391.
- [128] M. Buck, J. M. Chong, *Tetrahedron Lett.* **2001**, *42*, 5825–5827.
- [129] N. Pribut, M. D’Erasmus, M. Dasari, K. E. Giesler, S. Iskandar, S. K. Sharma, P. W. Bartsch, A. Raghuram, A. Bushnev, S. S. Hwang, S. L. Burton, C. A. Derdeyn, A. E. Basson, D. C. Liotta, E. J. Miller, *J. Med. Chem.* **2021**, *64*, 12917–12937.
- [130] M. Arai, K. Kamiya, D. Shin, H. Matsumoto, T. Hisa, A. Setiawan, N. Kotoku, M. Kobayashi, *Chem. Pharm. Bull.* **2016**, *64*, 766–771.
- [131] W. Oppolzer, R. N. Radinov, E. El-Sayed, *J. Org. Chem.* **2001**, *66*, 4766–4770.
- [132] Gawley, R.E., Zhang, X., Wang, Q., *Potassium Hydride. In Encyclopedia of Reagents for Organic Synthesis, (Ed.)*. **2001**, DOI 10.1002/047084289X.
- [133] C. A. Brown, *J. Org. Chem.* **1974**, *39*, 3913–3918.

- [134] W. Oppolzer, R. N. Radinov, *J. Am. Chem. Soc.* **1993**, *115*, 1593–1594.
- [135] R. C. Hoye, G. L. Anderson, S. G. Brown, E. E. Schultz, *J. Org. Chem.* **2010**, *75*, 7400–7403.
- [136] S. V. O’Neil, C. A. Quickley, B. B. Snider, *J. Org. Chem.* **1997**, *62*, 1970–1975.
- [137] L. Rubio-Pérez, R. Azpíroz, A. Di Giuseppe, V. Polo, R. Castarlenas, J. J. Pérez-Torrente, L. A. Oro, *Chem. – A Eur. J.* **2013**, *19*, 15304–15314.
- [138] F. Xue, X. Song, T. T. Lin, K. Munkerup, S. F. Albawardi, K. W. Huang, T. S. A. Hor, J. Zhao, *ACS Omega* **2018**, *3*, 5071–5077.
- [139] Q. Liang, K. Hayashi, D. Song, *ACS Catal.* **2020**, *10*, 4895–4905.
- [140] J. R. Araújo, W. R. Waldman, M. A. De Paoli, *Polym. Degrad. Stab.* **2008**, *93*, 1770–1775.
- [141] K. B. Wagener, J. M. Boncella, J. G. Nel, *Macromolecules* **1991**, *24*, 2649–2657.
- [142] B. Inci, K. B. Wagener, *J. Am. Chem. Soc.* **2011**, *133*, 11872–11875.
- [143] H. Li, G. Rojas, K. B. Wagener, *ACS Macro Lett.* **2015**, *4*, 1225–1228.
- [144] Sigma-Aldrich, “1,3-Dichloropropene” can be found under <https://www.sigmaaldrich.com/DE/en/product/aldrich/403733> (accessed 09.09.2022).
- [145] Sigma-Aldrich, “1,3-Dibromo-1-propene” can be found under <https://www.sigmaaldrich.com/DE/en/product/aldrich/276162> (accessed 09.09.2022).
- [146] A. P. Krapcho, J. F. Weimaster, J. M. Eldridge, E. G. E. Jahngen, A. J. Lovey, W. P. Stephens, *J. Org. Chem.* **1978**, *43*, 138–147.
- [147] G. V. Kryshnal, G. M. Zhdankina, S. G. Zlotin, *Mendeleev Commun.* **2002**, *12*, 57–58.
- [148] I. Kanwal, A. Mujahid, N. Rasool, K. Rizwan, A. Malik, G. Ahmad, S. A. A. Shah, U. Rashid, N. M. Nasir, *Catal. 2020, Vol. 10, Page 443* **2020**, *10*, 443.
- [149] R. Chinchilla, C. Nájera, *Chem. Soc. Rev.* **2011**, *40*, 5084–5121.
- [150] D. Chemin, G. Linstrumelle, *Tetrahedron* **1994**, *50*, 5335–5344.
- [151] M. Alami, B. Crousse, F. Ferri, *J. Organomet. Chem.* **2001**, *624*, 114–123.
- [152] M. Alami, B. Crousse, G. Linstrumelle, *Tetrahedron Lett.* **1994**, *35*, 3543–3544.
- [153] M. Alami, F. Ferri, G. Linstrumelle, *Tetrahedron Lett.* **1993**, *34*, 6403–6406.
- [154] J. N. Abrams, Q. Zhao, I. Ghiviriga, Minaruzzaman, *Tetrahedron* **2012**, *68*, 423–428.
- [155] P. Wu, M. Å. Petersen, A. E. Cohrt, R. Petersen, R. Morgentin, H. Lemoine, C. Roche, A. Willaume, M. H. Clausen, T. E. Nielsen, *Org. Biomol. Chem.* **2016**, *14*, 6947–6950.

- [156] S. Eisler, A. D. Slepko, E. Elliott, T. Luu, R. McDonald, F. A. Hegmann, R. R. Tykwinski, *J. Am. Chem. Soc.* **2005**, *127*, 2666–2676.
- [157] A. J. Butzelaar, M. Gauthier-Jaques, K. L. Liu, G. Brunklaus, M. Winter, P. Theato, *Polym. Chem.* **2021**, *12*, 4326–4331.
- [158] H. Rothfuss, N. D. Knöfel, P. Tzvetkova, N. C. Michenfelder, S. Baraban, A.-N. Unterreiner, P. W. Roesky, C. Barner-Kowollik, *Chem. – A Eur. J.* **2018**, *24*, 17369.
- [159] M. A. M. Alqarni, C. Waldron, G. Yilmaz, C. R. Becer, *Macromol. Rapid Commun.* **2021**, *42*, 2100035.
- [160] Y. Chen, L. Wang, H. Yu, Y. Zhao, R. Sun, G. Jing, J. Huang, H. Khalid, N. M. Abbasi, M. Akram, *Prog. Polym. Sci.* **2015**, *45*, 23–43.
- [161] S. Rathgeber, T. Pakula, A. Wilk, K. Matyjaszewski, K. L. Beers, *J. Chem. Phys.* **2005**, *122*, 124904.
- [162] H. Xu, F. C. Sun, D. G. Shirvanyants, M. Rubinstein, D. Shabratov, K. L. Beers, K. Matyjaszewski, S. S. Sheiko, *Adv. Mater.* **2007**, *19*, 2930–2934.
- [163] A. Nese, N. V. Lebedeva, G. Sherwood, S. Averick, Y. Li, H. Gao, L. Peteanu, S. S. Sheiko, K. Matyjaszewski, *Macromolecules* **2011**, *44*, 5905–5910.
- [164] Y. Q. Yang, X. D. Guo, W. J. Lin, L. J. Zhang, C. Y. Zhang, Y. Qian, *Soft Matter* **2012**, *8*, 454–464.
- [165] B. Zhang, F. Gröhn, J. S. Pedersen, K. Fischer, M. Schmidt, *Macromolecules* **2006**, *39*, 8440–8450.
- [166] L. Feuz, P. Strunz, T. Geue, M. Textor, O. Borisov, *Eur. Phys. J. E 2007 233* **2007**, *23*, 237–245.
- [167] B. M. Trost, C.-J. Li, *Modern Alkyne Chemistry: Catalytic and Atom - Economic Transformations*, Wiley, **2014**.
- [168] M. Arslan, G. Acik, M. A. Tasdelen, *Polym. Chem.* **2019**, *10*, 3806–3821.
- [169] R. Hoogenboom, *Angew. Chemie Int. Ed.* **2010**, *49*, 3415–3417.
- [170] I. Bae, H. Han, S. Chang, *J. Am. Chem. Soc.* **2005**, *127*, 2038–2039.
- [171] I. H. Lee, K. T. Bang, H. S. Yang, T. L. Choi, *Macromol. Rapid Commun.* **2022**, *43*, 2100642.
- [172] X. Liu, T. Han, J. W. Y. Lam, B. Zhong Tang, X. Liu, J. W. Y. Lam, B. Z. Tang, T. Han, *Macromol. Rapid Commun.* **2021**, *42*, 2000386.
- [173] J. He, N. Zheng, D. Xie, Y. Zheng, W. Song, *Polym. Chem.* **2020**, *11*, 1198–1210.
- [174] S. S. Sheiko, B. S. Sumerlin, K. Matyjaszewski, *Prog. Polym. Sci.* **2008**, *33*, 759–785.
- [175] H. il Lee, J. Pietrasik, S. S. Sheiko, K. Matyjaszewski, *Prog. Polym. Sci.* **2010**, *35*, 24–44.

- [176] D. Rosenbach, N. Mödl, M. Hahn, J. Petry, M. A. Danzer, M. Thelakkat, *ACS Appl. Energy Mater.* **2019**, *2*, 3373–3388.
- [177] J. Rolland, J. Brassinne, J. P. Bourgeois, E. Poggi, A. Vlad, J. F. Gohy, *J. Mater. Chem. A* **2014**, *2*, 11839–11846.
- [178] J. Du, G. Xu, H. Lin, G. Wang, M. Tao, W. Zhang, *Green Chem.* **2016**, *18*, 2726–2735.
- [179] M. Eberhardt, P. Théato, *Macromol. Rapid Commun.* **2005**, *26*, 1488–1493.
- [180] A. Das, P. Theato, *Chem. Rev.* **2016**, *116*, 1434–1495.
- [181] J. M. Noy, A. K. Friedrich, K. Batten, M. N. Bhebhe, N. Busatto, R. R. Batchelor, A. Kristanti, Y. Pei, P. J. Roth, *Macromolecules* **2017**, *50*, 7028–7040.
- [182] F. Cavalli, H. Mutlu, S. O. Steinmueller, L. Barner, *Polym. Chem.* **2017**, *8*, 3778–3782.
- [183] J. M. Noy, Y. Li, W. Smolan, P. J. Roth, *Macromolecules* **2019**, *52*, 3083–3091.
- [184] H. Shu, L. Chen, X. Wu, T. Wang, S. Wang, H. Tong, L. Wang, *J. Mater. Chem. C* **2022**, *10*, 1833–1838.
- [185] N. Van Herck, D. Maes, K. Unal, M. Guerre, J. M. Winne, F. E. Du Prez, *Angew. Chemie Int. Ed.* **2020**, *59*, 3609–3617.
- [186] V. X. Truong, A. P. Dove, *Angew. Chemie Int. Ed.* **2013**, *52*, 4132–4136.
- [187] O. Daglar, U. S. Gunay, G. Hizal, U. Tunca, H. Durmaz, *Macromolecules* **2019**, *52*, 3558–3572.
- [188] T. Zhao, V. P. Beyer, C. R. Becer, T. Zhao, V. P. Beyer, C. R. Becer, *Macromol. Rapid Commun.* **2020**, *41*, 2000409.
- [189] J. Ding, X. Du, M. Day, J. Jiang, C. L. Callender, J. Stupak, *Macromolecules* **2007**, *40*, 3145–3153.
- [190] L. Infante Teixeira, K. Landfester, H. Thérien-Aubin, *Macromolecules* **2021**, *54*, 3659–3667.
- [191] A. B. Lowe, *Polym. Chem.* **2014**, *5*, 4820–4870.
- [192] D. N. Schulz, S. R. Turner, M. A. Golub, *Rubber Chem. Technol.* **1982**, *55*, 809–859.
- [193] N. Shida, K. Ninomiya, N. Takigawa, K. Imato, Y. Ooyama, I. Tomita, S. Inagi, *Macromolecules* **2021**, *54*, 725–735.
- [194] S. V. Amosova, G. M. Gavrilova, V. I. Gostevskaya, A. V. Afonin, L. I. Larina, *Chem. Heterocycl. Compd. 1998 345* **1998**, *34*, 625–628.
- [195] M. Arisawa, T. Suzuki, T. Ishikawa, M. Yamaguchi, *J. Am. Chem. Soc.* **2008**, *130*, 12214–12215.

- [196] W. R. Xian, Y. He, Y. Diao, Y. L. Wong, H. Q. Zhou, S. L. Zheng, W. M. Liao, Z. Xu, J. He, *Inorg. Chem.* **2020**, *59*, 7097–7102.
- [197] “CN111170909A - Thioether compound and preparation method and application thereof - Google Patents” can be found under <https://patents.google.com/patent/CN111170909A/en?q=CN111170909A> (accessed 07.09.2022).
- [198] M. R. Uehling, A. M. Suess, G. Lalic, *J. Am. Chem. Soc.* **2015**, *137*, 1424–1427.
- [199] P. Mangeney, A. Alexakis, J. F. Normant, *Tetrahedron Lett.* **1986**, *27*, 3143–3146.
- [200] M. Ishizaki, O. Hoshino, *Heterocycles* **2002**, *57*, 1399–1402.
- [201] T. Nabeshima, N. Tsukada, K. Nishijima, H. Ohshiro, Y. Yano, *J. Org. Chem.* **1996**, *61*, 4342–4350.
- [202] S. J. Miller, S. A. Elomari (Chevron USA Inc), “US20080194444A1 - Diester-Based Lubricants and Methods of Making Same - Google Patents” can be found under <https://patents.google.com/patent/US20080194444A1/en?q=US2008194444A1> (accessed 07.09.2022).
- [203] R. Bernardini, A. Oliva, A. Paganelli, E. Menta, M. Grugni, S. De Munari, L. Goldoni, *Chem. Lett.* **2009**, *38*, 750–751.
- [204] B. M. Dufort, M. W. Tibbitt, *Mater. Today Chem.* **2019**, *12*, 16–33.
- [205] J. Lu, N. N. Ten Brummelhuis, M. Weck, *Chem. Commun.* **2014**, *50*, 6225–6227.
- [206] M. Firdaus, M. A. R. Meier, U. Biermann, J. O. Metzger, *Eur. J. Lipid Sci. Technol.* **2014**, *116*, 31–36.
- [207] J. Burden, P. L. Coe, C. R. Marsh, J. C. Tatlow, *J. Chem. Soc. Perkin Trans. 1* **1972**, 763–769.
- [208] D. A. Alonso, C. Nájera, M. Varea, *Helv. Chim. Acta* **2002**, *85*, 4287–4305.
- [209] Y. Zhao, G. Huang, C. Besnard, J. Mareda, N. Sakai, S. Matile, *Chem. – A Eur. J.* **2015**, *21*, 6202–6207.
- [210] V. V. Litvak, A. S. Kondrat’Ev, V. D. Shteimgarts, *Russ. J. Org. Chem. 2009 4511* **2009**, *45*, 1637–1643.
- [211] V. Dudutiene, A. Zubriene, A. Smirnov, J. Gylyte, D. Timm, E. Manakova, S. Gražulis, D. Matulis, *Bioorg. Med. Chem.* **2013**, *21*, 2093–2106.
- [212] R. Fernández De La Pradilla, S. Castro, P. Manzano, M. Martín-Ortega, J. Priego, A. Viso, A. Rodríguez, I. Fonseca, *J. Org. Chem.* **1998**, *63*, 4954–4966.
- [213] S. Masaki, N. Sato, A. Nishichi, S. Yamazaki, K. Kimura, *J. Appl. Polym. Sci.* **2008**, *108*, 498–503.

- [214] L. Lebreton, A. Andrady, *Palgrave Commun. 2019 51* **2019**, *5*, 1–11.
- [215] M. J. Kade, D. J. Burke, C. J. Hawker, *J. Polym. Sci. Part A Polym. Chem.* **2010**, *48*, 743–750.
- [216] O. Türünç, M. A. R. Meier, *Eur. J. Lipid Sci. Technol.* **2013**, *115*, 41–54.
- [217] O. Türünç, M. A. R. Meier, *Macromol. Rapid Commun.* **2010**, *31*, 1822–1826.
- [218] M. Lo Conte, S. Staderini, A. Marra, M. Sanchez-Navarro, B. G. Davis, A. Dondoni, *Chem. Commun.* **2011**, *47*, 11086–11088.
- [219] D. Goyard, T. C. Shiao, N. L. Fraleigh, H. Y. Vu, H. Lee, F. Diaz-Mitoma, H. T. Le, R. Roy, *J. Mater. Chem. B* **2016**, *4*, 4227–4233.
- [220] The Food and Agriculture Organization (FAO), “Specifications for Flavourings - Dodecanethiol” can be found under <https://www.fao.org/food/food-safety-quality/scientific-advice/jecfa/jecfa-flav/details/en/c/1902/> (accessed 07.09.2022).
- [221] M. Hudlicky, T. Hudlicky, *Patai Suppl. D, Chem. Halides Pseudo-Halides Azides* **2010**, 1021–1172.
- [222] E. Fromm, H. Benzinger, F. Schäfer, *Justus Liebigs Ann. Chem.* **1912**, *394*, 325–337.
- [223] T. P. Dawson, W. E. Lawson, *J. Am. Chem. Soc.* **1927**, *49*, 3125–3129.
- [224] C. M. Hu, F. Hong, B. Jiang, Y. Xu, *J. Fluor. Chem.* **1994**, *66*, 215–217.
- [225] D. F. Andres, E. G. Laurent, B. S. Marquet, H. Benotmane, A. Bensadat, *Tetrahedron* **1995**, *51*, 2605–2618.
- [226] J. Berthelot, Y. Benammar, C. Lange, *Tetrahedron Lett.* **1991**, *32*, 4135–4136.
- [227] M. C. Ford, M. Saxton, P. S. Ho, *J. Phys. Chem. Lett.* **2017**, *8*, 4246–4252.
- [228] M. Shimagaki, H. Koshiji, T. Oishi, *Phosphorus Sulfur Relat. Elem.* **1983**, *16*, 45–58.
- [229] N. Kutsumura, M. Iijima, S. Toguchi, T. Saito, *Chem. Lett.* **2011**, *40*, 1231–1232.
- [230] B. A. Haas, H.-U. Krachter, A. Haas, H.-U. Krachter, *Chem. Ber.* **1988**, *121*, 1833–1840.
- [231] E. A. Gormong, T. M. Reineke, T. R. Hoye, *ACS Macro Lett.* **2021**, *10*, 1068–1072.
- [232] D. J. Lippincott, R. T. H. Linstadt, M. R. Maser, B. H. Lipshutz, *Angew. Chemie Int. Ed.* **2017**, *56*, 847–850.

Publications

Publications arising from this Thesis

S. Baraban, L. Westendarp, H. Mutlu, P. Theato, Polymerization of Pentafluorophenyl vinyl sulfide Derivatives through *para*-Fluoro-Thiol Chemistry, *Macromol. Rapid Commun.*, *in preparation*.

Other Publications

Rothfuss, H.*, Knöfel, N.*, Tzvetkova, P., Michenfelder, N., Baraban, S., Unterreiner, A.-N., Roesky, P.W., Barner-Kowollik, C., *Chem. Eur. J.* **2018**, 24, 17475-17486.

*equal contributions

Conference Contributions

“Precise functional Polyethylenes *via* Sonogashira polycondensation”

S. Baraban, P. Theato

Poster presented on September 2021 at the online poster session of the GDCh-Makrosymposium 2021.

Acknowledgments

Vielen Menschen haben direkt oder indirekt zum Erfolg dieser Arbeit beigetragen, sodass ich nun meinen Dank aussprechen will.

An erster Stelle möchte ich PROF. DR. PATRICK THÉATO für die Aufnahme in seinem Arbeitskreis danken und natürlich auch für die stetig fortwährende Unterstützung auch „nach Vertragslaufzeit“. Du hat mir in chemischer Sicht ziemliche Narrenfreiheit gegeben, sodass ich mich sehr austoben konnte, wenn rückblickend auch nicht alles zielführend war, was da im Kolben gerührt hat. Nichtsdestotrotz konnte ich doch noch etwas „zu Papier“ bringen.

In diesem Zusammenhang möchte ich auch PROF. DR. MICHAEL MEIER für die Übernahme des Korreferats danken.

Weiterhin gilt mein besonderer Dank der „alten“ und „neuen“ 322-Truppe, namentlich erstmal Edgar & Martin als „alte Hasen“. Es war eine aufregende Zeit seit Mitte 2018, als wir noch voller Elan am Abzug standen. Die Komik in diesem Labor konnte nur durch die Kombination eurer eigenwilligen Charakterzüge entstehen („*Mais non, pu**in!*“). Ich bin gespannt, wo ihr (und ich) in 10 Jahren stehen und wünsche euch alles Gute weiterhin! Daran anschließend auch ein Danke an Andi und Stefan für die lustige Zeit als 322 eine richtige Boyband-Besetzung hatte! Zu fünft an drei Tischen und zwei gehen auch noch ins Gym. ;) Abschließend auch ein dickes Danke an die „next generation“ Sven und Nico Uli! Die Laborstimmung mit euch war so grandios, dass selbst die Wilhelms neidisch waren (und sich uns dann angebiedert haben!). Die Memes, die Songs und die schlechten Witze werde ich sehr vermissen! Ich kann nur hoffen, dass ihr mit meinem Nachfolger so happy seid wie ich mit euch war. *Magikarp!* In diesem Zusammenhang auch ein riesiges Dankeschön an meinen Vertiefer-HiWi Lars, der mit mir das Pentafluoro-Wunder bewirkt hat und gerade gegen Ende widerstandslos alles ausgeschüttelt und gesäult hat was man ihm vorgesetzt hat. Ich denke du bist in Zukunft in guten Händen und ich erwarte einen Paper-Regen der seinesgleichen sucht!

Direkt hierauf bezugnehmend auch ein riesiges Danke an Dr. Hatice Mutlu. Du hast mich ja irgendwie zu diesem Spaß hier zu anfangs überredet und nun auch durch die vielen Korrekturen bis zum Ende begleitet. Ein Lob an deinen stetigen Enthusiasmus und Willen, da muss ich mir definitiv etwas abschneiden. Weiterhin viel Erfolg auf der nächsten akademischen Stufe!

Wiederhin ein Dankeschön an die gesamte Gruppe, leider war das gemeinsame AK-Leben durch widrige Umstände etwas eingeschränkt aber ich hoffe das wird sich in Zukunft noch ändern. Auch ein Danke an alle, die „den Laden“ im Vordergrund und/oder Hintergrund am Laufen halten und gehalten haben: Dr. Dominik Voll, Evelyn Stühning, Vera Noga, Bärbel Seufert-Dausmann, Martina Ritter, Birgit Huber und im besonderen Katharina Kuppinger (ehemalige Elies; heimliche PhD Studentin). Abseits des nahen Laborumfeldes muss ich zudem

auch einigen „OClern“ danken: Eren und Luca für das eine oder andere Bier und dem guten AKW vor allem. Ich bin froh, so viele von euch gekannt zu haben, denn sonst wäre der Campus Süd eine Partywüste gewesen! Hierbei sei auch Mensa-Fabi gedankt. Daran angrenzend muss auch dem 322-Stammtisch bestehend aus Chris, Luca, Eren, Joel und 322 gedankt werden.

Weiterhin ein Danke für die tolle Zeit an meine lieben Kommilitonen Chris, Chrissy, Lari, Yannick, Tanja, Nico. Wir bleiben hoffentlich weiterhin in Kontakt.

Ein absolut GIGANTISCHES Danke muss ich natürlich an Sara aussprechen. Du hast mich in all den Jahren durch Tiefen und Höhen begleitet und kontinuierlich aufgebaut, unterstützt und mir den Rücken *freigehalten* und in den stressigsten Zeiten *zu* mir gehalten. Ein *liebes* Danke dafür.

Zum Schluss möchte ich noch meiner Familie danken. Ihr habt mich immer unterstützt und gerade auch in der letzten Zeit viel Verständlich zeigen müssen, da ich keine Zeit für euch hatte. Ich hoffe ich konnte euch etwas stolz machen. Danke für euren Rückhalt!